Formation of Cyclodextrin-Drug Inclusion Compounds and Polymeric Drug Delivery Systems Using Supercritical Carbon Dioxide

Heather E. Grandelli

Dissertation submitted to the faculty of the Virginia Polytechnic Institute and State University in partial fulfillment of the requirements for the degree of

Doctor of Philosophy

In

Chemical Engineering

Erdogan Kiran, Co-chair

Abby Whittington, Co-chair

Stephen Martin

Kevin Edgar

Robert Moore

August 30, 2013

Blacksburg, VA

Keywords: Supercritical carbon dioxide, cyclodextrin inclusion compounds, poly(lactide-co-glycolide), poly(ε-caprolactone), foaming

Formation of Cyclodextrin-Drug Inclusion Compounds and Polymeric Drug Delivery Systems Using Supercritical Carbon Dioxide

Heather E. Grandelli

ABSTRACT

New methods for the preparation of porous biomedical scaffolds have been explored for applications in tissue engineering and drug delivery. Scaffolds with controlled pore morphologies have been generated which incorporate cyclodextrin-drug inclusion complexes as the drug delivery component. Supercritical CO_2 was explored as the main processing fluid in the complex formation and in the foaming of the polymer scaffold. The co-solvents, ethanol, ethyl acetate and acetone, were explored in each stage, as needed, to improve the solvent power of CO_2.

The first goal was to promote cyclodextrin-drug complex formation. Complex formation by traditional methods was compared with complex formation driven by processing in supercritical CO_2. Complex formation was promoted by melting the drug in supercritical CO_2 or in CO_2 + co-solvent mixtures while in the presence of cyclodextrin. Some drugs, such as piroxicam, are prone to degradation near the drug's ambient melting temperature. However, this approach using CO_2 was found to circumvent drug thermal degradation, since drug melting temperatures were depressed in the presence of CO_2.

The second goal was to produce porous polymeric matrices to serve as tissue engineering scaffolds. Poly(lactide-*co*-glycolide) and poly(ε-caprolactone) were investigated for foaming, since these biomedical polymers are already commonly used and FDA approved. Polymer foaming with CO_2 is an alternative approach to conventional solvent-intensive methods for porosity generation. However, two major limitations of polymer foaming using CO_2 as the only processing fluid have been reported, including the formation of a non-porous outer skin upon depressurization and limited pore interconnectivity. Approaches to circumvent these limitations include the use of a co-solvent and controlling depressurization rates. The effect of processing parameters, including foaming temperatures and depressurization rate, as well as co-solvent addition, were examined in polymer foaming using CO_2. Drug release dynamics were compared for foams incorporated with either pure drug, cyclodextrin-drug physical mixture or cyclodextrin-drug complex. Pore morphology, polymer choice and drug release compound choice were found to alter drug release profiles.

Acknowledgements

I would first like to thank my primary Ph.D. advisor, Dr. Erdogan Kiran, to whom I am extremely grateful. His generosity, guidance, encouragement and never ending support have allowed me to find the way through my doctoral work at Virginia Tech and produce something of which I am proud. I am humbled to have been given the opportunity to work with him.

Thank you to my co-advisor advisor, Dr. Abby Whittington, for her guidance with the drug release aspects of my doctoral research and for her encouraging support. I am grateful to the other members of my advisory committee, Dr. Edgar, Dr. Martin and Dr. Moore, for their helpful discussions and guidance.

I must express my gratitude toward my undergraduate academic advisor, Dr. Gary Huvard, for always challenging me and for encouraging me to go to graduate school.

A special thanks to Michael Vaught and Dr. John Hassler for their dedicated help on the building and maintaining of the experimental equipment. I thank the departmental staff, Diane Cannaday, Tina Kirk, Jane Price and Nora Bentley for their help, and Stephen McCartney for his assistance with SEM analysis.

To my colleagues in the lab, Nunzia Falco, Shinya Takahashi, Sulamith Frerich and James Dickman, a special thanks for their support, stimulating conversations and advice. Thank you to undergraduate students, Bryce Stickle, Casey Bolin, Wes Sellers and Melanie Merrick for your help in the lab.

Finally, I want to express my appreciation to my friends and family. Especially to my parents, Connie and Pat, for their loving support and guidance and for always providing me with amazing opportunities. Thank you also goes to my brother, Patrick, for being so inspirational to me. A special thanks to John Quigley for his love, support and eternal optimism and for reminding me to always have fun. Thank you to my second family, Cathy, Craig, Jim and Laura, for always being there for me.

Table of Contents

List of Figures

List of Tables

Chapter I. Introduction

This dissertation reports on new methods in the preparation of porous biomedical scaffolds for applications in tissue engineering and drug delivery. Highly interconnected, low density porous scaffolds are desirable in tissue engineering applications and are conventionally generated using solvent-intensive techniques. A high pressure technique which employs supercritical CO_2 ($scCO_2$) as a foaming agent is an alternative to conventional organic solvent-intensive techniques, which is a safer approach to generating porosity in biodegradable polymers for use as tissue engineering scaffolds. Built-in drug release attributes can be achieved by incorporation of drug components into biomedical scaffolds and can potentially aid in the healing process when implanted into the body. However, many developed pharmaceuticals display very low aqueous solubility, which causes limited delivery of the drug in the body. Cyclodextrin-drug inclusion complex formation is a guest-host type association and is an approach to improve the aqueous solubility of hydrophobic drugs. Supercritical CO_2 and its mixtures with a small amount of an organic co-solvent are powerful processing fluids which hold high potential in the formation of cyclodextrin-drug inclusion complexes and in the foaming of polymers. This research has considered the use of these fluids at high pressure as an alternative to conventional solvent-intensive techniques in the generation of polymer foams incorporated with cyclodextrin-drug inclusion complexes as tissue engineering scaffolds with drug release attributes.

1.1 Supercritical Fluids

A supercritical fluid (SCF) is defined as a substance at a temperature and pressure above its critical values (T_c, P_c), at which conditions the distinction between the gas and liquid phase is no longer prevalent [1]. Figure 1 illustrates the phase boundaries for a pure component, with the supercritical fluid region shaded. In the supercritical region, molar volume or density can be altered by changing pressure without crossing into the two-phase region, as shown in Figure 2. This feature allows SCFs to function as tunable solvents, which also have low viscosity, no surface tension and high diffusivity.

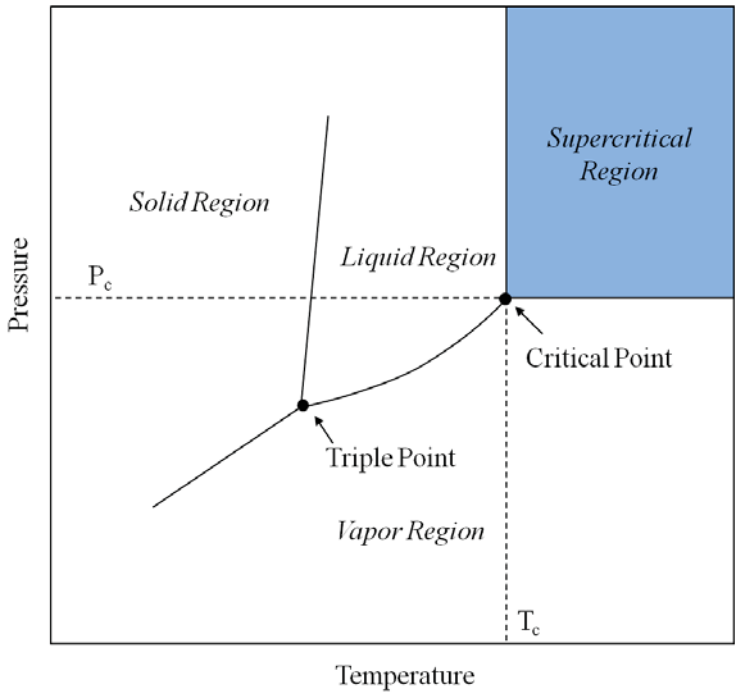

Figure 1. Phase diagram for a single component fluid, with the supercritical region shaded [1].

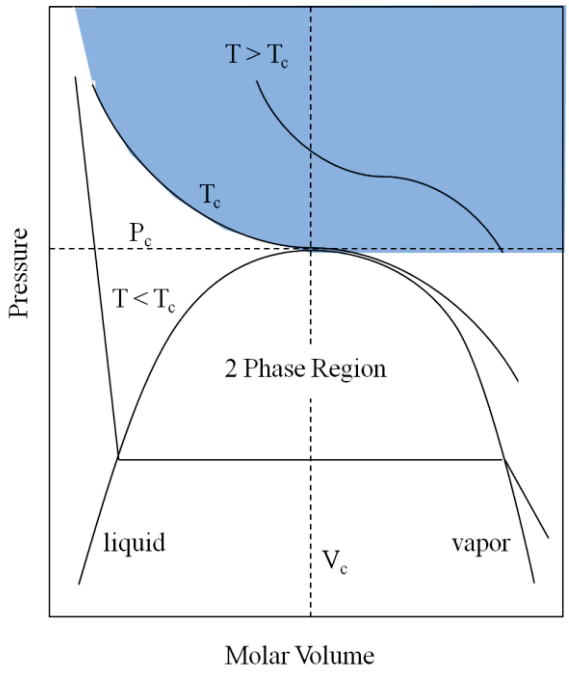

Figure 2. Volumetric behavior of a single component fluid as a function of pressure with the supercritical region shaded [1].

Carbon dioxide is the most widely used SCF due to its moderate critical point, non-toxicity, low cost and high natural abundance [2]. $scCO_2$ is of particular interest in the processing of biomedical devices, such as tissue engineering (TE) scaffolds and drug delivery systems, since it is non-toxic and leaves no residue [3, 4]. Typical SCF technologies currently investigated for use in the biomedical industry include particle formation [5], disinfection [6, 7], extraction [8], polymerization [9], and chromatography [3].

Despite its tunable solvent power, poor dissolution of most materials in $scCO_2$ limits the use of the fluid alone. This is especially true for high molecular weight polymers, where very high pressures are often required to achieve miscibility. For example, a biomedical co-polymer of interest in this research, poly(lactide-co-glycolide) with a 50/50 monomer ratio, does not dissolve

in pure CO_2 even at pressures up to 3000 bar at 50 ^oC [10]. An approach to improve the solvent power of $scCO_2$ and reduce miscibility pressures is the addition of a co-solvent [11, 12]. In TE applications, solvents which are Generally Recognized as Safe (GRAS solvents) by the Food and Drug Administration are preferable, as their residues are relatively non-toxic. Acetone, ethanol and ethyl acetate are a few examples of GRAS solvents. Table 1 provides the pure component critical parameters for CO_2 and the organic solvents explored in this research.

Table 1. Critical values for solvent with utility in the biomedical industry [13].

Fluid	P_c, MPa	T_c, ^oC
Carbon Dioxide	7.4 ± 0.015	31.0 ± 0.02
Ethanol	6.3 ± 0.4	240.9 ± 7
Acetone	4.8 ± 0.4	234.8 ± 2
Ethyl Acetate	3.9 ± 0.003	250.2 ± 0.5

The critical loci of binary fluid mixtures of CO_2 with acetone and ethanol are shown in Figure 3 and Figure 4, respectively. The critical loci of ethyl acetate - CO_2 mixtures are not available in the literature as a function of composition, but the PT projection has been provided and is shown in Figure 5 [14]. The critical point of the CO_2 + co-solvent mixture is dependent on the mixture composition, with T_c of the mixture taking on an intermediate value between the T_c of the pure components, while the P_c of the mixture takes on values greater than the P_c of either pure component [11, 12, 15].

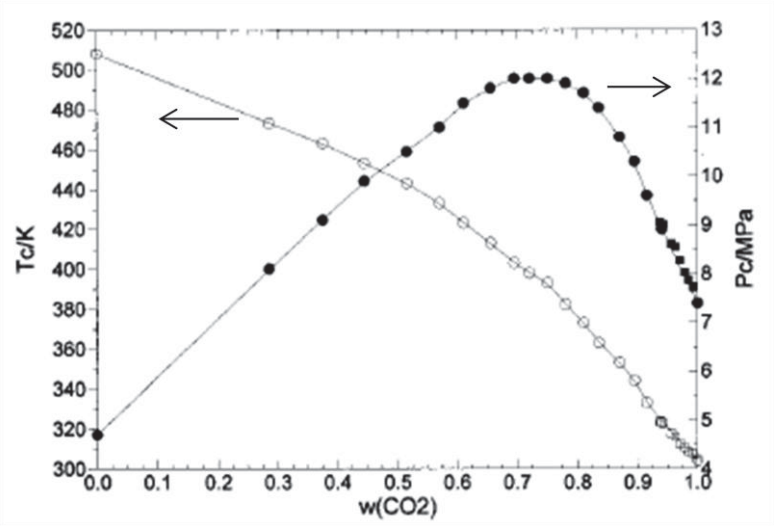

Figure 3. CO_2 + acetone critical parameters as a function of composition [11].

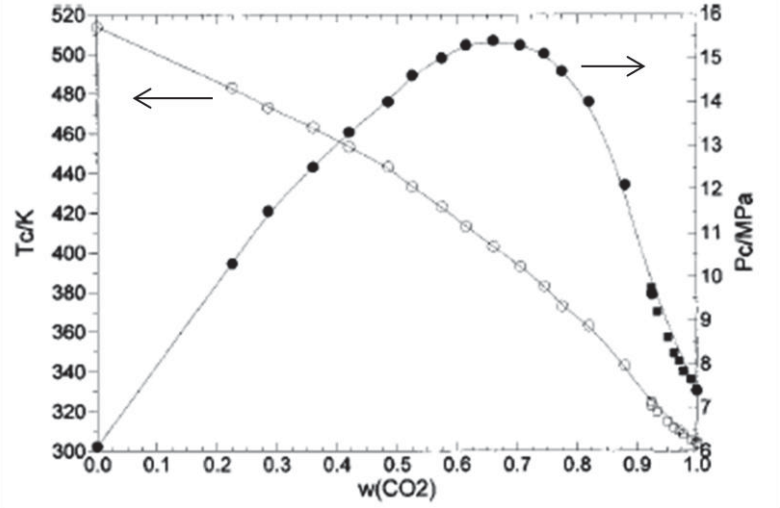

Figure 4. CO_2 + ethanol critical parameters as a function of composition [12].

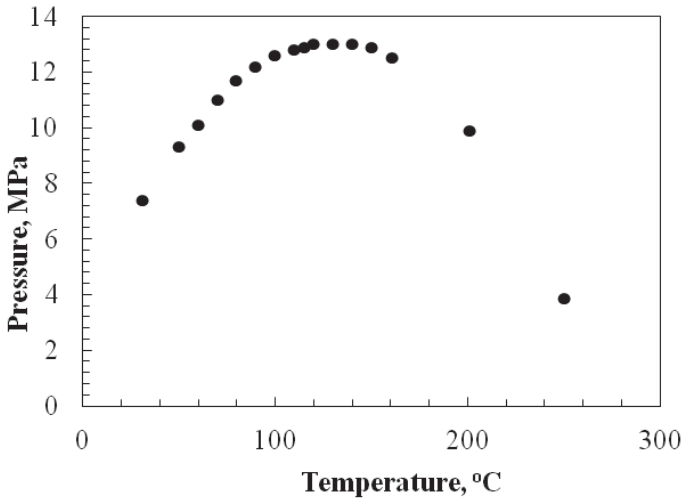

Figure 5. CO_2 + ethyl acetate critical loci PT projection [14].

1.2 Tissue Engineering Scaffolds and Drug Delivery Devices

TE is a field developed to resolve the shortage in tissue transplantations [16]. The approach employed in this field is to replace and repair damaged or defective tissues by developing appropriate biological substitutes [17]. Biomedical polymers used in TE and drug delivery are considered biomaterials, defined as materials that interface with a biological system to repair, improve or replace a tissue or function of the system [18, 19]. Biomedical polymers can be either naturally derived or synthesized. Natural polymers have the advantage of biocompatibility but lack material properties needed in many weight-bearing applications. The use of synthetic polymers poses the advantage of flexibility in chemistry giving rise to diverse physical and mechanical properties for a wide range of TE applications [18, 19]. Biomedical polymers have been used for the permanent replacement of connective tissues, including sutures, hip replacements, vascular grafts and lens replacement [20], as well as soft tissue replacement, tissue regeneration, blood contacting system, medical adhesives, orthopedics, dental materials, drug delivery and gene therapy [20, 21].

In TE, polymers are used to act as a scaffold for transplanted cells that mimics the extracellular matrix, provides a structure and organization for the cell growth, guides tissue regeneration and has adequate mechanical properties to withstand stresses common at the site of implantation [22]. Highly porous interconnected scaffolds are typically needed to promote in growth and the exchange of nutrients, oxygen and waste. Scaffolds for TE should be biocompatible (i.e. non-toxic) and biodegradable, such that a viable biological system remains once the function of the scaffold has been fulfilled [18].

Polymeric TE scaffolds are conventionally formed through solvent casting/porogen leaching [23], electrospinning [24] and thermally induced phase separation [25]. These methods all involve the use of harsh organic solvents, which is non-ideal in biomedical applications due to toxicity [26]. A safer alternative is the use of $scCO_2$ as a gas blowing agent in polymer foaming. In fact, CO_2 has been shown to be a powerful foaming agent for amorphous and semicrystalline biomedical polymers [27, 28]. In CO_2 foaming of polymers, CO_2 dissolves in the amorphous regions of the polymer reducing the glass transition and melting temperatures. A temperature or pressure quench can then be carried out to induce a thermodynamic instability in the polymer-CO_2 mixture. This instability results in the nucleation and growth of gaseous CO_2 domains within the polymer which remain as pores in the solidified polymer matrix [28]. Polymer foaming with CO_2 is illustrated in Figure 6.

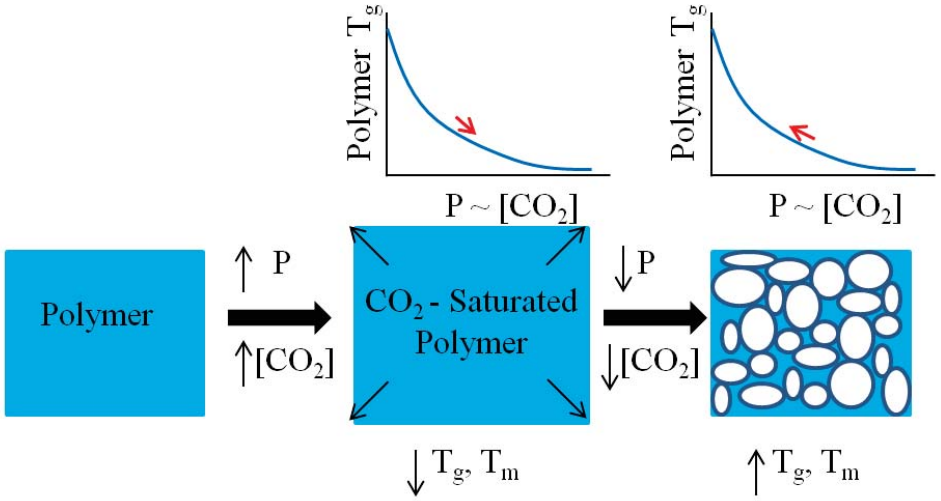

Figure 6. Illustration of polymer foaming with CO_2. Polymer becomes swollen with CO_2, lowering the glass transition and melting temperature (if semi-crystalline). Upon depressurization, CO_2 bubbles nucleate and grow as the glass transition and melting temperatures increase, causing polymer vitrification or crystallization locking in the porous structure.

Limitations of polymer foaming with CO_2 alone for TE applications, which are described in the literature [29] and confirmed in our experiments, include limited pore interconnectivity and the formation of a non-porous polymer skin layer on the surface of the foam. The addition of a small amount of GRAS organic co-solvent may help improve interconnectivity and limit skin formation [30]. This has already been explored in the foaming of poly(p-dioxanone) [30], poly(ε-caprolactone-co-lactide) [31] and poly(L-lactic acid) [32] with CO_2 + acetone mixtures in our lab and was further investigated with other biomedical polymers and co-solvents in this research.

A desirable feature of TE scaffolds is the incorporation of a bioactive compound, such as a drug or growth factor, which is released *in vivo* to aid the regeneration or healing process (e.g. promote cell growth, limit inflammation, prevent infection). In this situation the TE scaffold also acts as a drug delivery system [33]. Ideally, a drug delivery system will deliver the effective concentration of the bioactive compound locally to the affected area without initially exceeding the dosage in a burst release and without allowing the concentration to drop below the effective level throughout the treatment, as shown in Figure 7 [33, 34].

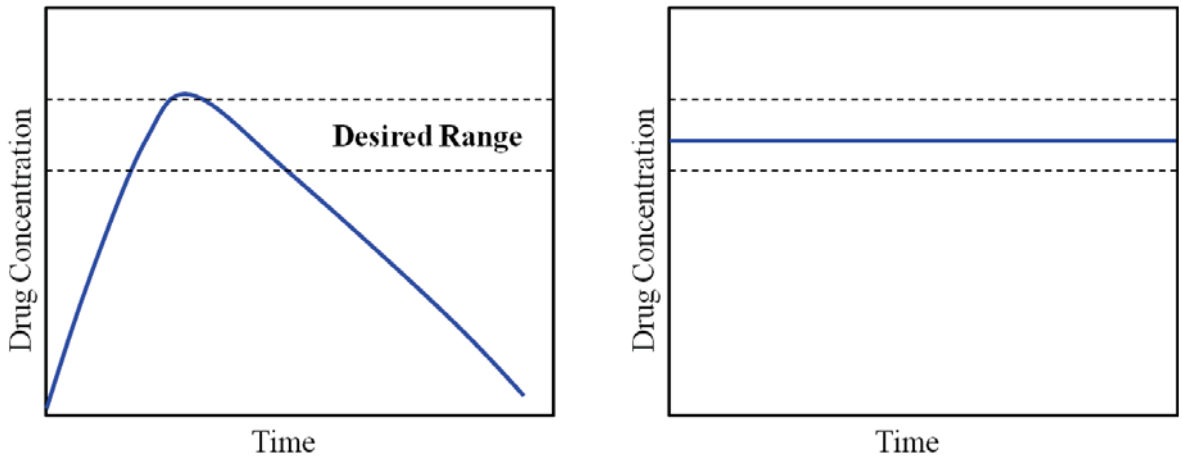

Figure 7. Typical (left) and ideal (right) drug release profiles [34].

The mechanism by which a bioactive molecule is released from the polymer matrix is a combination of diffusion and bulk erosion of the polymer (i.e. degradation/dissolution) [20, 35]. In either drug delivery mechanism the aqueous solubility of the bioactive compound is an important factor in the delivery and bioavailability of the molecule. Poor aqueous solubility of drugs is a serious limitation in the pharmaceutical industry, since about 40% of newly developed pharmaceuticals have very low aqueous solubility [36]. The low solubility is primarily due to

drug molecule hydrophobicity and limits the bioavailability of these drugs. In this research, the bioactive compounds investigated are all non-steroidal anti-inflammatory drugs (NSAIDs), which have low solubilities in water. NSAIDs, which constitute the most widely used drug type worldwide, have analgesic properties at low doses and anti-inflammatory properties at higher doses [37]. Table 2 lists the names of commonly used and commercially available NSAIDs, and Table 3 provides physical properties of NSAIDs investigated in this research.

Table 2. Commonly used NSAIDs separated by chemical class [37, 38].

Salicylates
Acetylsalicylic acid (aspirin)
Salsalate
Diflunisal

Nonacetylated Salicylates
Magnesium salicylate
Choline magnesium trisalicylate

Propionic Acid Derivatives
Fenoprofen calcium
Flurbiprofen
Ibuprofen
Ketoprofen
Naproxen
Naproxen sodium
Oxaprozin
Fenbufen

Fenamates
Mefenamic acid
Meclofenamate sodium
Flufenamic Acid

Naphthylalkanone
Nabumetone

Acetic Acids
Indomethacin
Sulindac
Tolmetin sodium
Acemetacin
Diclofenac
Etodolac

Oxicams
Piroxicam
Tenoxicam

Pyrrolo-pyrrole
Ketorolac tromethamine

Pyranocarboxylic Acid
Etodolac

Selective COX-2 Inhibitors
Celecoxib

Semiselective COX-2 Inhibitors
Meloxicam

Table 3. Physical properties of NSAIDs from (a) [39], (b) [40], (c) [41], (d) [42], (e) [43], (f) [44], (g) [45] at 37 ^{o}C.

Name/Structure	MW, g/mol	T_m, K	ΔH_m, kJ/mol	Solubility at 25 ^{o}C, mg/ml			
				Water	Ethanol	Acetone	Ethyl Acetate
Ibuprofen 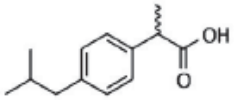	206.28[a]	347.2[a]	25.5[a]	0.021[a]	528[b]	699[d]	611[e]
Ketoprofen 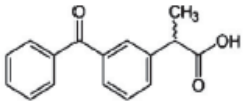	254.28[a]	367.7[a]	21.0[a]	0.124[a]	327[c]	-	523[c]
Naproxen 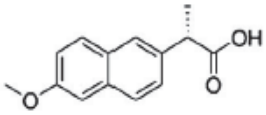	230.26[a]	427.6[a]	31.5[a]	0.0159[a]	57.1[b]	-	-
Piroxicam 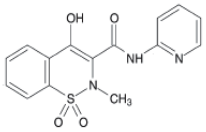	331.35[f]	471-476[f]	36.2[f]	0.0198[g]	-	-	-

1.3 Cyclodextrin Inclusion Compounds

Drug-cyclodextrin (CD) inclusion compound formation is an approach to improve the aqueous solubility of hydrophobic drugs. CDs, also known as cycloamyloses and cycloglucans, are cyclic oligosaccharides composed of α(1, 4)-linked glucose units which have the shape of a truncated cone or torus, as illustrated in Figure 8a [46]. The cavity is relatively non-polar compared to water, while the outer edge of the CD molecule is polar due to the presence of hydroxyl groups on the faces of the structure. The chemical structures of the three native CDs: α-, β- and γ-cyclodextrin which are composed of 6, 7, and 8 glucose units, respectively, are illustrated in

Figure 8b. Due to their unique chemical structure, CDs are interesting host molecules for hydrophobic guest molecules in aqueous solution [47]. In an inclusion compound or complex, a hydrophobic guest molecule can enter the cavity of a CD molecule, as illustrated in Figure 9 [48]. The complex takes on the hydrophilic character of the outside of the CD molecule, which can lead to improved aqueous solubility. When the inclusion complex is placed in aqueous solution, the guest molecules are released from the internal cavity of the CD through an equilibrium association/dissociation, which drives continuous release of the guest molecule [49].

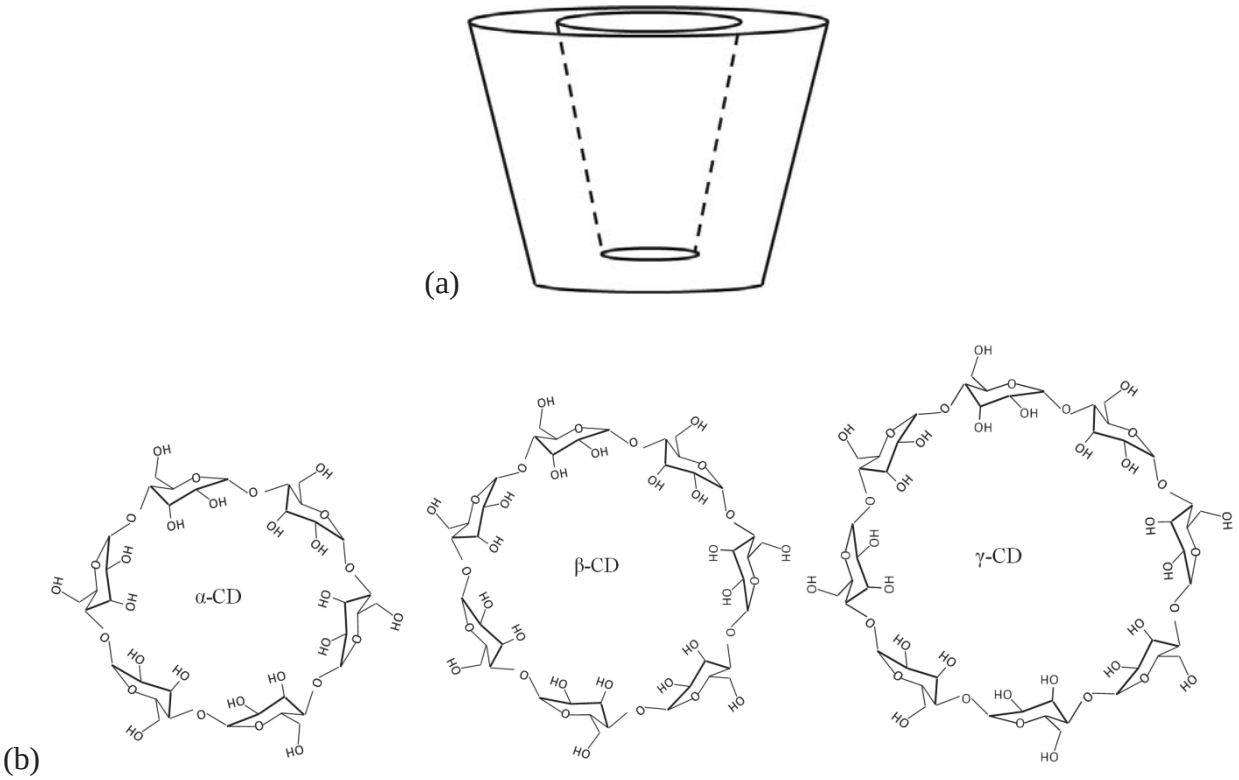

Figure 8. Geometry (a) and chemical structure (b) of native cyclodextrins.

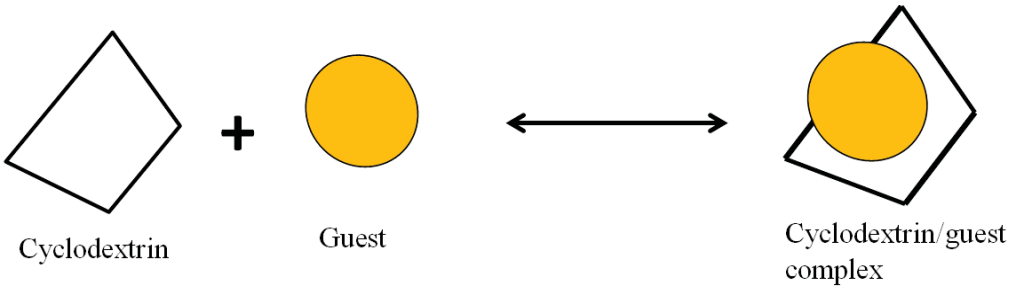

Figure 9. Equilibrium binding of a drug with CD in an inclusion compound formation [50].

CD-drug inclusion compounds have conventionally been prepared by solvent intensive methods, such as co-precipitation, lyophilization, spray drying and slurry or paste mixing which may also require high temperatures [51, 52]. Use of organic solvents can result in toxic residues unsuitable for TE and drug delivery applications, and high temperatures are non-ideal in processing of drug delivery devices since many bioactive compounds are thermally labile. Inclusion complex formation using $scCO_2$ as a processing fluid is thus an attractive alternative to conventional methods [53].

This dissertation reports on the promotion of CD-drug inclusion complex formation and the foaming of polymers incorporated with the inclusion compound using supercritical fluid mixtures for TE applications. Systematic studies of the interactions between small molecules (drugs) and macromolecules (CDs and polymers) were carried out in $scCO_2$ and its mixtures with GRAS co-solvents. Three papers based on the present research have already been published. These are:

(1) H. Grandelli, E. Kiran, High Pressure Density, Miscibility and Compressibility of Poly(lactide-co-glycolide) Solutions in Acetone and Acetone + CO_2 Binary Fluid Mixtures, The Journal of Supercritical Fluids 75 (2013) 159-171.

(2) H. Grandelli, B. Stickle, A. Whittington, E. Kiran, Inclusion complex formation of β-cyclodextrin and Naproxen: a study on exothermic complex formation by differential scanning calorimetry, Journal of Inclusion Phenomena and Macrocyclic Chemistry (2012) DOI 10.1007/s10847-012-0241-6.

(3) H.E. Grandelli, J.C. Hassler, A. Whittington, E. Kiran, Melting point depression of Piroxicam in carbon dioxide + acetone co-solvent mixtures and inclusion complex formation with β-cyclodextrin, The Journal of Supercritical Fluids 71 (2012) 19-25.

In the following chapters, the state of the art in CD-drug inclusion compound formation and polymer foaming using carbon dioxide are first reviewed (Chapters 2 and 3). The publications resulting from this research are then presented in Chapters 4, 5 and 6. In Chapters 7 and 8, the work done with polymer foaming is presented with resulting drug release studies. Chapter 9 provides conclusions drawn from this research and recommendations for future work.

Chapter II. Literature Review on Cyclodextrins

Cyclodextrins are cyclic oligosaccharides which have a torus or cup-like shape, as was illustrated in Figure 8a in Chapter I. The outside of the molecule is hydrophilic, while the cavity is hydrophobic. This unique structure lends CDs to host hydrophobic guest molecules causing the host-guest complex to become hydrophilic. As a result CDs have been explored as additives in the food, cosmetic and pharmaceutical industries to improve product stability and solubility [54].

2.1 Cyclodextrin Discovery and Synthesis

CDs were first described in a publication by Villiers in 1891 when he isolated a crystalline structure from the bacterial digestion of starch [51]. Villiers recognized the similarity in properties of his substance to those of cellulose, determined the chemical structure to be $(C_6H_{10}O_5)_2 \cdot H_2O$ and called his product "cellulosine" [51]. It was not until 12 years later that Austrian scientist, Franz Schardinger, provided the first detailed description of the CD synthesis and isolated the bacterial microorganism, *Bacillus macerans* [55]. Schardinger was able to isolate two distinct crystalline substances, one of which he determined to be Villiers' "cellulosine" and considered "crystalline dextrin" to be a better name for the compound. In the following years, Schardinger was able to isolate similar crystalline dextrins from other sources of starch using the same bacteria. Based on this experience, the bacteria used in the digest seemed to dictate the product, as opposed to the source of starch. He later changed the name of the dextrin products to α- and β-dextrin. CDs became known as Schardinger dextrins to honor him for his early work and discoveries [54].

Freudenberg and coworkers discovered the larger γ-dextrin in 1935, and in 1938 he determined the cyclic structure of these compounds and named them as CDs [56]. In 1954, Cramer published the chemical structure, cavity size, solubility, reactivity, complex formation abilities, and guest-stabilization of α-, β- , and γ-cyclodextrins, the structures of which are shown in Figure 8b. More recently physical properties which have been reported for the native cyclodextrins are shown in Table 4.

Table 4. Physical properties of native and substituted CDs found in marketed pharmaceutical products [57].

Cyclodextrin	Number of glucose units	Molecular Weight	Water solubility, g/100 ml	Dimensions, Å		
				Top Cavity Diameter	Outer Diameter	Depth
α-	6	972	14.5	4.7 - 5.3	14.2 - 15.0	7.8 - 8.0
β-	7	1135	1.85	6.0 - 6.5	15.0 - 15.8	7.8 - 8.0
γ-	8	1297	23.2	7.5 - 8.3	17.1 - 17.9	7.8 - 8.0

Until the 1970s, CDs could not be produced on an industrial scale due to the highly impure product obtained from the *Bacillus macerans* digestion, which was composed of about 60% α-, 20% β- , 20% γ-CD and a trace amount of larger ring cyclodextrins [46]. Technological advances in the 1970s, including engineering of the new CGTases which provided more specific digestion pathways for a more pure product, allowed for the industrial-scale production of CDs [58]. In 1948, Freudenberg suggested the possibility of larger ring CDs, which was then confirmed by French in 1965. Cyclodextrins with more than 8 glucose units have only been proven since the 1990s, and by 2002 larger CDs with several hundreds of glucose units had been reported [59].

In the 1990s, chemically modified CDs became of interest in the scientific community mainly due to the higher water solubility of the substituted CDs compared to their native analogues [56]. The high binding energy of crystalline α-, β- and γ-cyclodextrins drives the aqueous solubility of the native cyclodextrins down compared to their linear dextrin analogues [46]. In addition, β-CD molecules can also form intramolecular hydrogen bonds, decreasing their ability to hydrogen bond with surrounding water molecules to dissolve. Hydroxyl group substitution disrupts the crystallinity of CDs, which improves solubility. In fact, even substitution of a hydroxyl group with a hydrophobic moiety, such as a methoxy group, has been shown to increase aqueous solubility [60]. Highly water-soluble substituted CDs of commercial value include methylated β-CD, 2-hydroxypropylated β- and γ-CDs, sulfobutylated β-CDs, glucosyl- and maltosyl-β-CDs, acetylated β- and γ-CDs, and sulfated CDs.

An optimal degree of hydroxyl group substitution exists in terms of water solubility of the CD-based product [56] and is different for each CD derivative. Table 5 shows the optimal degree of substitution for some marketed pharmaceutical CDs with the corresponding aqueous solubility, and Figure 10 illustrates the chemical structures of the marketed substituted CDs.

Table 5. Physical properties of substituted CDs found in marketed pharmaceutical products [46].

Cyclodextrin	Molar substitution	Molecular weight, g/mol	Water solubility (25^{o}C), mg/ml
Hydroxypropyl-β-	0.65	1400	>600
Randomly Methylated-β-	1.8	1312	>500
Sulfobutylether-β-	0.9	2163	>500
Hydroxypropyl-γ-	0.6	1576	>500

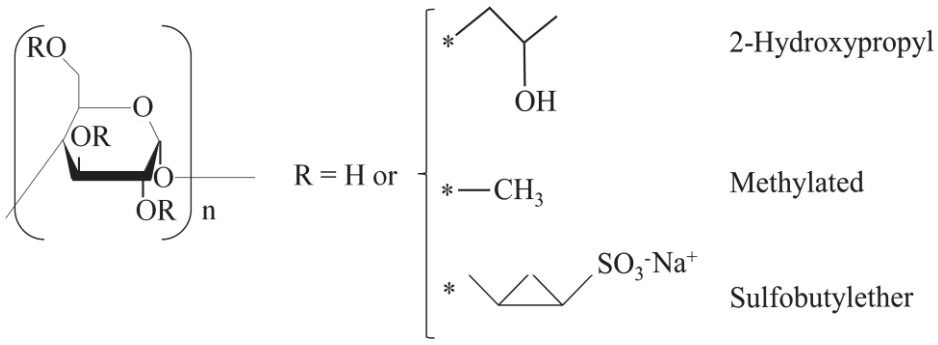

Figure 10. Chemical structures of substituted cyclodextrins; n = 7 for β-CDs and n = 8 for γ-CDs [61, 62].

In 1976 Japan marketed the first cyclodextrin-containing pharmaceutical agent, Prostarmon E™. Then in the 1980s Japan became the largest consumer of cyclodextrins, primarily in the food and cosmetic industries. Italy marketed one of Europe's first pharmaceutical products containing CD, Piroxicam-β-cyclodextrin tablets, in 1988. Since the 1990s, the US based company, Procter and Gamble, has been the world's largest industrial consumer of CDs. To date there are more than 30 pharmaceutical CD complexes available worldwide, which are listed in Table 6 [63].

Table 6. Commercially available CD-drug complexes [63].

Drug	CD	Product Name	Indication	Formulation	Company/Country
Alprostadil	α-CD	Rigidur	Erectile dysfunction	Intravenous	Ferring/Denmark
Aripiprazole	SBE-β-CD	Abilify	Antipsychotic/ antidepressant	Intramuscular	Briston-Myers Squibb/U.S. Otsuka Pharm Co./Japan
Benexate	β-CD	Ulgut, Lonmiel	Antiulcerant	Capsule	Teikoku/Japan Shionogi/Japan
Cefotian-hexetil	α-CD	Pansporin T	Antibiotic	Tablet	Takeda/Japan
Cephalosporin	β-CD	Meiact	Antibiotic	Tablet	Meiji Seika/Japan
Cetirizine	β-CD	Ceterizin	Antiallergic	Chewing tablet	Losan Pharma/ Germany
Chloramphenicol	M-β-CD	Clorocil	Antibiotic	Eye drop	Oftalder/Portugal
Chlordiazepoxide	β-CD	Transillium	Tranquilizer	Tablet	Godor/Argentina
Cisapride	HP-β-CD	Coordinaz, Prepulsid	GI mobility stimulant	Suppository	Janssen/Belgium
Dexamethasone	β-CD	Glymesason	Analgesic/ anti-inflammatory	Ointment	Fujinaga/Japan
Diclofenac Na	HP-γ-CD	Voltaren ophtha	Nonsteroid anti-inflammatory	Eye drop	Novartis/Switzerland
Diphenhydramin HCl, chlortheophyllin	β-CD	Stada-Travel	Travel sickness	Chewing tablet	Stada/Germany
Garlic oil	β-CD	Xind, Tegra, Allidex, Garlessence	Antiartherosclerotic	Dragees	Bipharm, Hermes/ Germany Parmafontana/U.S.
Hydrocortisone	HP-β-CD	Dexocort	Gingivitis	Mouthwash	Actavis/Iceland
Indomethacin	HP-β-CD	Indocid	Nonsteroid anti-inflammatory	Eye drop	Chauvin/France
Iodine	β-CD	Mena-Gargle	Throat disinfectant	Solution	Kyushin/Japan
Itraconazole	HP-β-CD	Sporanox	Esophageal candidiosis	Oral/IV	Janssen/Belgium, U.S.
Meloxicam	β-CD	Mobitil	Nonsteroid anti-inflammatory	Tablet/suppository	Medical Union Pharm/Egypt
Mitomycin	HP-β-CD	MitoExtra/ Mitozytrex	Anticancer	IV	Novartis/Switzerland
Nicotine	β-CD	Nicorette	Smoking cessation	Sublingual tablet	Pharmacia/Sweden
		Nicogum		Chewing gum	Pierre Fabre/France
Nimesulide	β-CD	Nimedex Mesulid Fast	Nonsteroid anti-inflammatory	Tablet Oral sachet	Novartis/Italy
Nitroglycerin	β-CD	Nitropen	Coronary dilator	Sublingual tablet	Nippon Kayaku/ Japan
Omeprazol	β-CD	Omebeta	Proton pump inhibitor	Tablet	Betafarm/Germany
OP-1206	γ-CD	Opalman	Buerger's disease	Tablet	Ono/Japan
PGE_1	α-CD	Prostavasin	Chronic arterial occlusive disease	Intraenterial infusion	Ono/Japan
		Edex		Intracavernous injection	Schwarz/Germany, U.S.
		Prostandin 500	Controlled hypotension for surgery	Infusion	Ono/Japan
PGE_2	β-CD	Prostarmon E	Induce labor	Sublingual tablet	Ono/Japan
Piroxicam	β-CD	Brexin	Nonsteroid anti-inflammatory	Tablet	Chiesi/Italy
		Flogene		Suppository	Ono/Japan
		Cicladol		Liquid	Ache/Brasil, Belgium, Fance, Germany, Netherlands, Scandinavia, Switzerland
Tc-99 Teoboroxime	HP-γ-CD	Cardiotec	Radioactive imaging agent	IV	Bracco/U.S.
Tiaprofenic acid	β-CD	Surgamyl	Analgesic	Tablet	Roussel-Maestrelli/ Italy
Voriconazole	SBE-β-CD	Vfend	Antimycotic	IV	Pfizer/U.S.
Ziprasidone mesylate	SBE-β-CD	Zeldox/Geodon	Antischizophenic	IM	Pfizer/Europe, U.S.

2.2 Cyclodextrin Inclusion Complex Formation

Due to their unique chemical structure, CDs are interesting host molecules for lipophilic guests. In an inclusion compound or complex, a hydrophobic guest molecule can enter the hydrophobic cavity of a CD molecule [48]. The complex takes on a hydrophilic character due to the hydroxyl groups present on the CD exterior. Thus, aqueous solubility and stability of lipophilic and/or labile compounds may be improved by complex formation with CDs. In CD complex formation no covalent bonds are broken or formed; therefore, the guest molecule is not chemically altered by the inclusion.

2.2.1 Conventional Preparation of Cyclodextrin Inclusion Compounds

Conventional methods of preparing CD inclusion compounds typically involve water as a solvent for the CD and an organic solvent for the guest compound. Conventional methods of forming CD inclusion complexes include co-precipitation, slurry, paste and dry mixing. Each of these methods involves the use of water as a processing fluid in varying quantities [64]. More recently, freeze drying and spray drying have become the more common techniques for preparing inclusion complexes [65-71], with spray drying being the most attractive method for industrial scale-up [72]. All of these methods employ some amount of organic solvent to dissolve the guest compound.

The co-precipitation method involves dissolving the host CD and guest compound in a suitable solvent and allowing the inclusion complex to precipitate [64]. This can be done in a few ways. Both the CD and the guest may be dissolved in heated water which is then allowed to cool with stirring. If the guest is not sufficiently soluble in water, an organic solvent is used to dissolve the

guest. The CD solution is mixed with the solution containing the guest compound. In both cases, complex formation results in precipitation of the inclusion complex which can be collected by filtration and washed to remove any uncomplexed drug. Co-precipitation is a suitable method on the laboratory scale. However, due to the large volume of water needed in the process, industrial scale-up is not practical.

In the slurry method, CD is mixed with water well beyond its solubility up to 45 wt% and the guest is added to the slurry [64]. As the inclusion complex is formed and precipitated, the free CD can then be dissolved and made available for complex formation. The cycle continues until the desired degree of complex formation is achieved. The complex is collected by filtration and dried.

In the paste method, only 20 wt% water/solvent solution is used in the guest-CD mixture, creating a high viscosity paste [64]. The complex formation must be carried out in a high shear mixer such as an extruder or kneading machinery. The product can be dried without filtration. The paste method is difficult to employ on the laboratory-scale due to the high shear processing needed. This process may also be unsuitable for labile guest molecules due to high temperatures and shear rates required to promote complex formation.

Dry mixing is also a method of inclusion complex formation [64]. Dry mixing is generally achieved by grinding or milling. Although some guests will complex with CDs within hours, most complex formation processes take days to weeks in the dry mixing process.

Spray drying involves dissolving or suspending the CD in water at a 1:10 mass ratio. The drug is added to the suspension as a solid or dissolved in a solvent. The complex is then isolated by spray drying the water solution [72]. The procedure for freeze drying is similar to spray drying with the exception of isolating the complex by lyophilization [72]. Spray drying [73-77] and freeze drying [78, 79] provide the highest inclusion yields of the conventional complex formation methods.

2.2.2 Cyclodextrin Inclusion Complex Formation in Supercritical CO_2

An alternative approach to conventional methods of preparing CD-drug inclusion complexes is the use of $scCO_2$ as the processing fluid. Benefits of using $scCO_2$ in CD-drug inclusion complexes include decreased use of organic solvents, limited adverse effect on drug stability through processing, and potential for improved inclusion efficiency. Complex formation efficiency is dependent on the conditions during CO_2 processing, including pressure, temperature, exposure time, molar ratio and the addition of ternary agents. The effects of pressure and temperature on the inclusion yield are dependent on the system. Optimum molar ratio, longer exposure times and the addition of appropriate ternary agents generally are found to improve inclusion yield. Typically the three processes illustrated in Figure 11 are employed in supercritical complex formation and can be described as stirred batch [80-83], static batch [84, 85] and continuous flow [62].

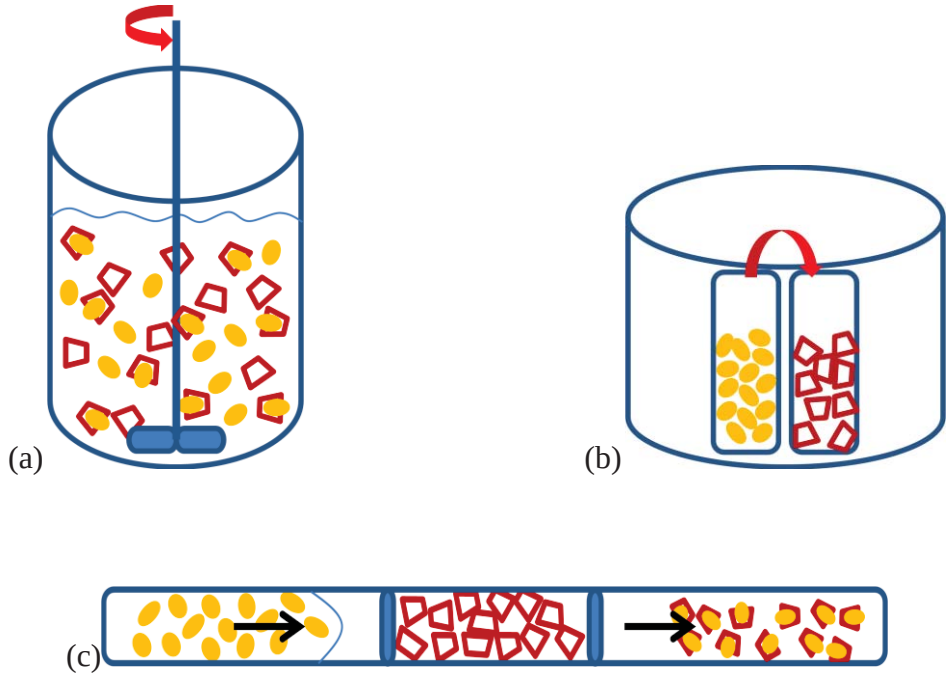

Figure 11. Common methods of generating CD-drug inclusion complexes using $scCO_2$ (a) stirred batch, (b) static batch and (c) continuous packed bed processes.

Each of these processes relies on the solubility of the drug in CO_2 resulting in a major drawback of using CO_2 - promoted complex formation since drug solubility in CO_2 is generally low. The CO_2 solubility of the NSAIDs investigated in this research is shown in Figure 12 at different temperatures as a function of pressure. The solubility of these drugs in CO_2 decreases in going from ibuprofen (IB) to ketoprofen (KP) to naproxen (NA) to piroxicam (PC). With lower solubility of drugs in CO_2, higher temperatures and pressures are shown to be required to achieve any drug dissolution. Thus, the lowest (pressure-temperature) P-T conditions are required to dissolve IB, while the most extreme P-T conditions are required to dissolve PC.

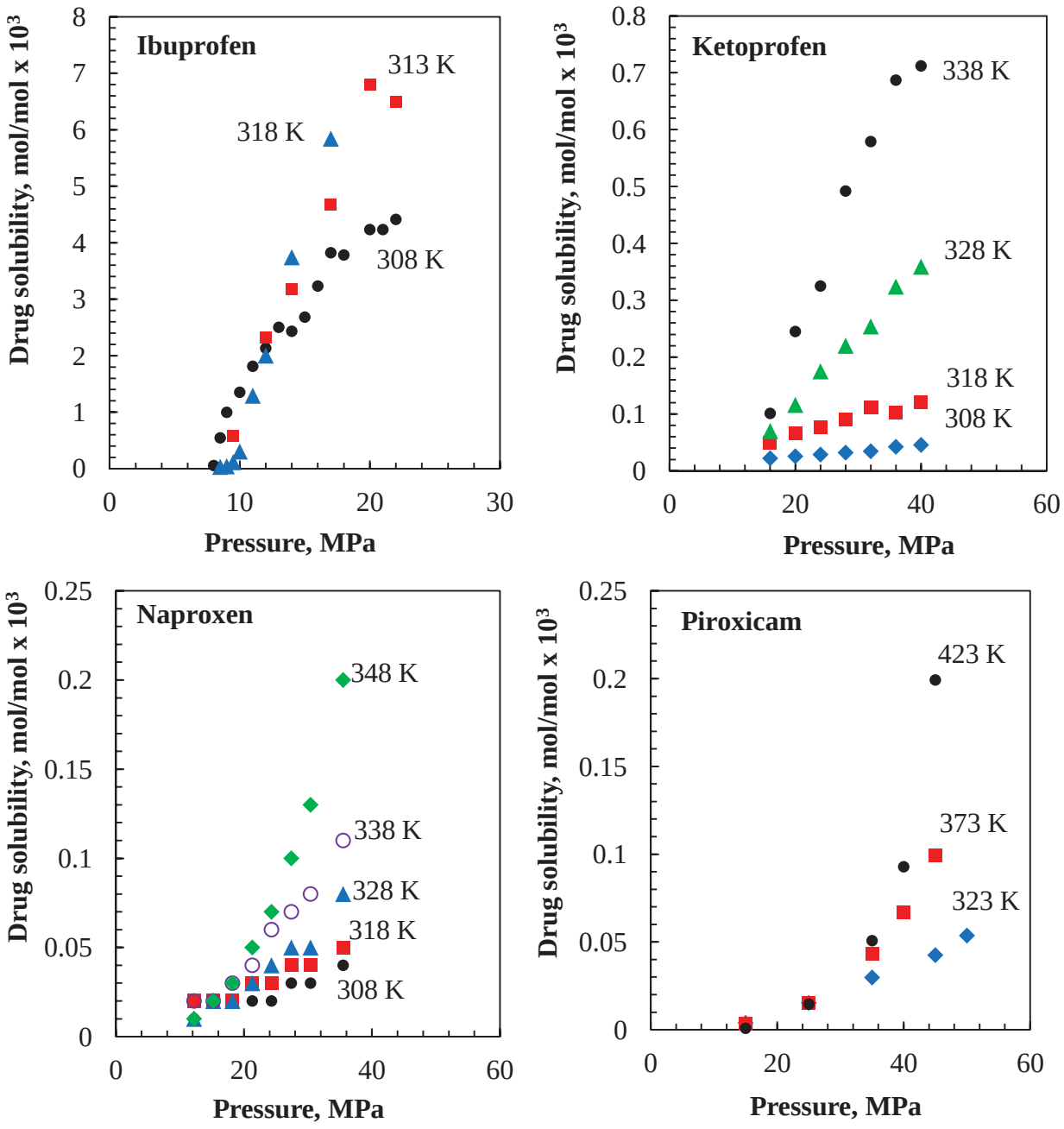

Figure 12. CO_2 solubility of drugs investigated in this research as a function of temperature and pressure. Data are shown for ibuprofen [86], ketoprofen [87], naproxen [88] and piroxicam [82].

The addition of a co-solvent to CO_2 has been shown to result in improved solvent power of the binary fluid mixture and thus, improved drug solubility has been reported in the ternary systems shown in Table 7. For each system, drug solubility was dependent on the co-solvent level, temperature and pressure. Higher co-solvent levels, temperatures and pressures each resulted in improved drug solubility.

Table 7. Literature available for solubility of drugs of interest in this research in CO_2 + co-solvent mixtures.

Solute	Co-solvent	Co-solvent, mass%	Temperature, K	Pressure, MPa	Reference
Naproxen	ethanol	1.75-5.25	323.1-333.1	11-17.9	a
	ethyl acetate	1.75-5.25	333.1	11-17.9	
	acetone	1.75-5.25	313.1-333.1	11-19.3	
	methanol	1.75-5.25	323.1-333.1	11-19.3	
Naproxen	ethanol	10-80	298	10	b
	acetone	15-75	298	10	
Naproxen	acetone	2.3-6.9	318.1-333.1	9.0-19.3	c
	ethyl acetate	3.4-10.2	333.1	11.0-17.9	
	methanol	1.3-3.9	323.1-333.1	11.0-19.3	
	ethanol	1.8-5.4	323.1-333.1	11.0-17.9	
	1-propanol	2.4-7.2	333.1	11.0-17.9	
	2-propanol	2.4-7.2	323.1-333.1	11.0-17.9	
Ibuprofen	ethanol	8-22	298	10	b
	acetone	6-23	298	10	

a [89], b [90], c [91]

Preparation of CD-drug inclusion complexes using $scCO_2$ has been reported, and the literature is summarized in Table 8. β-CD and its derivatives are the most commonly explored CDs in supercritical complex formation with drugs due to their appropriate cavity size for these guest molecules. Several groups have explored ternary agents or co-solvents as aids to improve drug solubility and complex formation efficiency [81, 92-95]. L-lysine, an essential amino acid for

humans, is the most commonly investigated ternary agent in supercritical complex formation due to its ability to interact with both the acidic drug, via electrostatic interactions, and the cyclodextrin, via hydrogen bonding. Van Hees, et al. were able to improve inclusion yield of β-CD:PC mixtures by about 20 % using L-lysine and citric acid addition was shown to improve the complex formation efficiency of micronazole base:HP-γ-CD mixtures by about 50 % [92]. Organic solvents have not been extensively investigated in supercritical complex formation techniques, although one study has been identified for the inclusion of triphenylphosphines into peracetylated-β-CDs using methanol as a co-solvent [96]. The potential use of the organic co-solvents ethanol, acetone and ethyl acetate in CD-drug inclusion complex formation using supercritical CO_2 was explored as a focus of this research.

Table 8. Summary of $scCO_2$ complex formation with successful CD-guest inclusion.

Reference	Guest	CD	Characterization Techniques	Comments
a	Simvastin	HP-β-CD	DSC, FTIR, SEM, XRD	SAS Method
b	NA	β-CD	DSC, FTIR, UV-Vis	
c	IB	TM-β-CD	DSC, FTIR, XRD	
	NA	TM-β-CD	DSC, FTIR, XRD	
	Flurbiprofen	TM-β-CD	DSC, FTIR, XRD	
d	IB	β-CD	DSC, SEM, XRD	CPD method
e	PC	β-CD	DSC, FTIR, UV-Vis	
f	PC	β-CD	DSC, UV-Vis	L-lysine as ternary agent
g	Micronazole	γ-CD	-	Citric acid as ternary agent
	Micronazole	HP-γ-CD	-	
h	Hydroxyflavone	β-CD	DSC, UV-Vis, XRD	
i	IB	TM-β-CD	DSC, FTIR, XRD	
	IB	DM-β-CD	DSC, FTIR, XRD	
j	IB	M-β-CD	DSC, XRD, SEM	Flow method
k	PC	β-CD	DSC, SEM, Solution	L-lysine as ternary agent
l	IB	β-CD	FTIR, XRD, SEM, DSC	Controlled particle deposition method
m	Itraconazole	β-CD	XRD, SEM, DSC	
n	Benzocaine	β-CD	FTIR, XRD	
	Bupivacaine	β-CD	FTIR, XRD	
	Mepivacaine	β-CD	FTIR, XRD	
o	KP	M-β-CD	DSC, XRD, FTIR	
p	PC	HP-β-CD	DSC, FTIR	L-lysine & polyvinyl pyrrolidone as ternary agents
q	KP	β-CD	DSC, FTIR	L-lysine as ternary agent
	KP	HP-β-CD	DSC, FTIR	L-lysine as ternary agent
r	Triphenylphosphine derivatives	Peracetylated-β-CD	UV	Methanol as co-solvent

a [97], b [80], c [98], d [84], e [82], f [92], g [81], h [99], i [83], j [62], k [93], l[85], m [100], n [101], o [102], p [103], q [95], r [96]

2.3 Characterization of Cyclodextrin Inclusion Compounds

CD inclusion compounds have typically been characterized by thermal and spectroscopic techniques. Commonly employed thermal analytical techniques include thermal gravimetric analysis and differential scanning calorimetry. Spectral analyses include Fourier transform infrared, nuclear magnetic resonance and ultraviolet-visible spectroscopy. Other characterization techniques include powder x-ray diffraction and high performance liquid chromatography. Typically a comparison is made between the analysis of the pure drug, the pure CD, the CD-drug physical mixture and the CD-drug inclusion compound. An extensive review of the characterization of CD inclusion complexes has been provided in the literature [104] and only the more common methods will be discussed in detail here. Characterizations carried out in this research are fully detailed in Appendix A. Solid state studies were preferred in this research to characterize CD-drug inclusion compounds to prevent dissociation of the complex in solution.

2.3.1 Thermal Gravimetric Analysis (TGA)

In typical TGA experiments the mass loss of a sample is precisely measured as a function of temperature at controlled temperature increase rates under inert atmosphere. The onset of thermal degradation is then determined as the temperature at which mass loss begins. Inclusion complex formation is known to improve the thermal stability of thermally labile drug molecules. Thus, thermal degradation temperatures of inclusion complexes may be observed at temperatures higher than the thermal degradation temperature of the pure drug [105]. This is illustrated in Figure 13. The drug and the CD each have a unique thermal degradation onset, as identified by the blue arrows in the figure. In the CD-drug physical mixture, two onsets are observed representing the thermal degradation of each component. The relative mass loss in each step of

the thermal degradation should be the same as the CD-drug mass ratio in the physical mixture. In a CD-drug inclusion compound, drug thermal degradation is shifted to a higher temperature, since the drug is protected and stabilized in the CD cavity. In the case of a partial inclusion compound mixture (i.e. physical mixture + inclusion compound), the drug weight loss can be related to the inclusion efficiency (i.e. amount of drug included in the CD cavity).

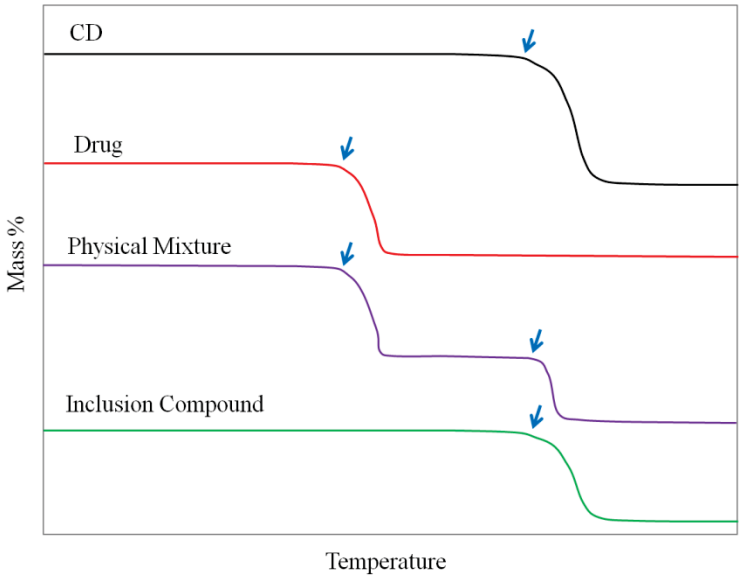

Figure 13. Example of TGA characterization for a drug molecule which forms a complex with CD (blue arrows indicate the onset of thermal degradation for each component).

2.3.2 Differential Scanning Calorimetry (DSC)

DSC thermograms show changes in heat flow through a sample as a function of temperature by comparing the sample to a reference, usually an empty DSC pan. Typically, a temperature increase or decrease scan is carried out at a controlled rate with the sample and reference pans under inert atmosphere. Phase state changes are observed as peaks in the heat flow versus temperature plots, since melting is an endothermic event and crystallization is an exothermic

event. A typical comparison is illustrated in Figure 14. The guest drug molecule, if crystalline, will display an endothermic melting peak on the heat flow curve upon temperature increase scans to temperatures above the melting point. If the drug has been included into the cavity of the CD molecule, peak shifting or broadening may be observed, as well as the appearance of new peaks not seen in the heating scans of the pure drug or pure CD [105]. More commonly, however, disappearance of the drug melting peak is observed if a CD-drug inclusion complex has been formed [104]. This is due to the inability of the guest to crystallize while isolated in the CD cavities. However, the absence of the drug melting peak indicates that the drug has become amorphous and does not indicate definitively that a CD-drug inclusion complex is the reason for drug amorphization. Thus, DSC alone cannot provide definitive proof of complex formation.

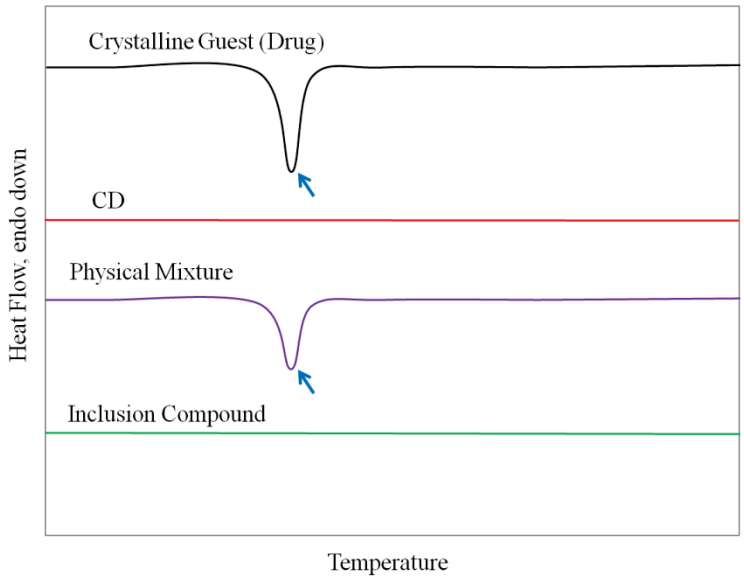

Figure 14. Example of DSC thermograms expected for a crystalline guest molecule which forms a complex with cyclodextrin (arrows indicate drug melting peak).

2.3.3 Fourier Transform Infrared Spectroscopy (FTIR)

FTIR spectra show characteristic wavenumber frequencies in the stretching and bending of the key chemical bonds of a molecule. In the comparison between pure drug, pure CD, CD-drug physical mixture and CD-drug inclusion compound, the spectrum of the physical mixture is an overlay of each pure component spectra. However, in the inclusion compound, peak intensities may change, some peaks may disappear [106] or peaks may shift to different frequencies [105] due to the CD-drug interaction.

2.3.4 Powder X-ray Diffraction (XRD)

XRD is a solid-state characterization technique used to identify phases of a crystalline compound and can provide information on the unit cell dimensions of a crystalline lattice. Changes in the crystallinity will be observed if an inclusion complex is present, although it is important to consider polymorphic transformations which may occur in the drug molecules during the complex formation processing. The diffraction pattern of a physical mixture is typically a sum of each component's pattern [104], while diffractograms of inclusion compounds display a new pattern not seen in the pure components. Often in the diffraction pattern of an inclusion compound a smooth, broad peak is observed which indicates the presence of an amorphous compound devoid of crystallinity. This is generally taken as an indication of a true complex.

2.3.5 Determination of Inclusion Complex Molar Ratio

CD inclusion complex formation in solution is an equilibrium process between complex formation and dissociation, defined by the following mechanism:

$$CD + drug \overset{K}{\leftrightarrow} CD \cdot drug$$

where *K* is the equilibrium constant, *CD* is free cyclodextrin, *drug* is free drug and *CD · drug* is the complex. *K* reflects the stability of the complex and is defined for 1:1 molar ratio complexes by the following equation:

$$K_{1:1} = \frac{[CD \cdot drug]}{[CD][drug]}$$

The stoichiometry of the complex varies depending on the CD-drug combination, which is illustrated in Figure 15.

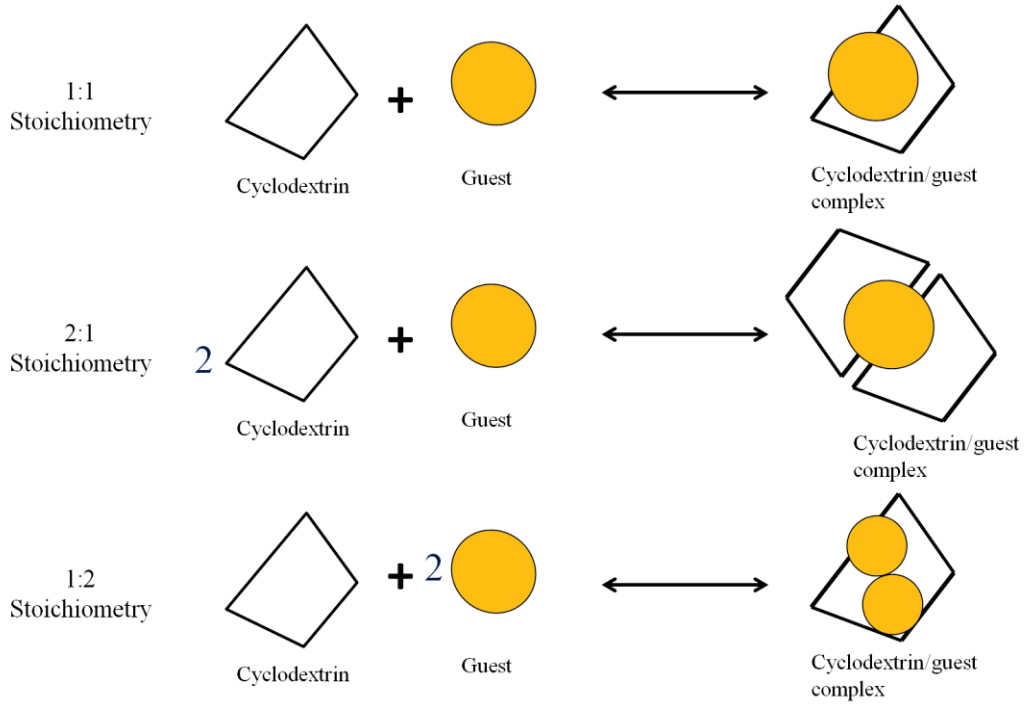

Figure 15. CD inclusion compounds and stoichiometry [50]

The ability of a guest compound to form an inclusion complex with a CD is limited by the size of the guest relative to the size of the CD cavity, as well as the thermodynamics of the system [47]. Each native CD is able to host different types of molecules based on the cavity diameter [50]. α-CD generally forms complexes with aliphatic molecules of low molecular weight, β-CD can form complexes with aromatics, and γ-CD can host macrocycles and other larger molecules [55]. Inclusion complexes most frequently form in a 1:1 molar ratio, although, guest-host molar ratios of 1:2, 2:1 1:3 3:1 and 2:3 have also been observed [50].

Solution based studies have been developed to elucidate the stoichiometry of specific CD-drug pairs, including Job's plots and Higuchi and Connors' phase solubility method. Less common methods include the Benesi-Hildebrand method [107] and thermal characterizations [108]. In each of these solution-based methods the drug solubility is monitored as a function of the CD content in the solution. Using Job's method, a plot is generated with drug solubility as a function of drug molar ratio. These are commonly prepared based on data acquired from NMR analyses [109]. A typical plot generated for a 1:1 complex using Job's method is illustrated in Figure 16. In a 1:1 complex the maximum of the parabolic curve occurs at a value of 0.5.

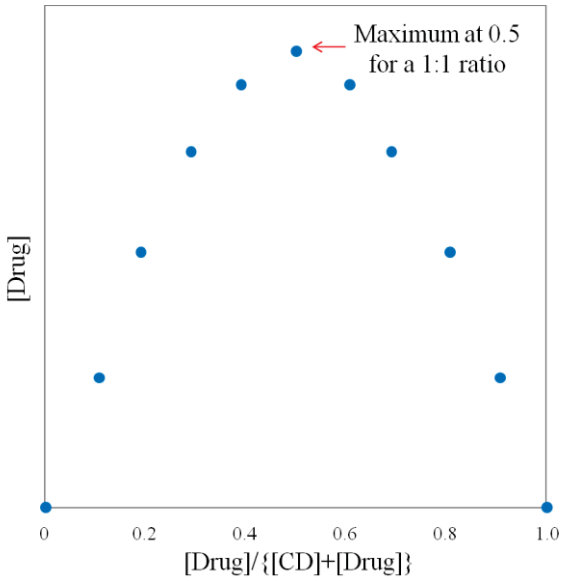

Figure 16. Typical Job's plot for a CD-drug mixture with a 1:1 molar ratio inclusion [109]

Higuchi and Connors have described a method used by many in the determination of thermodynamic properties and molar ratios for CD complex formation by studying the phase-solubility curves [110, 111]. In the phase-solubility approach, aqueous solutions are prepared with a range of CD concentrations. At a set temperature the drug is added in excess. After mixing, the solution is centrifuged and analyzed for drug concentration, usually by HPLC or UV-visible spectroscopy. A plot of drug solubility as a function of CD concentration is then generated, as shown in Figure 17. Depending on the stoichiometry of the complex, the phase-solubility curve can be quite different as shown in the figure.

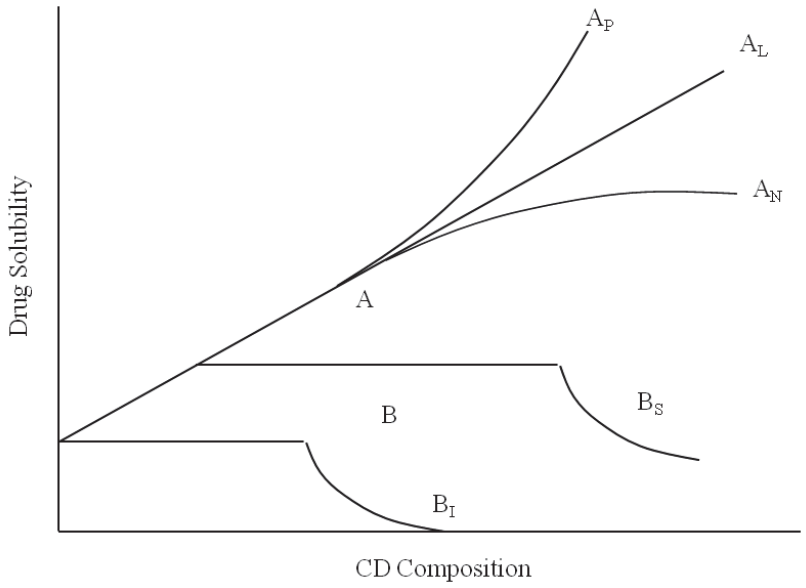

Figure 17. Phase-solubility technique [110]

The type of phase solubility behavior associated with each curve is indicated next to the curve in Figure 17. Type A behavior is characterized by improved drug solubility with increasing CD concentration due to complex formation of soluble compounds [111]. Three different behaviors are characterized as type A behavior. A linear increase in drug solubility with increasing CD concentration is classified as type A_L behavior, which indicates the formation of 1:1 molar ratio complex formation. Positive deviation from the A_L curve is classified as type A_P behavior and is characteristic of complex formation ratios high than 1:1 (i.e. more than one CD molecule complexes with one drug molecule). Negative deviation from the A_L curve is classified as A_N behavior and is rarely observed. A_N behavior indicates self-association of the drug or a change in the equilibrium constant.

Type B behavior is characterized by limited solubility of the CD-drug complex [111]. Two different behaviors are typically observed in B type phase solubility diagrams. B_S phase solubility behavior indicates that the complex has some solubility. Once the solubility of the complex is reached, the solubility stabilizes until higher CD concentrations complex and precipitate the drug. Type B_I behavior is described in the same way as type B_S behavior, except that the highly insoluble complex eliminates any measureable increase in drug solubility.

Based on the phase-solubility behavior, equilibrium constants can be calculated according to reported procedures [112-114]. The enthalpy and entropy changes can then be calculated from van't Hoff plots using the following equation:

$$\ln k = \frac{\Delta H^0}{RT} - \frac{\Delta S^0}{R}$$

This method has been employed to obtain thermodynamic parameters for many CD-guest systems which are reported in the literature [115-120]. Thermodynamics of complex formation are focused on the removal of bound water from the CD cavity and the penetration of the guest molecule into the CD cavity, similar to a hydrophobic interaction process. Generally the hydrophobic moiety of the guest compound is included in the CD cavity, while the polar or charged moiety of the guest is exposed to the bulk. An exception to this rule is the penetration of an aromatic hydroxyl, which will penetrate the CD cavity fully and hydrogen bond with a CD hydroxyl group. Thus, hydrogen bonding can also affect complex formation thermodynamics. Other thermodynamic considerations for complex formation include conformational changes that occur in the CD molecule upon complex formation. Complex formation is generally associated

with a large negative standard enthalpy change (ΔH^o) and either a positive or negative standard entropy change (ΔS^o), making complex formation largely an enthalpy-driven process. While the thermodynamic driving forces in complex formation are difficult to identify, they include van der Waals forces, hydrogen bonding, and hydrophobic interactions. [48]. Tables of experimentally determined thermodynamic data for various host-guest complexes have been provided in the literature [121].

Although widely used in the literature on CD inclusion compound formation, there is controversy on the validity of these simple solubility studies. For example, Loftsson, et al. reported that CD-drug inclusion complexes may self associate and create an environment suitable for further drug dissolution through a non-inclusion interaction [122]. Other methods for determination of thermodynamic properties of inclusion complex formation include conductometric methods [123], calorimetric methods [124], polarimetry [125], and nuclear magnetic resonance (NMR) [126].

2.4 Cyclodextrins and Polymers

In drug delivery applications, implantable biodegradable polymeric matrices can be used as sophisticated local drug delivery systems. Incorporation of CD:drug inclusion complexes into these systems is an approach to enhance local drug delivery from polymeric scaffolds by improving aqueous solubility of the drug.

2.4.1 Cyclodextrin – Incorporated Polymers

CD-incorporated polymeric systems can be obtained by simple physical mixing of the CD or inclusion complex with the polymer prior to or during processing. Sustained drug release profiles have been reported for systems which incorporate β-CD-drug complexes by physical mixing into polymer films for drug delivery applications [127, 128]. In a different approach $scCO_2$ was employed in the physical mixing of CDs into a polymer, followed by drug inclusion complex formation with CD in the film [129].

2.4.2 Cyclodextrin Inclusion with Polymers

CDs can form inclusion complexes with lipophilic, amphiphilic or bola-amphiphilic polymers by threading onto the polymer backbone [130]. CD-threaded polymers can be considered either polyrotaxanes or pseudo polyrotaxanes as illustrated in Figure 18. CDs forming inclusion complexes with the backbone of a polymer may be considered pseudo polyrotaxanes if bulky end groups are not present to lock in the threaded CDs, allowing dissociation at elevated temperatures or upon dissolution [131]. Polyrotaxanes are stable structures with bulky end groups to prevent dissociation [130, 132, 133].

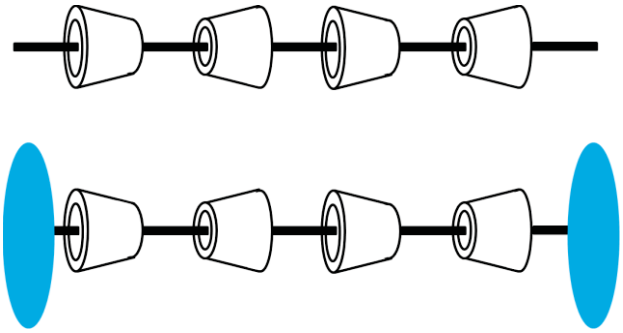

Figure 18. CD-threaded polymer chains forming pseudo polyrotaxanes (top) and polyrotaxanes with shaded stoppers (bottom) [130, 132]

2.4.3 Cyclodextrin – Based Polymers

CD-based polymers are generally prepared as one of the four general structures illustrated in Figure 19: CDs as pendant side groups on linear polymers, CD at the core of a star polymer, CDs as caps on the ends of polymer chains, and CDs as caps on the end of each branch of a star polymer [134].

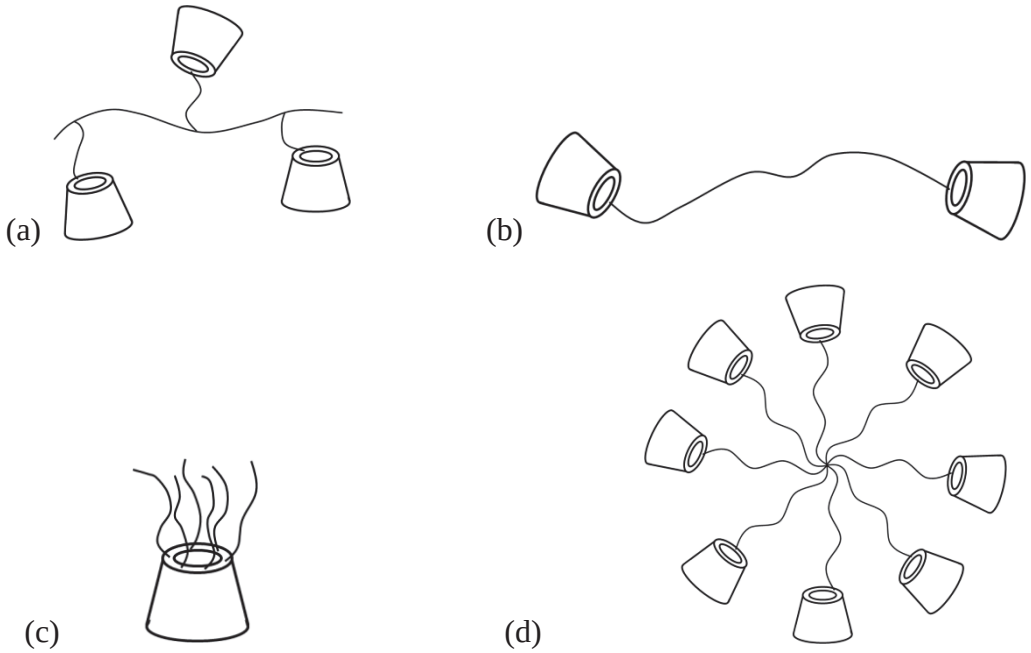

Figure 19. Common CD-based polymer structures (a) CD pendant groups, (b) CD caps on linear polymers, (c) CD core in star polymers, (d) CD-capped branches in star polymers [134]

CD-based polymers are generally synthesized either through polymerization of CD-based monomers or by modification of reactive polymers [134]. Copolymerization of CD-based vinyl or acryloyl monomers with other vinyl monomers is the most common approach to synthesizing CD-based polymers for TE and drug delivery applications [132]. Liu, et al. [135] reported a three step synthesis for obtaining mono-vinyl substituted β-CD, which was copolymerized with N-isopropylacrylamide to create linear CD-based copolymers.

Polymeric networks can be formed by chemical cross-linking of CDs using a cross-linking agent such as epichlorohydrin, diisocyanates, anhydrides and diepoxides, which are shown in Figure 20 [136, 137]. CDs themselves have also been reported as cross-linking agents for polymers [132, 138].

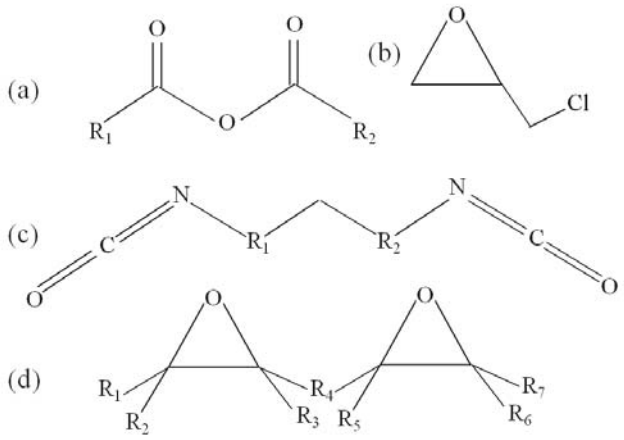

Figure 20. Typical cross-linking agents; (a) anhydrides, (b) epichlorohydrin, (c) diisocyantes, (d) diepoxides

Due to the harsh reaction conditions required in the chemical cross-linking of CDs, bioactive compounds usually cannot be incorporated until after network formation, which can result in low loading efficiency. An alternative to chemically cross-linked network formation is the reversible, physical cross-linking provided by CD inclusion complex formation [132, 139]. Figure 21 illustrates CD-based polymers of various architectures which can be used in the creation of self-assembling networks through complex formation with lipophilic polymer side chains.

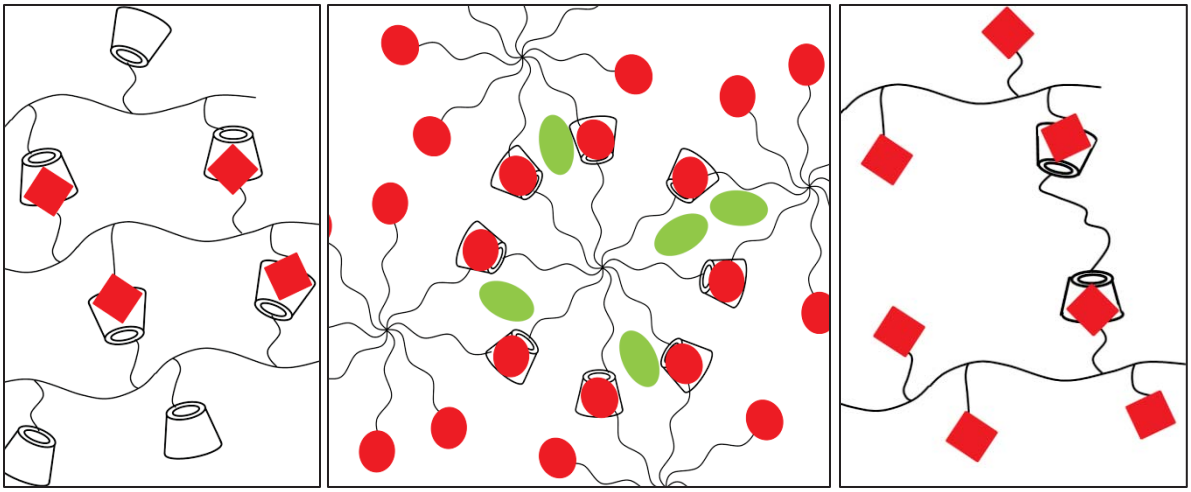

Figure 21.CD-polymer physical cross-links employing CD pendant groups (left), CD-capped star polymers with a bioactive compound (green ovals) incorporated into the network (center) and CD-capped linear polymers (right) [132].

Chapter III. Literature Review on Polymers in Tissue Engineering and Drug Delivery

Polymers used as TE scaffolds act as structures which mimic the extracellular matrix to support and guide new cell growth. TE scaffolds can also act as drug delivery devices by incorporating a drug delivery component. This chapter addresses TE scaffold properties, types of polymers used and processing methods described in the literature for generating TE scaffolds and drug delivery devices.

3.1 Scaffold Properties

The considerations for creating a biomedical scaffold for TE and drug delivery include biocompatibility, mechanical properties, structure, biodegradability, and interfacial adherence [140, 141]. Polymers which are used in TE applications can be either naturally or synthetically derived.

Biocompatibility is defined in TE as the ability of a material or device to be present in the body without causing damage to the host [142]. The variables related to the response of a tissue to an implant, include the interfacing cell type, the shape and size of the implant and the chemical and physical properties of the implant [18]. Biocompatibility is a material property which cannot be changed via processing. Naturally derived polymers typically pose the advantage in biocompatibility over synthetic polymers [140].

Ideally, a biomedical scaffold degrades safely as the new tissue regenerates. Biodegradation involves cleavage of bonds along the polymer backbone resulting in bulk polymer erosion. Biodegradable polymers should have the following characteristics in TE applications: (1) the body's inflammatory response should not be sustained after device implantation, (2) the shelf life of the material should be acceptable, (3) the degradation rate should be sufficiently matched to the tissue regeneration rate, (4) the mechanical properties should be acceptable as the material degrades, and (5) degradation products must also be biocompatible [18]. Synthetic control over degradation rates is provided by altering the monomer composition in biodegradable copolymers [140]. Generally natural polymers undergo enzymatic degradation, while synthetic polymers undergo hydrolytic degradation. A drawback of natural polymers undergoing enzymatic degradation is that the rate of degradation is dependent on the site of implantation, as enzyme concentrations may vary based on the biological site. The degradation of synthetic biodegradable polymers whose structure can be controlled via synthetic functionalization is more predictable, which is one reason synthetic polymers are of growing interest in biomedical applications. Functional groups susceptible to hydrolytic degradation are illustrated in Figure 22 and include esters, orthoesters, anhydrides, carbonates, amides, urethanes, and ureas [18].

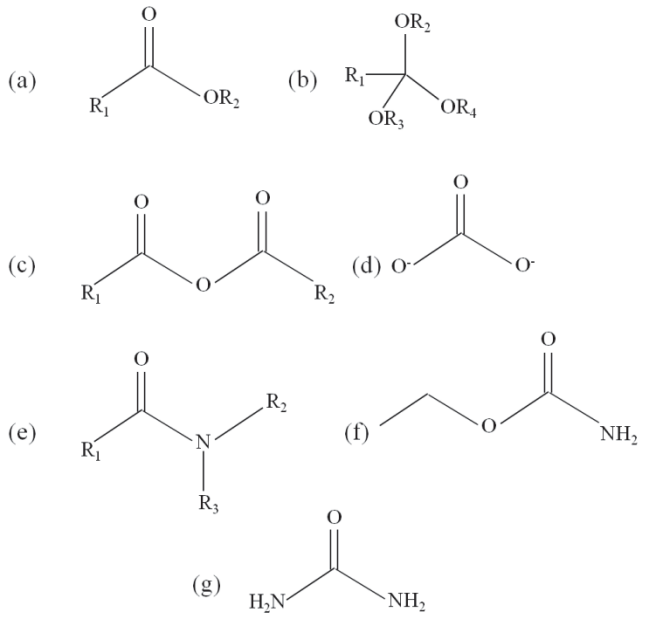

Figure 22. Chemical structure of hydrolytic functional groups; (a) esters, (b) orthoesters, (c) anhydrides, (d) carbonates, (e) amides, (f) urethanes, (g) ureas

The mechanical properties of a biomedical device should match closely with those of the mimicked material. Mechanical properties should also remain appropriate as the material degrades and as the damaged tissue regenerates. Properties of interest include adhesion, stiffness, toughness, swelling, and strength. Adverse effects of poorly correlated material properties could include implant brittleness, an induced inflammatory response, reduced cell adhesion, reduced gene expression, etc. [140]. Mechanical properties are dependent on the type of material used, as well as the processing of the material.

Scaffold structure is one of the most important attributes of TE and drug delivery devices and is controlled via processing of the polymer. Highly interconnected porous structures are desired in these applications such that the scaffold permits cell in-growth, allows transport of nutrients and waste in and out of the matrix and provides a structure for cell organization and growth [143].

3.2 Types of Polymers Used in Biomedical Applications

Typical polymers used in TE and drug delivery include both naturally derived and synthetic polymers. Proteins compose one branch of natural polymers used in TE and include collagen, elastin, albumin, gelatin, and fibrin. Polysaccharides make up another branch of natural polymers including alginate, chitosan and hyaluronic acid. Although applications exist for these materials in TE and drug delivery, the demand for synthetic polymers arises from the limitations in the mechanical properties of natural polymers. The types of synthetic polymers typically used in biomedical applications are aliphatic polyesters, polyurethanes, poly(ortho esters), polyanhydrides, poly(anhydride-*co*-imides), pseudo poly(amino acids), poly(alkyl cyanoacrylates), polyphosphazenes, and polyphosphoesters [18, 140]. Synthetic polymers are summarized with a specific focus on polyesters of interest in this research, poly(lactide-*co*-glycolide) (PLGA) and poly(ε-caprolactone) (PCL).

Polyurethanes are one of the most popular polymers used in the TE field and can be synthesized to be either biodegradable or non-biodegradable [144]. Non-biodegradable polyurethanes are excellent permanent implantable materials due to their good biocompatibility and mechanical properties. For the biomedical applications which do not require a permanent implant, biodegradable polyurethanes can be synthesized through a condensation polymerization of diisocyanates with alcohols and amines. In addition, biodegradable copolymers with soft segments can be obtained by polymerizing lysine diisocyanate with an aliphatic polyester [18, 144].

Poly(ester amides) have good mechanical and thermal properties [18]. The amide functionality allows poly(ester amides) to hydrogen bond. Degradation occurs via hydrolytic cleavage of the ester, while leaving the amide linkages intact and results in less acidic degradation products than other synthetic polyester-based materials [145]. Poly(ester amides) have been investigated as biodegradable sutures and water soluble materials for drug delivery.

Poly(ortho esters) have been developed as hydrophobic polymers which undergo surface erosion, as opposed to bulk erosion [18, 20]. Surface erosion is beneficial in controlled drug delivery. Four classes of poly(ortho esters) have been established, varying in synthesis and properties. Poly(ortho esters) find applications as biomaterials mainly in controlled drug delivery systems [146].

Polyanhydrides are the most studied polymers for drug delivery due to the hydrolytically labile anhydride backbone bonds and the hydrophobic nature of the materials [18, 20]. Degradation occurs mostly by surface erosion; however, evidence of bulk degradation exists as well. The most commonly used and FDA approved polyanhydride is a copolymer, poly[(carboxy phenoxy propane) – sebacic acid], which is used to deliver chemotherapeutic agents in the treatment of brain cancer. Polyanhydrides possess poor mechanical properties, which led to the copolymerization of anhydrides with imides producing poly(anhydrides-*co*-imides). The copolymers have been shown to maintain better mechanical properties throughout degradation and have been developed for injectable applications.

Naturally occurring poly(amino acids) are limited by poor mechanical properties and unwanted immunogenicity, providing an interest in synthetic poly(amino acids), or pseudo poly(amino acids) [18, 20]. Amino acid – based polymers linked by non-amide bonds have been synthesized and exhibit improved mechanical properties, stability and processing.

Poly(alkyl cyanoacrylates) are among the fastest biodegrading polymers with degradation times ranging from hours to days [18]. The degradation rate can be tailored to the application, since degradation is dependent on the length of the alkyl side chains. Poly(alkyl cyanoacrylates) have applications in biomedical adhesives and drug delivery systems.

Inorganic-organic polymers including phosphazenes, have been investigated as biodegradable biomaterials [18]. The backbone is made up of phosphorous and nitrogen in contrast to the carbon backbone in organic biomaterials and is not hydrolytically labile. However, biodegradable phophazenes can be synthesized via incorporation of organic ester segments into the backbone. The degradation rate of biodegradable phosphazenes is synthetically controlled by the side groups. Phosphazenes and their copolymers have applications in drug delivery and TE depending on the synthesis.

Phosphoesters constitute another interesting class of biomaterials with tunable properties through synthetic variation of the side chains [18]. The phosphate backbone bonds are subject to hydrolytic and enzymatic cleavage, producing phosphate, alcohols and diols as degradation products. Phosphoesters can be synthesized with a polymer to obtain various mechanical properties and have applications in drug delivery and TE.

Polyesters are widely used in biomedicine due to the many synthesis routes and the versatility in application [18]. Ester polymerization can occur via ring opening or condensation reactions, based on the monomer used. Ring opening polymerization is the more viable industrial method for producing higher molecular weight polymers using milder reaction conditions [20]. Aliphatic polyesters commonly used in the preparation of biomedical scaffolds are poly(lactic acid) (PLA), poly(glycolic acid) (PGA), their copolymers, poly(lactide-co-glycolide) (PLGA), and poly(ε-caprolactone) (PCL). PLA and PGA are also known as poly(lactide) and poly(glycolide), respectively, and the nomenclature is related to the synthesis of the polymer. Lactic acid is a chiral molecule with L and D forms. Therefore, PLA can be composed of purely the L-isomer, PLLA, purely the D-isomer, PDLA, or both isomers, PDLLA. PDLLA is amorphous, while PDLA and PLLA are semi-crystalline [147]. PLA, PGA, PLGA and PCL are water insoluble. The degradation pathway is via the hydrolytic cleavage of the ester, resulting in bulk degradation with non-linear erosion kinetics. The degradation rate of PLGA can be altered by changing the copolymer composition. Commonly used PLGA copolymer compositions are lactide:glycolide ratios of 50:50, 75:25 and 85:15. 50:50 PLGA degrades the fastest at about 1-2 months, 75:25 PLGA degrades in about 4-5 months, and 85:15 PLGA degrades in about 5-6 months [147]. Acidic degradation products of PLGA and PCL are known to cause an inflammatory response localized to the site of implantation, and the degradation rate of the polymer is accelerated in the acidic environment [148]. Mechanical and degradation properties are affected by the molecular weight, crystallinity, glass transition temperature (T_g) and hydrophobicity [20]. PLGA and PCL are the focus of this study, and properties of the homopolymers are provided in Table 9.

Table 9. Properties of polyesters investigated in this research.

Monomer	Polymer repeat unit	Abbreviation	T_g, °C	T_m, °C	% Crystallinity
Lactide	Poly(lactide)				
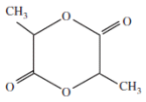	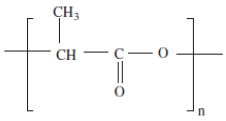	PLLA	50 - 80[a]	173-178[a,b,c,d]	37[a]
		PDLLA	55 - 60[b,c]	Amorphous	Amorphous
Glycolide	Poly(glycolide)				
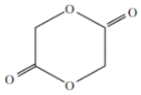	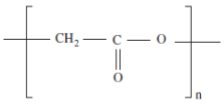	PGA	35 - 40[b]	225 - 230[b,d]	45-55[d,e]
Caprolactone	Poly(caprolactone)				
	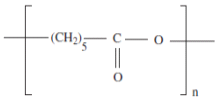	PCL	-60[b]	55 - 60[b]	50-71[e,f]

(a) [149], (b) [20], (c) [18], (d) [147], (e) [150], (f) [151]

3.3 Conventional Scaffold Preparation

Common methods of TE scaffold preparation include solvent casting/porogen leaching, thermally induced phase separation, electrospinning, lyophilization, templating and foaming [141, 143].

Solvent casting/porogen leaching involves pouring a polymer solution over a bed of porogens of uniform size, which can consist of salt, microspheres or particles. The solvent is evaporated under vacuum, followed by washing to leach out the porogens with an appropriate solvent. The advantage of porogen leaching is the resulting porous polymer structure with controlled and uniform pore size. However, the lengthy washing step can be destructive to the polymer structure or result in significant loss of an incorporated compound, such as a drug [141]. In

addition, organic solvents are commonly used to dissolve the polymer and may be used in the leaching step. A slightly modified method is melt porogen leaching, in which the polymer is melted instead of dissolved in organic solvent. This poses the advantage of limiting organic solvent use; however high temperatures are required which could damage thermally sensitive incorporated compounds [152] (e.g. proteins, thermally labile drugs).

Thermally induced phase separation (TIPS) is one of the most common methods for generating porous scaffolds and involves precipitation of the polymer from a liquid-liquid system [141]. TIPS techniques have been shown to result in highly porous interconnected scaffolds. However, processing is sensitive and highly variable, and organic solvents are used to dissolve the polymer [152]. In utilization of the TIPS technique for the generation of drug delivery systems, the affinity of the incorporated drug for the polymer must be higher than the drug's affinity for the solvent to ensure sufficient loading. An example of successful employment of the TIPS method was reported by Nam and Park [153] who produced porous scaffolds from PLA and PLGA. Dioxane was used as the polymer solvent and water was used as the antisolvent. Porous scaffolds were achieved with pore size and interconnectivity dependent on the polymer used and the temperature quench rate.

Electrospinning is a technique used in scaffold preparation which takes advantage of polymer jet formation from a charged nozzle to a grounded mandrel [141]. When the electric field induced at the nozzle exceeds the surface tension of the polymer, a string of polymer is ejected and deposited onto the grounded rotating mandrel. Electrospinning can yield nanoscale polymer fibers formed into a fibrous porous mesh. However, harsh organic solvents and high

temperatures are typically used in electrospinning making this process unsuitable for the incorporation of labile drugs.

Templating followed by particle leaching is a complex technique which involves repeated layering of micromachined salt particle polymer composite sheets, followed by leaching [141]. Highly controlled microporous structures can be obtained with complex morphologies using this method. Similar to solvent casting/porogen leaching, this templating process can result in insufficient drug loading due to the lengthy washing step [152].

Polymer foaming is a process which causes bubbles to form in a solidifying polymer. Conventional foaming techniques involve foaming during polymerization, or the use of a low boiling temperature organic solvent to foam the polymer [141].

Solvent casting/porogen leaching, TIPS, electrospinning, templating and conventional polymer foaming all employ organic solvents to initially dissolve the polymer. Although each process has its advantages, the use of harsh solvents is non-ideal in TE and drug delivery applications. Polymer foaming with carbon dioxide may offer an alternative pathway for successful generation of TE scaffolds and incorporation of drug delivery components which does not employ toxic solvents or require very high temperatures.

3.4 Supercritical CO_2 Scaffold Preparation

In TE and drug delivery applications, $scCO_2$ is an attractive alternative to conventional methods which employ organic solvents or may be energy intensive [29]. Most polymers are not highly

soluble in $scCO_2$; however $scCO_2$ can dissolve in many polymers. In these types of systems, a CO_2 swollen polymer exists in equilibrium with essentially pure CO_2 [154]. As a consequence of polymer impregnation with CO_2, the viscosity of the polymer is reduced, the glass transition temperature (T_g) and/or melting temperature (T_m) for semi-crystalline polymers, are reduced as a function of pressure, and the fluid diffusivity in the polymer is improved [155]. Although $scCO_2$ is the focus in this project, the techniques discussed have also been applied with other SCFs.

$scCO_2$ has been employed to produce TE and drug delivery scaffolds using techniques including rapid expansion of supercritical solutions (RESS), particles from gas saturated solutions (PGSS), gas antisolvent process (GAS), and supercritical antisolvent process (SAS) techniques [5, 152]. Foaming by expansion from $scCO_2$ is an approach to generate porous scaffolds [155], which may be incorporated into another supercritical processing technique, or can be a stand-alone process. In addition, $scCO_2$ can be used to extract residual solvent from TE devices processed with organic solvents [156].

RESS requires some degree of polymer solubility in $scCO_2$ at high pressures [5]. The polymer is dissolved in CO_2 at high pressure, and upon rapid depressurization, the polymer solubility in the CO_2 decreases appreciably and the polymer is precipitated in particle form. A temperature reduction is always observed upon rapid depressurization, resulting in a non-isothermal pressure quench. Precipitation of the polymer can occur by two mechanisms. A solid-liquid phase separation could occur directly upon depressurization, or a liquid-liquid phase separation could occur upon depressurization, followed by solidification. Incorporation of a soluble drug into the solution results in particle formation of a polymer/drug matrix. Narrow particle size distributions

are obtained from this nucleation and growth process. However, since most polymers and drugs have poor CO_2 solubility, the RESS process is limited in application [152].

PGSS takes advantage of the plasticizing effect $scCO_2$ has on polymers. Polymers in the presence of $scCO_2$ exhibit lowered T_g values, allowing CO_2 to dissolve into the amorphous polymer to obtain a saturated solution [152]. Upon depressurization of the solution through a nozzle, the liquid polymer is released and either foams or forms into particles by precipitation [5].

The GAS technique uses $scCO_2$ as an antisolvent in a ternary polymer/solvent/antisolvent system [5]. A polymer is dissolved in an organic solvent, and $scCO_2$ is added to the liquid solution causing the solution to expand. As the solvent power decreases with the addition of the $scCO_2$, polymer precipitation occurs in the form of microparticles. Particle size can be altered by adjusting the processing parameters [152].

The SAS technique also employs $scCO_2$ as an antisolvent, similar to the GAS process. However, the SAS method differs from the GAS process in the precipitation technique. Instead of adding the antisolvent to the polymer solution as in the GAS method, the polymer solution is sprayed into a chamber containing $scCO_2$. Smaller particles can be obtained with the SAS method compared to the GAS method [5].

The supercritical foaming process consists of two steps, illustrated in Figure 23. First, the polymer is contacted with $scCO_2$ at conditions needed to achieve saturation of the polymer.

After becoming saturated, the system is depressurized in the second step resulting in pore formation.

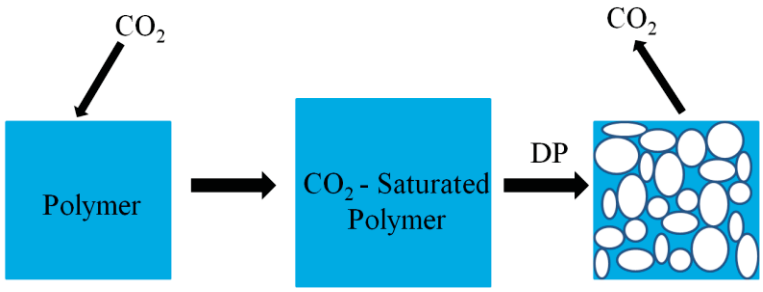

Figure 23. Illustration of polymer foaming using CO_2

Polymer exposure to $scCO_2$ is known to lower the T_g and T_m of the polymer in a pressure dependent manner as illustrated in Figure 24 [5]. This has been reported already for PCL [157]. For foaming to occur, the operating temperature must exceed the pressure dependent T_g of the polymer, allowing the $scCO_2$ to dissolve into the liquefied polymer. Upon depressurization of the polymer/$scCO_2$ system, thermodynamic instability causes nucleation of gas pockets which minimizes the free energy of the gas. Although phase separation can occur by both nucleation and growth and spinodal decomposition, nucleation and growth is widely accepted as the dominant phase separation mechanism in most supercritical foaming processes [155]. In addition, as the concentration of the $scCO_2$ decreases in the polymer, the polymer T_g increases, as shown in Figure 24. Pores are left in the place of the gas pockets as the polymer undergoes vitrification or crystallization. Many studies have been reported using $scCO_2$ as a polymer foaming agent for both TE applications and other industrial applications. Other industrial applications include mainly the production of insulation materials [158, 159] or membranes [160] and will not be the focus of this discussion.

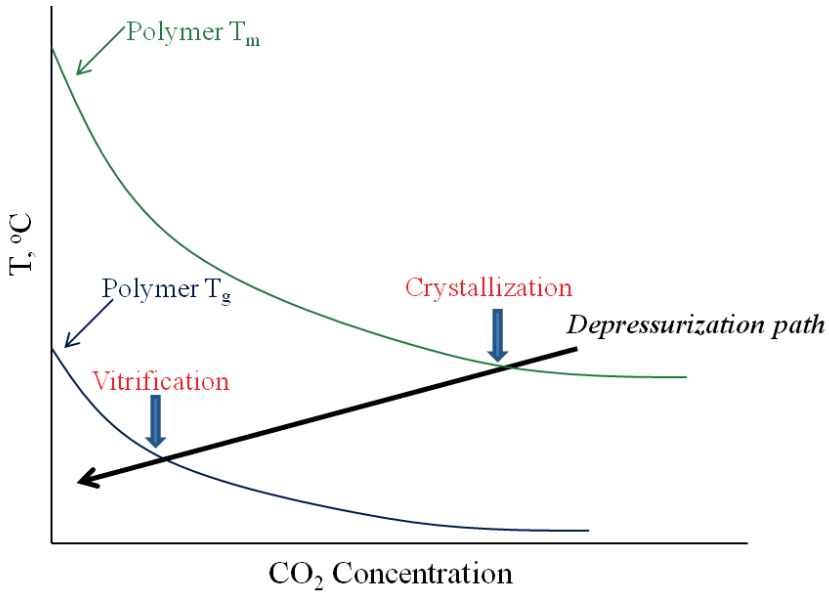

Figure 24. Phase diagram illustrating depressurization of polymer/CO_2 systems.

Foaming behavior of the semi-crystalline polymer, PCL, in scCO_2 was investigated by Kiran, et al. [161], in which morphological changes induced by CO_2 exposure were characterized by SEM and DSC. SEM images indicated that unprocessed PCL had a non-porous structure containing spherulitic crystalline domains. Temperatures up to 308 K and pressures up to 45 MPa were explored in the recrystallization and foaming of PCL. Increasing temperature or pressure promoted recrystallization of the polymer but did not result in pore formation, as the melt transition was not achievable at the conditions provided. However, at 308 K / 34 MPa PCL was melted in CO_2 and foamed upon expansion. Conditions of 308 K / 34 MPa resulted in pore diameters of about 1 μm. A further increase of temperature to 323 K / 34 MPa led to a heterogeneous morphology, common in semicrystalline polymers, containing spherulitic and porous domains. In the DSC heating scan of the CO_2 – exposed products, splitting of the PCL melting peak into two was observed, indicating the presence of two crystalline forms.

Differences in the crystalline forms are due to lamellar thickening or crystallization of formerly non-crystalline domains.

Siripurapu, et al. [162] attempted to created nanoporous foams by expansion from CO_2 with PMMA films. A constrained mold was used to limit CO_2 diffusion to the edges of the film. PMMA films were placed between two impenetrable plates and exposed to CO_2 at high saturation pressures (up to 34.5 MPa). Nanoporous structures were obtained at temperatures only slightly above the pressure dependent T_g.

Factors influencing the porosity and pore structure of the foamed polymer include the crystallinity of the polymer, the processing parameters, including exposure duration, temperature, and pressure, and the depressurization rate [152]. General trends have been recognized for pore structure dependence on temperature, pressure and depressurization rate. Increasing temperature generally lowers the solubility and increases the diffusivity of $scCO_2$ in the polymer, resulting in fewer pores with larger diameters [163, 164]. Increasing the pressure increases the amount of dissolved $scCO_2$ in the polymer, yielding more nucleation sites and a higher quantity of smaller pores. As a predominantly nucleation and growth phase separation, depressurization rate becomes an important parameter in the pore size evolution (i.e. sufficient time is necessary for pores to grow and generate interconnectivity). Faster depressurization rates result in the formation of a high pore density of small diameters, while slower rates yield larger pores with lower pore density. Depressurization rate has been shown to have a significant effect on the pore structure and interconnectivity and continues to be an area of interest [164]. A

parametric analysis performed by Tsivintzelis, et al. with polystyrene and PDLLA confirmed these trends [165] as well as the following studies.

Reverchon and Cardea [166] studied expansion from $scCO_2$ of polystyrene (PS) and cellulose acetate (CA). PS and CA foams were generated with microporous structures; however, nonporous skin formation was observed at all conditions. The expected temperature and pressure effects were seen with these systems: pore size increased, while pore density decreased with temperature, and pore size decreased, while pore density increased with pressure. The effect of contact time was also investigated. Longer contact times led to more uniform pore size distributions, as CO_2 was able to fully diffuse into the sample for homogeneous nucleation upon depressurization.

Tai, et al. [167] performed a systematic evaluation of PDLLA and PLGA foam structure based on polymer chemical composition, molecular weight and experimental parameters, including foaming temperature and pressure and depressurization rate. Polymers were foamed by expansion from $scCO_2$ in a single step batch process. Homogeneous porous structures were obtained with a nonporous skin layer for all polymers. PDLLA was found to provide more interconnected pore structures than PLGA. Pore size distributions as determined by micro-CT were narrower for PLGA than for PDLLA. Lower molecular weights resulted in larger pore sizes and more brittle foams. The copolymer concentration of PLGA was also found to have an effect on pore structure, and increasing glycolic acid content resulted in smaller pores with a narrower pore size distribution. Foams produced from lower molecular weight polymers were

found to be the most brittle. Increasing temperature produced foams with larger pores, higher pressures produced smaller pores and slower depressurization rates produced larger pores.

Limitations of foaming by expansion of CO_2 include skin formation at the polymer surface, limited pore interconnectivity, and poor mechanical properties [29]. Skin formation occurs at the surface of the polymer due to the rapid diffusion of gas out of the matrix. Incorporation of a salt porogen during foaming is an approach to prevent skin formation and improve interconnectivity, but maintains the same limitations of porogen leaching techniques, including loss of incorporated bioactive compounds [29, 152]. For example, Salerno, et al. reported the generation of bimodal pore size distributions in PCL scaffolds produced by a $scCO_2$ foaming and porogen leaching combined process [168]. $scCO_2$ is also non-ideal in the foaming of semi-crystalline polymers with a high degree of crystallinity due to the generation of heterogeneous porous structures [169], which are not always suitable for TE and drug delivery applications. Exploration of different polymers/copolymers/polymer blends, processing parameters and the addition of co-solvents can alter the $scCO_2$ foaming process.

A few authors have reported on the use of a co-solvent to enhance polymer foaming by a supercritical foaming technique. Kiran [31] has reported on the phase behavior and foaming process of PLLA and poly(caprolactone-*co*-lactide) in CO_2 and CO_2 + acetone mixtures. Foaming experiments were performed using PLLA in pure CO_2 and mixtures containing 1 and 4 wt% acetone. Addition of acetone in the foaming process promoted foaming in PLLA at much lower temperatures and pressures, compared to foaming with pure CO_2. In addition, larger pore sizes with a higher degree of interconnectivity were obtained with the addition of acetone. Non-

uniform pore structures are obtained from foaming of poly(caprolactone-*co*-lactide) using only $scCO_2$, and the addition of a small amount of acetone as a co-solvent was found to improve pore uniformity.

Tsivintzelis, et al. [169] employed various supercritical mixtures of ethanol and CO_2 in batch foaming of PCL. Heterogeneous porous structures of PCL foamed at temperatures well below its melting temperature using pure $scCO_2$ as the foaming agent were obtained, as expected. The addition of ethanol was found to promote the formation of uniform porous structures; however, skin formation was not prevented. Homogeneous porosity is directly related to the improved dissolution of the CO_2-ethanol mixtures into PCL, which is likely due to a solvent-induced viscosity reduction and/or a melting point depression. Typical temperature and pressure effects were observed with these systems regardless of the CO_2-ethanol mixture composition.

Polymer foaming with $scCO_2$ can also be incorporated into another industrially relevant process such as extrusion [170-175]. In an extrusion process, the addition of $scCO_2$ to the polymer decreases the polymer viscosity which reduces the shear forces acting on the solution. Lower operating temperatures are required in a $scCO_2$ extrusion due to the lowered T_g and T_m. Foaming occurs in $scCO_2$ extrusion when the polymer leaves the die through the nozzle. In the ambient conditions, $scCO_2$ diffuses radially outward from the extrudate creating pore size distributions along the radial dimension.

A supercritical solution extrusion process was developed by Kiran [31] for the preparation of porous structures with tubular geometries. Acetone was used as a co-solvent in the processing of

the biodegradable polymers PMMA and poly(caprolactone-*co*-lactide). Porous tubular scaffolds were obtained with pore diameters of about 50 μm.

Another area of interest in TE engineering and drug delivery is the supercritical extraction of organic solvents from particle-based drug delivery systems. For example, a double emulsion (water/oil/water) technique may be coupled with a $scCO_2$ extraction step to remove organic solvent from the drug-containing polymer microparticles [176, 177]. In the double emulsion technique, the drug is dissolved in an aqueous solution which is then emulsified with an organic polymer solution. The resulting solution is emulsified a second time with an aqueous solution containing a surfactant. The residual organic solvent contained in the microparticles usually exceeds the acceptable limit for TE or drug delivery applications, however, $scCO_2$ can be used to extract the organic solvent by diffusing into the polymer and leaching out the residual solvent [29].

3.5 Drug Delivery from Polymer Foams Prepared in Supercritical CO_2

Incorporation of bioactive compounds, including drugs, antibiotics, growth factors, genes, can supplement a TE scaffold to help prevent inflammation and infection, promote cell growth and provide necessary cell signaling capabilities for tissue regeneration. A simple way to incorporate bioactive compounds into scaffolds via the $scCO_2$ foaming technique is by physically mixing the compound into the liquefied polymer, which is saturated with $scCO_2$. The mild processing conditions applicable in $scCO_2$ foaming prevent damage to labile compounds such as proteins or drugs [29].

López-Periago, et al. [178] formed porous foams of PLLA and PMMA using $scCO_2$ processing by gas foaming and by a semicontinuous antisolvent (SAS) technique. A bioactive agent, triflusal, was incorporated into the foamed matrix. Triflusal was incorporated into the polymer through dissolution of the drug in CO_2 and diffusion through a membrane before being physically mixed with the polymer in a high pressure batch system. PMMA could be foamed, but a closed pore structure was obtained with a nonporous skin layer. A 15 wt% loading of triflusal was obtained. PLLA could not be foamed due to its highly crystalline morphology, and incorporation of triflusal resulted in triflusal crystal formation on the PLLA surface, making it a non-suitable drug delivery device.

Velasco and Benito [179] exposed PMMA-PLLA blends to CO_2 at 60 ^{o}C and pressures ranging from 120-260 bar in a batch foaming process. Polymer blends were created by polymerizing MMA with PLLA in the monomer solution. IB was incorporated at 10-20 wt% into the scaffolds prior to CO_2 exposure. Skin formation on the surface of all scaffolds was observed. Higher exposure pressures resulted in a higher degree of interconnectivity, which was attributed to higher diffusivity of CO_2 into the matrix. Higher concentrations of PLLA resulted in lower porosity and interconnectivity due to the higher degree of crystallinity. Interestingly, IB was found to possibly be acting act as a porogen, since higher porosities were achieved in samples containing the drug. IB was shown to be extracted by $scCO_2$ at longer processing times (> 24 hr). The release of IB was shown to be sustained and dependent on the polymer blend composition. Degradation behavior was found to be related to the porosity and hydration of the scaffold.

Hile, et al. [180] reported on the delivery of an active growth factor (protein) from PLGA foamed in $scCO_2$. Foams were generated from aqueous protein emulsions in a PLGA - methylene chloride solution which were saturated then foamed with CO_2. Growth factor release rates were found to be greater in the CO_2-produced foams when compared to foams generated by the solvent casting/porogen leaching technique. In addition, scaffolds produced by the CO_2 based technique were shown to prevent burst release behavior, releasing the protein at a relatively constant rate. However, residual methylene chloride concentrations in the foams were too high for in vivo use and required further solvent removal steps.

The literature has shown that foaming of biomedical polymers with $scCO_2$ holds promise in the generation of TE and drug delivery devices. However, the major limitations of foaming with CO_2 alone include the formation of a non-porous skin on the surface of the foam and poor interconnectivity of pores. A primary activity in this research is to investigate the ability of organic solvents as co-solvents as an approach to limit these adverse characteristics and improve the CO_2 foaming process. FDA-approved solvents, acetone, ethanol and ethyl acetate are being explored as co-solvents due to the abundant literature available on their mixtures with CO_2.

Chapter IV. Inclusion Complex Formation of β-cyclodextrin and Naproxen: A Study on Exothermic Complex Formation by Differential Scanning Calorimetry[1]

4.1 Abstract

Inclusion complex formation between β-cyclodextrin and Naproxen was investigated using differential scanning calorimetry (DSC) as a function of the β-cyclodextrin-to Naproxen molar ratio, ranging from 0:5:1 to 5:1. When these mixtures are heated above the melting temperature of Naproxen, an exothermic peak is observed at a temperature slightly higher than the melting peak of Naproxen. This peak, which has not been previously reported, has been interpreted as an exothermic energy of inclusion complex formation. The magnitude of this complex formation peak was found to be dependent upon the composition of the β-cyclodextrin and Naproxen mixture and increased in magnitude to a maximum value at a β-cyclodextrin:Naproxen molar ratio of 2:1. In addition, Naproxen recrystallization and re-melting peaks seen in the cooling and re-heating scans, respectively, decreased in magnitude with increasing molar ratio and totally disappeared for the mixture with 5:1 of β-cyclodextrin to Naproxen ratio indicative of complete inclusion of Naproxen in the cyclodextrin cavities. Complete inclusion was further reflected by the disappearance of key Naproxen peaks in Fourier transform infrared spectra of samples recovered from DSC experiments. The large excess of β-cyclodextrin needed to fully complex the Naproxen was found to be due to slow kinetics. Increasing the hold time after the initial

[1] Reproduced with permission from Springer. Copyright 2012. *H. Grandelli, B. Stickle, A. Whittington, E. Kiran, The Journal of Inclusion Phenomena and Macrocyclic Chemistry (2012) DOI 10.1007/s10847-012-0241-6.*

melting led to inclusion efficiencies up to 95% even for the 2:1 mixture. These experiments suggest that ratios of β-cyclodextrin:Naproxen 2:1 or greater facilitate the process by increasing the presence of cyclodextrin molecules in the close proximity of the drug molecules and lead to high efficiencies.

4.2 Introduction

Naproxen (NA) is a propionic acid derivative and is a type of non-steroidal anti-inflammatory drug commonly administered for the treatment of pain, inflammation and fever [38, 181]. Its selected properties are given in Table 10. The poor aqueous solubility of NA due to its hydrophobicity limits the bioavailability of the drug in the aqueous environment of the human body [182]. Inclusion complex formation with cyclodextrins (CDs) is an approach to improve the aqueous solubility via molecular encapsulation of the drug within the cavity of the more soluble CD molecule [183, 184].

Table 10. Reported physical properties of Naproxen [39] and β-cyclodextrin [55].

Compound	Chemical Structure	MW, g/mol	T_m, °C	ΔH_m, J/g	Water solubility (25 °C), mg/ml
Naproxen	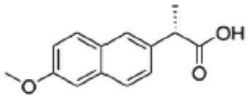	230.26	154.4	137	0.0159
β-cyclodextrin	See Figure 25b	1135.98	~ 300	-	18.5

CDs have indeed been explored extensively as additives in the pharmaceutical industry due to their unique ability to host and solubilize hydrophobic guest molecules including drugs [48, 55,

56, 184]. CDs are cyclic oligomeric polysaccharides composed of repeat glucose units which have a three dimensional structure similar in shape to a truncated cone or torus which is illustrated in Figure 25a [46]. The central cavity is relatively hydrophobic, and the outer edge of the molecule is hydrophilic [54, 63]. The three native CDs, α-, β-, and γ-CD, are produced by the enzymatic degradation of starch and differ from one another only in the number of repeat glucose units [48]. βCD, which is illustrated in Figure 25b, is the most commonly used CD due to the cavity size, availability and low cost [54, 55].

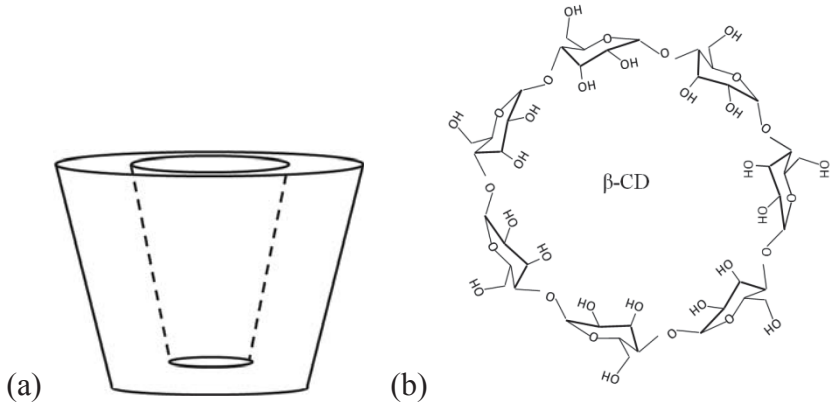

Figure 25. β-cyclodextrin (a) 3-dimensional torus structure and (b) chemical structure [185]

Complex formation is an equilibrium interaction described by the following equation:

$$a[CD] + b[drug] \overset{K}{\leftrightarrow} [CD \cdot drug]$$

where [*CD*] and [*drug*] represent uncomplexed CD and drug, respectively, [*CD* · *drug*] represents the complex, *K* is the stability constant for the complex, and a and b are the stoichiometric coefficients. The inclusion complex formation of NA with βCD and its

derivatives has been studied extensively by various techniques, including potentiometry [181], conductivity [181], fluorescence [181, 186, 187], nuclear magnetic resonance (NMR) [186, 188], mass spectroscopy [188], differential scanning calorimetry (DSC) [80, 98, 187, 189-193], x-ray diffraction (XRD) [98, 187, 189, 192, 193], thermogravimetric analysis (TGA) [189, 190, 192], ultraviolet-visible spectroscopy (UV-Vis) [80, 187, 189, 191-195], Fourier transform infrared spectroscopy (FTIR) [80, 98, 192, 193], hot stage microscopy [195], scanning electron microscopy [195], and molecular modeling [187, 194]. Stability constants of the NA-CD inclusion complexes, which can be used to calculate complexation stoichiometries and thermodynamic parameters of inclusion complex formation, including enthalpy and entropy changes, have previously been calculated based on spectroscopic characterizations utilizing a phase solubility method described by Higuchi [187, 189, 195] or a modified Benesi-Hildebrand equation [186, 188, 194]. Complex formation is generally associated with a large negative enthalpy change (ΔH) and either a positive or negative entropy change (ΔS), making complex formation largely an enthalpy-driven exothermic process [48]. In addition NA complexes with βCD, γCD and βCD derivatives formed in solutions have generally been reported as having a 1:1 stoichiometric ratio (where a = b) [181, 186, 188, 189, 194, 196, 197]. The stoichiometric ratios in nearly all guest-CD inclusion complexes that are reported in the literature are either 2:1, 1:1 or 1:2 [198]. Stoichiometries that differ from these have also been reported [199] but are attributed to poor inclusion efficiencies rather than any physical significance. It should be noted that these previously reported studies are all based on the behavior of CD solutions, and, to the authors' knowledge, stoichiometry of the inclusion complex, stability constants and thermodynamic parameters between NA and βCD, or the requirements of cyclodextrin-drug ratios to be used for

efficient complexation have not been previously reported for complex formation from physical mixtures in the absence of solvents.

DSC is an analytical technique commonly employed in the characterization of CD-drug inclusion complexes [104, 200]. In a typical DSC analysis for determination of complex formation, crystalline compounds which usually display distinct melting peaks in their DSC heating scans, appear amorphous if all the drug is included into the CD cavity. Observation of a drug melting peak is an indication of incomplete complex formation [104]. To the authors' knowledge, no additional peaks, which are not attributed to drug melting or recrystallization transitions, have been previously reported during or after the event of inclusion complex formation between Naproxen and βCD. FTIR is another analytical technique useful in the characterization of inclusion complexes. Spectra of CD-drug physical mixtures results in an overlay of the two pure component spectra, while spectra of CD-drug inclusion compounds can display new peaks which are not present in either pure component spectra [101, 201], or they can appear as the CD spectra alone, with no observation of the IR peaks of the included compound [95, 202].

The primary goal of this research was to examine the inclusion complex formation behavior of βCD and NA by DSC from their physical mixture via melting of the drug molecule. A comprehensive evaluation by DSC of the complex formation between βCD and NA at a wide range of βCD:NA molar ratios (from 0.5:1 to 5:1) is now reported. Further characterization by FTIR was carried out to verify observations from the DSC data. The results show that complexation via melting in physical mixtures is influenced by transport limitations and ratios of βCD:NA greater than 2:1 facilitate the process by increasing the presence of cyclodextrin molecules in the close proximity of the drug molecules and lead to high efficiencies.

4.3 Materials and Methods

Naproxen (NA) and β-cyclodextrin (βCD) were purchased from Sigma-Aldrich and used as received. DSC experiments were carried out in a Pyris Diamond DSC. 10 mg samples were prepared in the appropriate molar ratio, then mixed gently with a spatula and contained in a crimped aluminum DSC pan with a lid. The heating and cooling scans were carried out at a rate of 20 ^{o}C/min with a nitrogen purge of 10 ml/min. All heat values that are reported were normalized to the NA mass in the sample mixtures. FTIR spectra were acquired with a Digilab FTS 3100 spectrometer using a resolution of 4 cm^{-1} and 32 scans averaged in the wavenumber range of 4000 to 400 cm^{-1}. Samples were prepared at 1 wt% compositions into KBr discs for analysis. Four repeat samples were analyzed.

4.4 Results

DSC analyses were carried out for pure βCD, pure NA and for βCD:NA physical mixtures over a range of molar ratios from 0.5:1 to 5:1 (mol βCD:mol NA). Figure 26 shows the results for pure NA and pure βCD, displaying a T_m of 159 ^{o}C and a heat of melting of 129 J/g for NA in the first heating scan, and showing the removal of moisture from βCD above 100 ^{o}C. The variation between the melting temperatures obtained in DSC experiments from the literature data shown in Table 10 is due to differences in the heating rates employed during DSC experiments. Typically, a heating rate of 10 ^{o}C/min is employed in melting point determination by DSC; however, in these experiments a heating rate of 20 ^{o}C/min was used to sufficiently sharpen and resolve all

observed peaks. A faster rate of heating is known to cause a shift of the melting peak to higher temperatures, due to the kinetics of melting. The physical mixtures were first heated to 140 ^{o}C and held for 3 minutes to remove water from βCD, eliminating the broad dehydration peak. After cooling to 30 ^{o}C the samples were heated above the melting temperature of NA (T_m = 159 ^{o}C) to 180 ^{o}C and held at 180 ^{o}C for 1 minute, or heated to 165 ^{o}C and held for 60 or 120 min. The samples were then cooled to 30 ^{o}C, held at 30 ^{o}C for 1 minute and finally reheated to 180 ^{o}C.

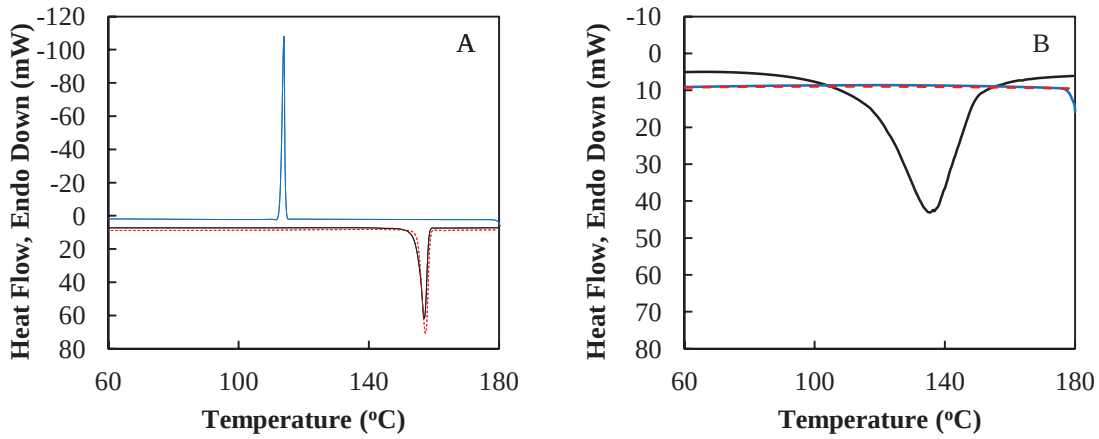

Figure 26. Pure component differential scanning calorimetry first heating (black, solid), cooling (blue, solid) and second heating (red, dotted) scans for (A) Naproxen and (B) β-cyclodextrin

DSC scans for 0.5:1 and 5:1 βCD:NA are individually shown in Figure 27 and Figure 28, respectively, to indicate that although the peaks for the 5:1 βCD:NA sample are significantly less pronounced than those for the 0.5:1 βCD:NA sample in the comparative plots shown in Figure 27, the peaks are indeed present and visible with the enlarged scale used in Figure 28. These scans were all generated with a 1 min hold time at 180 ^{o}C. The heating scan shown in plot A of each figure (in Figure 27 & Figure 28) contains two distinct peaks: (1) the endothermic melting

peak of NA at about 159 ^{o}C and (2) an exothermic peak at a temperature just higher than the NA melting peak. This peak has not been previously reported, to the authors' knowledge, and is evidence of the exothermic complex formation interaction occurring between βCD and NA upon NA melting. In the cooling scan of 0.5:1 βCD:NA shown in Figure 27B, an exothermic peak is seen, which is centered around 106 ^{o}C and is indicative of NA recrystallization. The heat of recrystallization (ΔH_c) for the 0.5:1 molar ratio sample was found to be significantly lower than the ΔH_m observed in the first heating scan, and ΔH_c for the 5:1 molar ratio sample was found to be zero, indicating that no fraction of the melted NA recrystallized in the cooling scan. Both observations are in contrast to the same DSC experiment carried out for pure NA (Figure 26A), where NA after undergoing its melting in the heating scan recrystallized completely in the cooling scan. Similarly, in the second heating scan in the pure NA case, a re-melting peak is observed which is similar in magnitude (but opposite in sign) to the respective recrystallization peak. In these DSC experiments on mixtures with βCD, when NA enters its molten state in the first heating scan, the drug molecules are able to enter the empty βCD cavities forming the complex. Then, in the cooling scan, only free uncomplexed NA is able to recrystallize, and in the re-heating scan, only the free NA is able to re-melt, causing a reduction in ΔH_c and in ΔH_{m2}, respectively.

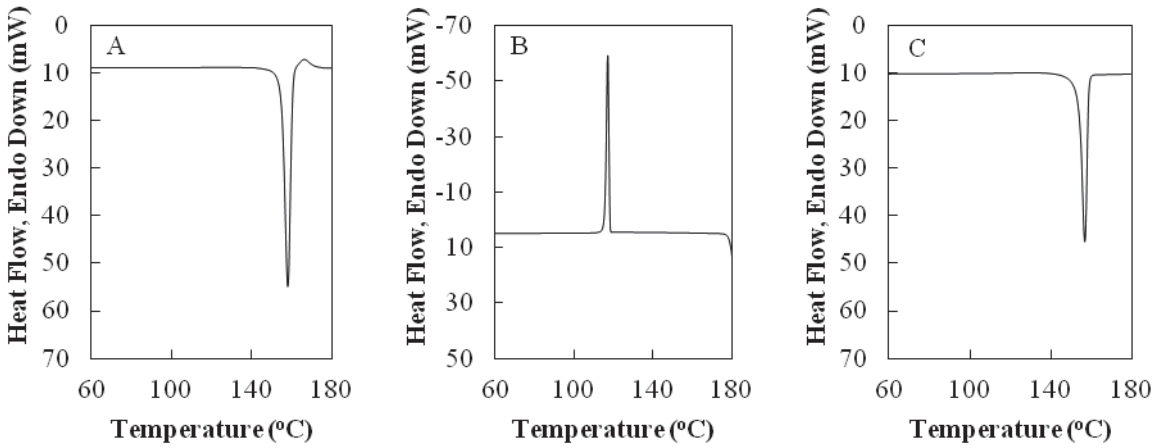

Figure 27. DSC scans of 0.5:1 β-cyclodextrin:Naproxen held at 180 oC for 1 min (A) 1st heating, (B) cooling and (C) 2nd heating

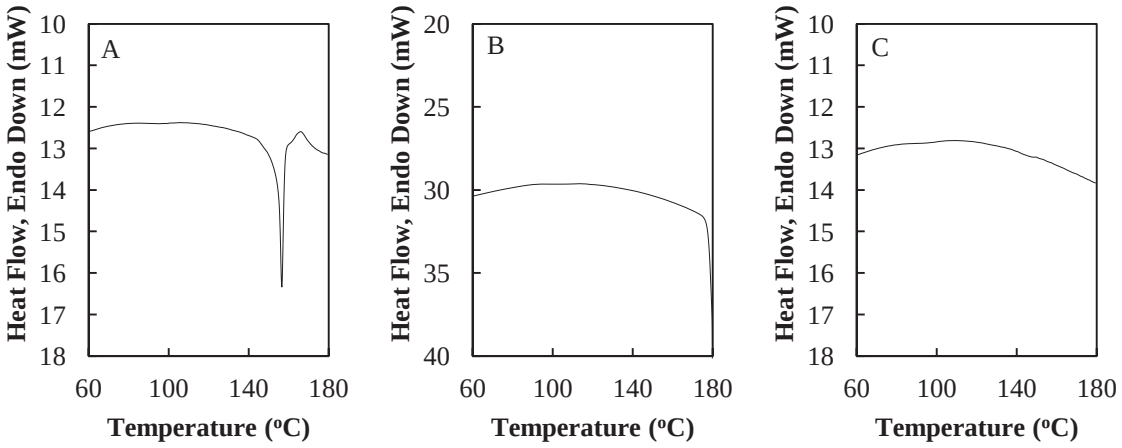

Figure 28. DSC scans of 5:1 β-cyclodextrin:Naproxen held at 180 oC for 1 min (A) 1st heating, (B) cooling and (C) 2nd heating

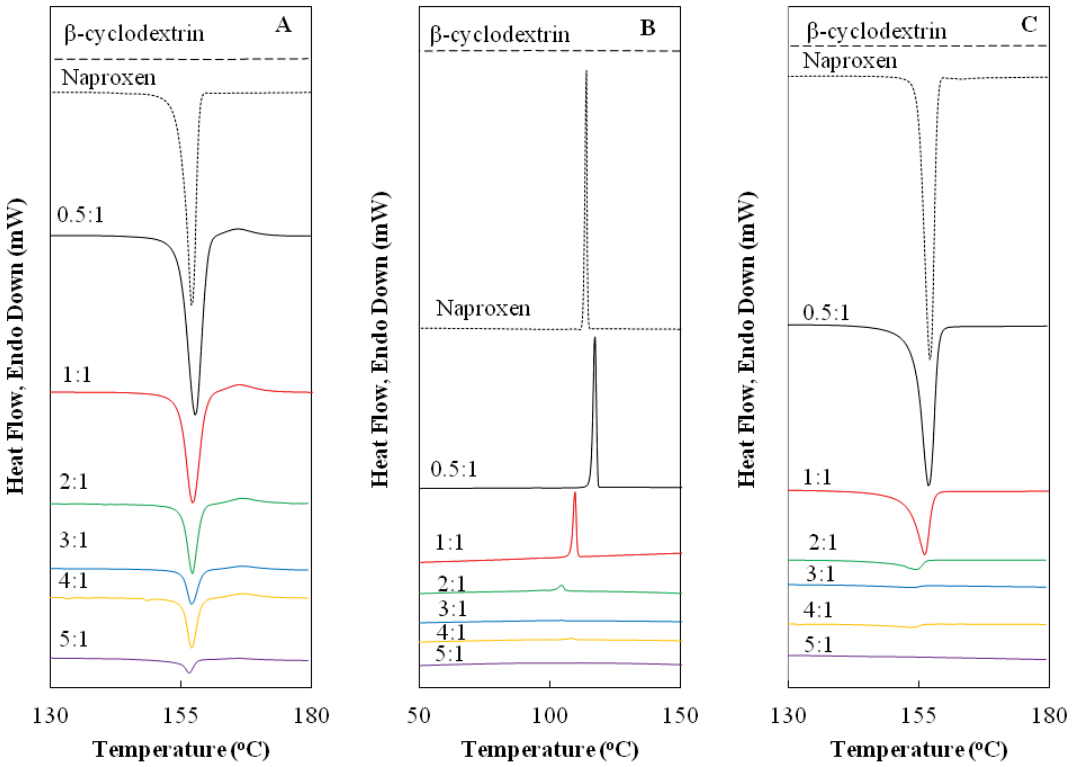

Figure 29. DSC scans for β-cyclodextrin:Naproxen physical mixtures held at 180 oC for 1 min (A) 1st heating scan, (B) cooling scan, (C) 2nd heating scan

Examination of the thermal behavior of the intermediate molar ratios between 0.5:1 and 5:1 provides further information on inclusion complex formation of NA with βCD. Figure 29 shows the comparative DSC scans during the 1st heating, cooling and the second heating scans for each mixture. Figure 30 shows the variation of the heat of melting, heat of complexation, heat of recrystallization, and heat of re-melting during the respective scans.

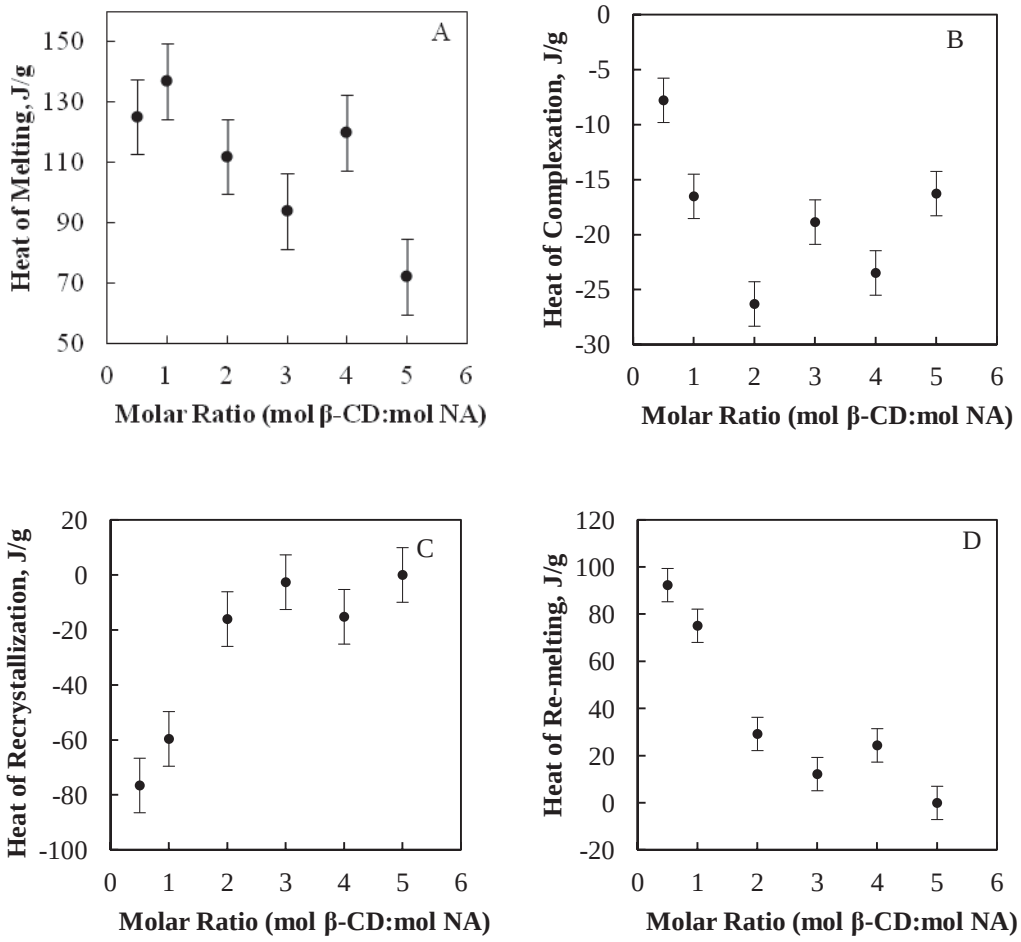

Figure 30. Heats for β-cyclodextrin:Naproxen physical mixtures from DSC experiments held at 180 ^{o}C for 1 min (four runs) (A) heat of β-cyclodextrin:Naproxen complexation, (B) heat of Naproxen recrystallization, (C) heat of Naproxen re-melting

The heat of complex formation, ΔH_{cf}, was found to increase in magnitude with increasing βCD molar composition up to a maximum value at a molar ratio of 2:1 [Figure 30A]. At molar ratios higher than 2:1, ΔH_{cf} maintained a value around -20 J/g. This initial increase in magnitude indicates an increase in the energy of complexation since more NA enters the βCD cavities; however, stabilization of the value may indicate a finite heat of complexation which exists for complex formation of the mixture. The magnitudes of the heat of recrystallization, ΔH_c and heat

of re-melting, ΔH_{m2}, decrease with increasing βCD molar composition, and the values are similar for each mixture. It should be noted that the peaks shown in Figure 29B & C generally shift to lower temperatures with increasing molar ratio. A possible explanation for the peak shift is the disruption of crystallinity and crystallizability due the increasing presence of the amorphous inclusion compound in the mixture after the first heating scan with increasing molar ratio. This would cause slower crystallization kinetics resulting in lower recrystallization temperatures, as well as a defect-laden semi-crystalline structure resulting in lower re-melting temperatures. Thus, higher molar ratios were found to promote inclusion complexation, leaving less free NA to recrystallize and re-melt. Since the magnitudes of recrystallization and re-melting peaks are similar at the same molar ratio, all of the inclusion complex formation must occur after the first melting of NA, and no further complex formation occurs upon melting in the second heating scan. The recrystallization and re-melting peaks completely disappear only for the 5:1 molar ratio mixture, suggesting that a large excess of βCD is needed for complete amorphization attributed to complex formation of NA with βCD by melt processing at 180 ^{o}C with a holding time of 1 min at this temperature. Inclusion efficiencies can then be calculated based on the heat of re-melting and pure NA heat of melting (ΔH_m^{NA} = 129 J/g) using the following relationship.

$$\% \, Inclusion = 100 * \left[1 - \frac{\Delta H_{m2}}{\Delta H_m^{NA}}\right]$$

The results that are plotted in Figure 31 show that the inclusion efficiency rapidly increases with increasing molar ratio of βCD to NA, basically approaching efficiencies of 90% and higher for CD:NA ratios of higher than 2.

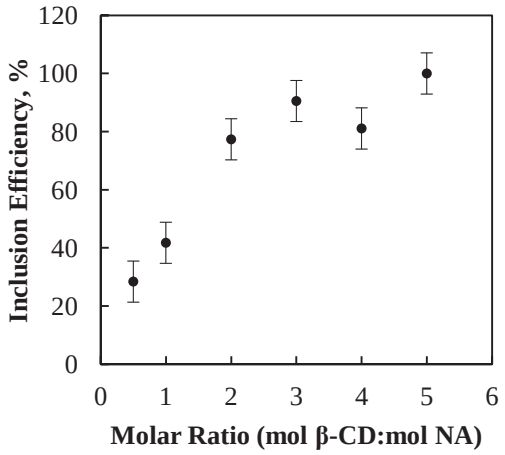

Figure 31. Calculated inclusion efficiencies for β-cyclodextrin-Naproxen prepared by melting in DSC experiments held at 180 ^{o}C for 1 min (based on heat of melting of pure Naproxen, ΔH_m^{NA} = 129 J/g)

The FTIR spectra shown in Figure 32 compare the spectra of pure βCD and NA with the spectra of the samples recovered after DSC experiments in the wavenumber range of 2000 to 800 cm^{-1}. Key NA peaks observed in this region include peaks at 1729, 1685, indicating the -C=O stretch, and the peak at 1228 cm^{-1}, indicative of the -O- stretch. The key βCD peaks include the asymmetric R-O-R stretch observed at 1158 cm^{-1} and the C-OH stretch observed at 1029 cm^{-1}. As the βCD:NA molar ratio is increased, the NA peaks become diminished. At molar ratios of 2:1 and higher, and in particular at the 5:1 molar ratio, NA peaks are no longer visible and the spectrum appears as pure βCD. The disappearance of the NA peaks in the FTIR spectra is a further indication of inclusion complex formation, and these data support the DSC results showing full inclusion being achieved only in the very high 5:1 molar ratio sample with the 1 min hold time at 180 ^{o}C.

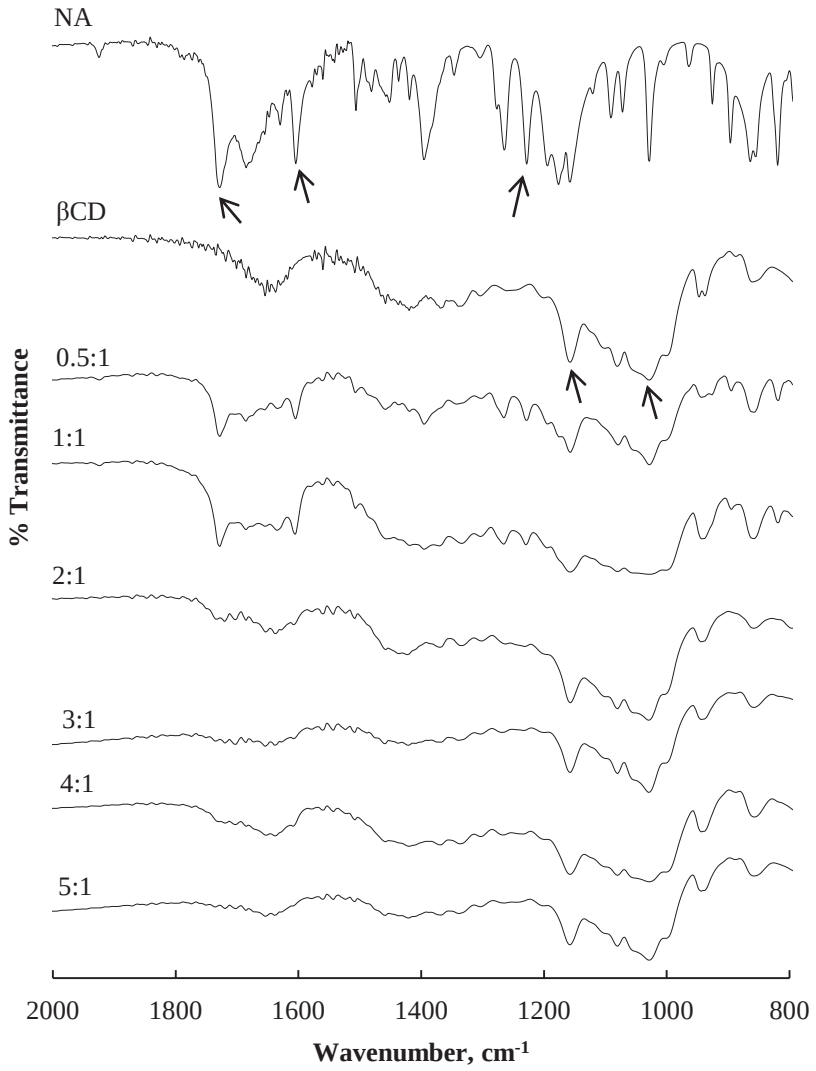

Figure 32. FTIR spectra of pure components compared to spectra of samples recovered from DSC experiments held at 180 ^{o}C for 1 min. Arrows show the key peaks at 1729, 1685, indicating the -C=O stretch and 1228 cm^{-1}, indicative of the -O- stretch in NA; and the asymmetric R-O-R stretch observed at 1158 cm^{-1} and the C-OH stretch observed at 1029 cm^{-1} in βCD.

Some degree of inclusion was achieved with all of the tested physical mixtures; however, only the 5:1 molar ratio mixture yielded a 100% inclusion by melt processing at 180 ^{o}C for 1 min. The large excess of βCD needed to include all of the NA was thought to be required due to transport or kinetic limitations in the static environment of the DSC pans or the short, 1 min, hold time after the initial melting. Thus, a series of additional experiments were performed by heating samples to 180 ^{o}C for 1 min in glass jars under a nitrogen purge with manual mixing to observe the effect of mixing on the inclusion efficiencies of 1:1, 2:1 and 3:1 βCD:NA mixtures. In addition, two more sets of DSC experiments were conducted in which the samples were heated and held above the melting temperature of NA, to 165 ^{o}C for 60 and 120 minutes to further observe whether kinetics were limiting the extent of inclusion complex formation. A lower temperature was chosen since these long exposure times to 180 ^{o}C were found to lead to some changes in the thermal behavior of NA, including doublet melting and recrystallization peaks. These changes were suspected to be due to changes in the crystalline form of NA from 60 and 120 min exposures to high temperatures rather than thermal degradation, since changes in FTIR spectra were not observed. No changes were observed in NA samples exposed to 180 ^{o}C for only 1 min, however.

Figure 33 shows the cooling and reheating scans for 1:1, 2:1 and 3:1 βCD:NA mixtures exposed to 165 ^{o}C for 60 min and compares the data with the samples exposed to 180 ^{o}C for 1 min. The recrystallization and remelting peaks are clearly less intense for samples exposed to 165 ^{o}C for 60 min when compared to the same molar ratio mixture exposed to 180 ^{o}C for 1 min

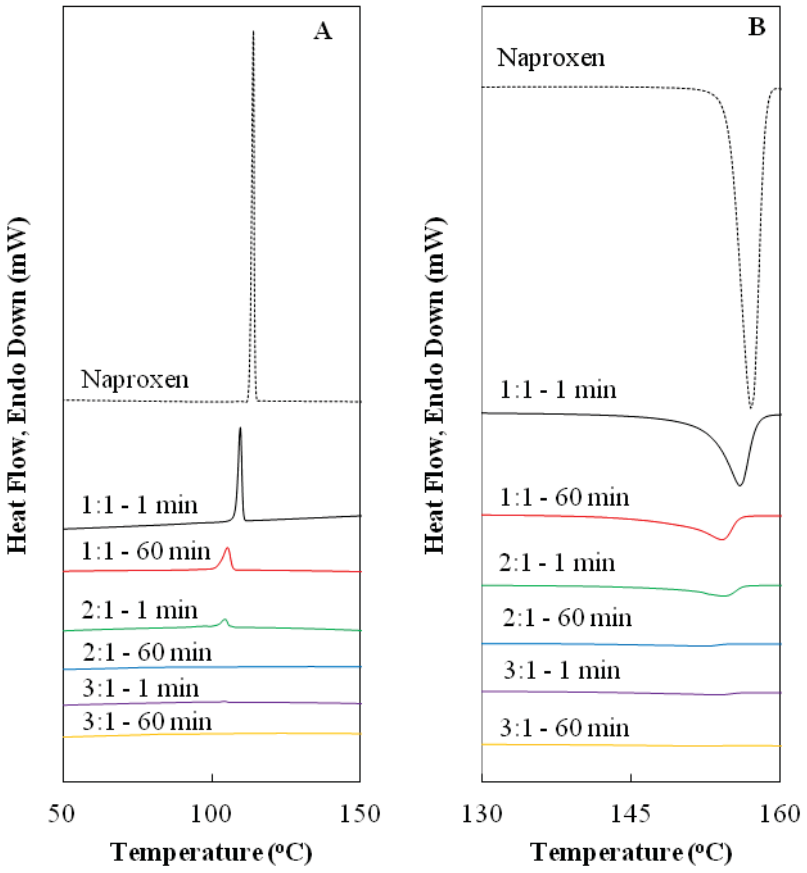

Figure 33. DSC comparison scans for β-cyclodextrin:Naproxen physical mixtures held at 165 °C for 60 min and at 180 °C for 1 min (A) cooling scan, (B) 2nd heating scan

Table 11 compares the results of the three different DSC experiments and the mixing experiments. The 120 min experiment was not carried out using the 3:1 mixture, since 100 % inclusion was achieved in the 60 min experiment. The results show no significant difference in inclusion efficiencies achieved with mixing versus samples prepared in DSC experiments held at 180 °C for 1 minute, indicating that inclusion is not necessarily limited due to absence of mixing in the static DSC experiments. However, a distinct influence of hold time above melting temperature is observed. Inclusions of 57%, 90% and 100% were achieved with 1:1, 2:1 and 3:1

molar ratio βCD:NA samples exposed to 165 ^{o}C for 60 min in the DSC. Furthermore, a hold time of 120 min yielded 57% and 95% inclusion efficiencies for 1:1 and 2:1 molar ratio samples. Inclusions achieved in 60 min and 120 min experiments for 1:1 and 2:1 molar ratio mixtures are within the same margin of error. Thus, exposures longer than 60 min do not seem to promote complex formation beyond the improved efficiency observed between 1 min and 60 min exposures. Figure 34, which compares the heat of remelting after different hold times above the melting temperature, shows the approach to essentially zero above 2:1 ratio molar ratio of CD to NA.

Table 11. Comparison of inclusion efficiencies (based on heat of melting of pure Naproxen, ΔH_m^{NA} = 129 J/g) obtained by melting Naproxen in the presence of β-cyclodextrin in (A) DSC experiments held at 180 ^{o}C for 1 minute, (B) mixed batches under nitrogen, (C) DSC experiments held at 165 ^{o}C for 60 minutes and (D) DSC experiments held at 165 ^{o}C for 120 min.

Molar Ratio	Inclusion Efficiencies, %			
βCD:NA	A	B	C	D
1:1	42	39	57	57
2:1	77	73	90	95
3:1	91	90	100	-

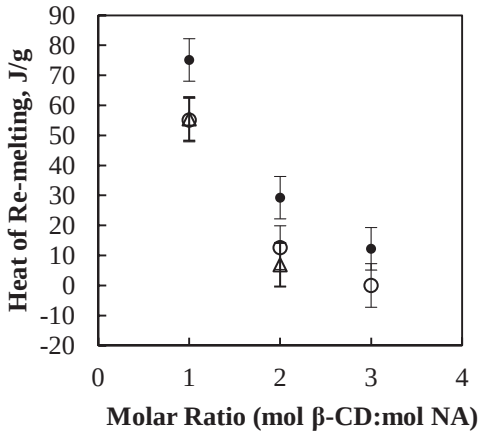

Figure 34. Heats of Naproxen remelting for β-cyclodextrin:Naproxen physical mixtures processed in DSC experiments held at 180 ^{o}C for 1 min (closed circles, four runs), experiments held at 165 ^{o}C for 60 min (open circles, three runs) and experiments held at 165 ^{o}C for 120 min (open triangles, three runs).

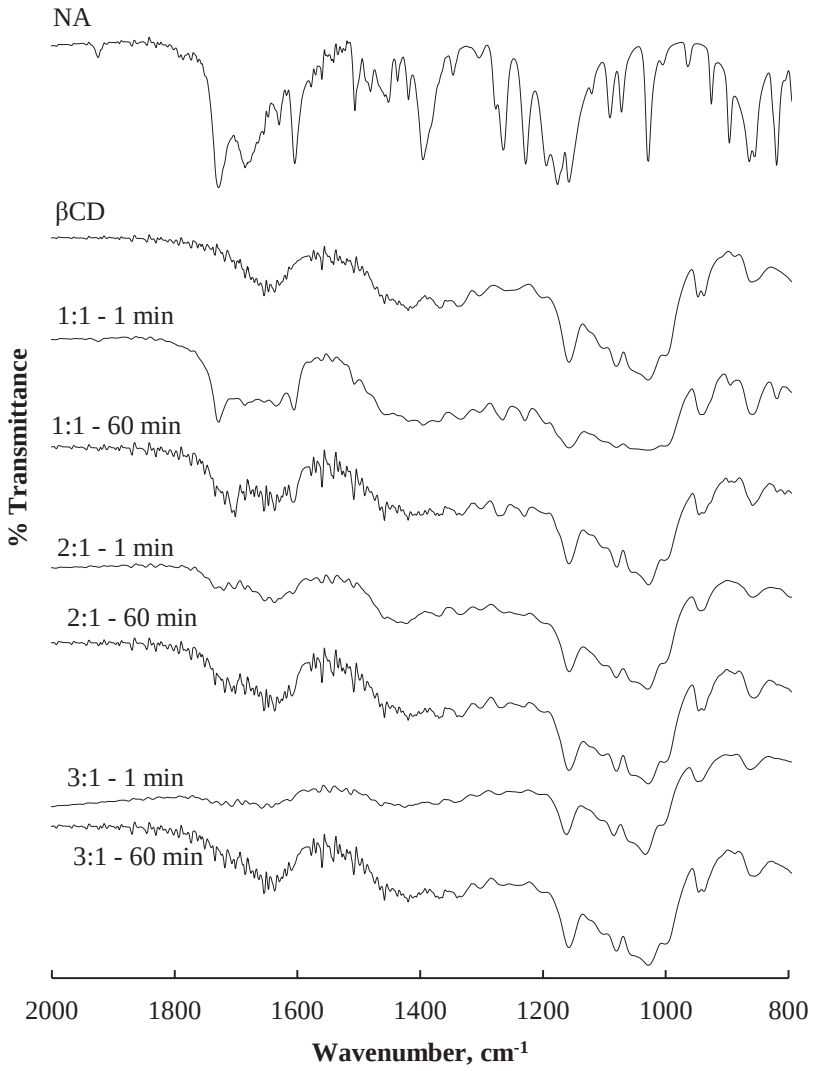

Figure 35. FTIR spectra of pure components compared to spectra of samples recovered from DSC experiments held at 180 ^{o}C for 1 min and DSC experiments held at 165 ^{o}C for 60 min.

At first sight, a 2:1 stoichiometry seems to be suggested by the data since, as Figure 34 shows, 90% inclusion was achieved with those physical mixtures. However, if an ideal stoichiometry of 2:1 existed for βCD:NA complexes, inclusions efficiencies greater than 50 % would not be possible in 1:1 mixtures. For the 1:1 mixture, a 60 min hold time resulted in a higher inclusion

efficiency of 57%, which did not improve further with hold time being increased to 120 min. It is possible that under efficient mixing conditions, inclusion efficiencies higher than 57% can be achieved which would be consistent with a 1:1 stoichiometry. Stoichiometric ratios of 1:1 are generally reported for CD:NA inclusion complexes based on solution complexation where transport limitations are less pronounced compared to solid state complexation [181, 186, 188, 189, 194, 196, 197].

The present observations indicate that the inclusion complex formation of βCD:NA mixtures by melting NA in DSC experiments is limited by transport kinetics, and sufficient time is needed for the molten NA to diffuse and enter the βCD cavities to achieve high inclusion efficiencies. This is achieved more readily when an excess of βCD is used, which naturally increases the presence of CD molecules in the close proximity of the drug molecules. The 2:1 βCD:NA molar ratio mixture appears to be a practical ratio needed to achieve a relatively high inclusion efficiency without going to high excess of βCD in forming the inclusion complex from melt without using solvents.

4.5 Conclusions

NA was found to form an inclusion complex with βCD upon melting in DSC heating scans, which was indicated by a reduction in NA melting peak intensity in repeat DSC heating scans, as well as by the reductions in NA FTIR spectral absorbance observed in samples recovered from DSC experiments. In addition, a unique exothermic peak was identified in the first DSC heating scans of βCD-NA physical mixtures, which was found to be indicative of inclusion complex formation. In cooling and re-heating scans, the amount of free, uncomplexed NA was found to

decrease with an increase in βCD:NA molar ratio, based on heats of recrystallization and re-melting, respectively. Full inclusion of NA was achieved by melting the drug in the presence of excess βCD in 3:1 and higher molar ratios of βCD:NA in physical mixtures in the DSC. However, essentially full inclusion of NA could be achieved with 2:1 molar ratio mixtures by holding at 165 ^{o}C for 1 hour in DSC experiments.

Acknowledgements

This research was funded by the National Science Foundation (CBET #0929978).

Chapter V. Melting Point Depression of Piroxicam in Carbon Dioxide + Co-solvent Mixtures and Inclusion Complex Formation with β-Cyclodextrin[2]

5.1 Abstract

This paper reports on the melting point depression and polymorphic transformations of Piroxicam in supercritical carbon dioxide and in mixtures with ethanol, acetone or ethyl acetate as co-solvents. It further reports on the formation of the inclusion complexes of Piroxicam which is liquefied in these fluid mixtures with β-cyclodextrin. It is shown that in carbon dioxide the melting temperature of Piroxicam is reduced by 17 ^{o}C, from 200 ^{o}C to 183 ^{o}C. The melting temperature was further depressed in mixtures containing a small amount of a co-solvent. The largest melting point depression was 37 ^{o}C and was observed in the fluid mixture containing 10 wt % ethanol. Piroxicam that was melted and recrystallized in carbon dioxide or carbon dioxide + co-solvent mixtures displayed distinct differences in its infrared spectra, thermal behavior and x-ray diffraction patterns as compared to its unprocessed form. Melting in CO_2 and CO_2 + co-solvent mixtures was found to lead to a polymorphic transformation of Piroxicam from the β crystal form (cubic) to the α crystal form (needle). It was further found that melting of Piroxicam in 90:10 wt% CO_2:Ethanol fluid mixture promotes inclusion complex formation with β-cyclodextrin leading to a 1:1 molar ratio complex. Inclusion complex formation via melting in supercritical fluid mixtures is now being proposed as a new processing methodology.

[2] Reproduced with permission from Elsevier. Copyright 2012. *H. Grandelli, J.C. Hassler, A. Whittington, E. Kiran, The Journal of Supercritical Fluids 71 (2012) 19-25.*

5.2 Introduction

Poor dissolution behavior due to hydrophobicity limits the bioavailability of many pharmaceutical agents, including the non-steroidal anti-inflammatory drug Piroxicam (PC). One approach to improve dissolution is the molecular encapsulation of drugs into a compound with an inherently higher solubility, such as cyclodextrins (CDs), through a process known as inclusion complex formation [55] [Figure 36a]. Cyclodextrins are cyclic oligosaccharides which have the shape of a truncated cone or a torus. These cup-like molecules are able to host guest molecules in their hydrophobic internal cavities, and the inclusion complex takes on the hydrophilic character of the exterior of the CD molecule [56]. Native CDs are prepared by the enzymatic degradation of starch and include α-, β- and γ-CDs [48], which differ from one another only in the number of repeat glucose units. The chemical structure of βCD, containing 7 repeat glucose units, is illustrated in Figure 36b. Other CD derivatives of pharmaceutical relevance are substituted with various functional groups and include hydroxypropyl-βCD, sulfobutyl ether-βCD, methylated βCD, hydroxypropyl-γCD and maltosyl-βCD [54].

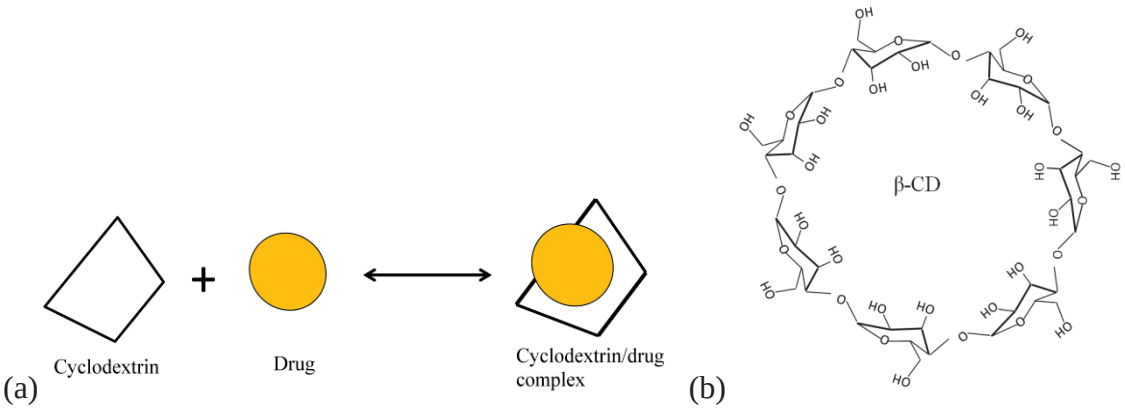

(a) (b)

Figure 36. (a) Cyclodextrin – drug inclusion complex formation, (b) β-cyclodextrin chemical structure

CD-drug inclusion complexes are formed through different processes including kneading, co-precipitation from solvents [64], freeze drying, spray drying [55] and supercritical fluid processing [62, 81]. Kneading and co-precipitation methods do not typically provide high inclusion efficiencies and involve large amounts of water or toxic organic solvents. Freeze drying and spray drying can provide high inclusion efficiencies but typically involve the use of toxic organic solvents. Inclusion complex formation techniques employing supercritical CO_2 as the primary processing fluid are emerging [53, 62, 80-83, 93, 97, 98, 100, 101, 103, 201, 203, 204] as an alternative which reduces the use of organic solvents with potential for high inclusion efficiencies [82, 103]. However, the majority of reported supercritical inclusion complex formation techniques, while effective, are limited by the drug solubility in CO_2 [62]. Thus, some researchers have investigated the addition of ternary agents, such as L-lysine, to promote complex formation in the solid state by improving drug solubility in CO_2 [82]. Even though liquid state complex formation by melting the drug could be an alternative and effective method for promoting complex formation, no such study, to the authors' knowledge, has hitherto been reported in the literature.

Differential scanning calorimetry (DSC) is a technique commonly employed in the characterization of CD inclusion complexes [104]. Crystalline compounds which display distinct melting peaks in their DSC scans, such as Piroxicam (PC), usually appear amorphous in DSC scans of the complex if all the drug is included into the CD cavity. Observation of a drug melting peak after a complex formation experiment is an indication of incomplete complex formation [104]. In recent studies conducted in the authors' laboratory, it was observed that when CD:drug physical mixtures were heated beyond the melting point of the drug and then

cooled, and then reheated, the melting peak of some drugs became diminished or disappeared completely, indicating that complex formation could be occurring upon drug melting in the DSC pans. As an example, Figure 37 shows the DSC heating, cooling and reheating scans of a 1:1 molar ratio physical mixture of βCD and PC. During the first heating scan, an endothermic peak indicating PC melting is observed near 200 ^{o}C. However, neither a crystallization nor a re-melting peak is observed in the cooling and re-heating scans after the initial heating stage, which indicates that PC had become amorphous. To better understand the thermal behavior of PC, thermogravimetric analyses (TGA) were also carried out. The TGA results were extremely significant in showing that PC was starting to degrade as it was melting at 200 ^{o}C. This is illustrated in combined TGA and DSC plots shown in Figure 38, which indicates that the amorphization of PC was more likely due to thermal degradation rather than inclusion complex formation. Although PC may form an inclusion complex with βCD upon melting, the simultaneous onset of thermal degradation with melting does not permit melt processing of PC. A viable approach to circumvent thermal degradation upon melting would be to depress the melting temperature of PC.

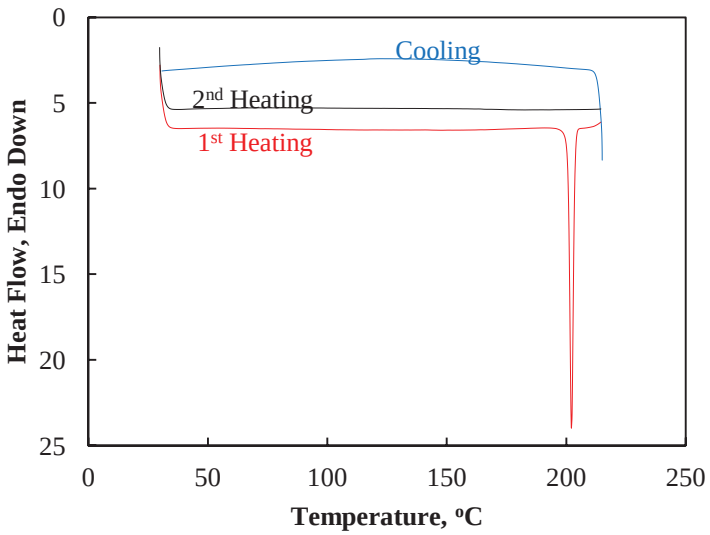

Figure 37. Differentical scanning calorimetry scans for 1:1 β-cyclodextrin:Piroxicam

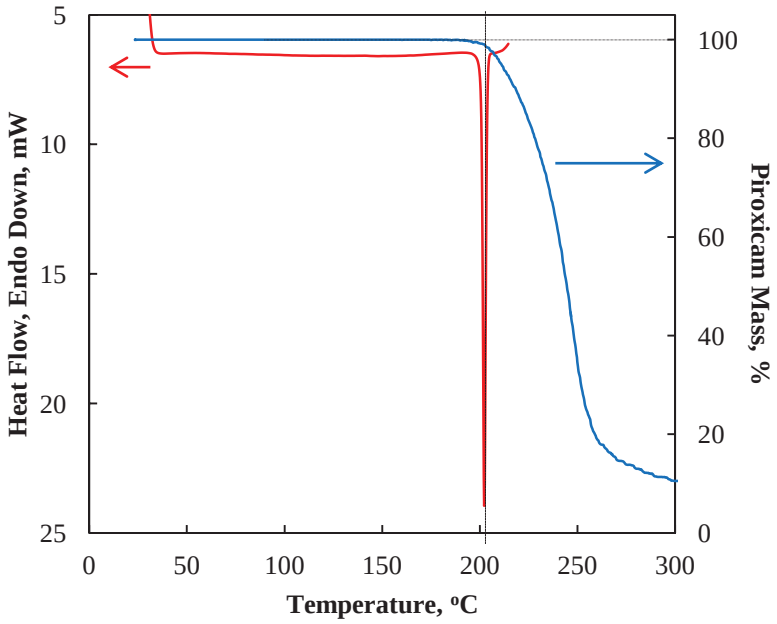

Figure 38. Differential scanning calorimetry heating scan of 1:1 β-cyclodextrin:Piroxicam and thermogravimetric analysis of Piroxicam

Melting point depression in supercritical carbon dioxide has been demonstrated in the literature for semi-crystalline polymers [32, 205-207] or small molecules such as the drug molecules, Ibuprofen [208, 209] and Naproxen [210]. In the studies with these drug molecules reported in the literature, the first melting point method was used, in which the initial appearance of melting was recorded. Melting temperatures of each drug were shown to be pressure dependent, and the results are reproduced in Figure 39 for comparison. The melting temperature of Ibuprofen decreases linearly from 76 ^{o}C to 48 ^{o}C with increasing pressure up to 10 MPa. Increasing the pressure above 10 MPa does not lead to a further reduction in the melting temperature. The melting temperature of Naproxen in CO_2 decreases linearly with increasing pressure up to at least 30 MPa from the ambient value of 154 ^{o}C to 140 ^{o}C at 30 MPa. Higher pressures were not reported. To the authors' knowledge, PC melting in CO_2 or CO_2 + co-solvent mixtures has not been previously reported in the literature. Due to the thermal instability of the drug at its melting temperature, melting point depression of PC is of particular interest since by melting at lower temperatures, thermal degradation of PC may be avoided and thereby allowing its melt processing for complex formation with CDs.

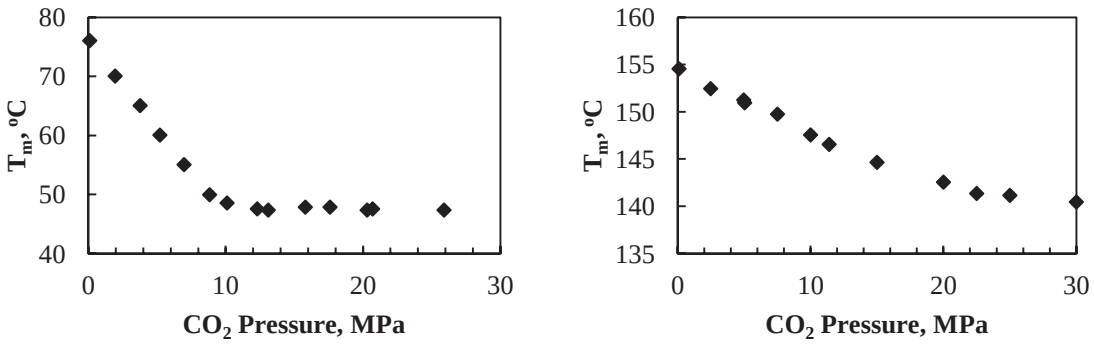

Figure 39. Reported pressure dependent melting temperatures of RS-(±)-ibuprofen (left) [208] and S-(+)-naproxen (right) [210] in pure CO_2. (Data has been re-plotted from the original references).

An interesting characteristic of PC is its ability to form polymorphs upon recrystallization from solutions with various solvents. The polymorphs are readily characterized by FTIR, DSC, NMR and powder XRD and have been reported in the literature [211]. Two forms, needle (α form) and cubic (β form) are commonly observed [211-214] when crystallized from solutions in ethanol and benzene, respectively. The infrared spectrum of PC, whose chemical structure is illustrated in Figure 40, displays a sharp key peak indicative of the -NH- stretch in the range of 3340-3395 cm^{-1}, which varies within this region depending on the crystalline form. This peak is reported to appear at 3393 cm^{-1} in the α form and at 3341-3340 cm^{-1} in the β form [211, 212]. Thermal analyses by DSC show that the melting of the α form occurs at 199.7 ^oC with a heat of melting of 112.96 J/g, while the melting of the β form occurs at 202.6 ^oC with a heat of melting of 110.28 J/g [211, 213]. The XRD patterns of the α and β forms display distinct differences [211]. Crystalline precipitation into various PC polymorphic structures has also been reported from CO_2 + co-solvent fluid mixtures with acetone, ethyl acetate and dichloromethane [215]. All the samples precipitated from these fluid mixtures were found to be the needle, α form of PC based

on SEM characterization. Prior work on semicrystalline polymers such as poly(4-methyl-1-pentene) [216] and syndiotactic polystyrene [217] had shown that pressure can be used as a tuning parameter in mixtures of CO_2 with co-solvents to promote different polymorphic states. In addition, exposure to supercritical carbon dioxide has been reported to result in the polymorphic transformations of small crystalline drug molecules, such as Ibuprofen, Flurbiprofen, Ketoprofen and Naproxen [53]. Thus, it was of interest to explore if polymorphic transformation of PC could be achieved in mixtures of carbon dioxide with ethanol, and explore further the extent and the nature of the polymorphic transformations of Piroxicam in mixtures of carbon dioxide with acetone and ethyl acetate. The earlier study on polymorphic transformation of PC in carbon dioxide + co-solvent mixtures [33] had not reported on the outcome from mixtures with ethanol due to high co-solvency effects observed in this mixture at the relatively low temperatures (40 ^{o}C) that were explored.

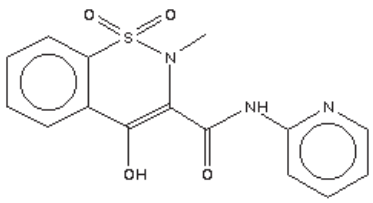

Figure 40. Chemical structure of Piroxicam

The primary goal of this research was to create a pathway for drug-CD complex formation with the drug in its molten, liquid state rather than from its solutions. Since PC was found to thermally degrade when the melting temperature was reached, a method for depressing the melting temperature was necessary. The melting point of PC was found to be depressed in the presence of carbon dioxide and mixtures with the co-solvents ethanol, acetone or ethyl acetate.

PC was further found to undergo a polymorphic transformation upon recrystallization from the liquid phase in these solutions. Finally, PC was melted while in contact with βCD in carbon dioxide and ethanol solutions to achieve complex formation. Thus, this paper reports for the first time on the melting point depression of PC, polymorphic transformations of PC when recrystallized from the liquid phase, and complex formation of PC and βCD with PC in the molten state, all in solutions of carbon dioxide and its mixtures with ethanol, acetone or ethyl acetate.

5.3 Materials and Methods

5.3.1 Materials

Piroxicam and β-cyclodextrin were purchased from Sigma and used as received. ACS reagent grade ethanol, acetone and ethyl acetate were purchased from Sigma. Carbon dioxide was supercritical fluid extraction grade and was purchased from Airgas.

5.3.2 Methods

Fourier transform infrared (FTIR) characterizations were carried out on a Digilab Excaliber HE Series FTS 3100 spectrometer using KBr disks.

Characterizations by differential scanning calorimetry (DSC) were carried out using a Pyris Diamond DSC. Sample masses of about 5 mg were placed in aluminum pans with lids and crimped before the experiments. Experiments were performed with a heating rate of 20 ^{o}C/min and a nitrogen purge at 10 ml/min.

A PANalytical X-Pert PRO x-ray diffractometer was utilized in the powder x-ray diffraction measurements.

5.3.2.1 Melting Point Depression in CO_2 and CO_2 + Co-solvent Mixtures

Melting point depression experiments were carried out in a high pressure view-cell with an internal volume of 23.0 cm^3 equipped with sapphire windows. Internal pressure and temperature were continuously monitored and recorded by computer using a flush mounted Dynisco diaphragm pressure transducer and thermocouple, respectively. The cell was first loaded with 1 g of PC and the desired amount of co-solvent, if used, and then charged with CO_2 for a total solvent mass of 12 g. CO_2 was charged from a transfer vessel to the view-cell system using a high pressure liquid pump. The mass of CO_2 charged to the view-cell was determined by mass loss from the transfer vessel using a high capacity (6100 g) balance with 0.01 g accuracy (Mettler PM6100). The vessel was heated by four symmetrically positioned 65 Watt cartridge heaters at a rate of about 1 ^oC/min and pressure was allowed to increase with temperature in constant volume experiments. The melting temperature was recorded as the temperature at which all of the drug was in the liquid phase, which was visually observed as the point at which an immiscible liquid drug layer appeared at the bottom of the view-cell. After cooling to room temperature, the system was discharged and the collected sample was dried under vacuum at 80 ^oC to remove residual solvent.

5.3.2.2 High Pressure Complex Formation in CO_2 + Ethanol

The same high pressure view-cell system used in the melting point depression experiments was employed in the high pressure complex formation experiments. 500 mg of a 1:1 molar ratio physical mixture of βCD:PC and the desired amount of co-solvent were added to the cell. The vessel was then charged with CO_2 for a total solvent mass of 12 g and then heated to the melting point of PC and held there for 1.5 h. Pressure was allowed to increase with temperature. The mixture was magnetically stirred throughout the 1.5 h exposure. The heaters were turned off and the vessel was then allowed to gradually cool to room temperature while mixing the sample. The sample was collected after depressurizing and was dried under vacuum at 80 ^{o}C to remove any remaining co-solvent.

5.4 Results

5.4.1 Melting Point Depression of Piroxicam in CO_2 and CO_2 + Co-solvent Mixtures

Melting point depression experiments with PC were carried out with pure CO_2 as the solvent, as well as with mixtures of CO_2 with ethanol, acetone or ethyl acetate as co-solvents at 5 wt % and 10 wt % co-solvent levels. The results are shown in Table 12 and Figure 41. A melting point depression of 17 ^{o}C was observed in pure CO_2 at 35 MPa. The melting point was further reduced with the addition of a co-solvent. The highest melting point depression was obtained with a 90:10 wt % CO_2:Ethanol mixture, which decreased the melting point by 37 ^{o}C to 163 ^{o}C at 29 MPa. Acetone decreased the melting point of PC to a lesser extent. The addition of ethyl acetate to CO_2 solutions did not lower the melting point beyond the melting point in pure CO_2 (183 ^{o}C). Literature data on the solubility of Piroxicam in mixtures of ethanol, acetone or ethyl acetate in carbon dioxide is limited. The values that are reported are at low temperatures, but

indicate strong co-solvency in carbon dioxide + ethanol mixtures [215]. Even though the exact reason for the higher melting point depression in ethanol is not known at present, the data suggests that melting point depression is promoted in solvent mixtures with the component of higher polarity and is improved by the effect of co-solvency in CO_2-ethanol mixtures.

Table 12. Piroxicam melting conditions in CO_2 and CO_2 + co-solvent mixtures.

Sample	T_{melt}, °C	P, MPa
Unprocessed	200	Ambient
Carbon Dioxide	183	35
95:5 wt% CO_2:Ethanol	176	41
90:10 wt% CO_2:Ethanol	163	29
95:5 wt% CO_2:Acetone	179	22
90:10 wt% CO_2:Acetone	172	23
95:5 wt% CO_2:Ethyl acetate	183	23
90:10 wt% CO_2:Ethyl acetate	182	22

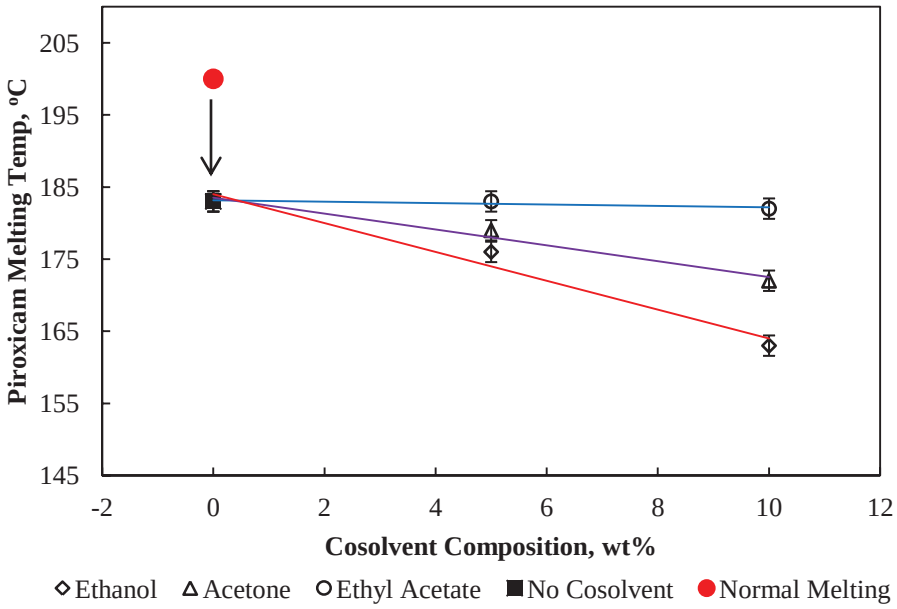

Figure 41. Melting behavior of Piroxicam in pure CO_2 and CO_2 + co-solvent mixtures with ethanol, acetone or ethyl acetate; error bars represent one standard deviation based on four melting point depression experiments in CO_2

PC as received has a slightly yellow or off-white color. When PC undergoes thermal degradation the color darkens, changing from yellow to brown and eventually turning black. Some color change indicative of thermal degradation was observed after the melting point depression experiments, and the extent of the change was dependent on the fluid mixture used in the experiment. The color change was the lowest in samples obtained from mixtures in which the melting temperature of PC was the lowest. More specifically, the color of PC recovered from melting in pure CO_2 had changed from off-white/yellow to brown, while PC recovered from melting in 90:10 wt% CO_2:Ethanol solutions did not show any noticeable change. The absence of color change in carbon dioxide + ethanol mixture is a strong indicator that in this mixture, melting was being achieved at a low enough temperature to avoid the onset of thermal

degradation, and could therefore be employed in melt processing of PC in complex formation experiments. The absence of thermal degradation was confirmed by FTIR characterization as well.

5.4.2 Polymorphic Transformations

Figure 42-Figure 44 show the FTIR spectra, the DSC scans and the XRD patterns, respectively, of the unprocessed PC, PC after melting in pure CO_2, and PC melted in 90:10 wt % CO_2:co-solvent mixtures. Based on the DSC and FTIR data which are summarized in Table 13, the PC as received was characterized as the cubic, β crystal form. However, melting of PC in CO_2 and CO_2 + co-solvent mixtures all resulted in recrystallization of PC into the needle, α crystal form.

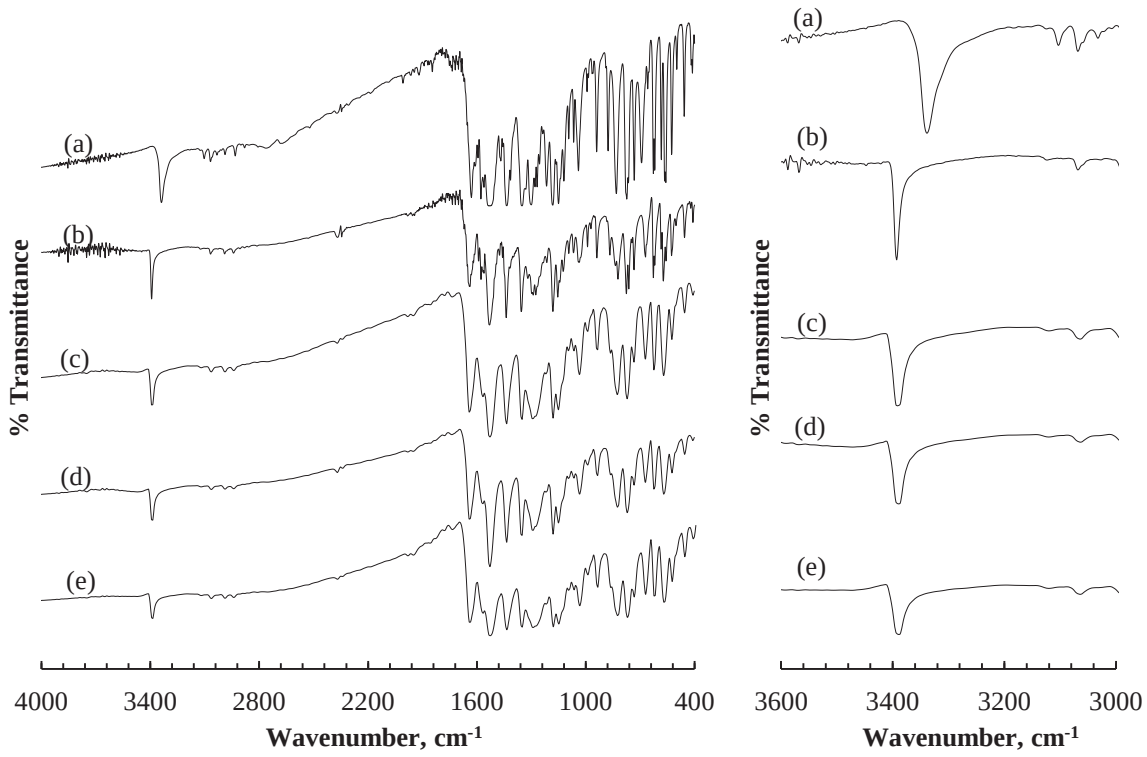

Figure 42. FTIR spectra of Piroxicam over the full range (left) and in the expanded range from 3600 to 3000 cm^{-1} (right) (a) as received, and after melting in (b) CO_2, (c) 90:10 wt% CO_2:Ethanol, (d) 90:10 wt% CO_2:Acetone, (e) 90:10 wt% CO_2:Ethyl Acetate

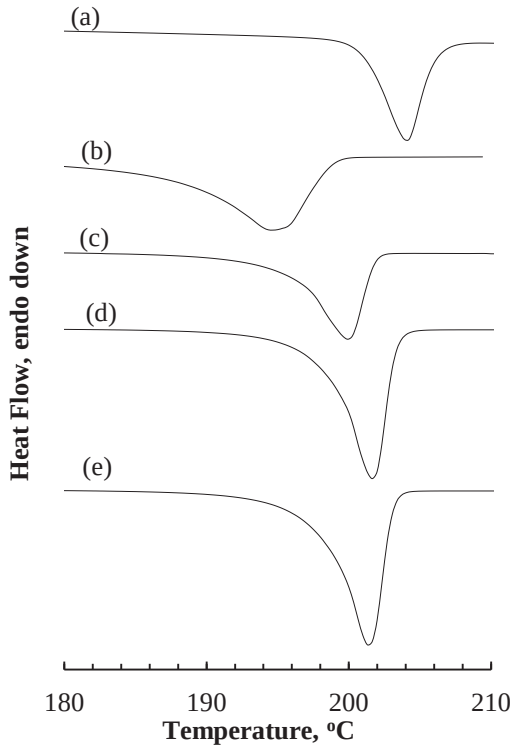

Figure 43. DSC heating scans of Piroxicam (a) as received, and after melting in (b) CO_2, (c) 90:10 wt% CO_2:Ethanol, (d) 90:10 wt% CO_2:Acetone, (e) 90:10 wt% CO_2:Ethyl Acetate

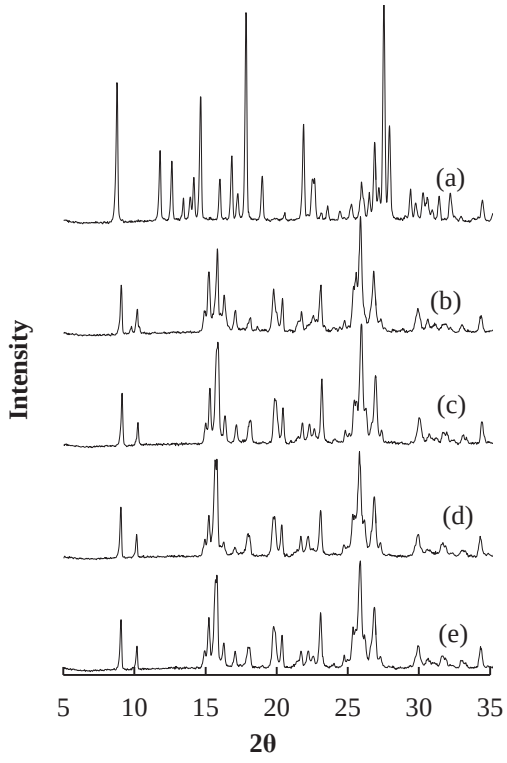

Figure 44. XRD patterns of Piroxicam (a) as received, and after melting in (b) CO_2, (c) 90:10 wt% CO_2:Ethanol, (d) 90:10 wt% CO_2:Acetone, (e) 90:10 wt% CO_2:Ethyl Acetate

Table 13. Summary of Piroxicam characterization data from FTIR [Figure 42] and DSC [Figure 43] experiments.

Sample	T_m, °C	ΔH_m, J/g	-NH- peak , cm^{-1}	Crystal Form
Reported [30]	202.6	110.28	3341	β-cubic
Reported [30]	199.7	112.96	3393	α-needle
Unprocessed PC	200	103	3338	β-cubic
PC - CO_2	194.7	84.7	3393	α-needle
PC - CO_2 - ethanol	199.9	98.6	3391	α-needle
PC - CO_2 - acetone	201.7	104.2	3390	α-needle
PC - CO_2 - ethyl acetate	201.3	105.4	3390	α-needle

The FTIR data show distinct differences between the unprocessed PC, the PC melted in CO_2 and the PC melted in CO_2 + co-solvent mixtures. The main differences are observed from 3400 to 3300 cm^{-1}, where the -NH- band is found. In the unprocessed PC, the peak is seen at 3339 cm^{-1}, which is typical for the β crystal. However, in the melted samples the peak is seen at about 3393 cm^{-1}, which is typical for the α crystal form. The -NH- peak shifts due to the differences in hydrogen bonding in the two crystal forms. The DSC data show that the melting temperature and the heat of melting for PC recrystallized after melting in pure CO_2 were significantly lower than the values obtained for unprocessed PC and for PC recrystallized after melting in CO_2 + co-solvent mixtures. The difference is likely due to thermal degradation which may have occurred upon melting of PC in pure CO_2, which, as indicated earlier, had shown some color change. The extent of degradation is by no means extensive as the XRD patterns show that the material still retains crystallinity.

The XRD patterns that are shown in Figure 44 correspond to the XRD patterns for the α and β crystal forms reported in the literature [211]. The main peaks for the β crystal form are seen in the unprocessed PC at 2θ values of 8.8, 11.8, 12.7, 14.7, 16.0, 16.8, 17.9, 19.0, 21.9, 26.9, 27.5, and 27.9^{o}. The peaks for the PC samples melted in CO_2 and all CO_2 + co-solvent mixtures displayed XRD patterns which were distinctly different from the unprocessed PC with main peaks at 2θ values of 9.1, 10.2, 15.2, 15.8, 23.2, 25.9 and 26.8^{o}. The diffraction patterns of the PC samples melted in CO_2 and CO_2 + co-solvent mixtures are consistent with the reported diffraction pattern of the α crystal form.

5.4.3 Liquid State High Pressure Complex Formation

High pressure complex formation experiments with PC and βCD were performed in a 90:10 wt% CO_2:Ethanol fluid mixture at 29 MPa. In melting point depression experiments PC was found to be melted in this mixture at 163 ^oC with a heating rate of 1 ^oC/min. However, longer exposure times at 163 ^oC led to thermal degradation of PC. Thus, a lower exposure temperature of 160 ^oC was used in which PC was found to melt after a 45 minute exposure time, which is equivalent to a much lower rate of heating. Due to the kinetic nature of melting, lower melting points are expected from lower heating rates. Although optimization of the exposure time for complex formation efficiency was not performed in this study, temperature and exposure time were chosen such that PC would be in the molten state without thermal degradation. Thus, the high pressure complex formation experiment was performed at 160 ^oC and 29 MPa with a 1.5 h exposure time. Figure 45-Figure 47 show the FTIR, DSC and XRD results, respectively, for the βCD-PC product. Both βCD and PC key peaks are observed in the FTIR spectrum. The product spectrum appears to be nearly identical to pure βCD, with the exception of a few PC peaks, which are seen at 1529 and 1352 cm^{-1}, indicative of the R-CO-NHR stretch and the asymmetric O=S=O stretch, respectively, in the PC molecule. The DSC heating scan of the complex which is shown in Figure 46 displayed a small endothermic peak at 192 ^oC with a heat of 20.2 J/g-PC. This peak indicates the presence of a small amount of crystalline, uncomplexed PC being present in the sample. PC melted in a 90:10 wt% CO_2:Ethanol fluid mixture has a heat of melting of about 98.6 J/g, which indicates a complex formation efficiency of 80 % by this process. The XRD pattern of the product, when compared with that of the pure components, does not represent the crystallographic orientation of either pure compound, but contains new XRD peaks. The new peaks can be attributed to a new crystalline form arising from the crystallization of the

inclusion complex. New crystalline forms have been previously reported also for inclusion complex formation between crystalline guests, such as Ibuprofen and Flurbiprofen, with the crystalline cyclodextrin, 2, 3, 6-tri-*O*-methyl-βCD **[53]**.

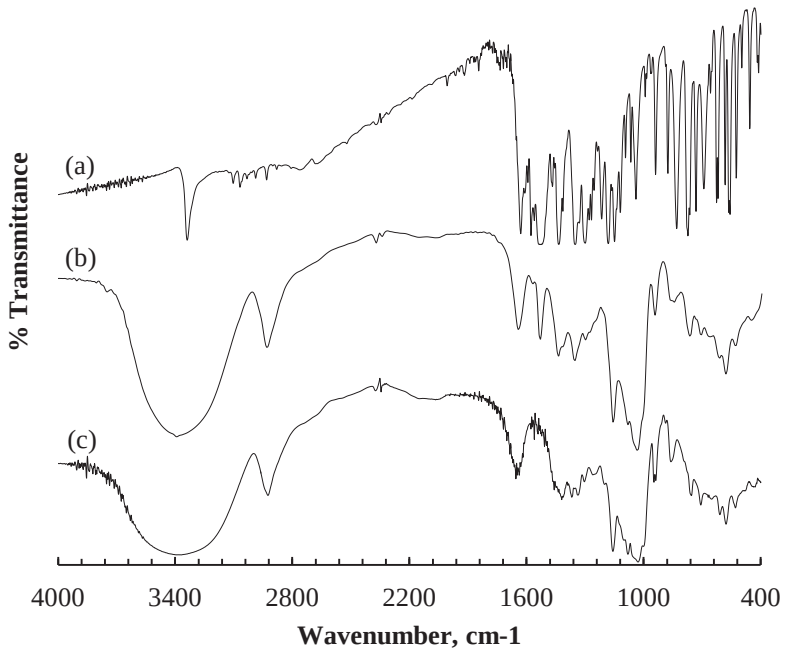

Figure 45. FTIR spectra of (a) Piroxicam, as received, (b) 1:1 molar ratio β-cyclodextrin:Piroxicam exposed to 90:10 wt% CO_2:Ethanol at 160 ^oC for 1.5 hours, (c) β-cyclodextrin, as received

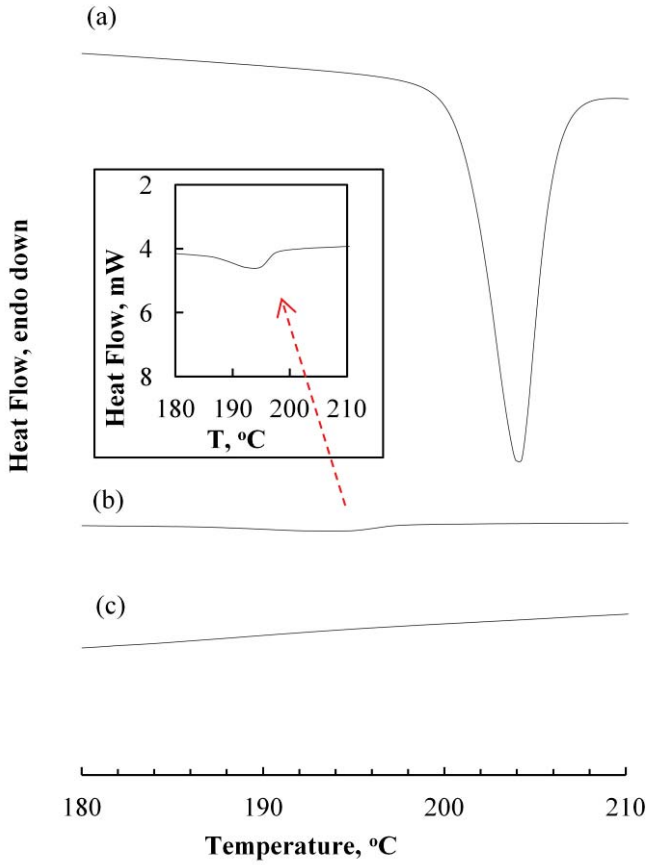

Figure 46. DSC heating scans of (a) Piroxicam, as received, (b) 1:1 molar ratio β-cyclodextrin:Piroxicam exposed to 90:10 wt% CO_2:Ethanol at 160 ^{o}C for 1.5 hours (enlarged view in the box), (c) β-cyclodextrin, as received

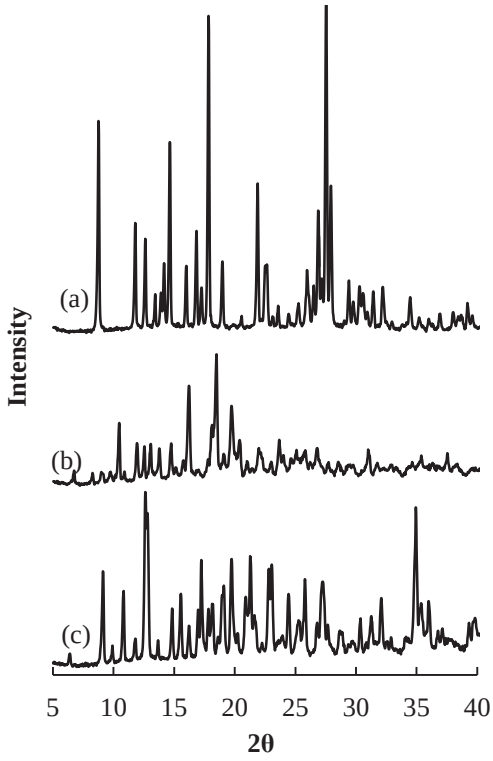

Figure 47. XRD patterns for (a) Piroxicam, as received, (b) 1:1 molar ratio β-cyclodextrin:Piroxicam exposed to 90:10 wt% CO_2:Ethanol at 160 ^oC for 1.5 hours, (c) β-cyclodextrin, as received

These evaluations of the thermal, spectral and x-ray characterizations confirm that the βCD-PC physical mixture was converted to an inclusion complex via melting of PC in a 90:10 wt% CO_2:Ethanol fluid mixture at 160 ^oC over an exposure time of 1.5 h that was explored.

5.5 Conclusions

This study has shown that the melting point of Piroxicam can be significantly depressed in CO_2 or mixtures of CO_2 with a co-solvent such as ethanol, acetone or ethyl acetate. Ethanol as a co-solvent was observed to lead to the largest melting point depression without leading to any

thermal degradation, while ethyl acetate as a co-solvent provided no further melting point depression beyond what was observed in pure CO_2. In addition, melting in CO_2 and CO_2 + co-solvent mixtures resulted in a polymorphic transformation of PC from the β crystal form to the α crystal form. Finally, melting point depression was shown to provide a new pathway for efficient inclusion complex formation of βCD:PC which was promoted by PC melting.

Acknowledgements

This research was funded by the National Science Foundation (Award # CBET 0929978).

Chapter VI. High Pressure Density, Miscibility and Compressibility of Poly(lactide-*co*-glycolide) Solutions in Acetone and Acetone + CO_2 Binary Fluid Mixtures[3]

6.1 Abstract

High pressure density, miscibility and compressibility of poly(lactide-*co*-glycolide) (PLGA) solutions in acetone and in acetone + CO_2 mixtures were determined at 75, 100, 125 and 150 ^oC at pressures up to 400 bar. The experiments were carried out in a special variable-volume view-cell system which permits continuous real-time monitoring of the pressure, temperature, transmitted light intensity, and the position of a movable piston which allows continuous determination of the cell internal volume and, thus the solution density, as pressure is altered. The liquid-liquid (LL) phase boundaries are assessed from the variation of transmitted light intensity with pressure while the liquid-vapor (LV) or liquid-liquid-vapor (LLV) phase boundaries are assessed from the variation of density with pressure as, upon formation of vapor phase, the density shows an abrupt decrease and varies without a further change in pressure. Isothermal compressibilities are also evaluated from the variation of density with pressure by generating functional correlations of density with pressure. Data are reported for the PLGA:Acetone:CO_2 compositions with the ratios (in wt%) of 0:89:11, 5:84.5:10.5, 10:85:5, 10:80:10 and 10:90:0. The observations of phase boundaries, densities and the compressibilities are discussed in terms of the effect of varying the polymer concentration while maintaining the

[3] Reproduced with permission from Elsevier. Copyright 2013. *H. Grandelli, E. Kiran, The Journal of Supercritical Fluids 75 (2013) 159-171*.

CO_2:acetone ratio the same, or by varying the CO_2:acetone ratio and maintaining the polymer concentration unchanged. These LL boundaries display lower solution temperature (LCST) behavior, and the densities and compressibilities display the complexities of the relative extent of the association of carbon dioxide with polymer versus acetone.

6.2 Introduction

Poly(DL-lactide-co-glycolide) (PLGA), -[(CH_3)CH-COO]$_m$-[CH_2-COO]$_n$-, is a biodegradable polyester which is of significance in tissue engineering and drug delivery applications. Processing of these polymers in supercritical fluids such as CO_2 is of continuing interest due to the non-toxicity of CO_2 and the potential it offers for the development of matrices with desirable drug release characteristics, or microstructured features for cell attachment and proliferation for tissue regeneration [5, 28-32, 152, 161, 167, 176, 177, 218-224].

Despite the attractiveness of carbon dioxide being a benign processing fluid, the solubility of polymers, especially of PLGA in pure carbon dioxide is low [10, 224, 225]. Indeed, the data reported in the literature shows that even for 5 wt% solutions of PLGA with 85:15; 75:25, and 65:35 lactide:glycolide ratios, pressures above about 1800, 2000, and 3000 bar, respectively, are required to achieve miscibility with pressures becoming higher with increasing glycolide content in the copolymer [10, 225]. Miscibility of polylactide, corresponding to the limiting composition with no glycolide content, still requires pressures above about 1400 bar. The solutions of PLGA in CO_2 show upper critical solution temperature (UCST) type behavior which is in contrast to the LCST type behavior observed in the PLA + CO_2 system. The UCST-type behavior in PLGA solutions has been interpreted as suggesting that the exchange energy is weighed more toward

polymer-polymer interactions rather than cross interactions [10, 225]. Exchange energy is a measure of the difference between the "polymer-CO_2" cross-interactions relative to the "polymer-polymer" and "CO_2-CO_2" like-like interactions and, in the regular solution theory or in the original Flory-Huggins solution theory, that predict only UCST type behavior, like-like interactions are indeed greater than the cross interactions. However, a later publication in which FTIR measurements were carried out to identify the spectral shifts resulting from absorption of CO_2 into films made of different polymers including poly(methyl methacrylate) (PMMA) and the PLGA copolymers with the same compositions [223] reported the presence of a weak specific interaction between CO_2 and PLGA similar to those observed in CO_2 + PMMA. Model descriptions based on a modified lattice theory that accounts for complex formation between a polymer segment and μ number of molecules of solvent S according to $P + \mu S \leftrightarrow PS_\mu$ were then shown to be effective in describing the phase boundaries for these PLGA + CO_2 systems [223, 226].

Miscibility pressures can be reduced by changing the fluid from CO_2 to other supercritical chlorinated or fluorinated solvents, such as trifluoromethane (CHF_3), chlorodifluoromethane ($CHClF_2$), dichloromethane (CH_2Cl_2) and chloroform ($CHCl_3$) [10, 224, 225, 227, 228]. The reductions are especially significant in chlorinated solvents. An alternative approach to lower miscibility pressures is to use mixtures of CO_2 with organic solvents, such as acetone, which is the approach taken in the current study. Use of binary fluid mixtures provides flexibilities in tuning the miscibility conditions and solution properties with pressure or temperature using the solvent composition as an additional coordinate. Mixtures of CO_2 with acetone as solvents for polymers with carbonyl groups presents an additional feature in that CO_2 can interact and

associate with both the carbonyl group of acetone and the carbonyl groups of the polymer chain. The relative extent of such interactions may vary with prevailing pressure or temperature conditions and the relative concentrations of the components. These interactions not only alter the miscibility pressures, but also influence the overall properties of the solutions with respect to density and/or compressibilities.

The interactions of CO_2 with polymers is traditionally explored with FTIR measurements of the shifts in the carbonyl [-C=O] absorption band in the presence of CO_2 as a function of pressure [229-231]. Shifts arise from the weak acid-base interactions between the carbon on CO_2 and the carbonyl group in the polymer [232]. The frequency of the vibration of the carbonyl group is reduced, shifting the wavenumber to higher values. However, shifts in the carbonyl stretching frequencies are not free of complications, as these shifts may be affected by other factors such as dielectric effects [231, 233]. Changes in the absorption bands associated with the bending mode of CO_2 , specifically the splitting in the in-plane bending mode, have been used to more reliably distinguish the "free" CO_2 versus CO_2 that is associated with the polymer and, thus, to quantify the strength of the specific interactions between CO_2 and the polymer carbonyl groups [231]. It is also noted that free-volume effects, which are ultimately linked to density, must also be taken into account [233]. The wavenumber shift of the carbonyl band in CO_2-exposed polymers reaches a limit at higher pressures obtained from higher CO_2 loading due to increased mobility of CO_2, which is interpreted as being a result of an increased number of CO_2-CO_2 interactions competing with CO_2-carbonyl interactions [230].

Interactions of CO_2 with acetone have also been addressed in the literature [234-236]. Publications based on *ab initio* calculations and Raman studies conducted at pressures up to about 8 MPa report that CO_2 interacts with acetone leading to the formation of an "Acetone-CO_2" 1:1 electron donor-acceptor complex [236, 237], where the carbon atom in CO_2 is the electron acceptor center, and the oxygen atom of the carbonyl group is the electron donor center. Splitting of the CO_2 bending vibration was taken as a spectral signature of complex formation. A recent study [235] based on FTIR experiments conducted at 50 ^oC at pressures up to 22 MPa indicates that at pressures above 8.5 MPa, the stoichiometry of the complex changes to "Acetone-$(CO_2)_2$". This was interpreted as being related to the compressibility of CO_2, and that at higher pressures the complex of two CO_2 molecules interacting with one acetone molecule becomes the preferred conformer.

The changes in the extent of interactions between CO_2 and acetone were considered in describing the trends observed in excess volume behavior in mixtures containing 10, 25, 50 and 75 wt% carbon dioxide [238]. The data were indicative of mixtures with high CO_2 content being more sensitive to pressure, whereas mixtures with high acetone concentration were more sensitive to temperature. In another study in which densities and compressibilities were investigated in solutions of poly(ε-caprolactone) (PCL) in acetone + CO_2, the observations could be interpreted if one were to assume that CO_2-acetone and CO_2-PCL interactions would both decrease with temperature but with a higher rate of decrease in CO_2-PCL interactions leading to the release of some of the "bound" CO_2. It was further assumed that at lower temperatures CO_2-PCL interactions were stronger than CO_2-acetone interactions but became less favored above a cross-

over temperature around 125 ^{o}C. The increase in "free" CO_2 would then lead to an increase in the isothermal compressibility in the solution.

In these earlier studies with "acetone + CO_2" and "PCL + acetone + CO_2" density data were limited, as the measurements were single point measurements conducted at selected pressure conditions at each temperature. An approach for continuous density measurements, which employs a long stroke-length linear variable differential transformer (LVDT) to monitor the position of a movable piston in a variable-volume view cell [239], was recently revitalized in our laboratory in a comprehensive study of the volumetric properties of mixtures of ethyl acetate + CO_2 [240]. The real-time continuous measurement of density as a function of pressure or temperature provides functional descriptions of the pressure/temperature dependence of density, allowing the quantification of thermodynamic parameters, such as compressibility and, in the case of mixtures, the precise assessment of the conditions for LV or LLV phase boundaries.

In the present study, we have explored the miscibility of PLGA in acetone (which is a solvent that is Generally Recognized as Safe (GRAS) by the Food and Drug Administration) and acetone + CO_2 fluid mixtures. This is within the broad program in which binary fluid mixtures of CO_2 with organic solvents such as acetone are being evaluated in our laboratory for their utility in processing of polymers for biomedical applications. In prior publications, we reported on the high pressure volumetric and other physical properties, such as viscosity, of acetone + CO_2 mixtures [11, 238], as well as on the miscibility and foaming of poly(L-lactic acid) [32] poly(p-dioxanone) [30], and poly(ε-caprolactone-co-lactide) [31], and on the miscibility of poly(ε-caprolactone) [241, 242] and its blends with PMMA [243] in these mixtures. These polymers all have carbonyl groups in their backbone. This paper reports on the phase behavior, density and

isothermal compressibilities of PLGA + acetone + CO_2 solutions which have been evaluated at different temperatures as a function of pressure. The volumetric properties are found to show a complex dependence on temperature, pressure and composition, in addition to how the association of CO_2 with polymer may alter the free volume and chain flexibility. Therefore, continuous density profiling of the solutions and isothermal compressibilities are now explored as possible macroscopic probes that can provide further insights into the dynamics of such interactions.

6.3 Materials and Methods

6.3.1 Materials

Poly(DL-lactide-co-glycolide) (PLGA) with 50:50 lactide:glycolide ratio was purchased from Boehringer Ingelheim (Resomer RG 504 H). The weight average molecular weight and polydispersity index as determined by gel permeation chromatrography analyses conducted in our laboratory were M_w = 65,000 with a PDI = 2.02. Acetone (99.5% purity, ACS reagent grade) was purchased from Sigma. Carbon dioxide (99.8% purity) was purchased from Airgas.

6.3.2 Experimental System Description and Operational Procedures

Experiments were carried out using a high pressure variable-volume view-cell, which is illustrated in Figure 48. The system has been modified from a previously reported version of the same vessel [11], which now incorporates a long stroke-length LVDT for continuous sensing of the position of the movable piston in the variable-volume section of the view-cell, and a mounting stage for the vessel which is on a hinge that allows 90^o rotation between the vertical

position (for loading) and the horizontal position for observation of the full height of the interior of the cell across the sapphire windows. When in the upright position, the part of the cell above the sapphire window is not visible across the windows. However, when the view cell is rotated by 90^{o}, to the horizontal position, the entire cross-section of the cell interior becomes observable. The two sapphire windows allow the assessment of the phase state of the solution by either visual observations or by optical recording of transmitted light intensities. The pressure and temperature in the cell are monitored using a flush mount Dynisco diaphragm pressure transducer that also incorporates a J-type thermocouple with accuracies of 0.07 MPa and +/- 0.5 ^{o}C, respectively. Pressure, temperature, transmitted light intensity, and the piston position are continuously recorded with a dedicated computer using a data acquisition board (National Instruments) and customized software that allows recording of data at desired sampling rates (typically 0.5 s intervals). The maximum internal volume of the view cell corresponding to the piston being at its all the way out position is 23.0 cm^3. The volume is reduced by moving the piston inwards by applying pressure to the pressurizing fluid (ethanol) on the back side of the piston using the pressure generator. The volume changes are recorded with an accuracy of +/- 0.1 cm^3. From the piston position, the internal volume of the cell is determined, which then allows determination of the densities (in g/cm^3) from the initial mass loading (M, in grams) with accuracies within 1%.

In a typical experiment, the total mass loading of polymer plus the solvent mixture was maintained in the range of about 12-13 g. The view-cell is first loaded with accurately weighed amount of PLGA powder and acetone from a graduated syringe. The cell is then closed and CO_2 is charged from a pre-loaded transfer vessel by opening the inlet valve. The amount of CO_2

charged is determined from the mass loss of the transfer vessel using a high capacity (6100 g) balance with 0.01 g accuracy (Mettler PM6100). After loading, the cell is heated to the desired temperature using four symmetrically positioned heater cartridges while the solution is mixed with a magnetic stirring bar. After equilibration at a desired temperature, pressure is increased, with the aid of the pressure generator, to achieve homogeneous conditions. Pressure scans are then performed by lowering the pressure at a controlled rate while recording the pressure, temperature, piston position, and transmitted light intensity with the dedicated computer.

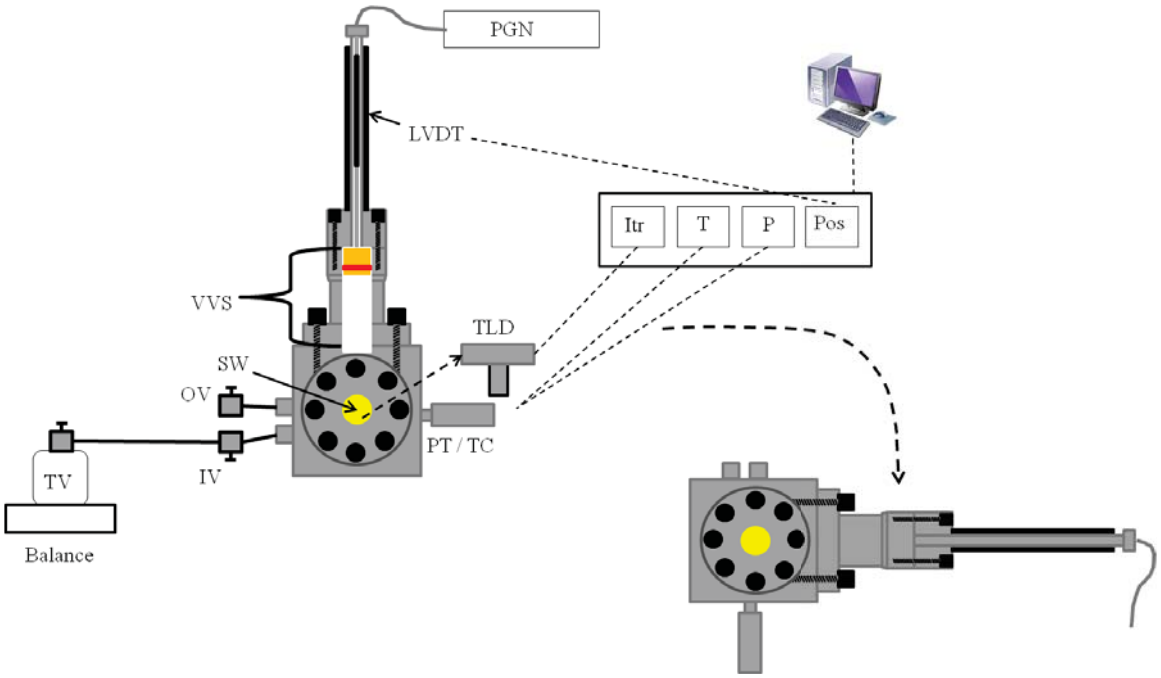

Figure 48. Schematic diagram of the view-cell system in the upright and tilted positions. PGN – pressure generator; VVS – variable volume section; TV – CO_2 transfer vessel; LVDT – linear variable differential transformer; PT/TC – pressure transducer/thermocouple; TLD – transmitted light detector; SW – sapphire windows; OV – outlet valve; IV – inlet valve; Itr – transmitted light intensity; T – temperature; P – pressure; Pos – piston position.

6.4 Results and Discussions

Miscibility conditions, densities and compressibilities were determined for PLGA:Acetone:CO_2 mixtures with 0:89:11, 5:84.5:10.5, 10:85:5, 10:80:10 and 10:90:0 wt% ratios. The experiments were conducted at 75, 100, 125 and 150 ^oC and at pressures up to 400 bar. These compositions were selected to explore (a) the effect of polymer concentration (for 0, 5 and 10 wt% polymer) while maintaining the acetone:CO_2 ratio in the solvent mixture unchanged at 89:11 wt%, and (b) the effect of CO_2 level (at 0, 5 and 10 wt%) while maintaining polymer concentration unchanged at 10 wt%.

Polymer concentrations higher than 10 wt% presented difficulties in mixing with the stir bar; and CO_2 levels higher than 10 wt% presented difficulties in achieving homogeneous conditions at 400 bar at the temperatures under investigation. The results are discussed below in two parts, first addressing the effect of polymer concentration, and then the effect of the CO_2 content.

6.4.1 Effect of Varying Polymer Concentration in the Same Solvent Mixture

6.4.1.1 Densities

Density profiles were generated starting from homogeneous liquid conditions at 400 bar and reducing the pressure at a rate of about 1.75 bar/s while recording the piston position at 0.5 s intervals. The results are shown in Figure 49 & Figure 50.

Figure 49 shows the density profiles generated for each of the PLGA solutions in an 89:11 wt% acetone:CO_2 fluid mixture at specified temperatures. From the homogeneous liquid phase at 400 bar, density decreases with a decrease in pressure. At a certain pressure, densities undergo a

sharp change, and then any further change in density (or volume) occurs without a change in pressure. These pressures correspond to the LV phase boundary conditions for each mixture at the respective temperatures. The experimental procedure employed in the present study which generates about 1500 data points along each isotherm permits capturing these points of demarcation in density with high precision. The onset of this slope change defines the LV phase boundary. As will be discussed in the next section, the 5 and 10 wt % PLGA solutions show also a liquid-liquid phase separation at 125 and 150 ^{o}C as assessed from the changes in the transmitted light intensities. The occurrence of LL phase separation is however not discernible from the variation of density with pressure. This indicates that the differences in the densities of the polymer-lean and polymer-rich phases that form upon LL phase separation are not large. This is in contrast to LV or LLV phase separation, which is accompanied with a significant change in density. The density profiles show that the change in density becomes sharper upon appearance of a vapor phase at the higher temperatures where the vapor phase forms from the solution that has already undergone LL phase separation. At the lower temperatures of 75 and 100 ^{o}C, the solutions undergo only LV phase separation, and the density change is not as abrupt. These suggest that transition into LLV region may be a faster process and be dominated by the behavior of the polymer lean-phase which should be closer in its behavior to the solvent mixture. The sharp change in density at 125 and 150 ^{o}C is indeed similar to the manner in which density change accompanies LV phase transition in the solvent mixture itself. The dynamics of the density change at the lower temperatures (75 and 125 ^{o}C) as the liquid solution is undergoing only LV phase separation may potentially be affected by the extent of association of CO_2 with the polymer and its more gradual release to contribute to the vapor phase. In the already LL

phase separated state, the polymer lean-phase would be expected to contain the larger portion of CO_2 that is not associated with polymer and can be more readily transformed to the vapor phase. Other features of density profiles in Figure 49 are that, at a given pressure, densities are lowered at higher temperatures, which is as should be. Figure 50 compares the solutions of various PLGA concentration in an 89:11 wt% acetone:CO_2 fluid mixture at selected temperatures. Increasing polymer concentration led to an increase in overall solution density. This is normally to be expected since density of the polymer is greater than that of the solvent.

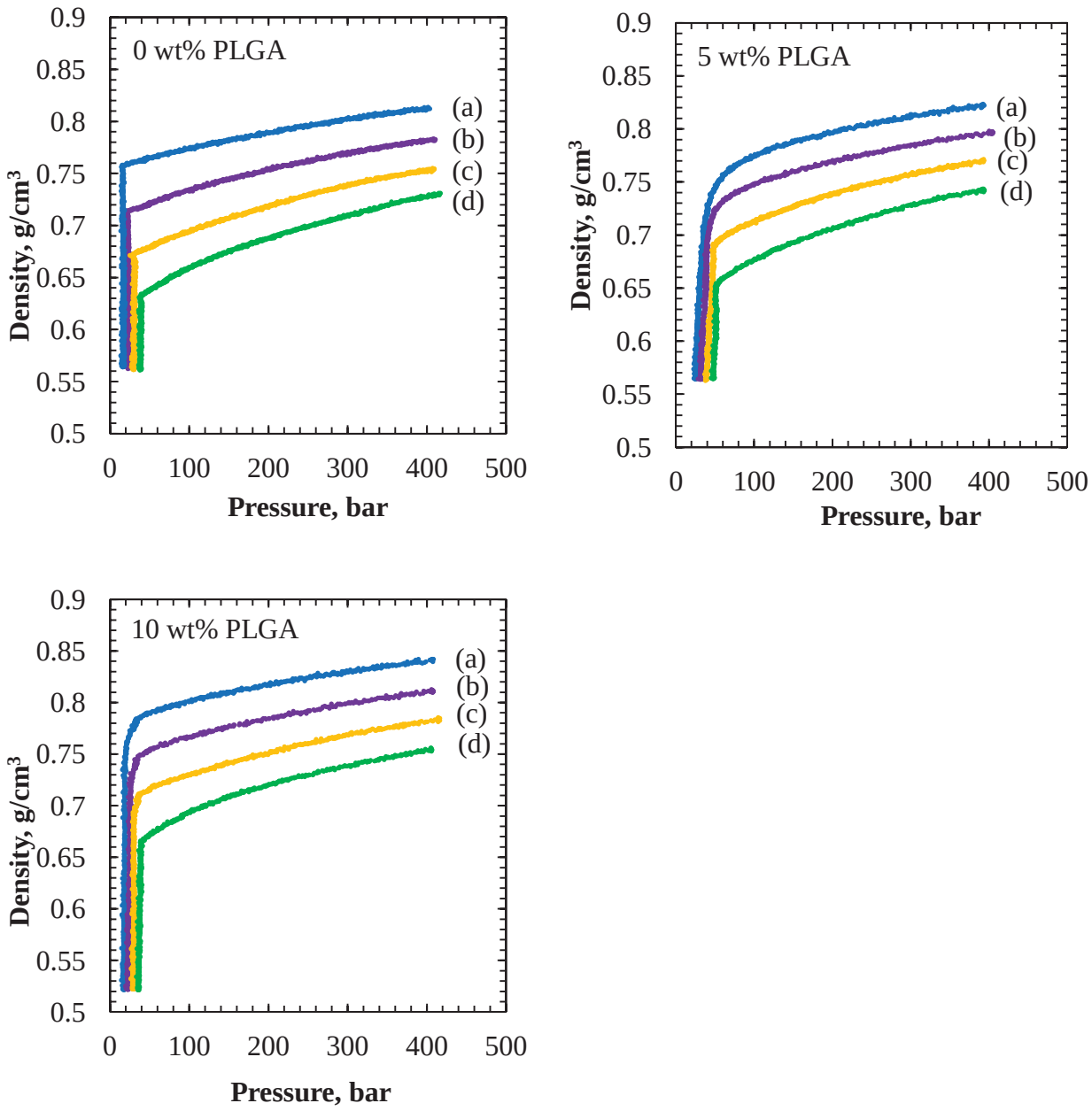

Figure 49. Density profiles for PLGA in an 89:11 wt% Acetone:CO_2 fluid mixture at (a) 75 ^{o}C, (b) 100 ^{o}C, (c) 125 ^{o}C, (d) 150 ^{o}C.

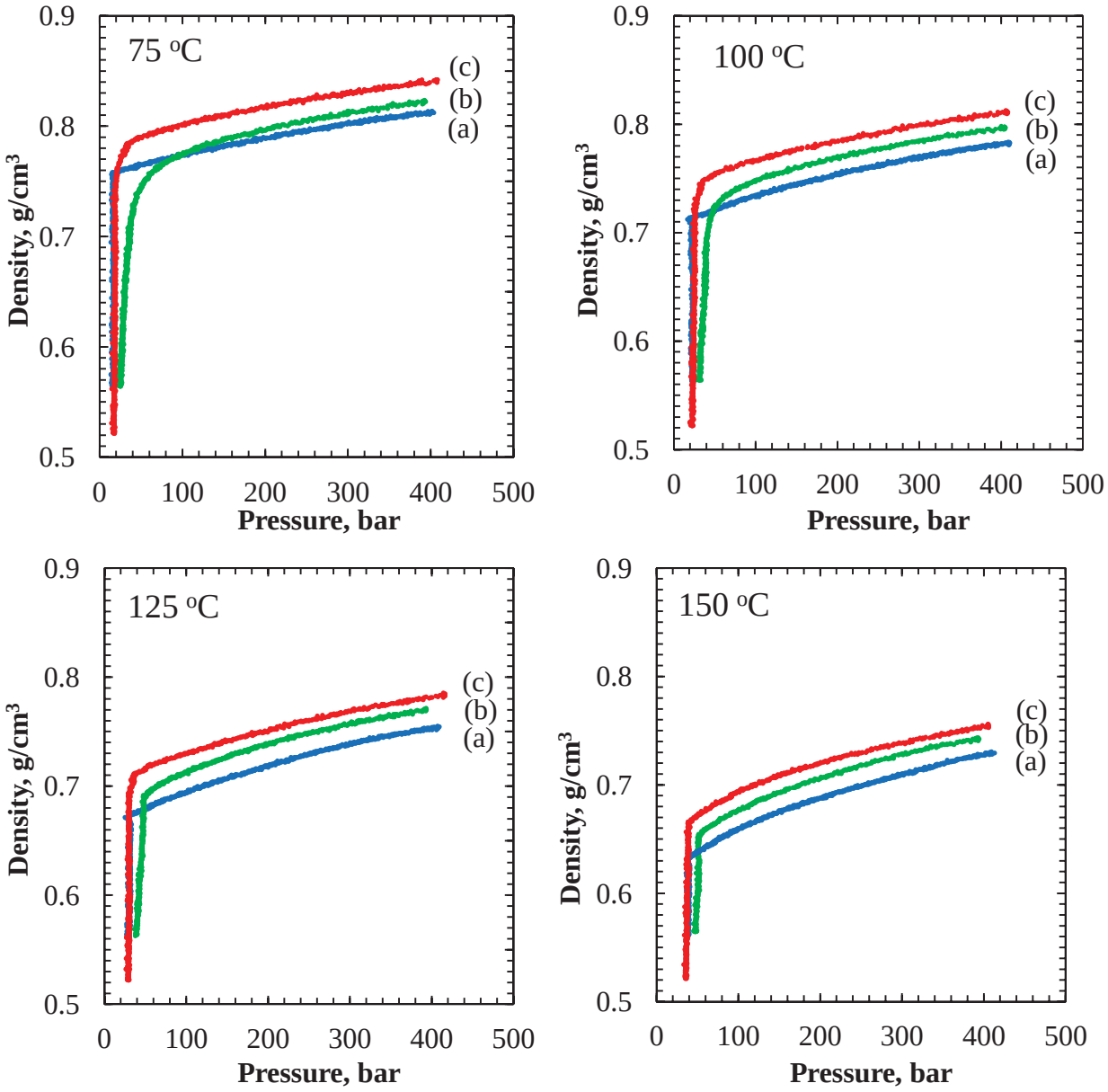

Figure 50. Density profiles for PLGA solutions in 89:11 wt% Acetone:CO_2 mixture with total solution PLGA:Acetone:CO_2 compositions of (a) 0:89:11, (b) 5:84.5:10.5, (c) 10:80:10 (wt%).

6.4.1.2 Miscibility and Liquid –Liquid Phase Separation Conditions

Figure 51 shows the variation of normalized transmitted light intensity (I/I_o) during reduction of pressure from 400 bar at 125 and 150 ^oC in 5 and 10 wt% PLGA solutions in 89:11 wt% acetone:CO_2 mixtures. The transmitted light intensities essentially go to zero when the solutions undergo LL phase separation. The LL phase separation occurs at higher pressures at higher temperatures, which is typical of systems showing LCST-type behavior. At 75 and 100 ^oC, similar experiments did not show LL phase separation. At those temperatures polymer solutions undergo only LV phase separation as captured in the density profiles shown in Figure 49. The polymer solutions at 125 and 150 ^oC display both the LL phase boundary (observed at higher pressures) and the LLV phase boundary (observed at lower pressures). The polymer-free solvent mixture remains homogeneous until the mixture crosses its LV boundary at low pressures.

Table 14 shows the LL, LV, and the LLV phase boundary pressures that have been determined from Figure 49 and Figure 51. These boundaries are show in Figure 52 in the pressure-temperature coordinates. The LCST-type behavior of the LL phase boundary in these solutions is reflected in the positive slope of the boundary, where at a given pressure increasing the temperature causes phase separation, or as temperature is increased higher pressures are required for miscibility. An interesting feature of the data in Table 14 is the observation that LV phase separation pressures in the polymer-free solvent mixture and in the 10 wt% polymer solution are very similar, but in the 5 wt% polymer solution this boundary is observed at higher pressures. This is suggestive of a lesser extent of association of CO_2 with the polymer or acetone at this lower polymer concentration, or of the presence of a greater amount of free CO_2 which may be

potentially contributing to the formation of a vapor phase without requiring as much reduction in pressure as in the other solutions.

Table 14. Summary of phase boundaries for various concentrations of PLGA in an 89:11 wt% Acetone:CO_2 solvent mixture.

		Phase Boundary, bar		
T, ^{o}C	wt% PLGA	LL	LV	LLV
75	0	-	25	-
	5	-	41	-
	10	-	21	-
100	0	-	33	-
	5	-	42	-
	10	-	28	-
125	0	-	44	-
	5	80	-	48
	10	49	-	31
150	0	-	45	-
	5	119	-	52
	10	91	-	38

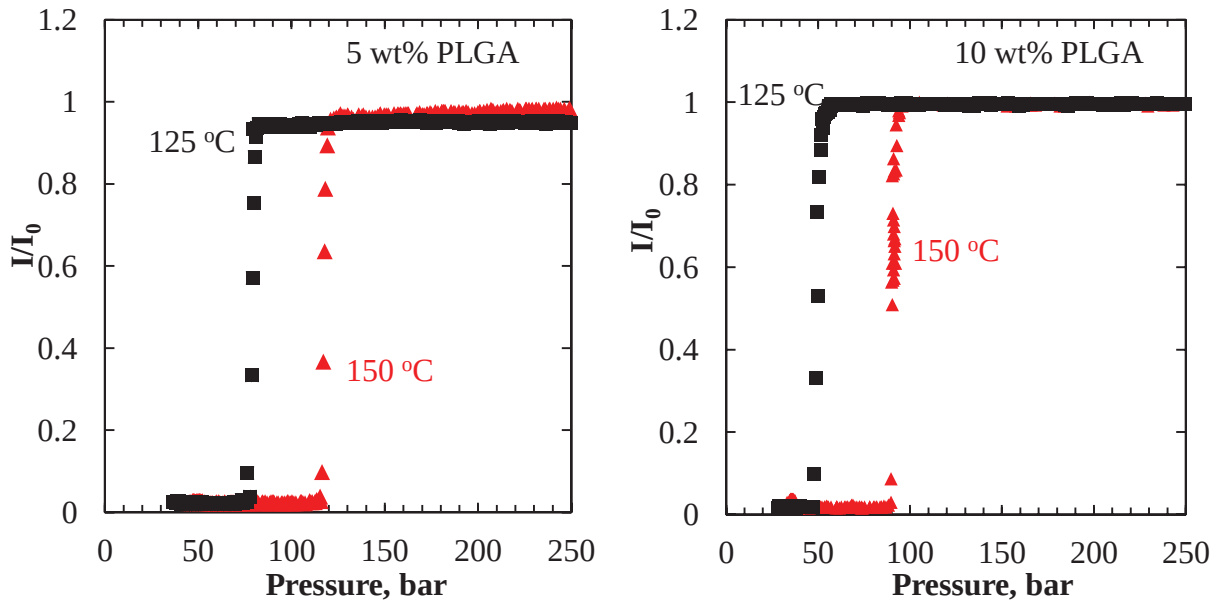

Figure 51. Transmitted light intensity as a function of pressure for determination of LL phase boundaries of PLGA in an 89:11 wt% Acetone:CO_2 fluid mixture.

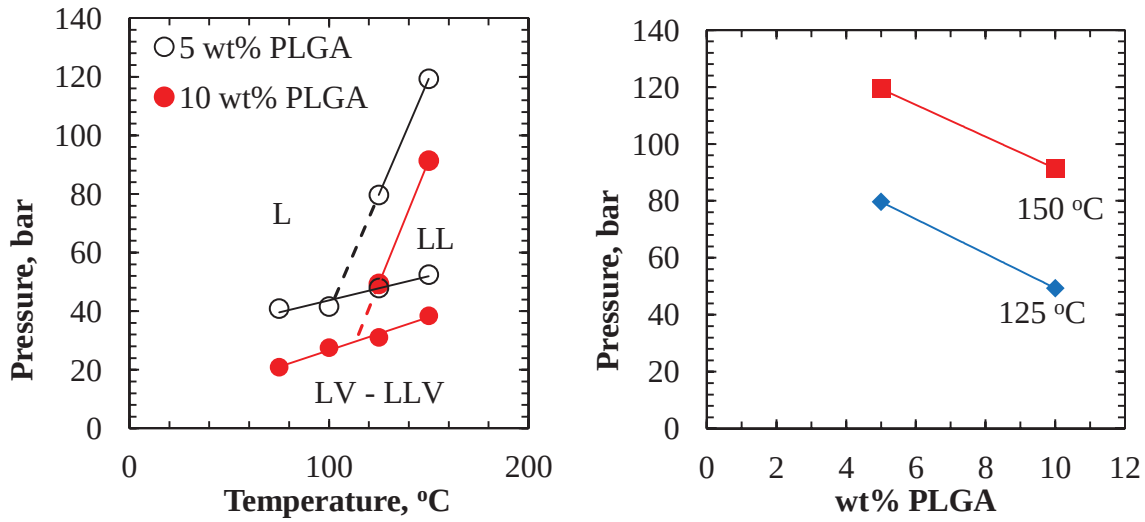

Figure 52. Phase boundaries for various concentrations of PLGA in an 89:11 wt% Acetone:CO_2 fluid mixture (left – dashed lines are extrapolations of the LL boundary) and corresponding demixing pressures at two temperatures as a function of PLGA concentration (wt%) (right).

6.4.1.3 Isothermal Compressibilities

The densities for each solution at pressures above their LV or LLV boundary have been correlated as a function of pressure and the correlations are given in Table 15. These functions have then been used in generating the isothermal compressibilities using the relationship $k_T = (1/\rho)(d\rho/dP)_T$. The results are shown in Figure 53 for the solvent and the solution with 5 and 10 wt% polymer. At a given temperature, compressibilities all decrease with pressure, which is as expected. The changes in compressibilities with temperature, however, do not show a simple trend. Even though, at a given pressure, compressibilities of all the solutions increase in going directly from 75 to 150 ^oC, this increase does not follow a regular trend at the intermediate temperatures of 100 and 125 ^oC. This is further illustrated in Figure 54 which compares the compressibilities of the solutions at each temperature.

As noted earlier and shown in Figure 50, densities of these solutions increase with polymer concentration, and therefore, other things being equal, one would anticipate that the compressibilities may decrease in going from the solvent to the solutions containing the polymer. This is in fact observed in Figure 54 when the solvent compressibilities (curves a) are compared only with the 10 wt% polymer solution (curves c). However, compressibility behavior of the 5 wt% solution (curve b) does not follow an in-between trend and becomes higher at all pressures at 125 ^oC.

As discussed in the introduction, in mixtures containing CO_2, acetone and a polymer with carbonyl groups, such as PLGA, one must be cognizant of the complex dynamics of association of CO_2 with acetone versus the carbonyl groups in polymer. As already noted, in mixtures of

acetone + CO_2, at pressures above 8.5 MPa acetone associates with two CO_2 molecules [235] and the excess volumes are more sensitive to pressure in mixtures with high CO_2 content, but more sensitive to temperature in mixtures with high acetone content [238]. The association of CO_2 with the carbonyl groups of polymers is influenced by the accessibility of the carbonyl groups and, in the case of solutions of poly(ε-caprolactone) in acetone + CO_2 mixtures, data were suggestive of CO_2-polymer interactions being stronger than CO_2-acetone interactions at lower temperatures. However, this behavior is reversed at higher temperatures leading to an increase in free "CO_2" and consequently to increased compressibilities [242]. The higher compressibilities observed at 125 ^oC in 5 wt% solution of PLGA in the present study suggests the presence of an increased fraction of "free" CO_2 in the mixture. In the previous section, it was also noted that the LV phase separation in the 5 wt% polymer solutions was observed at a slightly higher pressures, which was further suggestive of the presence of greater amount of free CO_2 in this solution.

The mechanistic reasons for lessening association of CO_2 with polymer or acetone at 125 ^oC and this lessening (if it is an outcome of temperature) being greater in the 5 wt% polymer solution is not clear. It should be however noted that the differences are relatively small. At high pressures, for example, at 400 bar range, the compressibilities of all the solutions become very close to each other and are in the range 0.5-2 $x10^{-4}$ bar^{-1}. At lower pressures, for example at 100 bar, the compressibilities are higher and are in the range 2-3 x 10^{-4} bar^{-1} at 75 and 100 ^oC. What is interesting is that these values, even though small, essentially double at 125 ^oC to a range of 4-$5x10^{-4}$ bar^{-1}, and remains at this range at 150 ^oC. Clearly, temperature is the significant factor that alters the extent of association of CO_2 with carbonyl groups in the polymer vis-a-vis acetone and promotes formation of "free" CO_2 which is more compressible. It is interesting to further

note that in a 5 wt% solution of poly(ε-caprolactone) in an essentially similar 89:11 wt% acetone:CO_2 solvent, it was also at 125 ^oC that the polymer solution was found to display compressibilities higher than that of the solvent [242], similar to the present observations. These observations strengthen the argument that CO_2-carbonyl group interactions must indeed be significantly weakened at around 125 ^oC. If more of the CO_2 is associated with polymer in the 10 wt% PLGA system than in the 5 wt% PLGA case, the formation of free CO_2 may be relatively slower, and this may be a plausible cause for the greater compressibility displayed by the 5 wt% polymer solution. The effect of relative concentration of CO_2 in the solution is further explored in the following sections.

Table 15. Density correlations for PLGA in an 89:11 wt% Acetone:CO_2 fluid mixture.

[PLGA], wt%	Temperature, ^oC	$\rho = f(P, bar)$	R^2 Value	P range, bar
0	75	$\rho = -1E\text{-}07P^2 + 0.0002P + 0.756$	0.9970	60-400
	100	$\rho = -2E\text{-}07P^2 + 0.0003P + 0.7102$	0.9983	
	125	$\rho = -2E\text{-}07P^2 + 0.0003P + 0.6649$	0.9990	
	150	$\rho = -3E\text{-}07P^2 + 0.0004P + 0.6224$	0.9980	
5	75	$\rho = -3E\text{-}07P^2 + 0.0003P + 0.746$	0.9947	80-380
	100	$\rho = -3E\text{-}07P^2 + 0.0003P + 0.721$	0.9967	
	125	$\rho = -3E\text{-}07P^2 + 0.0004P + 0.6806$	0.9982	
	150	$\rho = -4E\text{-}07P^2 + 0.0004P + 0.64$	0.9987	
10	75	$\rho = -2E\text{-}07P^2 + 0.0002P + 0.7812$	0.9953	60-400
	100	$\rho = -2E\text{-}07P^2 + 0.0002P + 0.745$	0.9966	
	125	$\rho = -2E\text{-}07P^2 + 0.0003P + 0.7041$	0.9983	
	150	$\rho = -4E\text{-}07P^2 + 0.0004P + 0.6578$	0.9969	

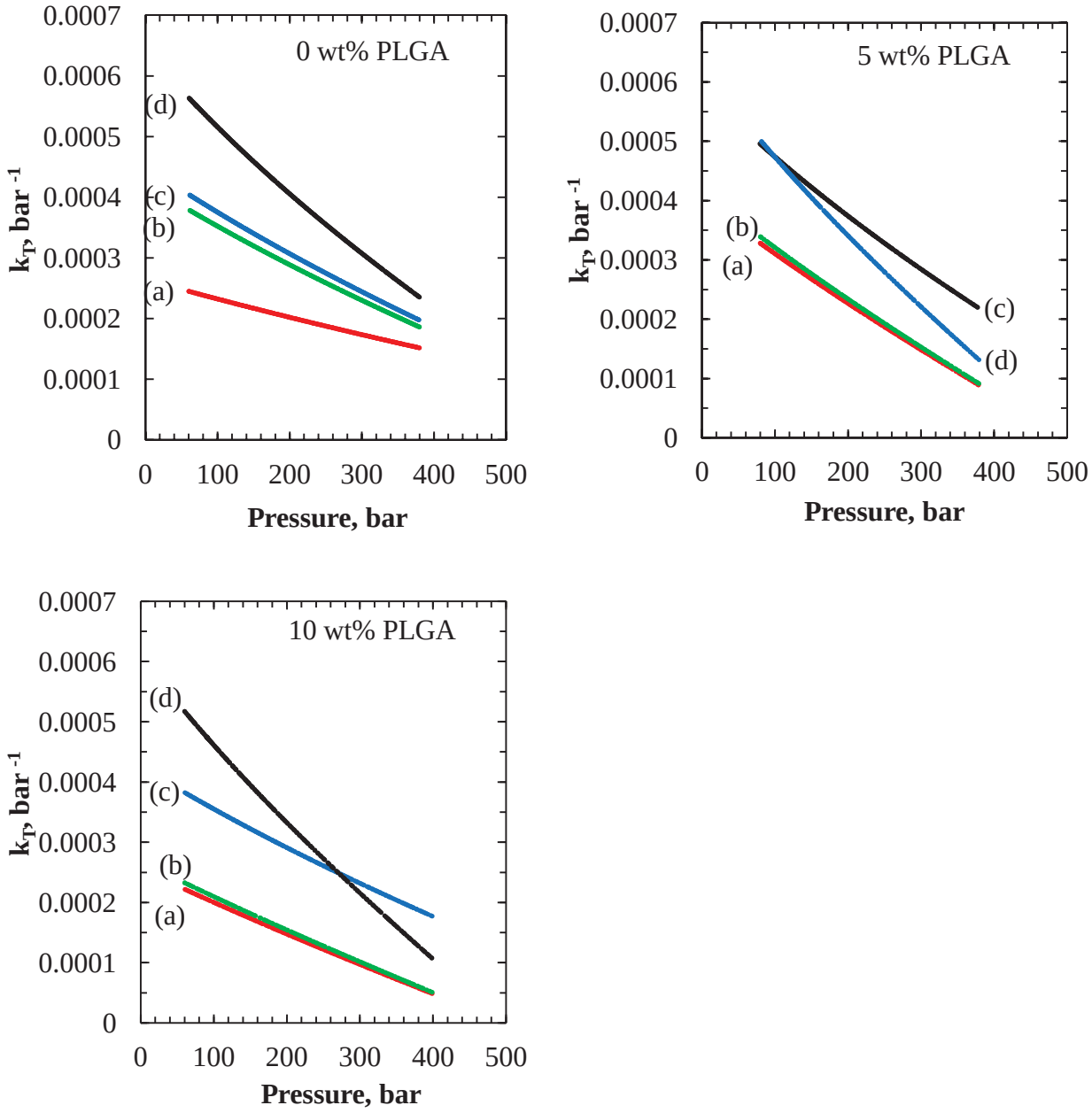

Figure 53. Isothermal compressibilities for PLGA in an 89:11 wt% Acetone:CO_2 fluid mixture at (a) 75 ^{o}C, (b) 100 ^{o}C, (c) 125 ^{o}C, (d) 150 ^{o}C.

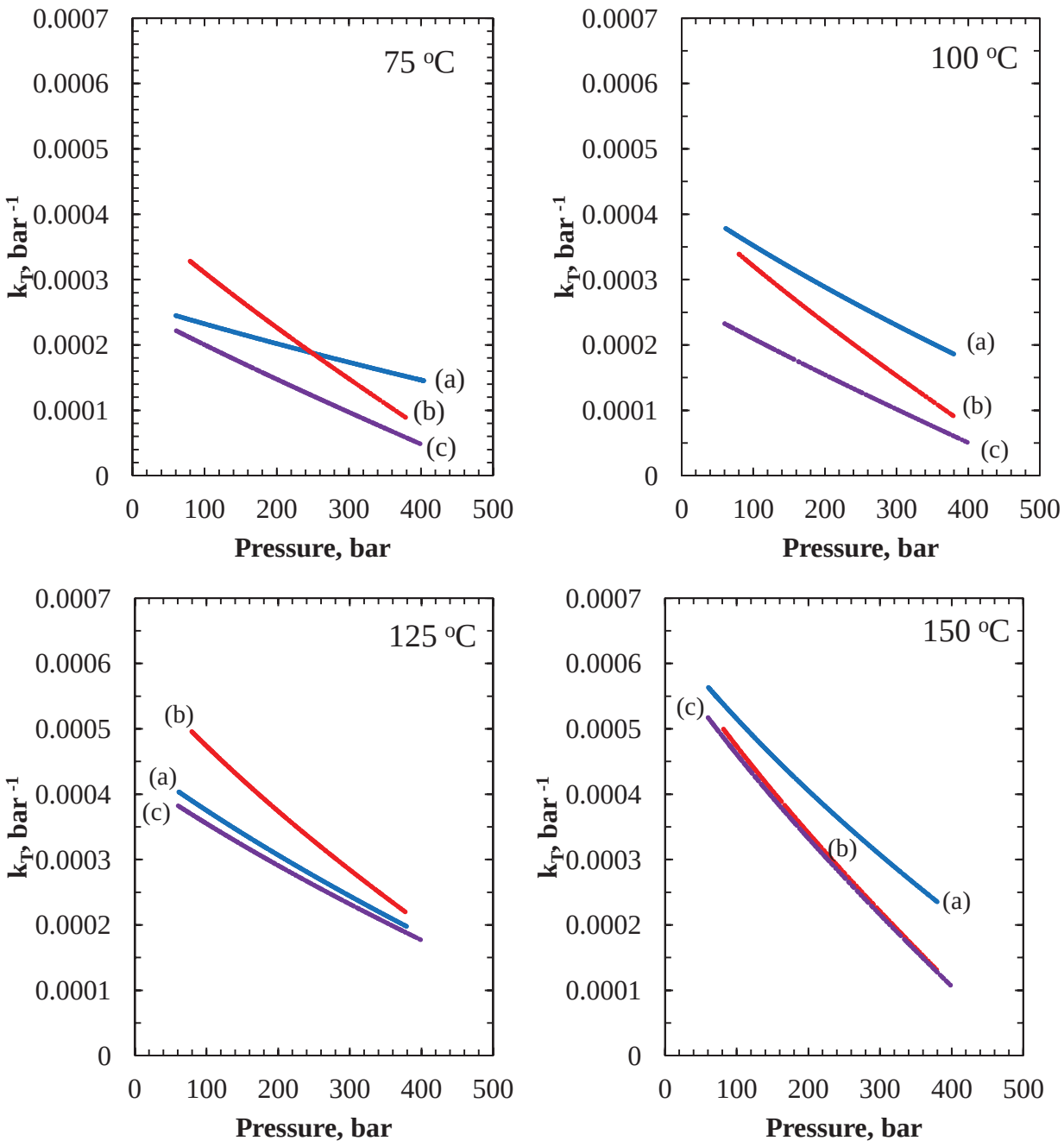

Figure 54. Compressibilities of PLGA solutions in 89:11 wt% Acetone:CO_2 with total solution PLGA:Acetone:CO_2 compositions of (a) 0:89:11, (b) 5:84.5:10.5, (c) 10:80:10 (wt%).

6.4.2 Effect of Varying CO_2 : Acetone Ratio in 10 wt% Polymer Solutions

The effect of changing the acetone:CO_2 ratio in the solvent on the miscibility, density and compressibility was explored for 10 wt% solutions of PLGA. CO_2 levels of 0, 5 and 10 wt% were examined corresponding to acetone:CO_2 ratios of 100:0; 94:4:5.6; 89:11, or the total solution compositions of 10:90:0, 10:85:5 and 10:80:10 (PLGA:Acetone:CO_2 in wt%).

6.4.2.1 Densities

Density profiles at 75, 100, 125, and 150 ^oC were again generated starting from homogeneous conditions at 400 bar, and reducing the pressure at a rate of 1.75 bars/s while recording the piston positions at 0.5 s intervals. The results are shown in Figure 55 and Figure 56. Figure 55 shows that, as expected, in each solution, densities increase with pressure and decrease with temperature.

The 0 wt% CO_2 solution remains a homogeneous liquid at all the temperatures and pressures evaluated. By increasing the mass fraction of CO_2 in the solvent mixture, densities were decreased at a given temperature. This is illustrated more explicitly in Figure 56. As shown, density reduction becomes greater at higher temperatures. This observation at first sight is against expectations since compressed CO_2 and mixtures of CO_2 + acetone at high pressures have densities higher than that of pure acetone, and, as such, polymer concentration being the same, one would anticipate higher densities upon increase in the CO_2 content. The lower densities suggest that the association of CO_2 with polymer must be reducing the packing density of the polymer chains by acting as “spacers” between chains, thereby leading to increases in total volume for the systems.

Density isotherms for the solution containing 5 wt% CO_2 display the sharp change in the density at low pressures when the vapor phase appears. As will be shown in the next section, this solution does not undergo a prior LL phase separation during pressure reduction, and the pressures where the sharp change in the density occurs represent the LV phase boundaries for this solution at the respective temperatures. The LV transitions are very sharp, similar to acetone + CO_2 mixtures without polymer, shown in Figure 49. The rapid appearance of the vapor phase in these solutions suggests that CO_2 is mostly associated with acetone at this level of addition. The behavior of the solution with 10 wt% CO_2 has already been discussed in Section 6.3.1 and shown in Figure 49. Here the large changes in the density are associated with LLV phase transition at 125 and 150 ^{o}C, and with the LV phase transition at 75 and 100 ^{o}C. In this solution, it is the LLV transition that shows itself with a more abrupt change in density, which is interpreted as reflecting the behavior of the polymer-lean phase.

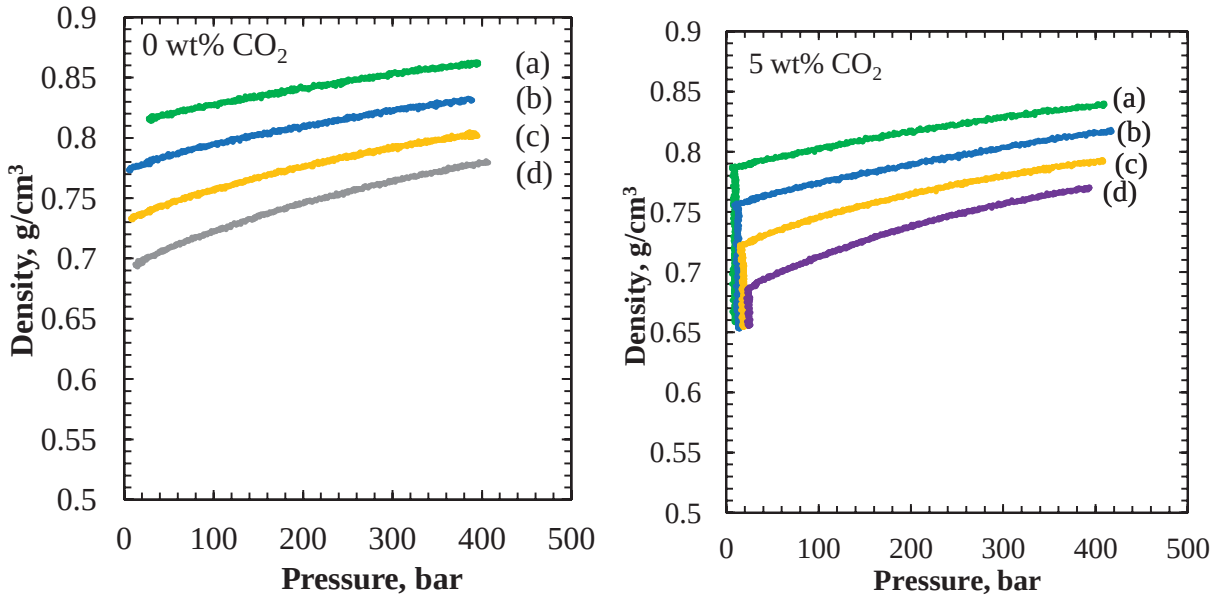

Figure 55. Density data for 10 wt% PLGA in acetone:CO_2 mixtures of different composition at (a) 75 ^{o}C, (b) 100 ^{o}C, (c) 125 ^{o}C, (d) 150 ^{o}C.

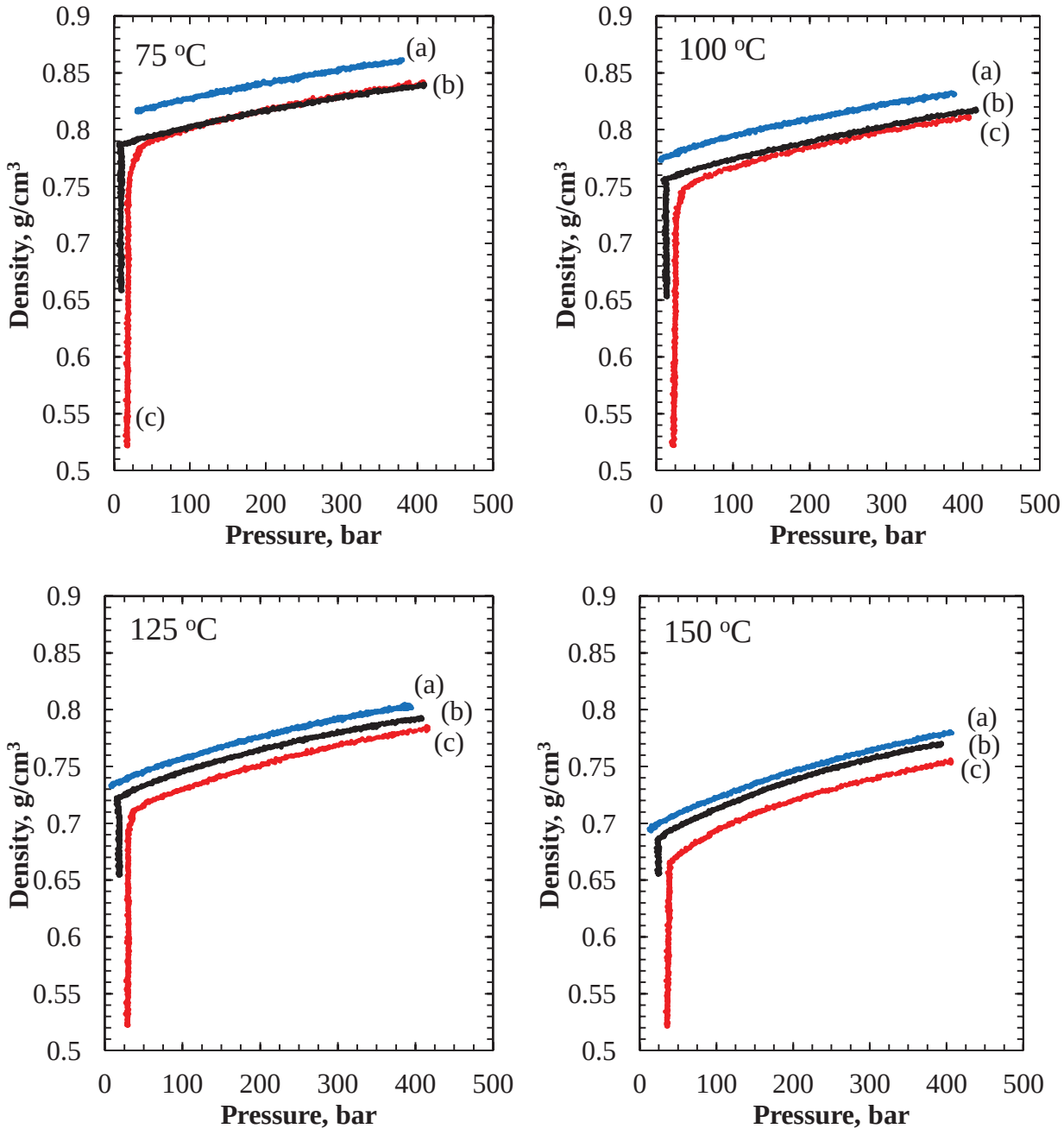

Figure 56. Density vs Pressure data for PLGA:Acetone:CO_2 mixtures of the following compositions (a) 10:90:0, (b) 10:85:5 and (c) 10:80:10.

6.4.2.2 Miscibility and Liquid-Liquid Phase Separation Conditions.

The 10 wt% PLGA was found to be soluble in pure acetone at all T/P conditions explored, since no change was observed in the transmitted light intensifies during pressure scans. The LL and LLV phase boundaries observed in the solution with 10 wt% CO_2 have been discussed in Section 6.3.1.2 in Figure 51 and Figure 52. In the solution with 5 wt% CO_2, LL phase separation was observed only at 150 ^{o}C. At lower temperatures, lowering the pressure led to only LV phase separation, which is displayed clearly in the density profiles. For this system, LL phase separation conditions were determined also at 160 and 170 ^{o}C to generate the broader picture of the LL and LLV domains. Figure 57 shows the change in transmitted light intensity along the pressure reduction paths at 150, 160, and 170 ^{o}C. Table 16 shows the P/ T conditions at the LV and LLV boundaries for the solution with 5 wt% CO_2. Figure 58 shows a comparative plot of the phase boundaries for solutions with 5 and 10 wt% CO_2 content. As expected, the phase boundaries shift to higher pressures and to lower temperatures with increasing CO_2 content, reflecting the reduction in the solvent quality.

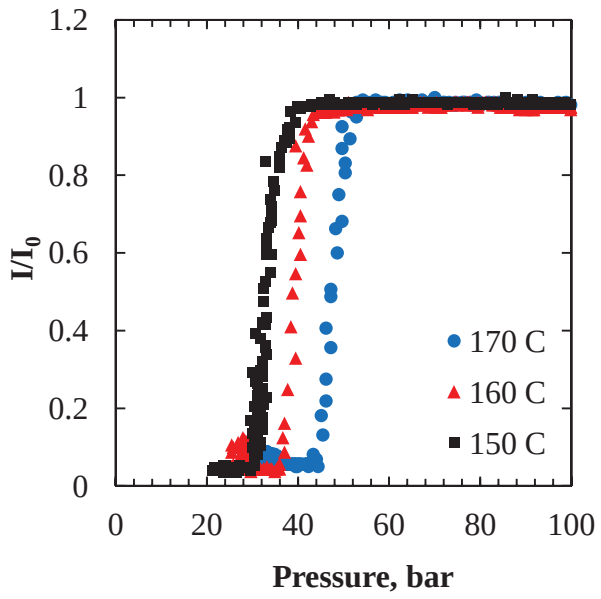

Figure 57. Transmitted light intensity as a function of pressure for determination of LL phase boundaries of 10 wt% PLGA - 85 wt% Acetone - 5 wt% CO_2.

Table 16. Summary of phase boundaries for 10 wt% PLGA – 85 wt% Acetone – 5 wt% CO_2 solvent mixtures.

	Phase Boundary, bar		
T, °C	LL	LV	LLV
75	-	9	-
100	-	13	-
125	-	19	-
150	38	-	25
160	43	-	28
170	51	-	33

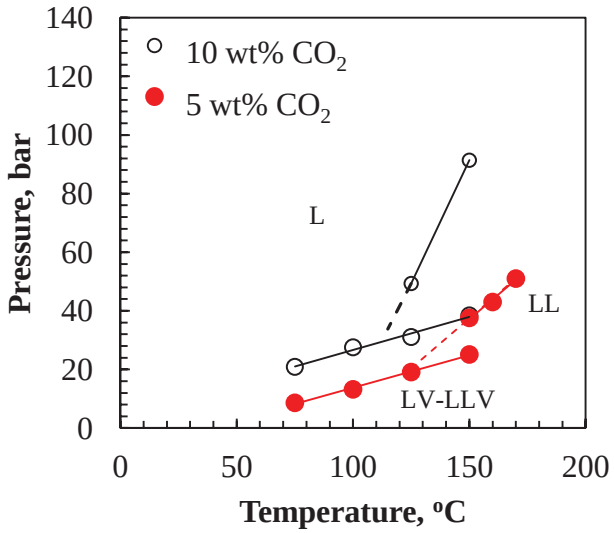

Figure 58. Phase boundaries for 10 wt% PLGA in two Acetone:CO_2 fluid mixtures

6.4.2.3 Isothermal Compressibilities

Table 17 provides the density correlations as a function of pressure for the solutions with 0 and 5 wt% CO_2 content based on the data presented in Figure 55. The correlations for the solution with 10 wt% CO_2 content was already given in Table 15. Isothermal compressibility data generated from these functions at the respective temperatures are shown in Figure 59. The compressibilities show a regular increase with temperature and a regular decrease with pressure. Figure 60 compares the compressibility behavior of 10 wt% PLGA solution in acetone and in solvent mixture with 5 and 10 wt% CO_2 at different temperatures. The data shows that the compressibilities in acetone and in solution with 5 wt% CO_2 are very similar at 75 and 100 ^{o}C, with values in the range 2.5 x 10^{-4} bar^{-1} and 1.5 x10^{-4} bar^{-1}. The compressibilities increase at temperatures 125 ^{o}C and above, essentially doubling to values in the range 4x10^{-4} bar^{-1} to 2x10^{-4} bar^{-1}, and 5.5x10^{-4} bar^{-1} to 2.5x10^{-4} bar^{-1}, respectively. The compressibility of the solution containing 10 wt% CO_2 is lower at 75 and 100 ^{o}C, but becomes very similar at 125 ^{o}C, and then

appears to be lower at 150 °C at high pressures. From the reduction in density in solutions with higher CO_2 content displayed in Figure 56, an increasing trend in compressibilities would have been expected but does not appear to be the case. A qualitative interpretation would suggest that, when CO_2 associates with the carbonyl groups of the polymer, if it indeed functions as a spacer to lower the density, it must be decreasing the chain flexibility leading to lower compressibilities. The data suggest that the extent of the polymer-CO_2 interactions become more prevalent as a greater fraction of the carbonyl groups in the chain are engaged with CO_2 with increasing CO_2 content.

Table 17. Density correlations for 10 wt% PLGA in different Acetone:CO_2 fluid mixtures.

[CO_2], wt%	Temperature, °C	ρ = f (P, bar)	R^2 Value	P range, bar
0	75	$\rho = -1E\text{-}07P^2 + 0.0002P + 0.8118$	0.9964	30-380
	100	$\rho = -1E\text{-}07P^2 + 0.0002P + 0.7759$	0.9968	
	125	$\rho = -2E\text{-}07P^2 + 0.0003P + 0.7336$	0.9984	
	150	$\rho = -2E\text{-}07P^2 + 0.0003P + 0.6938$	0.9988	
5	75	$y = -1E\text{-}07x^2 + 0.0002x + 0.786$	0.9971	30-380
	100	$y = -9E\text{-}08x^2 + 0.0002x + 0.7562$	0.9980	
	125	$y = -2E\text{-}07x^2 + 0.0003x + 0.7205$	0.9984	
	150	$y = -3E\text{-}07x^2 + 0.0004x + 0.6794$	0.9991	

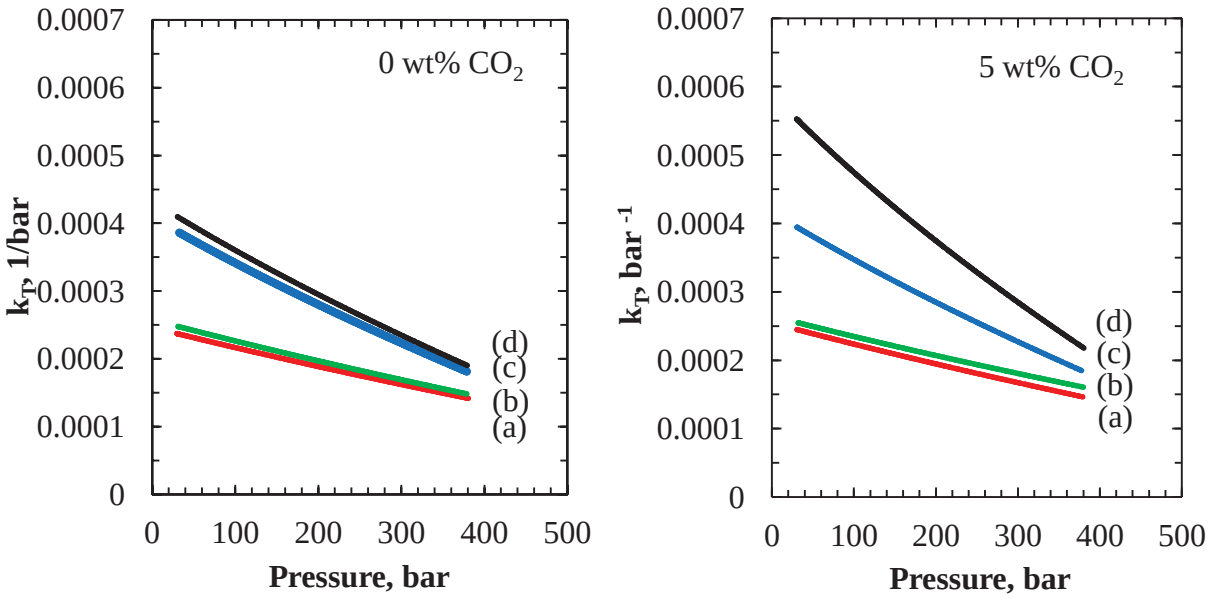

Figure 59. Isothermal compressibilities for 10 wt% PLGA in acetone:CO_2 mixtures at (a) 75 ^{o}C, (b) 100 ^{o}C, (c) 125 ^{o}C, (d) 150 ^{o}C.

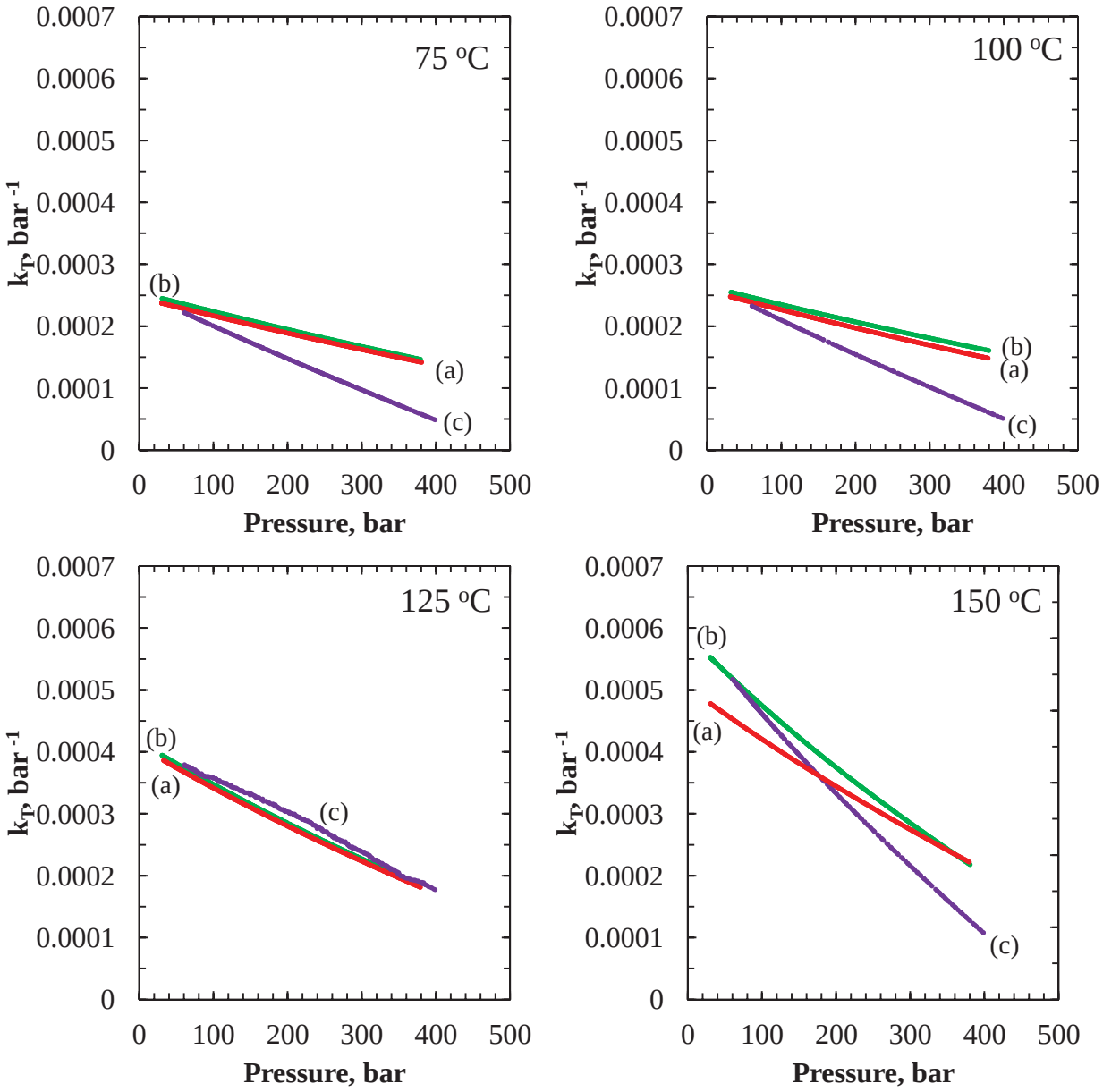

Figure 60. Compressibilities for PLGA:Acetone:CO_2 mixtures of the following compositions (a) 10:90:0, (b) 10:85:5 and (c) 10:80:10

6.5 Further Discussion

The present findings point to the complexities arising from the changes in the relative polymer-CO_2, polymer-acetone and CO_2-acetone interactions as a function of temperature, pressure and composition. No prior FTIR work has been reported that has attempted to look at these pair-wise interactions in ternary mixtures of CO_2 + co-solvent + polymer with carbonyl groups, and publications on the densities of such ternary systems are also rare. In a prior study which reports on 5 wt% PCL solutions in CO_2-acetone mixtures containing 0, 5, 10, 20, 40 and 60 wt% CO_2 at 75 ^oC [242], densities were found to increase with increasing CO_2 content at pressures above 200 bar. At pressure below 200 bar, densities were found to increase up to 20 wt% CO_2 content, but at higher CO_2 additions they were observed to decrease. In the present study with PLGA, densities are observed to decrease even for the relatively low CO_2 levels that have been explored. The present results on the effect of CO_2 are also in contrast to the densities that were reported for 5 wt% solutions of PMMA in a CO_2-acetone mixture with 1, 2, and 4 wt% CO_2 content, where the densities of the solutions were found to increase with increasing CO_2 content in the mixture [241]. In that study, density measurements were also reported for 5 wt% PCL solutions in CO_2-acetone mixtures with the same, 2 and 4 wt%, CO_2 levels. Compared to the PMMA solutions, the PCL solutions displayed slightly lower densities (at 100 ^oC, in solutions with 4 wt% CO_2, densities were in the range 0.83-0.87 g/cm^3 for PMMA solution; but 0.82-0.87g/cm^3 for PCL solution), which would imply higher free volume in the PCL solution and, other things being equal, lower viscosities. To the contrary, PCL solutions were found to display higher viscosities, which can be interpreted as arising from PCL chains undergoing greater chain expansion than PMMA, indicating that the CO_2-acetone mixture acted as a better solvent for PCL than for PMMA. In the present study, the density values for 5 wt% PLGA solutions in CO_2-acetone

mixture with 5 wt% CO_2 are in the range of 0.75-0.81 g/cm^3, which are lower than that for the case with PMMA or PCL solutions. Based on density measurements, the likelihood of association of CO_2 with the carbonyl groups leading to increased spacing in between the polymer chains must increase going from PMMA to PCL and then to PLGA.

As depicted in Figure 61, interaction of CO_2 with PMMA will be in the side groups of the chain, yet in PCL and PLGA will be along the backbone. In PMMA the associated CO_2 would not be expected as functioning as spacers between chains. The difference in PCL and PLGA is in the higher frequency of appearance and the closer spacing of carbonyl groups in the backbone chain of PLGA. In PCL, upon association of CO_2 with carbonyl groups there may be spreading of the chains, but due to the space in between the carbonyl groups, as illustrated in the figure, chains can assume a different conformational state and may not necessarily exhibit a significant expansion of the free volume between the chains. In PLGA, the effect of associated CO_2 acting as a spacer between the chains is expected to be the greatest. Even though not shown in the figure, it is easy to visualize that if the carbonyl groups with bound CO_2 groups were on the same sides of the neighboring chains, the expansion of the chains would be even greater. It is thus not surprising to see significantly lowered densities for PLGA solutions upon addition of CO_2. Clearly, more of the carbonyl groups will be associated with increasing CO_2 content in the mixture leading to greater density reduction, but it is also easy to visualize that this may lead to significant hindrance of chain backbone flexibility, thereby reducing the compressibility as is observed for the case of 10 wt% CO_2.

It is instructive to look at the compositions investigated with a different perspective by considering the relative amounts of the three components not by their mass amounts but in terms of the number of moles of CO_2, acetone, and the carbonyl groups to have a better sense of the fraction of carbonyl groups that may be associated . We will focus only on the ternary mixtures with PLGA:Acetone:CO_2 with wt% ratios of 5:84.5:10.5; 10:8.5:5; 10:80:10. Recognizing that the repeat unit in PLGA has a molecular weight of 130 grams and each repeat unit has 2 carbonyl groups, these compositions can be expressed equivalently in terms of the mole ratios of Carbonyl Groups:Acetone:CO_2 as 0.077:1.56:0.24 ; 0.154:1.57:0.11 and 0.154:1.45:0.22. Or, if further normalized to 1 mole of carbonyl group, the compositions can be expressed in rounded values as 1:20:3; 1:10:0.7; and 1:9.4:1.4. These numbers are very helpful in immediately indicating that the mixtures have excess acetone for each mole of carbonyl group to the tune of 10 or 20 to 1, or for each mole of CO_2 to the tune of 7 or 14. Therefore, in terms of association effects between acetone and polymer, or acetone and CO_2 one does not anticipate much of a difference in these three solutions. What is significantly different is the number of moles of CO_2 available for each mole of carbonyl group, which is 3:1 in the 5 wt% polymer solution; 1.4:1 in the 10 wt% polymer solution with 10 wt% CO_2 and 0.7:1 in the 10 wt% polymer solution with 5 wt% CO_2. In the 10 wt% polymer solutions with a CO_2:carbonyl group ratio of greater than 1, a greater likelihood of in-between chain separation through association of CO_2 with the carbonyl groups, and consequently lower densities, can be anticipated as the data display. The 5 wt% polymer solution with 3:1 CO_2 to carbonyl group ratio suggests that, there will be more CO_2 association with acetone, or, if held within the polymer, 2 of the 3 CO_2 molecules will have to be in “free form” and can be available to promote LV phase separation leading to observation of the

LV boundary at higher pressures that in 10 wt% polymer solution. This further supports the arguments presented in Section 6.3.1.2.

The present study thus highlights the significance of the potential interactions of the components that may undergo complex formation with CO_2 in considering the thermophysical behavior of polymer solutions in mixture fluids. In the selection of compositions to investigate, one should give consideration to molar ratios in addition to masses. It would be interesting to explore the viscosity of these PLGA solutions in a future study to assess the consequences of competitive association of CO_2 with the carbonyl groups on the polymer chain versus acetone on the chain flexibility and the flow dynamics at different temperatures and pressures. It will be especially important to look at the changes at around 125 ^{o}C, where the compressibility data suggest that changes occur in the relative extent of the association of CO_2 with polymer versus acetone. Spectroscopic studies below and above 125 ^{o}C would be especially informative in understating the dynamics of complexation of CO_2 between polymer versus acetone.

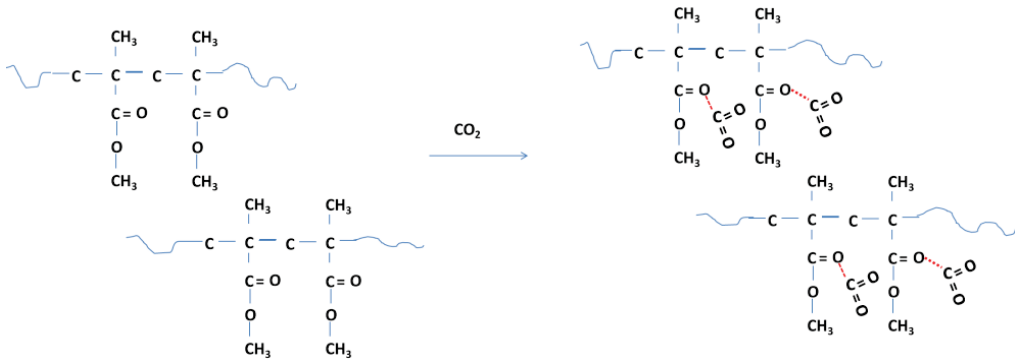

a.

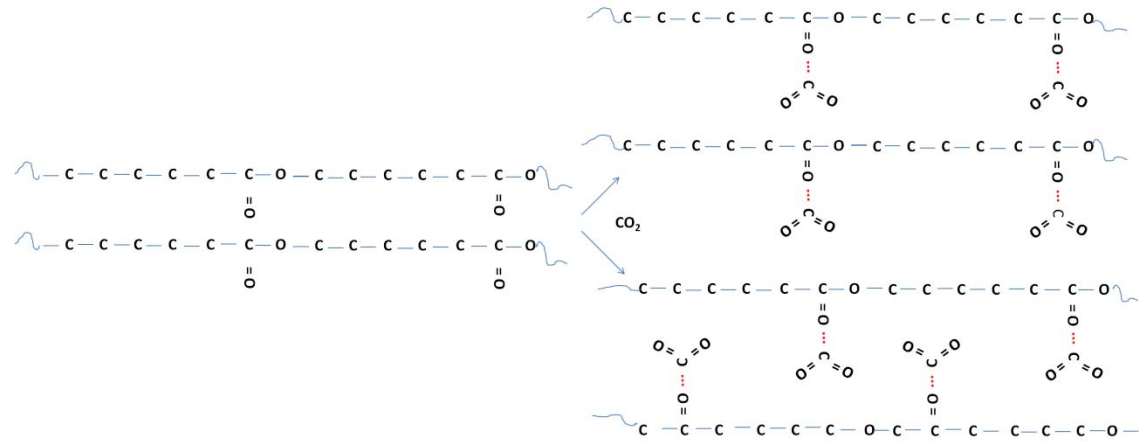

b.

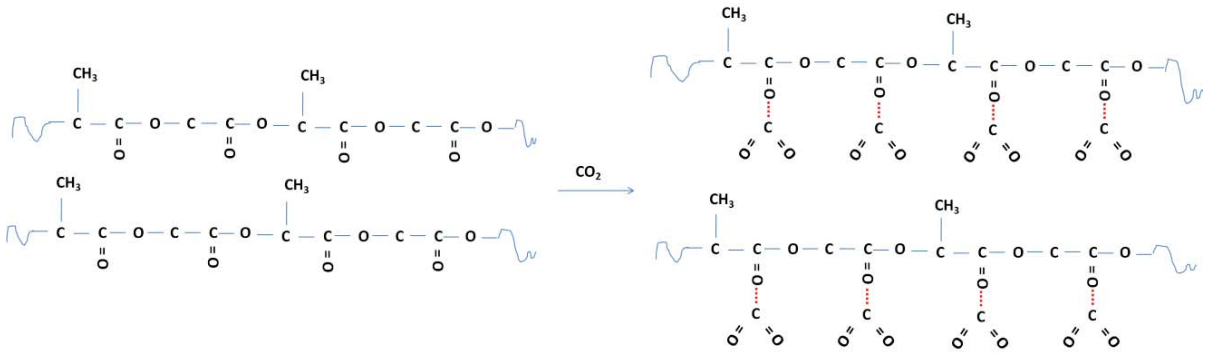

c.

Figure 61. Consequences of CO_2 association with the carbonyl groups in (a) PMMA; (b) PCL and (c) PLGA in terms of CO_2 acting as spacers between backbone chains and leading to changes in density and or compressibilities in their solution in CO_2 + acetone mixtures.

6.6 Conclusions

Solutions of PLGA in CO_2-acetone mixtures display a LCST type LL phase boundary. Miscibility pressures increase with increasing CO_2 content in the solvent mixture. Continuous recording of the density as a function of pressure at a given temperature helps identify the LV or LLV phase boundaries, as well as development of density–pressure correlations from which compressibilities are generated. Documentation of density along with compressibility provide insights on the complex dynamics of changes in the extent of association of CO_2 with the polymer versus acetone as a function of pressure and/or temperature especially around 125 ^{o}C, above which the data suggests that CO_2-polymer interactions vis-a-vis CO_2–acetone interactions are most likely reduced. The results further show that with increasing amount of CO_2 in the solutions, densities as well as compressibilities decrease. This is interpreted as evidence of CO_2 association with the carbonyl groups in the polymer chain, which acts as spacers thereby reducing density, but also reducing chain flexibility and thus reducing compressibility.

Acknowledgements

This research was in part supported by the National Science Foundation (Award # CBET 0929978).

Chapter VII. Generation of Polymer Foams using Carbon Dioxide and Co-solvents

7.1 Abstract

Foaming of the biomedical polymers, PLGA and PCL, using CO_2 was explored as an approach to generate tissue engineering scaffolds. The effect of the foaming parameters, including temperature, pressure and depressurization rate (DPR) on the resulting pore structure was investigated. The following general trends were recognized. Increasing the foaming temperature causes an increase in pore size, increasing pressure results in a decrease in pore size and an increase in pore density, and reducing the DPR results in increased pore size. Co-solvent addition was then explored as an approach to circumvent non-porous skin formation at the surface of the polymer foam and to improve pore interconnectivity. Acetone, ethanol and ethyl acetate were investigated as co-solvents at 0.2 wt% concentrations in CO_2. Acetone addition resulted in a reduction in skin formation in PCL and improved pore interconnectivity in both polymers, while ethanol as a co-solvent resulted in pore deformation and collapse and ethyl acetate was not shown to improve interconnectivity but reduced skin formation on the bottom surface of PLGA foams. Average pore diameters varied widely based on the processing parameters and co-solvent addition. Smaller pores for PLGA were obtained with CO_2 foaming at 35 ^{o}C / 12.1 MPa / fast DPR, generating a fairly uniform closed pore structure with average pore diameters of 100 ± 29 μm. Larger pores for PLGA were 878 ± 274 μm and were obtained with CO_2 foaming at 35 ^{o}C / 12.1 MPa / slow DPR. Porosities of PLGA foams generated were in the range of 93 - 97 % by volume. Smaller pores for PCL were obtained by foaming with CO_2 at 35 ^{o}C / 16.0 MPa / fast DPR, generating average pore sizes of 57 ± 26 μm . Larger pores for

PCL were found to be 1143 ± 313 μm and were generated with CO_2 foaming at 35 ^oC / 9.2 MPa / slow DPR. PCL foam porosities were in the range of 70 - 72 % by volume.

7.2 Introduction

PLGA and PCL are of interest in the biomedical field as tissue engineering (TE) and drug delivery devices, as these polymers are biocompatible and biodegradable. In TE applications, low density, highly interconnected networks are desired to promote cell growth into the scaffold and allowing nutrient, oxygen and waste transport through the device. Methods for generating polymeric TE scaffolds include phase separation (temperature or pressure induced), solvent casting/porogen leaching, electrospinning, lyophilization, templating and foaming [141, 143]. In each of these methods, organic solvents are employed to dissolve the polymer. Residual solvents can lead to toxicity of the scaffold causing it to be unsuitable for TE applications. The use of supercritical CO_2 in place of toxic organic solvents is a safer alternative to generating biomedical scaffolds, and polymer foaming with CO_2 has been shown to be an effective method for generating low density foams [28].

The CO_2 foaming process was previously described in Chapter III and will be briefly summarized again here. CO_2 is first dissolved into the polymer, which is facilitated by bringing the polymer to the liquid state by raising the temperature. Foaming is then induced by bringing about a thermodynamic instability via either a pressure or a temperature quench, resulting in nucleation of CO_2 gas bubbles within the polymer. The bubbles then remain as pores within the solidified polymer. The glass transition or melting temperature of the polymer is depressed as CO_2 dissolves in the polymer. A foaming temperature should be chosen such that the polymer is

in the liquid state at high pressure, or when CO_2 is dissolved in the polymer, but becomes solidified via crystallization or vitrification upon depressurization to ambient pressure. This is described graphically in Figure 24 in Chapter III.

The processing parameters in the foaming process, including temperature, pressure and depressurization rate are known to influence the resulting pore structure [152]. General trends have been recognized for pore structure dependence on temperature, pressure and depressurization rate. Increasing temperature generally lowers the solubility of CO_2 in the polymer and increases the diffusivity of $scCO_2$ in the polymer, resulting in fewer nucleation sites, and thus, fewer pores with larger diameters [163, 164]. Increasing the pressure increases the amount of dissolved $scCO_2$ in the polymer, yielding more nucleation sites and a higher quantity of smaller pores. Faster depressurization rates result in the formation of a high pore density of pores with small diameters, while slower rates yield larger pores accompanied by lower pore density. Depressurization rate has been shown to have a significant effect on the pore structure and interconnectivity and continues to be an area of interest [164]. A parametric analysis of CO_2 foaming of polystyrene and PLA [165] and a separate study with PLGA and PLA [167] foams produced by CO_2 foaming confirmed these trends. A systematic study was performed also in this research with PLGA (50/50) and PCL to verify these relationships between processing parameters and the resulting pore morphology.

PLGA is a good candidate for CO_2 foaming due to its low glass transition temperature and the high solubility of CO_2 in the polymer. PLGA is foamed with CO_2 at relatively modest pressures

and temperatures. For example, PLGA foams were successfully generated at 35-40 ^{o}C and 10-20 MPa [244]. PLGA has been studied extensively for CO_2 foaming [28, 180, 221, 245, 246].

Foaming studies with PCL are not as abundant as those with PLGA, although such work has been reported [161]. Foaming conditions of 308 K / 34 MPa resulted in reported pore diameters of about 1 μm. A further increase of temperature to 323 K / 34 MPa led to a heterogeneous morphology, common in semicrystalline polymers, containing spherulitic and porous domains.

Drawbacks to CO_2 foaming include the formation of a non-porous skin layer at the surface of the foam [166, 167] and limited interconnectivity of pores. A non-porous skin layer is formed on the surface of the foam during the pressure quench step in CO_2 foaming. Skin formation is due to more rapid diffusion of CO_2 from the outer layer of the polymer than from the bulk polymer, causing earlier onset of vitrification or crystallization at the surface. An approach to circumvent these drawbacks with CO_2 foaming is to add a small amount of an organic co-solvent to the fluid. Co-solvents can improve the solvent power of CO_2 with even very small additions. Acetone, ethanol and ethyl acetate were investigated in this research as co-solvents to improve the CO_2 foaming process. These solvents were chosen due to the abundant literature available on their mixtures with CO_2 [11, 12, 240] and due to their relative non-toxicity and FDA approval.

The critical points for these mixtures with CO_2 were provided in Figure 3-Figure 5 in Chapter I and were found to be composition dependent. At all CO_2:co-solvent compositions, the critical temperature takes on an intermediate value between the critical temperatures of the pure components. The critical pressure takes on a value higher than the critical pressure of the co-

solvent at low CO_2 compositions, and a value higher than the critical pressure of either pure component at higher CO_2 compositions. The co-solvent addition levels explored in this research were very low (0.2 wt%), thus, the critical point of the fluid mixture is expected to be nearly identical to the pure CO_2 critical point.

The solubility parameter, which is the square root of the cohesive energy density, provides a numerical figure for predicting the extent of interaction between two compounds [247]. Materials with similar solubility parameters, δ, are expected to be miscible. The solubility parameters of the investigated co-solvents are shown in Table 18, and the CO_2 solubility parameter is displayed graphically at a range of pressures and temperatures in Figure 62.

Table 18. Solubility parameters for co-solvents and polymers investigated [247].

Sample	δ, $MPa^{1/2}$
Acetone	20.3
Ethanol	26.5
Ethyl Acetate	18.2
PLGA	22.3
PCL	20.3

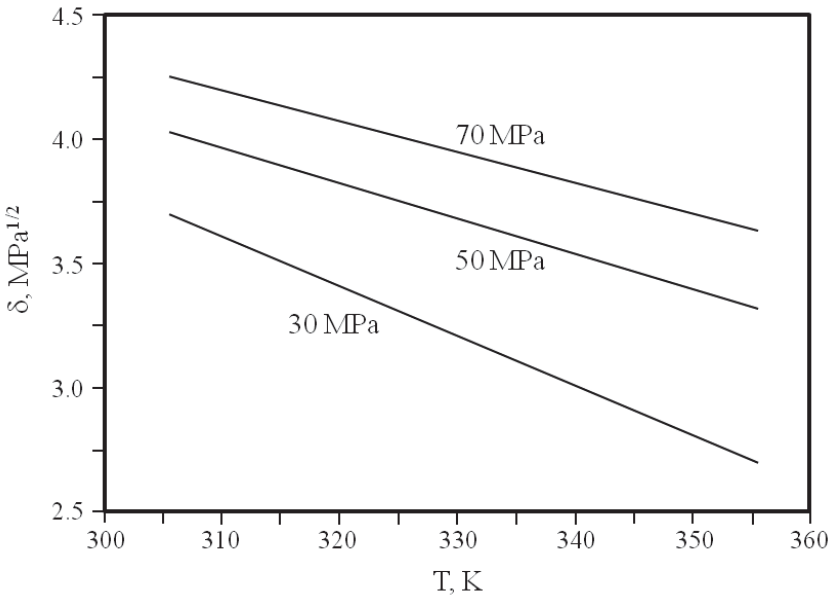

Figure 62. Solubility parameter of CO_2 as a function of temperature and pressure [248].

According to the solubility parameter values listed in Table 18 and displayed in Figure 62, CO_2 is not a good solvent for either of the polymers investigated in this research, and this was confirmed in experimental observations. However, the three co-solvents, acetone, ethanol and ethyl acetate, have solubility parameters much closer to those of the polymers. Acetone is expected to be the best solvent for both polymers, but especially for PCL since the solubility parameters are similar. Ethanol has the weakest solvent power for both polymers, with ethyl acetate being more powerful than ethanol. The solubility parameter of mixtures is calculated by averaging the solubility parameters by volume. Since very small amounts of co-solvents (50 μL; 0.2 wt%) are being added to the foaming process carried out in this research, the solubility parameter is not expected to be changed much in the binary solvent mixture and should be relatively close to that of the CO_2 alone.

A few authors have reported on the use of a co-solvent in polymer foaming by a supercritical foaming technique. Foaming of PLLA and poly(caprolactone-*co*-lactide) in CO_2 and CO_2 + acetone mixtures has been reported [31] with mixtures containing 1 and 4 wt% acetone. PLLA foaming was reported to be promoted at much lower temperatures and pressures generating foams with larger pore sizes and a higher degree of interconnectivity, compared to foaming with CO_2 alone. Pore uniformity was improved with CO_2 + acetone foaming of poly(caprolactone-*co*-lactide). A separate group reported use of CO_2 + ethanol mixtures in the foaming of PCL [169]. The addition of ethanol was found to promote the formation of uniform porous structures; however, skin formation was not prevented. Homogeneous porosity was attributed to the improved dissolution of the CO_2-ethanol mixtures into PCL, due to a solvent-induced viscosity reduction and/or a melting point depression.

In this chapter, the effects of foaming parameters and co-solvent addition on the resulting pore structure of biomedical foams generated by CO_2 foaming are investigated.

7.3 Materials

Resomer RG 504 H, poly(DL-lactide-co-glycolide) with a 50/50 monomer ratio, was purchased from Boehringer Ingelheim and used as received. PLGA was stored with desiccant in a refrigerator at 4 ^{o}C to protect the polymer from moisture and prevent degradation. Poly(ε-caprolactone) was purchased from Sigma Aldrich and ground into powder form with a mechanical grinder before using. Both polymers were characterized by gel permeation chromatography (GPC) using a Waters 1515 isocratic HPLC pump and a Waters 2414 refractive index detector. Tetrahydrofuran (THF) was used as the solvent and purge fluid. Therefore, THF

compatible columns (WAT044228 & WAT044240) were used. PLGA (50:50) and PCL were dissolved separately in THF at a concentration of 1 mg/ml. Weight average molecular weight (M_w), number average molecular weight (M_n) and polydispersity (PDI) were determined for each and are listed in Table 19. The bulk density of PCL as reported by Sigma is 1.145 g/cm^3 [249], and the density of PLGA as reported by Polyscience, Inc. is 1.34 g/cm^3 [250].

Table 19. Molecular weights of PLGA and PCL determined by GPC.

Polymer	M_w (g/mol)	M_n (g/mol)	PDI
PLGA	65,000	32,000	2.02
PCL	65,000	44,000	1.48

Ibuprofen, piroxicam, β-cyclodextrin and 2-hydroxypropyl-β-cyclodextrin were purchased from Sigma Aldrich and used as received. Characterizations of these compounds, the drug:CD physical mixtures and the drug:CD inclusion compounds are provided in detail in Appendix A.

7.4 Methods

7.4.1 Polymer Foaming

Polymer foams were prepared by CO_2 foaming using the high pressure view-cell apparatus illustrated in Figure 63. The view-cell is equipped with two large (1 in. diameter) sapphire windows for observation of the foaming process with the sample contained in a glass vial with a diameter of 0.385 in. The path followed in the foaming process is graphically illustrated in Figure 64. In a typical foaming experiment, the polymer is placed into the glass vial which is then placed into the vessel. The co-solvent, if used is added by syringe to the vessel outside of

the vial, so as not to soak the polymer in pure co-solvent. The vessel is closed to seal and then heated to the soak temperature (T_{soak}), the temperature at which the sample is first exposed to CO_2, using four symmetrically positioned heater cartridges. CO_2 is then charged to the vessel to the soak pressure (P_{soak}) by opening the inlet valve and pumping, if needed. In each experiment T_{soak} was maintained at 50 ^oC and P_{soak} was maintained above 10 MPa. At these conditions, PLGA is above its ambient pressure glass transition temperature (T_g = 46 - 50 ^oC), which is known to be depressed to lower values when exposed to CO_2. At 50 ^oC, PCL is not above its ambient pressure melting temperature (T_m = 55 - 60 ^oC), but under CO_2 exposure at pressures above 10 MPa, 50 ^oC has been described in the literature to be sufficient to melt the polymer [157]. The liquid state at each soak condition is confirmed in these experiments visually, as each polymer underwent a decrease in apparent volume upon CO_2 exposure, indicating the densification of the polymer as it changed from the solid (powder) to the liquid state. Upon liquefaction, the polymers also become transparent. The reason for bringing the polymers to the liquid state in the soaking step of the foaming process, is to accelerate diffusion of CO_2 into the polymers. Thirty minutes, which was chosen as the soak time (t_{soak}), was found to be sufficient to fully saturate the polymer with CO_2, as longer soaking times (up to 6 hours) did not result in changes in the eventual foam structure or density. After 30 minutes at the soaking conditions, the temperature was reduced to the foaming temperature (T_{foam}) allowing pressure to drop with temperature to the foaming pressure (P_{foam}). P_{foam} is not a controlled parameter but was still recorded in each experiment. The cooling step takes about 30 minutes, resulting in a total CO_2 exposure time of about 1 hour. The depressurization rate (DPR) was qualitatively defined as either fast (exit valve fully opened / depressurization < 15 s) or slow (depressurization ~ 5 min) to ambient pressure conditions, which results in a temperature drop in the sample. This

temperature drop is not detected on the thermocouples in the vessel, but is known to occur during an adiabatic expansion. The faster DPR will result in a greater extent of temperature reduction than the slow DPR, as indicated in Figure 64. After depressurization the vessel was opened to recover the foamed polymer. After foaming, the density was approximately determined knowing the polymer mass and measuring the cylindrical volume of the foam. The calculated foam density values are only approximate as volume determination assumes perfect cylindrical geometry.

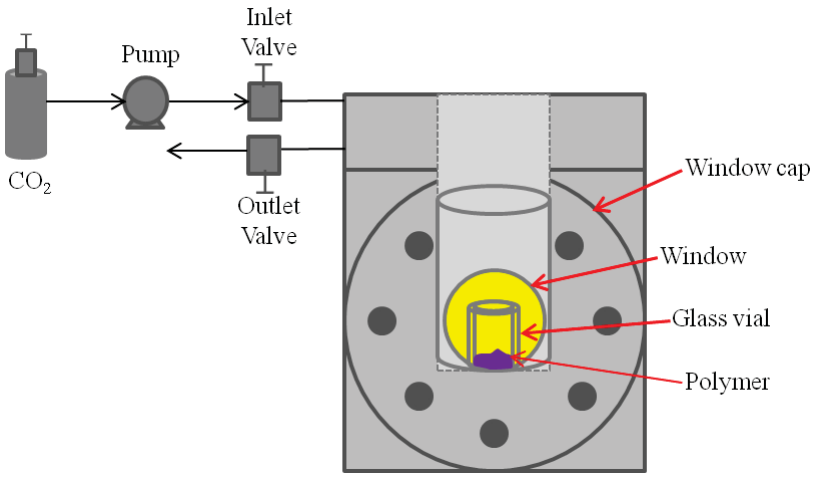

Figure 63. View-cell apparatus used in foaming experiments.

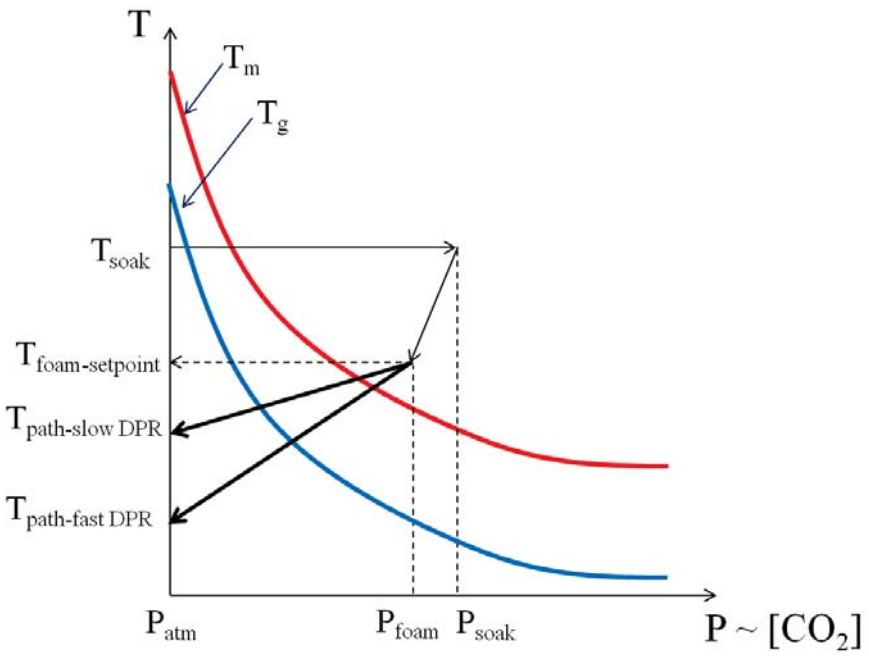

Figure 64. Illustration of foaming procedure carried out in high pressure foaming experiments.

7.4.2 Thermal Analyses

Differential scanning calorimetry (DSC) and thermogravimetric analysis (TGA) were carried out to characterize polymers before and after foaming. DSC heating scans were acquired using a 10 ^{o}C/min heating rate from -10 ^{o}C to 90 ^{o}C. The heating scans for the unprocessed polymers are the second heating scans, to display the thermal behavior of the polymer after erasing its thermal history in the first heating scans. TGA weight loss curves were obtained by heating the sample to 600 ^{o}C at a rate of 10 ^{o}C/min.

7.4.3 Foam Characterization

Foams were recovered from glass vials by carefully breaking the vial and pulling the glass off of the foam. This procedure did not damage or alter the foams in any way. The volume of the

foams was calculated, assuming a cylindrical geometry. The diameter and height of the foams were obtained using a caliper micrometer.

Brunauer, Emmett and Teller (BET), a physical gas adsorption technique, was carried out on a Quantachrome Instruments BET-Autosorb 1-C for foam surface area and pore size distribution determination. The foamed samples were placed into a 9 mm cell and then degassed by the system at 30 ^{o}C for 15 minutes. An 11-point analysis was then carried out using nitrogen was as the adsorption gas. This experimental setup was inadequate for the analysis of foams generated in this study, as the C values (an indication of test validity) were reported to be outside of the valid test range. The reason for the poor BET analysis results could include experimental setup and the sample preparation. The foam pores were found to be too large for adsorption of nitrogen to be quantified, suggesting a different gas may be used instead. In addition, at least 1 gram of sample should be used to accurately quantify the surface area and pore size distribution by BET in this setup. Since the density of these foams is very low (~ 0.04 - 0.4 g/cm^3), a large sample holder (~ 2.5 - 25 cm^3) would be required to achieve a 1 gram sample loading of intact foams. An alternative procedure would be to crush the foams prior to BET analysis to reduce the volume of the sample.

In lieu of BET analyses, image analysis of scanning electron micrographs was used to obtain average pore diameters. Micrographs were acquired on a LEO Zeiss 1550 field-emission scanning electron microscope (SEM). Polymer foams were prepared by freeze fracturing with liquid nitrogen to present a cross-section of the porous structure for imaging, and foams were then sputter coated with palladium and platinum for 120 s. Average pore diameters and standard

deviations were calculated using at least 10 pores per foam. Interconnectivity was able to be visually confirmed if openings to other pores were observed within pore cell walls, as seen in the SEM micrographs.

7.5 Results

7.5.1 Effect of Foaming on Polymers

The effect of the foaming process on the polymers, PLGA and PCL, was investigated by DSC and TGA. The DSC analyses of PLGA before and after CO_2 treatment for foaming are shown in Figure 65. In both heating scans the glass transition temperature of PLGA is observed as a small endothermic peak followed by a baseline shift. The peaks in the PLGA heating scans are magnified in the scale used in Figure 65. Peak integrations yield heats of 2.9 J/g and 3.9 J/g for the unprocessed and foamed PLGA, respectively, which are relatively small values as these peaks are associated with the perturbation of the glass transition rather than the glass transition itself. The glass transition temperature of the unprocessed PLGA was found to be 49.9 ^{o}C, while the T_g of foamed PLGA was shifted to a higher value of 53.0 ^{o}C. Shifting of the T_g to higher temperatures in the foamed PLGA likely results from the extraction of low molecular weight compounds, such as residual monomer or solvent, from the unprocessed polymer during the CO_2 exposure. Lower molecular weight components, when incorporated into polymers, reduce the T_g due to an increase in free volume. In the foaming process, CO_2 tends to extract low molecular weight components from polymers, which appears to be the case with PLGA.

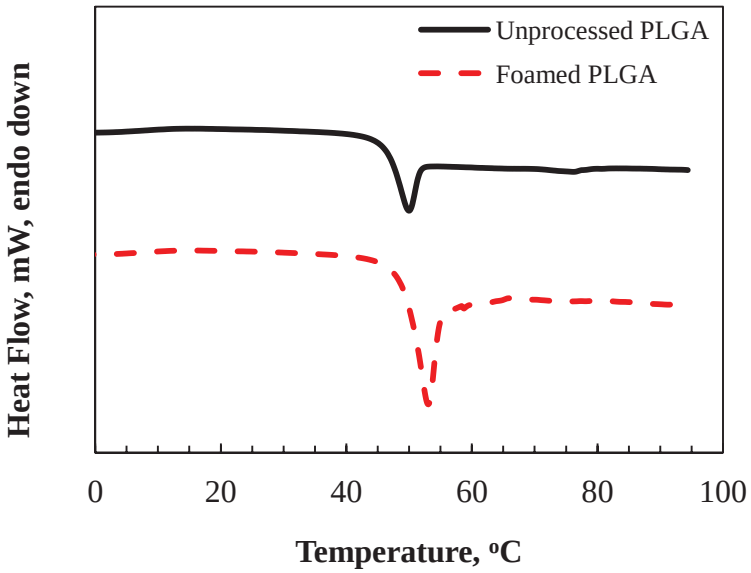

Figure 65. DSC heating scans of PLGA before and after CO_2 treatment for foaming.

The TGA thermograms for PLGA before and after CO_2 foaming are shown in Figure 66. The thermograms overlap nearly exactly, and the foamed PLGA does not display any mass loss that can be attributed to residual CO_2 in the foam.

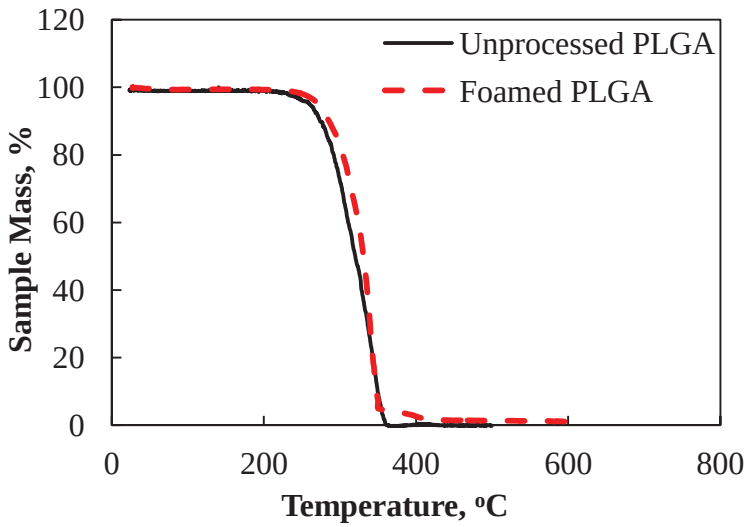

Figure 66. TGA thermograms of PLGA before and after CO_2 treatment for foaming.

The DSC heating scans for PCL before and after CO_2 foaming are shown in Figure 67. The crystalline melting peak of unprocessed PCL is observed at 56.4 ^{o}C with a heat of melting of 67.7 J/g. In the foamed PCL, the melting peak is still observed but has shifted to a temperature of 60.5 ^{o}C with a heat of melting of 74.5 J/g. The melting peak in the foamed PCL also appears to be broadened compared to the melting peak of the unprocessed polymer. Both melting peaks contain a very shallow but broad shoulder peak which begins at about 40 ^{o}C. PCL exposed to CO_2 is known to undergo lamellar thickening leading to higher melting temperatures and higher heats of melting. This effect was reported previously [161].

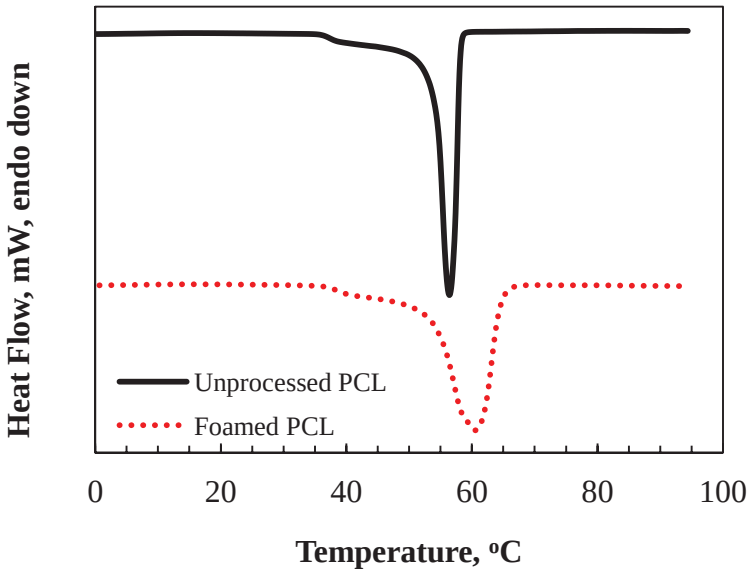

Figure 67. DSC heating scans of PCL before and after CO_2 treatment for foaming.

Figure 68 shows the TGA thermograms of PCL before and after CO_2 foaming. The mass loss curves are nearly identical for the unprocessed and the foamed PCL samples, and no mass loss associated with residual CO_2 in the foamed polymer is observed.

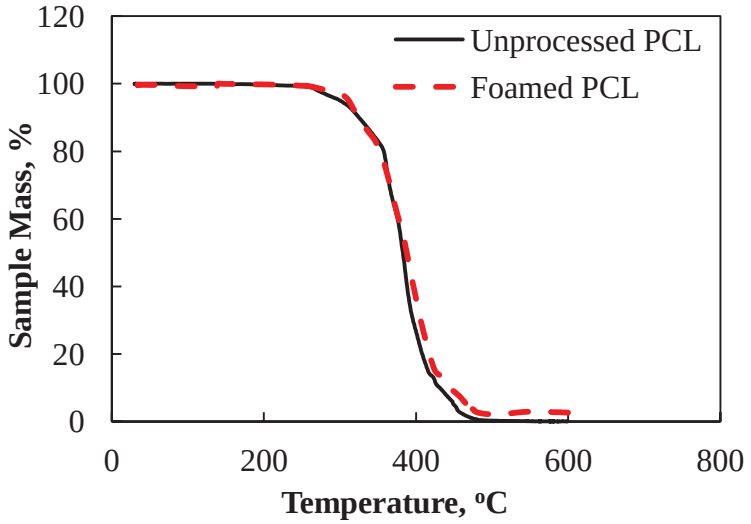

Figure 68. TGA thermograms of PCL before and after CO_2 treatment for foaming.

These thermal analyses do not provide evidence for retained CO_2 in either of the polymers after foaming, indicating that nearly all of the CO_2 was removed from the polymers during the depressurization step.

7.5.2 Effect of Processing Conditions on Pore Morphology

The effect of T_{foam}, P_{foam}, and DPR was investigated for PCL and PLGA foams generated using only CO_2 as the processing fluid. It should be noted that the shape of the resulting foams is like that of a cylinder with a very small cone-shaped void left in the bottom of the cylinder, as shown in Figure 69, where the void is exaggerated for illustration. No part of the polymer was left on the bottom of the vial, but the foam had a tendency to rise during the foaming process. The same phenomenon was observed with both PLGA and PCL foams, but the void was much shallower in PCL as PCL does not expand as much as PLGA. It appears that, since the foaming is constrained in the radial direction, the foam presses against the walls of the vial as it expands radially, causing the foam to arch upward.

The foams were freeze fractured along the vertical dimension for SEM imaging of the foam's entire cross-section. This is illustrated as the black line through the center of the illustrated foam in Figure 69. In foams with very sharply arched voids, the SEM images display the bottom arched surface of the polymer foam, as well as the porous cross-section.

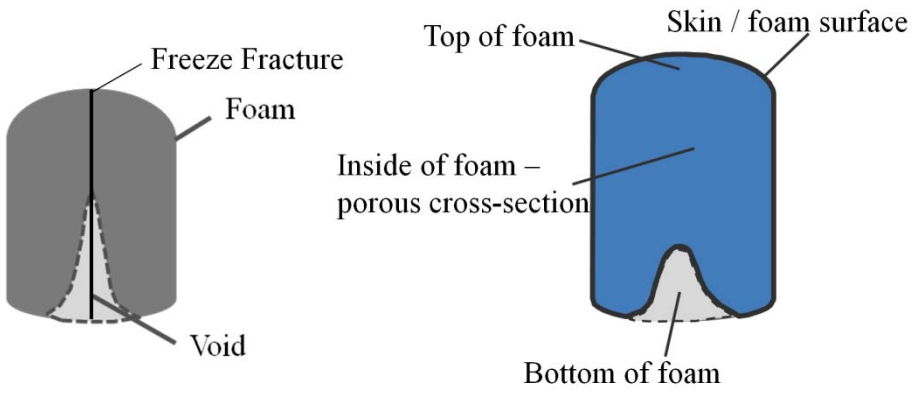

Figure 69. Shape of polymer foams produced in foaming experiments. A cone-shaped void was created as the polymer rose off the bottom of the vial in the foaming process (left). When freeze-fractured, a porous cross-section was exposed (right).

7.5.2.1 Foaming of PLGA

SEM images are shown for PLGA in Figure 70. The base foaming scenario for PLGA is shown in Figure 70a, which was carried out at the conditions of 35 ^{o}C / 12.1 MPa / fast DPR. A fairly uniform closed pore structure was formed with pore diameters of 100 ± 29 μm. A non-porous skin layer is formed on the outer foam surfaces with a thickness of about 10 μm. The density of the base case PLGA foam was found to be 0.090 g/cm^3 compared to the unprocessed PLGA density of 1.34 g/cm^3, corresponding to a porosity of 93%.

From the base foaming scenarios, an experiment was performed modifying one of the processing parameters (T_{foam}, P_{foam}, and DPR) at a time to investigate the effect of each variable individually on the foam structure. For PLGA the foam structure was most significantly altered by changing the DPR, as shown in Figure 70b. Slower pressure reduction rates extend the duration of the polymer plasticization, allowing the pores to grow larger before the polymer solidifies. PLGA

pores were much larger than those formed with a fast DPR, with average pore diameters of 878 ± 274 μm. Although pores were allowed to grow to much larger sizes with slower DPRs, the pores did not become open to other pores to improve interconnectivity. The density of the slowly depressurized foam was found to be about 0.036 g/cm^3, which corresponds to a porosity of about 97%.

The effect of raising the foaming temperature is shown in Figure 70c, where a foaming temperature of 40 ^{o}C was employed instead of 35 ^{o}C. In PLGA, average pore size diameters decreased to 82 ± 16 μm. The difference is pore size is not statistically significant from the base foaming scenario.

The effect of P_{foam} is shown in Figure 70d. For PLGA, pore sizes increased to 184 ± 34 μm when P_{foam} was reduced from 12.1 MPa to 9.2 MPa. Pore size has been shown to decrease with increasing foaming pressures while increasing pore density [167] and has been attributed to a higher number of CO_2 bubble nucleation sites present at higher pressures giving rise to the generation of a higher number of pores (increased pore density) with a decrease in average pore diameter.

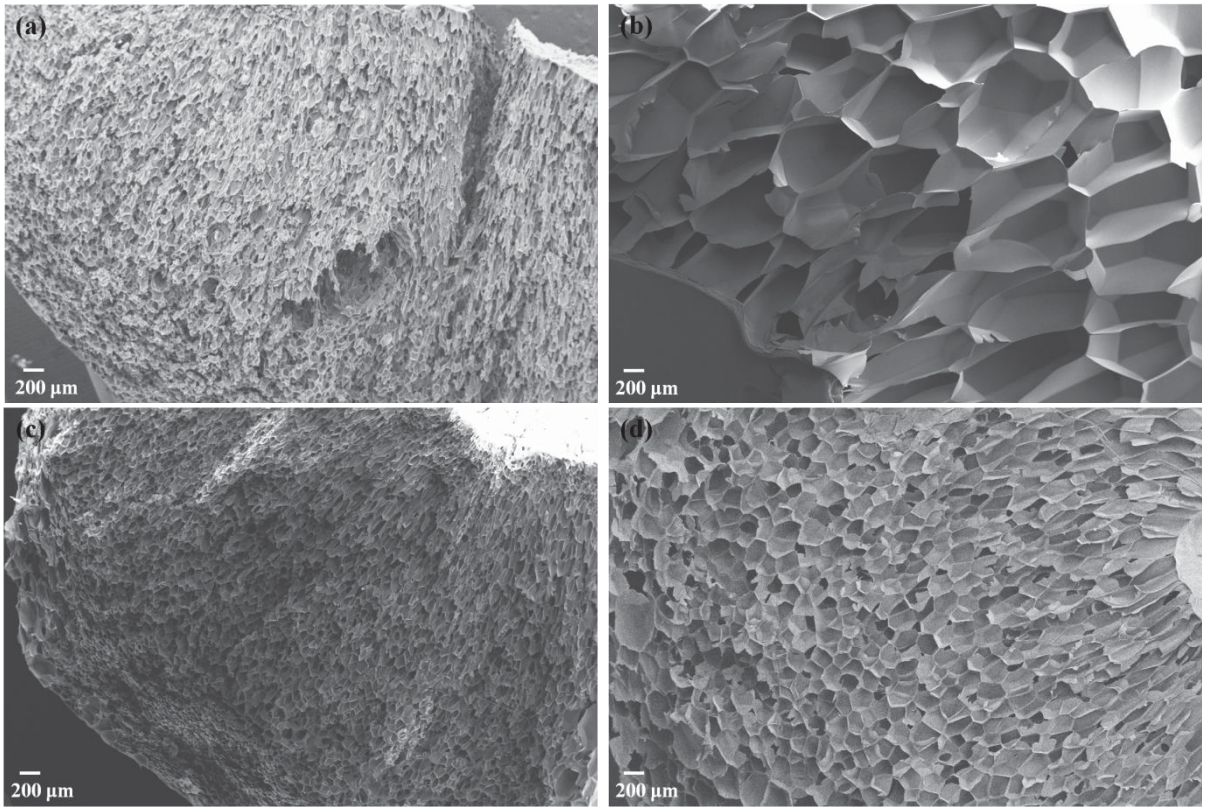

Figure 70. SEM images of PLGA foams produced from different processing conditions of (a) 35 ^{o}C / 12.1 MPa / fast DPR, (b) 35 ^{o}C / 12.1 MPa / slow DPR, (c) 40 ^{o}C / 12.1 MPa / fast DPR and (d) 35 ^{o}C / 9.2 MPa / fast DPR.

7.5.2.2 Foaming of PCL

Different foaming conditions were explored for PCL as well, and the SEM micrographs are shown in Figure 71. In the base foaming scenario for PCL (35 ^{o}C / 9.2 MPa / fast DPR) shown in Figure 71a, a mildly interconnected porous structure is observed with average pore diameters in the range of 181 ± 28 µm. The density of the PCL base case foam was found to be 0.326 g/cm^3, which corresponds to a porosity of 72%. The skin layer in PCL is much thicker than the skin formed in PLGA foams with thicknesses of about 150 µm, and interestingly, the skin layer

in PCL contains very small pores separated by sharp boundaries. The boundaries resemble those reported earlier for PCL exposed to CO_2, which was attributed to the growth impingement of spherulites during crystallization [161]. The skin layer of these foams, thus, appears to have recrystallized during the foaming process, as CO_2 escapes faster from the outer surface of the polymer than from the inside. The skin layer in PCL foams is more closely examined in Figure 72a and b, which shows PCL foamed with CO_2 at two different conditions, corresponding to the same conditions shown in Figure 71a and c, respectively. The pores in the PCL skin layer are much smaller than pores found in the bulk of the foam with average diameters of 2 ± 0.6 μm.

The effect of the DPR is shown in Figure 71b for PCL, where pore sizes increased to average diameters of 1143 ± 313 μm. The density of the slowly depressurized PCL foam was found to be 0.348 g/cm^3 compared to a bulk density of 1.145 g/cm^3, which corresponds to a porosity of 70%. This is actually an increase in density from the base case foam, although pore sizes increased in size. This is due to the very low pore density found in the slowly depressurized PCL foam, resulting in relatively large domains of un-foamed, dense PCL between pores. Increasing the foaming temperature resulted in PCL average pore diameters of 181 ± 63 μm, which is nearly the same as in the base foaming scenario. The effect of foaming pressure is shown in Figure 71d. In PCL, higher foaming pressures resulted in a decrease in pore size, as expected, with average pore diameters of 57 ± 26 μm when P_{foam} was increased to 16.0 MPa.

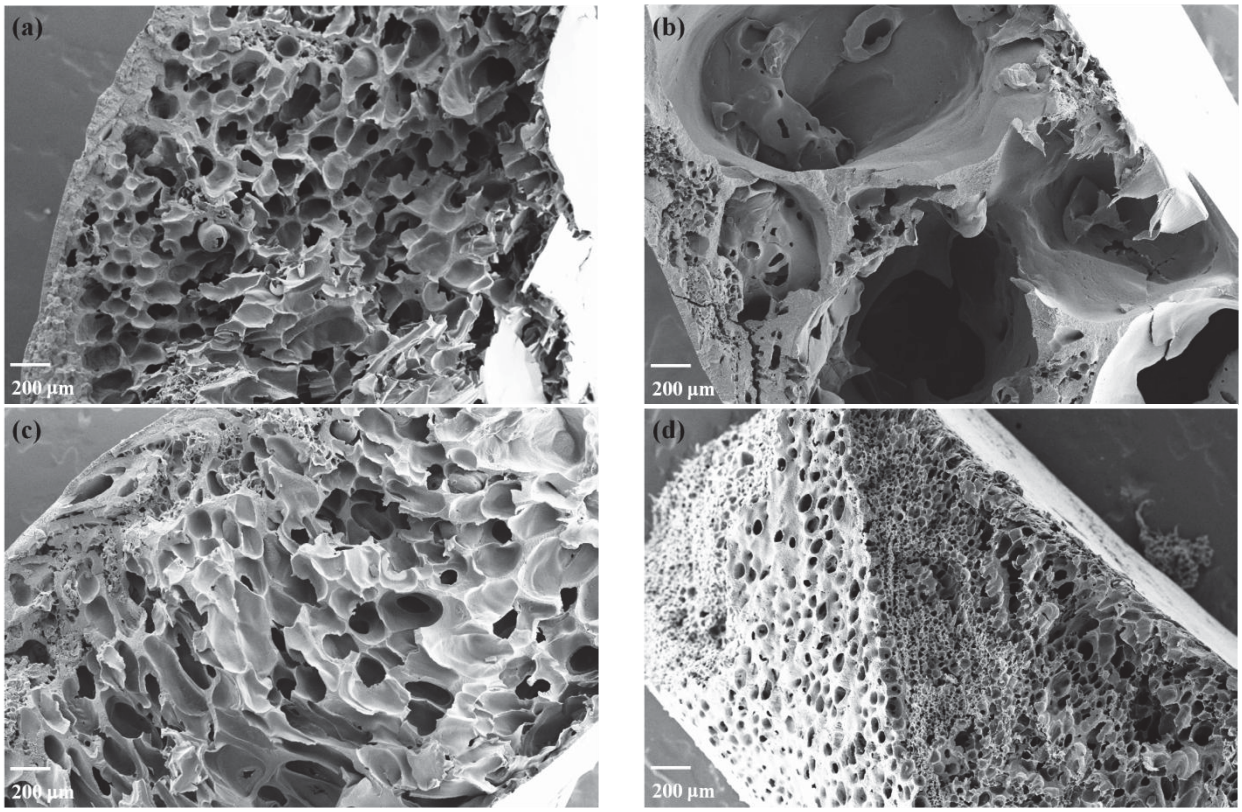

Figure 71. SEM images of PCL foams produced from different processing conditions of (a) 35 ^{o}C / 9.2 MPa / fast DPR, (b) 35 ^{o}C / 9.2 MPa / slow DPR, (c) 40 ^{o}C / 9.2 MPa / fast DPR and (d) 35 ^{o}C / 16.0 MPa / fast DPR.

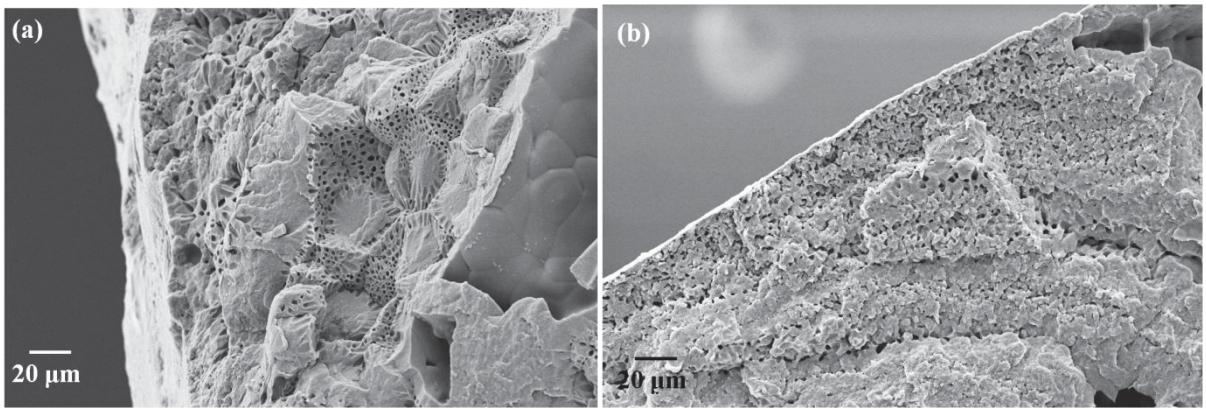

Figure 72. SEM images of PCL foam skin produced by CO_2 foaming at (a) 35 ^{o}C / 9.2 MPa / fast DPR and (b) 40 ^{o}C / 9.2 MPa / fast DPR.

7.5.3 Effect of Co-solvent Addition on Pore Morphology

Co-solvents, acetone, ethanol and ethyl acetate were explored as an approach to improve the CO_2-foaming process for generation of TE scaffolds by limiting non-porous skin formation on the foam surface and improving pore interconnectivity. A volume of 50 μL of each co-solvent was added to the system prior to charging with CO_2. Since the total CO_2 mass charged to the system in these experiments was about 24 g, the co-solvent addition corresponded to about 0.2 wt% in the binary solvent mixture. Co-solvent additions of up to 200 μL were investigated but were found to lead to pore collapse or even gel-like polymer solutions after depressurization due to the higher concentration of residual co-solvent.

7.5.3.1 PLGA Foamed with Co-solvents

The PLGA foams generated with a 0.2 wt% co-solvent addition are shown in Figure 73 and compared to a PLGA foam produced from the same conditions in the absence of co-solvent. The bottom (see Figure 69 for designation of bottom and top surface of the foam) of the foam produced with acetone addition is shown in Figure 73b, and the foam exhibits a lack of skin formation on the bottom surface, although skin formation was still observed at the top surface. Looking into the larger pores on the bottom surface, openings to other pores were observable indicating some degree of interconnectivity. Average pore sizes of PLGA foamed with CO_2 + 0.2 wt% acetone were found to be 147 ± 65 μm, which is slightly smaller than the average pore diameter of PLGA foamed with CO_2 alone. The foam density achieved with acetone addition was found to be 0.068 g/cm^3, corresponding to a porosity of 95%. Ethanol addition resulted in the generation of very non-uniform pores with some very large pore diameters of 582 ± 239 μm. As indicated by the rippled appearance of the pore walls, ethanol resulted in the partial or total

pore collapse in this foam, as shown in Figure 73c. This could indicate that ethanol was not able to escape fully from the polymer during the depressurization process. Interconnectivity does not appear to be improved with the addition of ethanol to the PLGA foaming process, as openings to pores are not found within visible pores. Ethyl acetate addition, like acetone, also led to the formation of pores at the bottom surface of the foam, as shown in Figure 73d. Pores were however found to be very non-uniform in size and shape, with average pore sizes of 194 ± 110 μm. Interconnectivity does not seem to be improved with the use of ethyl acetate as a co-solvent.

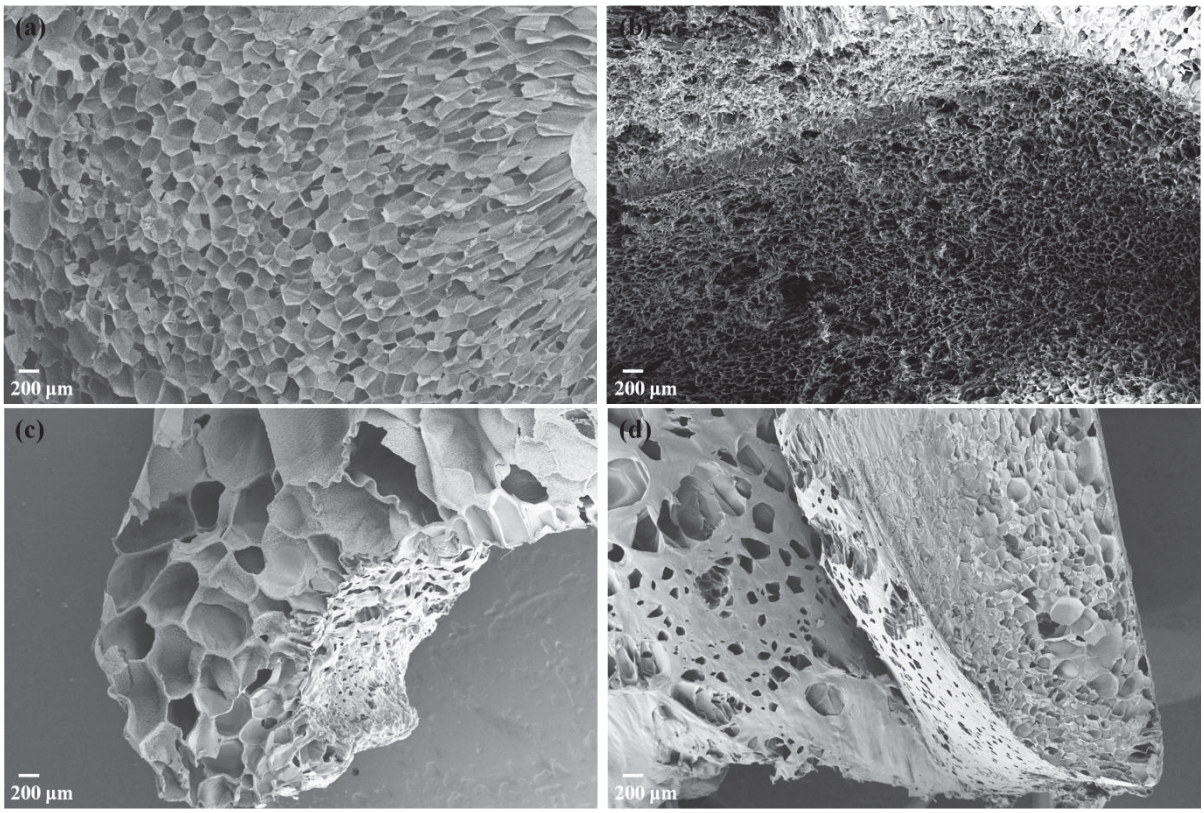

Figure 73. SEM images of PLGA foams generated by CO_2 foaming (35 ^{o}C / 9.2 MPa / fast DPR) with the addition of 0.2 wt% of the following co-solvent: (a) none, (b) acetone, (c) ethanol and (d) ethyl acetate.

7.5.3.2 PCL Foamed with Co-solvents

PCL foams generated with 0.2 wt% co-solvent addition are shown in Figure 74 and compared with a foam generated under the same conditions in the absence of co-solvent but using the same foaming conditions. The addition of acetone seemed to lead to greater non-uniformity with larger pores formed in the bottom half of the foam (left in the image) and smaller pores formed in the top half of the foam (right in the image), as shown in Figure 74b. This uneven pore size distribution may be due to non-uniform acetone distribution in the polymer. The upper half of the foam has average pore diameters of 111 ± 15 μm, while the bottom half has average pore diameters of 322 ± 42 μm. Overall average pore diameters of 179 ± 94 μm were observed using acetone as a co-solvent in PCL foaming. The density of the PCL foam generated with acetone addition was found to be 0.334 g/cm^3, which corresponds to a porosity of 71%. Ethanol addition led to a highly non-uniform pore structure with large pores up to 1 mm in diameter separated by bundles of smaller pores less than 50 μm in diameter. Average pore diameters were found to be 107 ± 98 μm. Residual ethanol in the polymer after foaming may have resulted in pore collapse, which caused a decrease in pore interconnectivity. The addition of ethyl acetate resulted in increased PCL pore sizes with average pore diameters of 265 ± 62 μm. No significant change in interconnectivity was observed by SEM. Co-solvent addition in CO_2 foaming of PCL did not reduce skin formation with any of the three co-solvents explored.

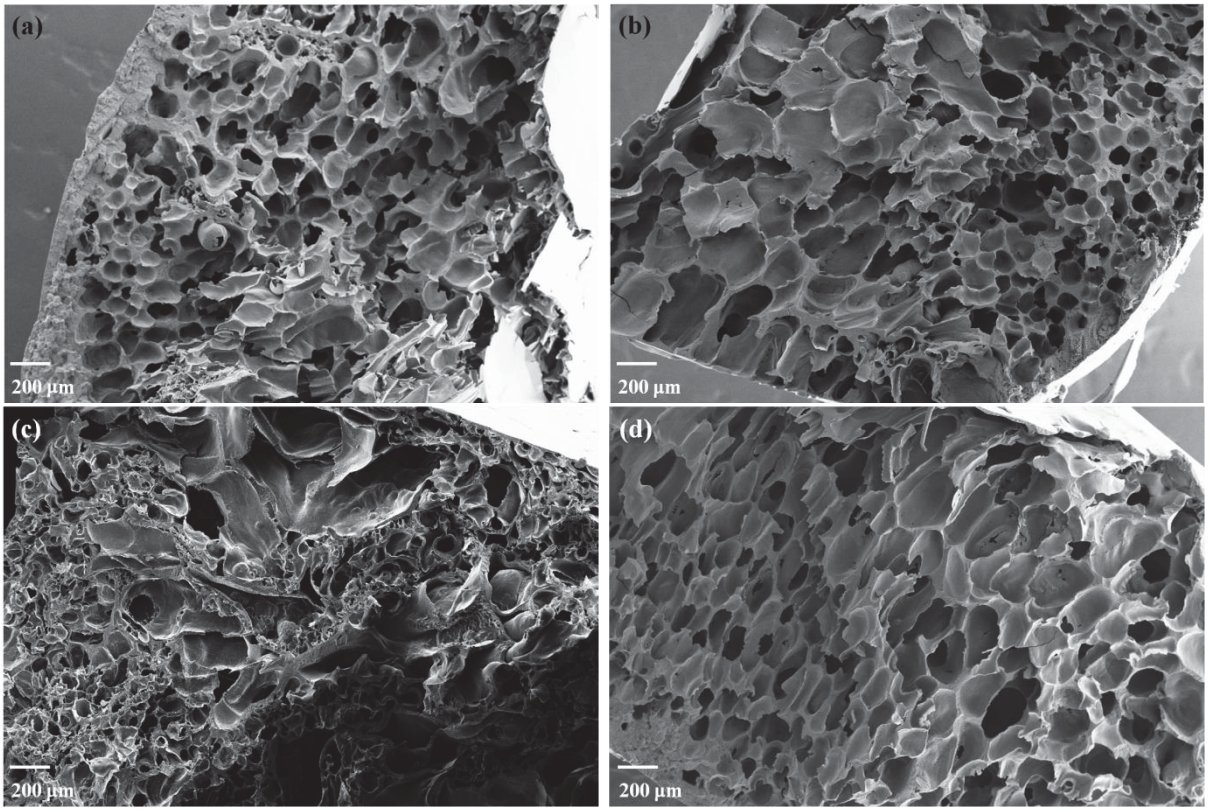

Figure 74. SEM images of PCL foams generated by CO_2 foaming at 35 ^{o}C / 9.2 MPa / fast DPR with the addition of 0.2 wt% of the following co-solvent: (a) none, (b) acetone, (c) ethanol and (d) ethyl acetate.

7.6 Conclusions

The effects of foaming parameters, T_{foam}, P_{foam}, DPR on the resulting foam structure of PCL and PLGA foams were examined and found to be consistent with reported trends. Acetone was found to improve interconnectivity in PLGA foams and limit skin formation at the bottom surface of PLGA foams, but did not result in any significant improvements in PCL foams. Ethanol was found to be a poor co-solvent in PLGA and PCL foams, as residual solvent caused pore deformation and collapse in both polymers. Ethyl acetate as a co-solvent in the foaming process did not result in any significant improvements in pore structure for PLGA or PCL. Thus,

acetone will be further explored as a co-solvent in polymer foaming with the incorporation of drug release components, as will be described in Chapter VIII.

Chapter VIII. Incorporation of Drug Release Components into Polymer Foams

8.1 Abstract

PLGA and PCL foams were generated using CO_2 and CO_2 + 0.2 wt% acetone, which were incorporated with drug release components, including pure drug, drug:CD physical mixtures and drug:CD inclusion compounds. All foams were generated from the same foaming conditions of 35 ^oC / 9.2 MPa / fast depressurization rate (DPR). The effect of the incorporation of drug release components on the resulting foam structures was studied by SEM, and drug release dynamics were studied using UV-Vis spectroscopy. Incorporation of drug release components into foams was found to result in increased pore diameters, which was attributed to the T_g or T_m depression of the polymer foams containing drug release components, allowing an extended duration of bubble growth before vitrification. Drug release studies revealed more complete release of drug release components from PCL foams than from PLGA foams. This arises from the liquid-like state of the amorphous regions in PCL in the drug release studies (37 ^oC) giving rise to free volume which allows drug diffusion from these regions. PLGA, on the other hand, is glassy at the conditions in the drug release studies, limiting diffusion of the drug out of the polymer matrix. In many foams, similar release behavior from foams containing drug:CD physical mixtures and drug:CD inclusion compounds was observed, suggesting that physical mixtures may undergo inclusion complex formation in situ during the foaming process. Drug release dynamics from 50/50 PLGA/PCL polymer blends were also studied and were shown to provide some insight into the distribution of the drug delivery component within the blend. Furthermore, acetone addition in the foaming process with the polymer blend was shown to

promote more even distribution of the drug release component between the two polymers. The present observations suggest that controlling the foaming process and adjusting the PLGA/PCL blend ratio can lead to tailored drug release profiles.

8.2 Introduction

In this chapter the generation of biodegradable polymeric TE scaffolds and drug delivery devices with supercritical carbon dioxide is explored and the resulting drug release behavior is reported. Biodegradable polymeric scaffolds are desirable in TE applications and regenerative medicine, and built in drug release attributes of these scaffolds can aid in the healing and regeneration process by incorporating drugs into the device.

As discussed in Chapter III, biodegradable polyesters were explored in this research, specifically PLGA (50/50 monomer ratio) and PCL. FDA approval has been granted for use of PLGA and PCL in biomedical applications, and abundant literature is available on the processing of these polymers with $scCO_2$ [27, 161] [30-32]. Carbon dioxide is not a good solvent for these polymers but can dissolve in the polymer to bring about morphological changes, including altered crystallinity [27, 161] and pore formation for polymer foaming [30-32].

Two different NSAIDs were chosen as the model drug release compounds in this study: piroxicam (PC) and ibuprofen (IB). These drugs display limited aqueous solubility as shown in Table 7 in Chapter II, which results in poor bioavailability in the body. To improve solubility of these drugs, two cyclodextrins (CDs) were investigated as host molecules. A native CD, β-CD, was used to host IB and a substituted CD, HP-β-CD, was studied as a potential host molecule for

PC. Pure drug, drug:CD physical mixture and drug:CD inclusion complex were individually incorporated into polymer prior to foaming. The drug release behavior of the scaffolds is expected to be dependent on the nature of the drug release component, the type of polymer employed and the pore morphology of the scaffold.

8.3 Materials

Piroxicam, ibuprofen, β-cyclodextrin and 2-hydroxypropyl-β-cyclodextrin were purchased from Sigma Aldrich and used as received without further purification. All drug release components were in powder form. Resomer RG 504 H, poly(DL-lactide-co-glycolide) with a 50/50 monomer ratio, was purchased from Boehringer Ingelheim and used as received. Poly(ε-caprolactone) was purchased from Sigma Aldrich and ground into powder form with a mechanical grinder before using. The IB:β-CD and PC:HP-β-CD inclusion compounds were prepared using a high pressure complex formation method which takes advantage of melting point depression of the drugs in CO_2. The high pressure method and characterizations of these compounds are described in Appendix B.

8.4 Methods

8.4.1 Incorporation of Drug Delivery Component

The drug delivery component consisting of pure drug, drug:CD physical mixtures or drug:CD inclusion complex, was physically mixed with the polymer prior to the foaming process. All of the components were in powder form and could be mixed by gentle grinding with a mortar and pestle. The mixture was placed into a small vial and the same types of foaming experiments as

optimized in Chapter VII were carried out. Samples were first exposed to CO_2 (+ co-solvent, if used) at 50 ^oC / 10.3 MPa for 30 minutes. The system was then cooled to 35 ^oC allowing pressure to drop with temperature to 9.2 MPa. Finally the system was depressurized by fully opening the exit valve causing the pressure to drop to ambient conditions in less than 10 s. Two sets of foams were generated. In the first set of foams generated, IB, IB + β-CD physical mixture and IB + β-CD inclusion compound were incorporated into PLGA foams. Then, in a different set of foams, PC, PC + HP-β-CD physical mixture and inclusion compound were incorporated into not only PLGA, but also in PCL and 50-50 PLGA-PCL blends. The effect of the drug delivery component on the foam structure was investigated by SEM, as described in Section 7.4.3.

8.4.2 Compression Molding

Compression molded polymer + PC drug release component disks were prepared for comparison with the foams in drug release studies. 100 mg samples were prepared containing polymer with either 2 wt% PC, 10 wt% PC:HP-β-CD physical mixture or 10 wt% PC:HP-β-CD inclusion compound. Drug release components were incorporated into the polymer prior to compression molding by gentle grinding with a mortar and pestle. Sample mixtures were then poured into a metal cylindrical die and heated to 70 ^oC. A Carver laboratory press was used to apply 5000 lbs of force to the polymer while maintaining the temperature at 70 ^oC for 1 minute. The compressed sample was then allowed to cool to room temperature by turning off the heaters.

8.4.3 Drug Release Studies

Drug release dynamics were measured from polymer foams containing a drug release component of either pure drug, drug:CD physical mixture or drug:CD inclusion complex. Each foam was submerged in 3 mL of a neutral (pH ~ 7.2) phosphate buffered saline (PBS) solution and placed on a rocker table at 37 ^{o}C with gentle rocking agitation at about 60 rpm. During sampling, all of the PBS was removed by pipette and replaced with 3 mL of fresh media. The amount of drug in the removed PBS was determined spectrophotometrically using an Ocean Optics UV-Vis instrument and analyzed with SpectraSuite software. The drug concentration vs absorbance calibration was obtained using solutions with known concentrations at wavelengths of maximum absorbance (λ_{max}) of 265 nm for IB and 334 nm for PC. Each experiment was carried out in triplicate (n=3). Averages and standard deviations are reported.

8.5 Results

8.5.1 PLGA Foams with Ibuprofen (IB) and β-cyclodextrin (β-CD) Drug Release Components

PLGA foams containing drug release components based on IB and β-CD are shown in Figure 75 and compared with pure PLGA foamed by the same process. Each foam was generated using CO_2 alone at a soak condition of 50 ^{o}C / 10.3 MPa / 30 min and a foaming condition of 35 ^{o}C / 9.2 MPa / fast DPR. It should be noted that at the soak conditions, IB, as discussed in Appendix B, is in the liquid state. A 10 wt% composition of drug release component was selected since higher additions led to foam crumbling. Drug release components incorporated into these PLGA foams were 10 wt% IB, 10 wt% IB:β-CD physical mixture (1:1 mol:mol) and 10 wt% IB:β-CD inclusion compound (1:1 mol:mol).

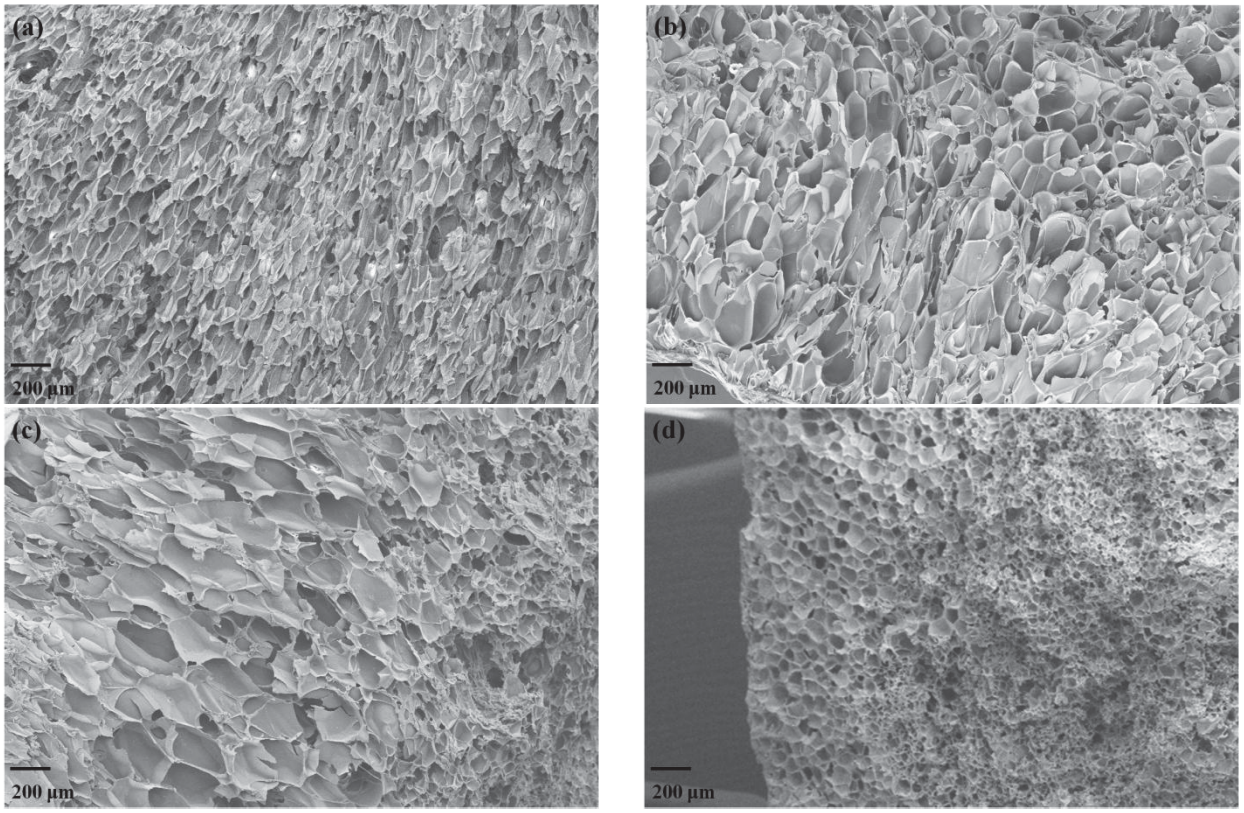

Figure 75. PLGA foams produced by CO_2 foaming at 35 ^{o}C / 9.2 MPa / fast DPR incorporated with (a) no drug release component, (b) 10 wt% IB, (c) 10 wt% IB:β-CD physical mixture (1:1 mol:mol) and (d) 10 wt% IB:β-CD inclusion complex (1:1 mol:mol).

The foam generated without the addition of a drug release component shown in Figure 75a, was found to have average pore diameters of 100 ± 29 µm, while average pore diameters for foams incorporated with 10 wt% IB, 10 wt% physical mixture (PM) and 10 wt% inclusion compound (IC) were found to be 151 ± 32 µm, 159 ± 132 µm and 57 ± 31 µm, respectively. The formation of larger pores as a result of incorporation of drug release components was not initially expected, since the addition of immiscible components to polymer foaming processes has been reported to decrease the pore size due to heterogeneous nucleation [251]. The larger pores suggest that a

longer time was allowed for cell growth before polymer vitrification. To further investigate this possibility, the thermal characteristics of the PLGA foams containing IB and β-CD based drug release components were studied by DSC to explore whether the glass transition temperature of the polymer had been altered in the presence of the drug release components. To erase the thermal history of the foams, foamed samples were first heated to 100 ^{o}C then cooled and reheated. The second heating scans from DSC runs at 10 ^{o}C/min are shown in Figure 76 which displays the PLGA glass transition temperature of each foam. As seen in the figure, the addition of IB or IB + β-CD physical mixtures resulted in a T_g depression of about 7 ^{o}C in PLGA foams, compared to foams which do not contain any drug release component. However, addition of the IB + β-CD inclusion compound (IC) depressed the T_g of PLGA to a lesser extent of 4 ^{o}C. Due to depression of the T_g, the time allowed for pores to grow during depressurization is further extended, resulting in the generation of larger pores. Based on the DSC heating scans, the larger pore sizes would be expected for foams incorporated with IB and the IB:β-CD physical mixture followed by IB:β-CD inclusion compounds and then PLGA alone. The T_g trend observed in DSC heating scans is consistent with what is observed in the SEM images in Figure 75.

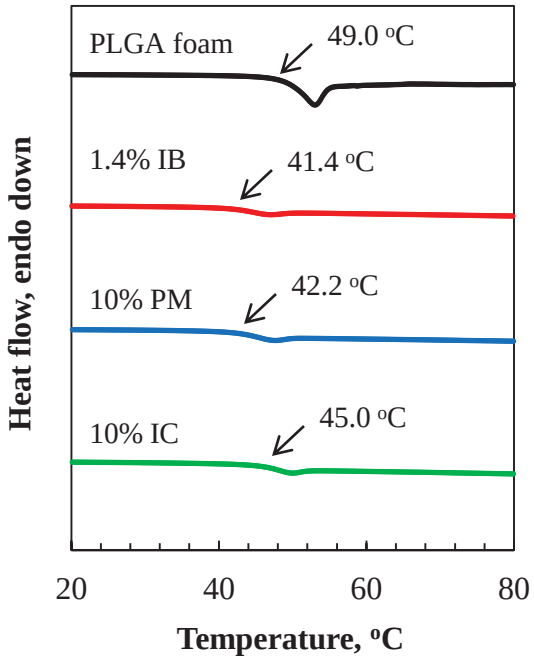

Figure 76. Effect of the incorporation of drug release components on the T_g of PLGA foams. Second heating scans are shown, as a first heating scan was carried out to erase thermal history of the polymer.

An additional feature of Figure 75 is that the foams incorporated with pure IB, pure β-CD and the IB:β-CD physical mixture were found to contain particles inside the pores, which suggests the presence of the crystalline drug release components. This is expected to affect the drug release behavior, as the drug contained within the pores of the foam is expected to be released more rapidly than drug contained within the polymer matrix. Drug release studies were carried out at 37 °C, which is below the T_g of PLGA, resulting in very low free volume from which drug molecules can diffuse. Thus, the drug contained within the pores can be released easily if directly exposed to the drug release media, which would be possible if some degree of interconnectivity exists. The drug contained within the polymer matrix cannot be easily released

until PLGA undergoes swelling or hydrolysis, which will then open up free volume for drug diffusion out of the matrix.

8.5.2 Drug Release Dynamics from PLGA Foams with Ibuprofen and β-cyclodextrin Components

8.5.2.1 Effect of the Incorporated Drug Release Component

Drug release studies were carried out to determine the effect of the pore structure and of the incorporated component on drug release dynamics from PLGA foams. The amount of IB incorporated into the foams used in the drug release studies was maintained at 1.4 wt%, since this corresponds to the amount of IB present in the 10 wt% physical mixture (1:1 mol:mol) or CD inclusion compound (1:1 mol:mol). Figure 77 shows the effect of the different incorporated compounds on the IB release from PLGA foams containing 1.4 wt% IB, 10 wt% IB:β-CD physical mixture and 10 wt% IB:β-CD inclusion complex.

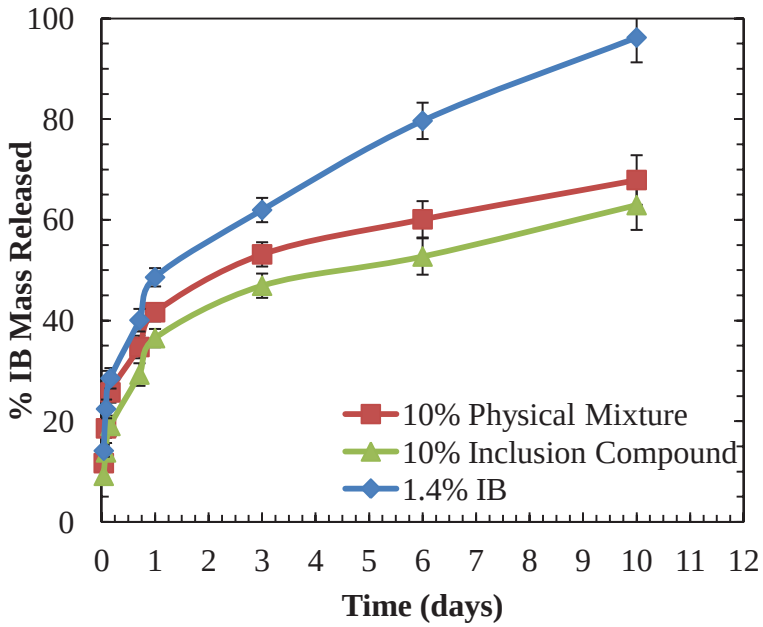

Figure 77. Comparison of drug release behavior of PLGA foams incorporated with different drug release components (n=3).

In all of the foams the release is sustained over the 10 day release study, although release rates clearly decline after the first 24 hours. The initial fast release suggests that the IB on the surface of the foams is initially released, followed by a slower release from within the foam, either from pore surfaces or from within the polymer matrix. Comparing the release components, the foam containing IB alone as the drug delivery component displays a faster and higher IB release than the foams containing either the physical mixture (PM) or the inclusion complex (IC). Considering the aqueous solubility of IB is 0.021 mg/ml [39] and is 18.5 mg/ml for β-CD [57] at 25 ^{o}C, this trend is counterintuitive. Other factors being equal, the IC would be expected to exhibit the faster and more complete drug release due to the improved solubility of the complex compared to IB alone. It should be noted that the release profiles of the IC and the PM are very similar, and may result from the PM forming a complex during the foaming process. To further

investigate the potential complex formation at the foaming conditions, a PM was subjected to the same procedure as the foaming procedure but in the absence of polymer. Analyzing the mixture after processing by DSC showed that about 90% of the crystalline, uncomplexed IB remained in the PMs after both, the CO_2 and the CO_2 + acetone, processing. However, in the polymer + PM + CO_2 (+ co-solvent) mixtures it is possible that the IB still becomes included into the β-CD cavity at these conditions, as the potential synergistic effects in these complex systems cannot be overruled.

The presence of particles in the pores of the foams containing pure IB and the PM could explain a higher release from those foams. As indicated earlier, the SEM images in Figure 75 further suggest that the IC is contained within the bulk of the polymer rather than within the pores, due to the absence of particles within the pores and the smaller pore sizes that were observed. If most of the inclusion complex is actually contained within the bulk of the polymer rather than inside the pores, it is not unreasonable to see a slower release from the foam containing the inclusion complex, as discussed in the previous section.

8.5.2.2 Effect of the Pore Morphology from Foaming Process

The effect of the foaming conditions on the drug release behavior from PLGA foams was investigated by comparing foams generated by fast versus slow DPRs. DPR was selected as the varied processing parameter since pore structure is most significantly affected by the DPR as was shown in the SEM images in Figure 70. Figure 78 displays the drug release behavior from PLGA foams incorporated with 1.4 wt% IB generated by CO_2 foaming with a fast and a slow DPR. The drug release profiles of the two different foams are nearly identical for the first 72

hours. Then the release becomes higher and reaches its plateau value for the foam generated by slow depressurization. It should be noted that average pore sizes for the fast DPR PLGA foam were 151 ± 32 μm, while the slow DPR PLGA foam had average pore diameters of 878 ± 274 μm. Even though the release of IB during the first 72 hours does not seem to be affected by pore size, the later stage of release is clearly showing higher release from the foam with larger pores (slow DPR), which is as would be expected.

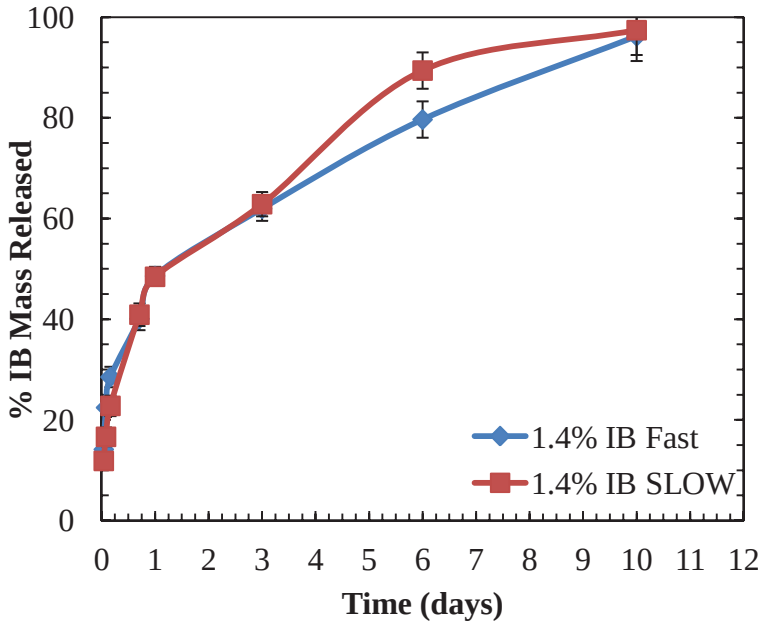

Figure 78. Comparison of IB release behavior from PLGA foams generated using a 'fast' DPR and a 'slow' DPR at 35 ^{o}C / 9.2 MPa (n=3).

8.5.2.3 Effect of Co-solvent Addition

The effect of co-solvent addition on drug release dynamics was then investigated with foams incorporated with a physical mixture of IB and β-CD, and the IB release profiles are shown in Figure 79. The release rate and total percent release from all of these foams were similar,

although co-solvent addition led to a slightly higher percent release of IB by the end of the 10 day study. Foams generated with acetone as a co-solvent led to the highest drug release levels, while ethanol or ethyl acetate addition resulted in foams with similar but lower IB release by the end of the 10 day study. As was shown in the SEM images in Figure 73 from Chapter VII, foams generated with acetone as a co-solvent displayed a higher level of interconnectivity compared to foams generated with ethanol or ethyl acetate as a co-solvent, which would suggest that a higher drug release would be expected from the foams generated with acetone addition. The observations from the drug release studies appear to be consistent with the pore morphologies in the respective systems.

An additional feature displayed in Figure 79 is the short time drug release behavior. As shown in the case of the foam generated without the use of a co-solvent, the short time release is higher while long time release is lower compared to the foams generated with co-solvent addition. This suggests that the physical mixture has a greater propensity to form the inclusion complex in the presence of co-solvents. This is evidenced by the slower release at short times seen in the foams generated with co-solvent addition. While all mixtures likely contain some fraction of IC as a result of the processing, it appears from the IB release behavior that the foams generated with co-solvent addition contain a higher fraction of the inclusion complex than the foam generated with CO_2 alone. Again, this notion of complex formation was not displayed in the DSC analysis of PMs exposed to CO_2 and CO_2 + acetone at the same conditions as the foaming process, as 90% of the IB remained uncomplexed. However, the observations in foaming and drug release behavior point to the plausible synergistic effects promoting the inclusion complex formation of

the PM during the processing of the polymer, especially as competitive carbonyl group interactions have been shown to affect molecular association as described in Chapter VI.

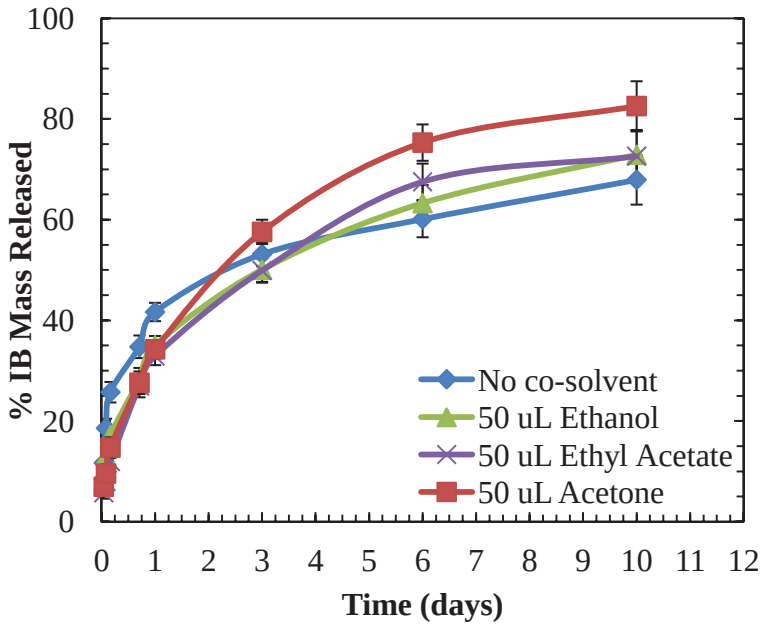

Figure 79. Release of 1:1 molar ratio IB:β-CD physical mixture from PLGA foams generated with the use of different co-solvents at 35 ^{o}C / 9.2 MPa / fast DPR (n=3).

8.5.3 Polymer Foams with Piroxicam (PC) & 2-Hydroxypropyl-β-cyclodextrin (HP-β-CD) Drug Release Components

8.5.3.1 PLGA Foams

Foams incorporated with PC and HP-β-CD based drug release components are shown in Figure 80. Each foam was generated using CO_2 alone at a soak condition of 50 ^{o}C / 10.3 MPa / 30 min and a foaming condition of 35 ^{o}C / 9.2 MPa / fast DPR. Foams incorporated with 2 wt% PC, 10 wt% physical mixture and 10 wt% inclusion compound were found to have pore diameters of

362 ± 68 μm, 274 ± 45 μm and 143 ± 41 μm, respectively, compared to the PLGA foam without any drug release component incorporated, which was found to have an average pore diameter of 100 ± 29 μm. Thus, pore sizes were found to be much larger in PLGA foams containing PC:HP-β-CD drug release components. The thermal behavior of the PLGA foams was investigated to further study this phenomenon, and the resulting DSC (second) heating scans are shown in Figure 81. As shown in the figure, the T_g of PLGA is depressed in the foams incorporated with PC:HP-β-CD drug release components by about 4 ^oC, with the depression being similar for each of the foams, regardless of the incorporated component. The T_g depression would permit an extended duration of pore growth in the foaming process, leading to larger pores, which is consistent with the SEM images.

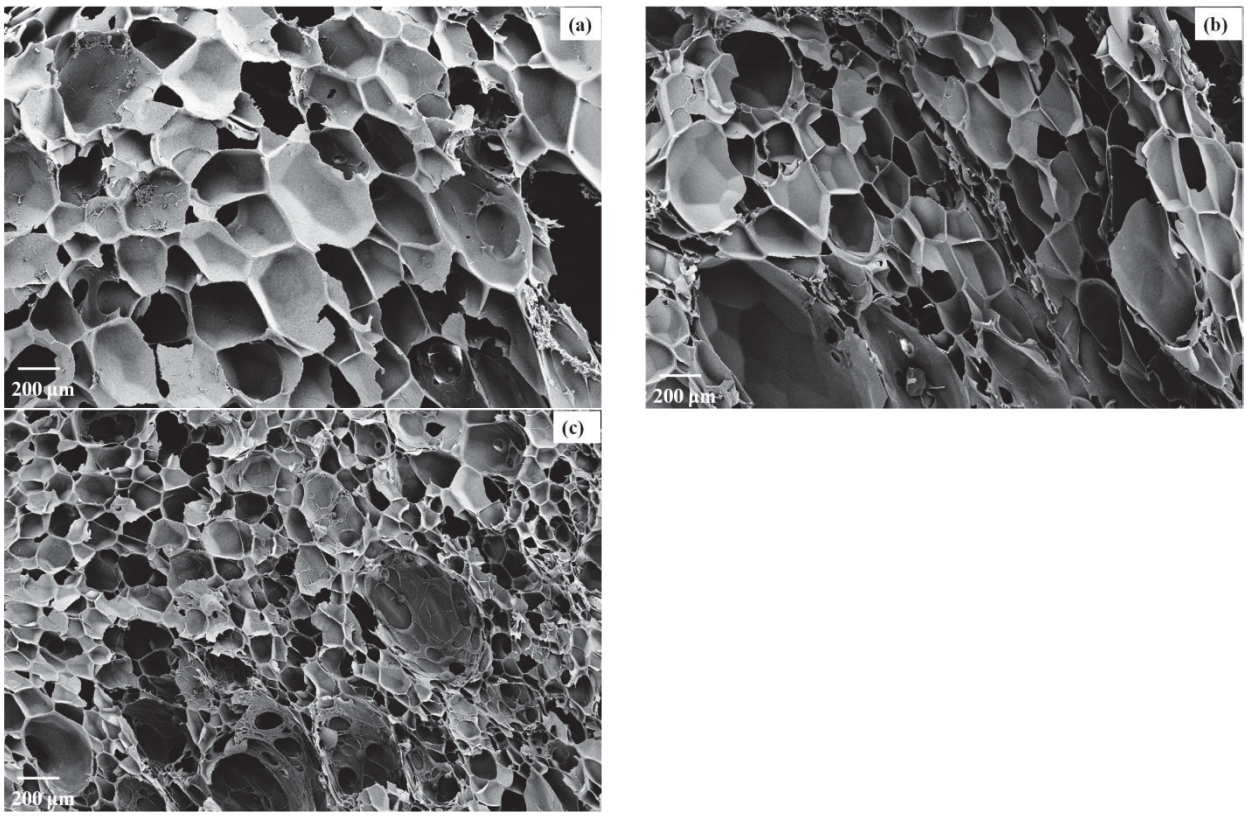

Figure 80. PLGA foams generated by CO_2 foaming (35 ^{o}C / 9.2 MPa / fast DPR) incorporated with (a) 2 wt% PC, (b) 10 wt% PC:HP-β-CD physical mixture (1:1 mol:mol) and (c) PC:HP-β-CD inclusion complex (1:1 mol:mol).

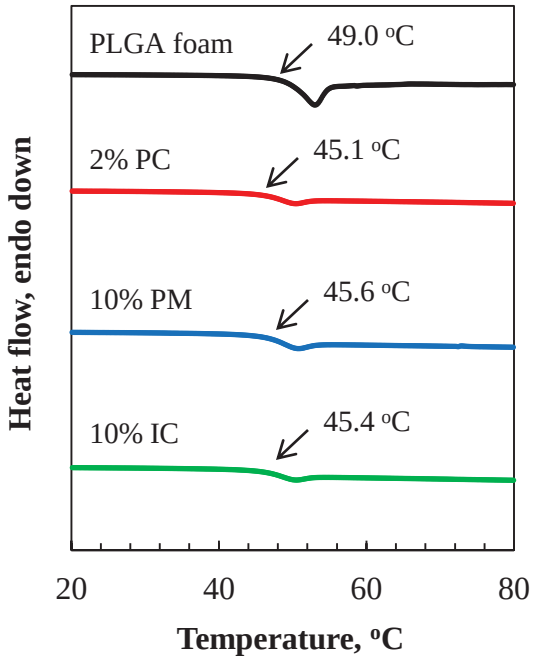

Figure 81. Effect of the incorporation of drug release components on the T_g of PLGA foams. Second heating scans are shown, as a first heating scan was carried out to erase thermal history of the polymer.

The pores generated in the foams incorporated with PC:HP-β-CD drug release components were much larger than those observed in the foams incorporated with IB and β-CD based drug release components in, which cannot be sufficiently rationalized strictly based on observation of T_g depression of the polymer in polymer-drug composite foams. Another factor to consider in the resulting pore morphology of these foams is the solubility of the incorporated drug in CO_2. In going from IB to PC, there is a significant reduction in CO_2 solubility, as was shown in Figure 12 in Chapter II. The solubility is shown again here at the P-T conditions similar to those employed during foaming in Figure 82. Solubility data was not available for PC at 308 K, and the information at 312.5 K is provided in the figure as an estimate instead. Based on the trend seen in Figure 12 from Chapter II, PC solubility in CO_2 decreases with decreasing temperature, thus,

the very sparing solubility shown in Figure 82 is still higher than what would be expected at 308 K. From this solubility information it is known that IB is at least 300 times more soluble in CO_2 than PC at 308 K and 10 MPa. The difference in solubility between IB and PC suggests that IB will be much better dispersed in the polymer than PC due to the dissolution of the drug in CO_2. In addition, from the DSC studies in Appendix A, it is known that IB undergoes slow recrystallization from the melt, indicating that IB will be in the liquid state during and even after foaming has taken place. PC, on the other hand, remains in the solid state during the entire foaming process, aside from very small amounts which dissolve in CO_2. The presence of a dispersed molten drug vs solid drug particles is likely to affect the resulting foam structure as reflected by the differences in average pore diameters.

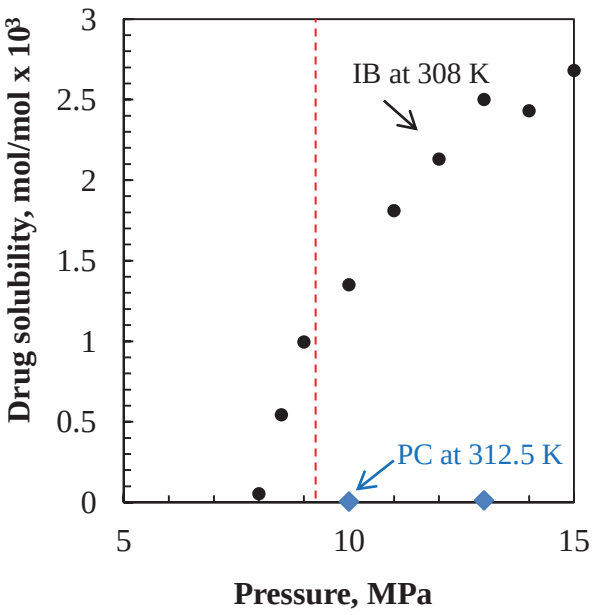

Figure 82. Ibuprofen [62] and piroxicam [252] solubility in CO_2 at conditions similar to foaming conditions. Dashed red line indicates the solubility at the foaming pressure of 9.2 MPa.

It is important to also note that foams generated with the PC:HP-β-CD inclusion complex display smaller pores, as was the case with IB:β-CD for similar reasons of the IC being better distributed in the polymer matrix. The dispersion of the PC:HP-β-CD inclusion compound in the PLGA matrix may have been further improved beyond what was observed in the PLGA + IB:β-CD mixtures due to the presence of the hydroxypropyl group on the HP-β-CD, which would be expected to improve CD miscibility with PLGA.

8.5.3.2 PLGA Foams Generated with Acetone Addition

Acetone was investigated as a co-solvent at 0.2 wt% in PLGA foams incorporated with PC:HP-β-CD inclusion compound. Foams were generated at a soak condition of 50 ^{o}C / 10.3 MPa / 30 min and a foaming condition of 35 ^{o}C / 9.2 MPa / fast DPR. SEM micrographs of the foam generated with CO_2 alone and the foam generated with CO_2 + 0.2 wt% acetone are compared in Figure 83. In the foam produced with acetone addition, the pore walls are rippled, which is evidence of residual acetone in the foam after depressurization leading to pore deformation and collapse. This is, at first sight, surprising, since the same acetone addition level in the PLGA without an incorporated drug release component did not lead to pore deformation, as was shown in Figure 73 in Chapter VII. This morphological observation suggests that acetone is being retained to a greater degree in the foams incorporated with CD:drug release components, which may possibly be arising from carbonyl group interactions between PC and acetone. In addition, interconnectivity may have been reduced with the addition of acetone to this PLGA foam, especially as the interconnectivity in the PLGA foam generated without acetone addition shown in Figure 83a is already relatively high compared to other PLGA foams. The bottom surface of the foam incorporated with the PC:HP-β-CD inclusion compound produced with acetone

addition, shown in Figure 83c, displays numerous pore openings, evidence of a lack of skin formation, even though skin formation was still found to occur on the top surface of the foam.

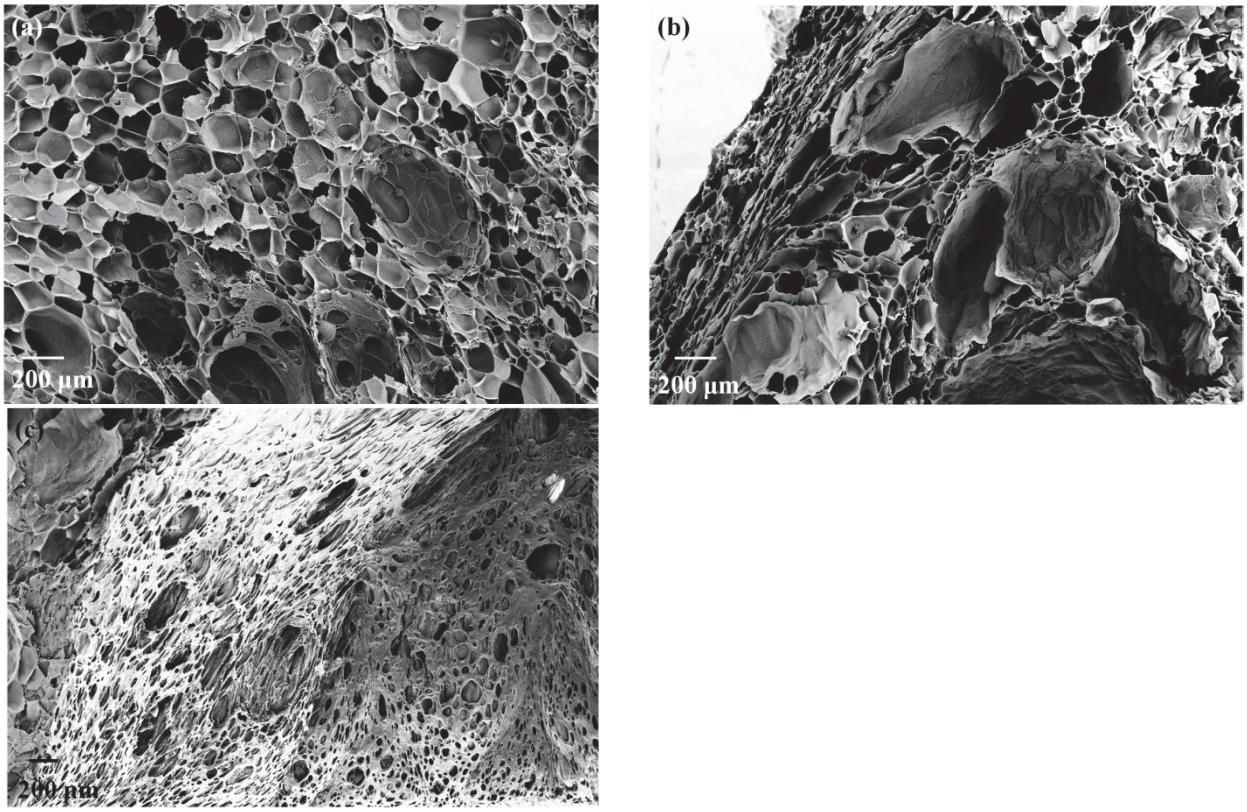

Figure 83. PLGA foams generated by foaming at 35 ^{o}C / 9.2 MPa / fast DPR incorporated with 10 wt% PC:HP-β-CD inclusion complex (1:1 mol:mol) using (a) only CO_2, (b) CO_2 + 0.2 wt% acetone (cross-section of foam) and (c) CO_2 + 0.2 wt% acetone (bottom surface of foam).

8.5.3.3 Piroxicam Release Dynamics from PLGA Foams

Figure 84 shows the effect of the drug release component incorporated into PLGA foams generated with both, CO_2 alone and CO_2 + 0.2 wt% acetone. As shown, with all of these PLGA foams the drug release levels are relatively low, with total PC released being less than 25 wt% of the total PC contained in the foams at the end of the 17 day study. The extent of the PC release reaches a plateau in all of these PLGA foams within 24 hours, with only small amounts of PC being released afterwards. The drug released in the first day is likely due to the drug confined to the surfaces of the polymer exposed to the PBS solution. However, the very slow release after 24 hours suggests that a significant portion of the drug is contained within the bulk polymer, which depends on the swelling of hydrolysis of PLGA to open up some free volume from which the drug can diffuse. Assuming an evenly dispersed drug within the polymer, a small amount of PC will continue to be released until the PLGA is completely degraded, which is approximately 3 months for this polymer, according to the supplier.

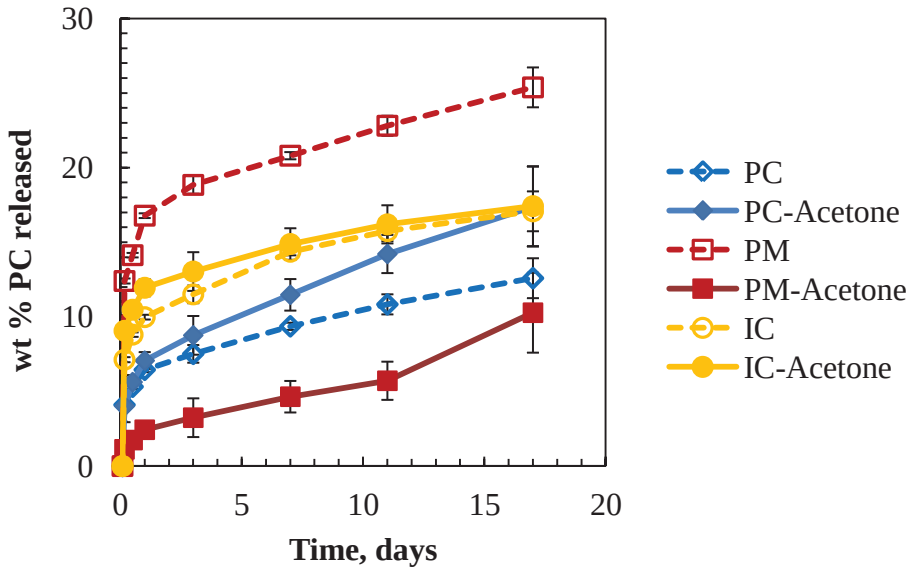

Figure 84. Effect of the drug release component on the drug release behavior from PLGA foams generated using CO_2 only (solid lines) and CO_2 + 0.2 wt% acetone (dashed lines) (n=3).

In the foams produced with CO_2 only, the fastest and most complete release is observed from the PLGA foam containing the PM, followed by the IC and then the PC alone. Here also it appears that the inclusion compound is better incorporated into the bulk of the polymer material, rather than excluded into the pores, leading to a slower release dependent on the swelling or hydrolysis of PLGA.

In the foams generated with CO_2 + 0.2 wt% acetone, the PC and IC incorporated foams displayed similar release profiles, which were also very close to their release profiles in the CO_2 – foamed samples. The amount of drug released from the foam containing the PM was, however, reduced in the CO_2 + acetone – foamed sample in comparison with the CO_2 – foamed sample. As noted with the SEM images of PLGA foamed with CO_2 + acetone in Figure 83b in the previous section, there is a high possibility of acetone interaction with both the drug and the

polymer. This interaction may be promoting the formation of the IC from the PM during the foaming procedure. This was further investigated using the same processing technique as used in the foaming process but in the absence of polymer. It was found that a 1:1 molar ratio physical mixture of PC and HP-β-CD, when exposed to either CO_2 alone or CO_2 + 0.2 wt% acetone at the same conditions resulted in about 20 wt% IC, based on PC melting transitions seen in DSC heating scans. This indicates that physical mixtures of PC and HP-β-CD are able to form an inclusion complex under the foaming conditions, which may lead to similar drug release behavior from foams containing the PM and the IC.

It should be noted that the effect of the drug release component cannot be examined strictly independent of the foam structure, since the incorporated compound was also found to affect the foam structure, as shown in Figure 80. To study the drug release independently, polymer discs incorporated with the different drug release components were formed by compression molding. Figure 85 shows the effect of the drug release component from compression molded PLGA discs containing 2 wt% PC, 10 wt% PC:HP-β-CD physical mixture (PM) or 10 wt% PC:HP-β-CD inclusion compound (IC). The PM displayed the fastest and highest drug released during the study, followed by the IC and then PC alone. PC would be expected to display the slowest release, as PC is not very water soluble (0.0198 mg/ml at 25 ^{o}C [45]). Complex formation of PC with HP-β-CD increases the aqueous solubility of PC, recalling that the solubility of HP-β-CD is > 600 mg/ml at 25 ^{o}C [46]. However, no significant increase in PC is displayed from the disc containing the IC beyond the release from pellets containing only PC. The high PC release from the disc containing the PM, suggests that the presence of HP-β-CD does indeed enhance the delivery of PC from these PLGA discs, although inclusion complex formation may not be

necessary. The presence of CDs within relatively hydrophobic polymers, such as PLGA, has been reported to improve the wettability of the polymer [253], which may in itself be enough to aid in the diffusion of PC from the polymer to the PBS solution.

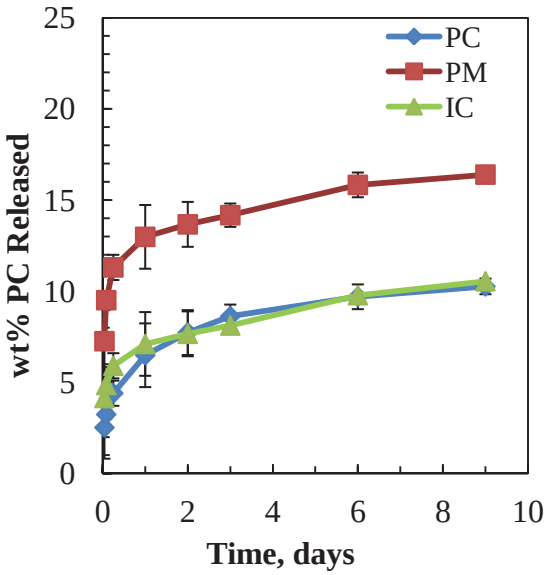

Figure 85. Effect of the drug release component from compression molded PLGA pellets (n=3).

8.5.3.4 PCL Foams and PCL + PLGA Blend Foams

PCL was also investigated as a foam material incorporated with PC and HP-β-CD based drug release components. Foams were generated at a soak condition of 50 ^{o}C / 10.3 MPa / 30 min and a foaming condition of 35 ^{o}C / 9.2 MPa / fast DPR. SEM images were only acquired for the foams containing the PC:HP-β-CD inclusion complex. The micrographs of the foam generated with CO_2 alone and of the foam generated with CO_2 + 0.2 wt% acetone are compared in Figure 86. The average pore diameter for the foam generated with CO_2 alone is 259 ± 46 μm and 413 ± 130 μm for the foam generated with acetone addition. For comparison, the PCL foam generated from CO_2 foaming at the same conditions without incorporation of a drug release component

resulted in an average pore diameter of 181 ± 28 μm, while the foam generated with acetone addition resulted in an average pore diameter of 179 ± 94 μm, as was shown in Figure 74. The incorporation of PC:HP-β-CD inclusion complex resulted in an increase in average pore diameter, which is likely due to melting point depression of the PCL by the presence of drug molecules, as was seen for T_g depression in PLGA foams. Melting point depression, similar to T_g depression, extends the duration of pore growth during foaming, which results in the generation of larger pores.

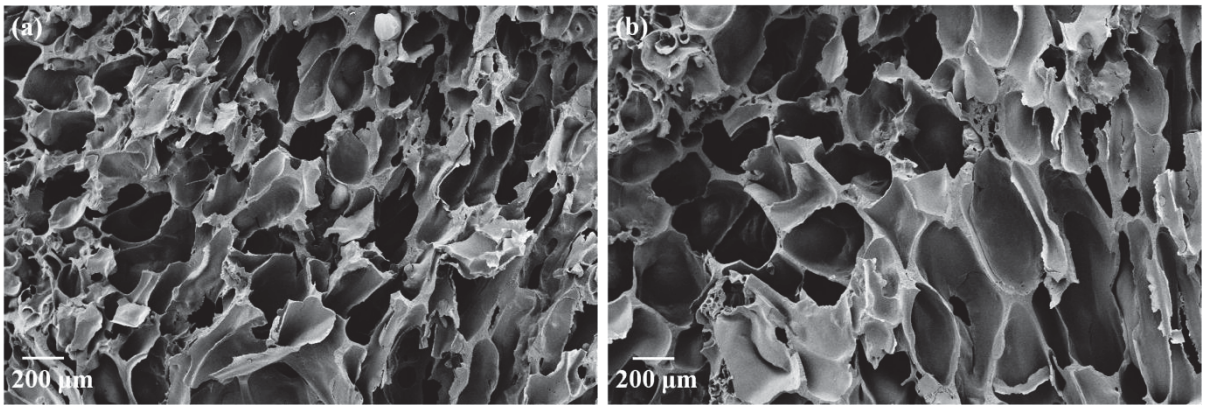

Figure 86. PCL foams generated by foaming at 35 ^{o}C / 9.2 MPa / fast DPR incorporated with 10 wt% PC:HP-β-CD inclusion complex (1:1 mol:mol) using (a) only CO_2 and (b) CO_2 + 0.2 wt% acetone.

50-50 wt% blends of PCL and PLGA were also explored as foams incorporated with PC:HP-β-CD inclusion compound. Foams were generated at a soak condition of 50 ^{o}C / 10.3 MPa / 30 min and a foaming condition of 35 ^{o}C / 9.2 MPa / fast DPR. A comparison of a PLGA-PCL blend foam generated with CO_2 alone is compared with a foam generated with 0.2 wt% acetone addition in Figure 87. The 50-50 PCL-PLGA blend foamed with CO_2 alone displayed an average pore diameter of 134 ± 58 μm, while the foam generated with the addition of acetone

had an average pore diameter of 142 ± 55 μm. Both foams have highly non-uniform pores, and some degree of interconnectivity was observed upon closer inspection. Large sections of the samples appear to be non-porous in both foams. It is not clear whether these sections are indeed non-porous or if they are interfacial boundary layers which have formed between PCL-PLGA domains.

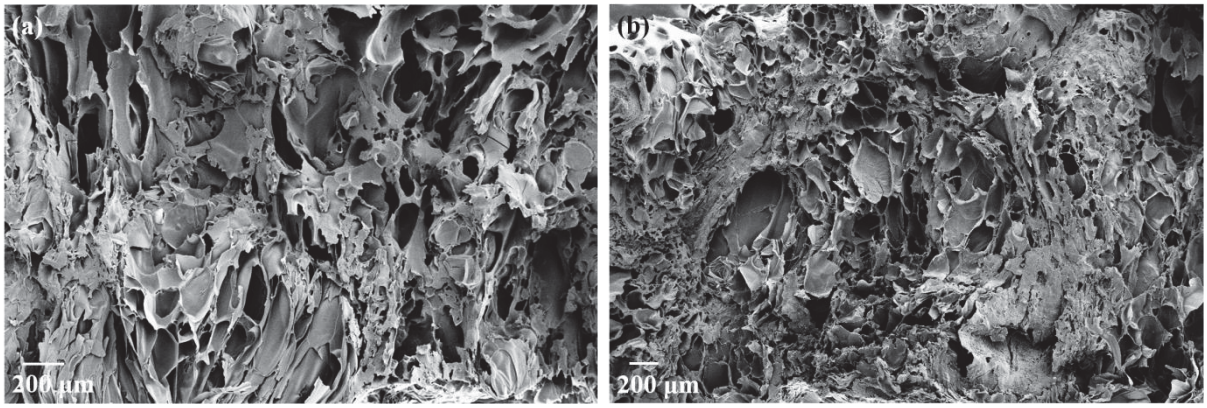

Figure 87. 50/50 PLGA-PCL foams generated by foaming at 35 ^{o}C / 9.2 MPa / fast DPR incorporated with 10 wt% PC:HP-β-CD inclusion complex (1:1 mol:mol) using (a) only CO_2 and (b) CO_2 + 0.2 wt% acetone.

8.5.3.5 Piroxicam Release Dynamics from PCL and PCL + PLGA Blend Foams

The drug release profiles from PCL foams incorporated with different PC drug release components and foamed using both, CO_2 and CO_2 + 0.2 wt% acetone, are shown in Figure 88. Drug release from PCL foams is much higher than the release from PLGA foams, as 25-67 % of the total drug was released from these foams. Furthermore, the PC release level reached a plateau after 7 days, which is in contrast to about 1 day for PLGA foams. PCL is a semi-crystalline polymer with a T_g of about -60 ^{o}C and a T_m of about 55-60 ^{o}C [20]. Since PCL is

highly crystalline (50 – 71 % crystallinity), the polymer is solid at room temperature, even though it is above its T_g. However, the amorphous regions of PCL are liquid-like and have free volume in which it can assume different chain conformations. This free volume provides pathways for incorporated drug release components to diffuse out of the amorphous domains of PCL during drug release studies at 37 ^oC, leading to faster and more complete drug delivery from PCL foams than from PLGA foams.

In PCL foams produced with CO_2 alone, the fastest release dynamics were displayed in the foams containing the PM, followed by pure drug and then the inclusion complex. In addition, the release from PCL foams plateaus after about 24 hours in PBS solution, although the release is not yet complete. The remaining fraction of drug release component is likely contained within regions of PCL which are bounded by crystalline domains and will not be released until the polymer starts to degrade.

The release of PM and IC was higher from the foams generated with CO_2 + acetone, although pure PC release was similar in foams generated with both, CO_2 and CO_2 + acetone. As shown earlier, the pore diameters are much larger in foams generated with the CO_2 + acetone mixture, suggesting that the diffusion of the drug release component is facilitated from the larger pores.

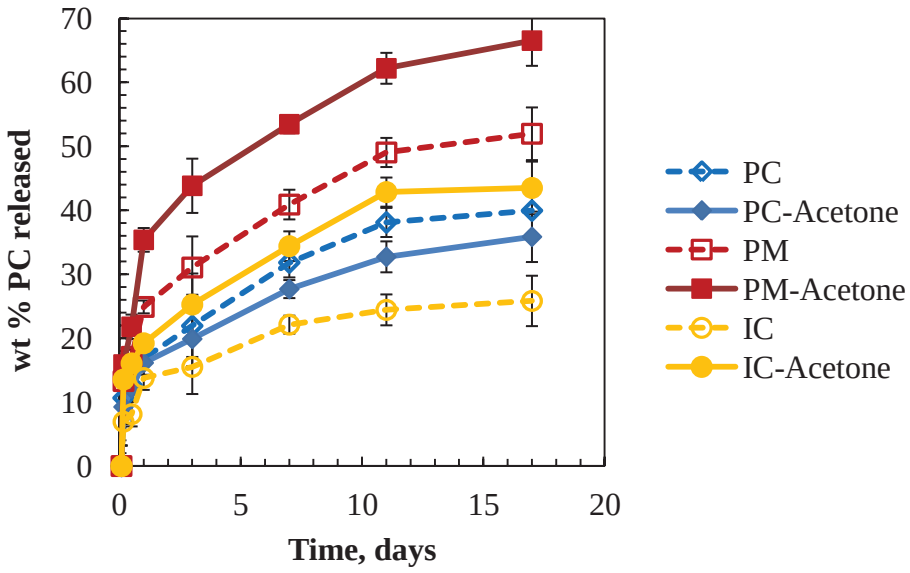

Figure 88. Effect of the drug release component on the drug release behavior from PCL foams generated using CO_2 only (solid lines) and CO_2 + 0.2 wt% acetone (dashed lines) (n=3).

To examine the effect of the drug release component independent of foam structure, non-porous PCL discs were compression molded (70 ^{o}C / 5000 lbs / 1 min) which contained each of the different drug release components. The compression molding temperature was chosen such that the PCL would be melted while the PC would remain in the solid state. Figure 89 shows the PC release profiles from the discs. The fastest release was observed in the PCL disc containing PC alone, with the physical mixture displaying a slower release, followed by the inclusion complex with the slowest release. Interestingly, the short time release from the disc containing the inclusion complex displays a higher release than the pure PC or the physical mixture. However, after 12 hours, the inclusion complex release rate declines, and the release of pure PC and the physical mixture become higher. This is in contrast to the trend observed with the PCL foams where the fastest release was observed from the pellet containing the physical mixture, although incorporation of the IC also resulted in the slowest release in PCL foams. These differences

arise due to differences in pore structure resulting from the incorporated drug release component, as well as the type of incorporated drug release component, itself. The release of each drug release compound was found to be faster in discs compared to the foams, which is likely due to the decreased volume of the PCL discs compared to the foams, which facilitates diffusion of the drug from the smaller volume of the disc.

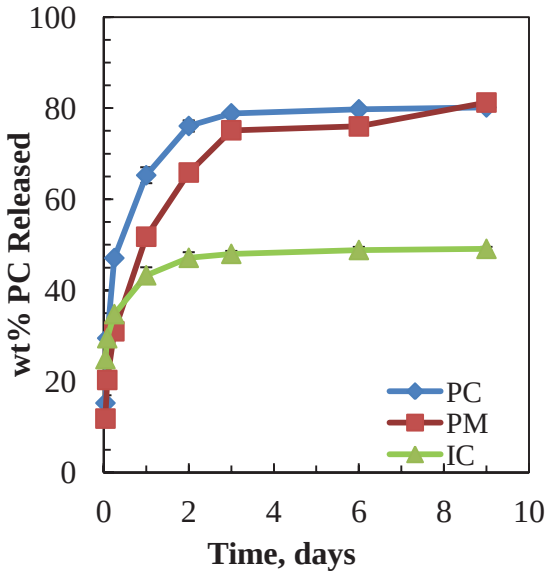

Figure 89. Effect of incorporated drug delivery component in PCL pellets prepared by compression molding (n=3).

The effect of the drug release component on the release behavior from 50/50 PLGA-PCL foams generated with both, CO_2 alone and CO_2 + 0.2 wt% acetone, is shown in Figure 88. In this polymer blend, the drug release behavior appears to be most influenced by the presence of PCL. Looking at the foams generated using CO_2 alone, the short time release behavior of the PM is almost exactly the same as that of the IC. However, after 3 days, the IC release reaches a plateau, while the PM continues release at a similar rate as the pure PC. The combined behavior

of the PM as the IC and the pure PC, suggests that the PM has partially formed an IC in the CO_2 processing. In the PCL/PLGA foam prepared with CO_2 + acetone foaming, the behavior of the PM and the IC are almost exactly the same, suggesting PM has formed the IC, which is promoted more fully with the addition of acetone to the process.

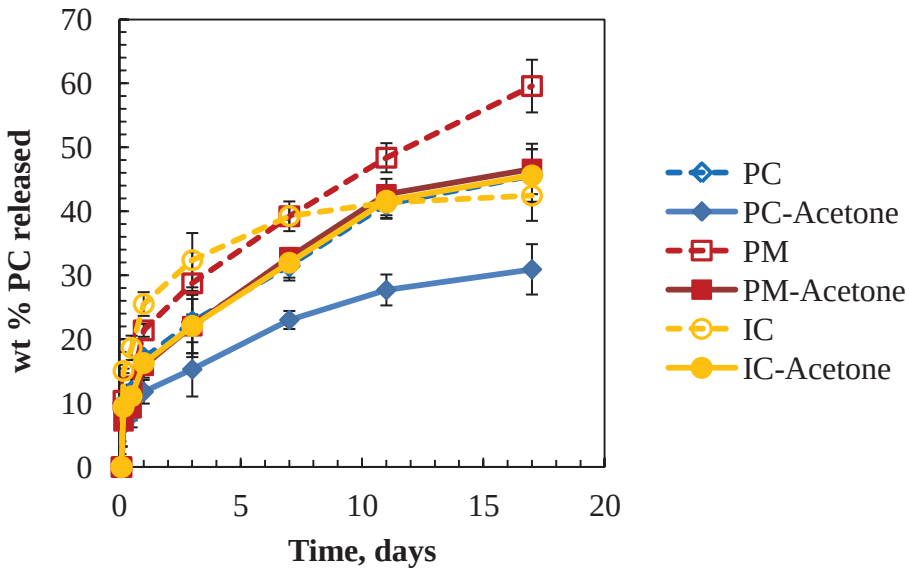

Figure 90. Effect of the drug release component on the drug release behavior from 50/50 PLGA/PCL foams generated using CO_2 only (solid lines) and CO_2 + 0.2 wt% acetone (dashed lines) (n=3).

8.5.3.6 Effect of Polymer Choice on Piroxicam Release

Figure 91-Figure 93 compare the drug release kinetics from PCL, PLGA and 50/50 PCL/PLGA foams generated using CO_2 or CO_2 + 0.2 wt% acetone. In all of these scaffolds, PCL foams exhibit a higher release than PLGA foams. As discussed in the previous sections, the amorphous regions in PCL contain free volume since the polymer is well above its T_g, creating pathways for drug diffusion into the PBS solution. In contrast, PLGA is below its T_g, and very low free

volume within the amorphous polymer leads to very slow release of every drug release component from the foams.

Other factors being equal, the 50/50 PCL/PLGA blend would at first sight be expected to display intermediate release behavior between that of each pure polymer, but this is not always the case. Drug release rates will be dependent upon the distribution of the drug release component in the polymer blend. The fraction of the drug release component which is contained within the amorphous domains of PCL is expected to be released within the first 24 hours, while the fraction of drug contained within the PLGA matrix is expected to be released very slowly over the 17 day study. Thus, the release kinetics can be used as an indicator of drug distribution in the foams. The drug release profiles from foams generated using CO_2 alone suggest that PC may be contained within the amorphous regions of PCL, as the PC release from PCL and PCL/PLGA blends are nearly identical. The sustained but slower release observed in the PCL/PLGA foam after 7 days is likely to be PC release from the PLGA domains. Applying the same argument to the polymer blend foamed with CO_2 + 0.2 wt% acetone, a greater fraction of PC would be contained within the PLGA as indicated by the intermediate release rate from the PCL/PLGA blend foam.

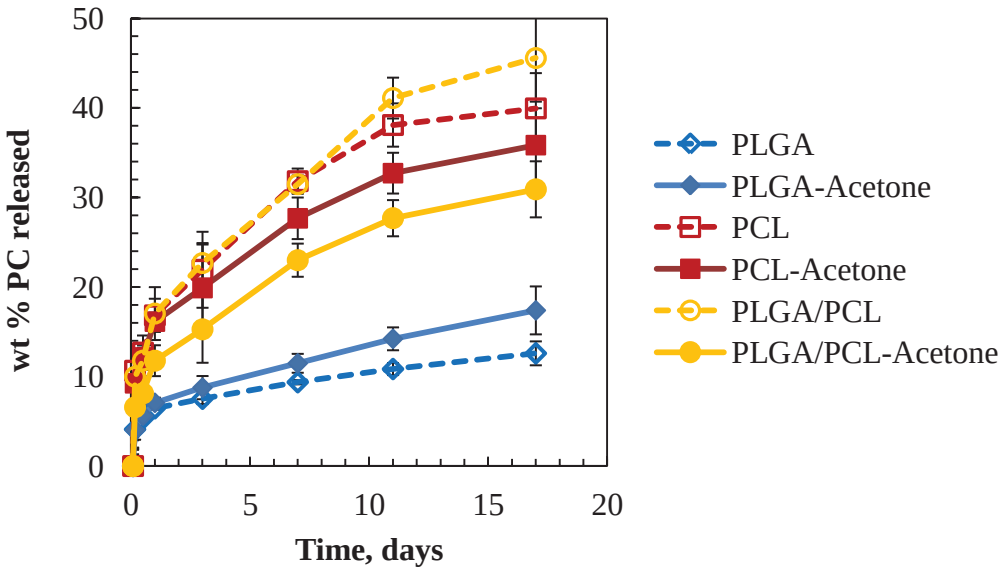

Figure 91. Effect of the polymer material on the drug release behavior from foams incorporated with 2 wt% PC and generated using CO_2 only (solid lines) and CO_2 + 0.2 wt% acetone (dashed lines) (n=3).

The trends observed in Figure 91 are also observed in Figure 92 where the drug release component has been changed to the PM, and the same discussion regarding drug release profiles can be applied here. The drug release profiles from the different polymers suggest that acetone addition promotes a more even distribution of the drug release component into both polymers in the PLGA/PCL blend foams, leading to an intermediate drug release profile between what is observed in each pure polymer.

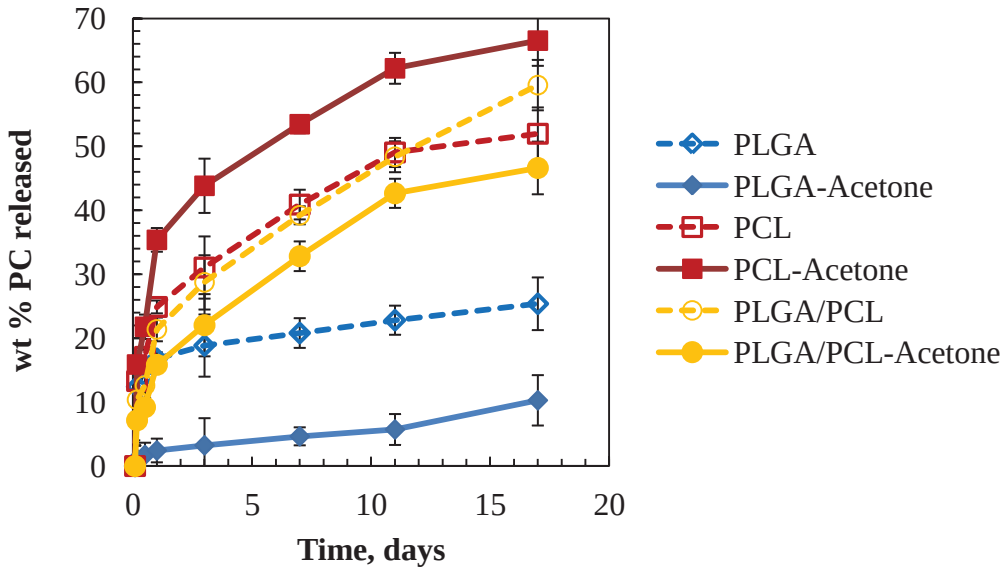

Figure 92. Effect of polymer material on drug release behavior from foams incorporated with 10 wt% PM and generated using CO_2 only (solid lines) and CO_2 + 0.2 wt% acetone (dashed lines) (n=3).

Figure 93 shows the release of the IC from each type of polymer generated with CO_2 only and CO_2 + acetone. Interestingly, release of the IC from the polymer blend is fastest and highest in the foams generated with CO_2 only. Again, however, the release of the IC is brought into the intermediate range with the addition of acetone as a co-solvent, suggesting more even distribution of the drug release component between the two polymers.

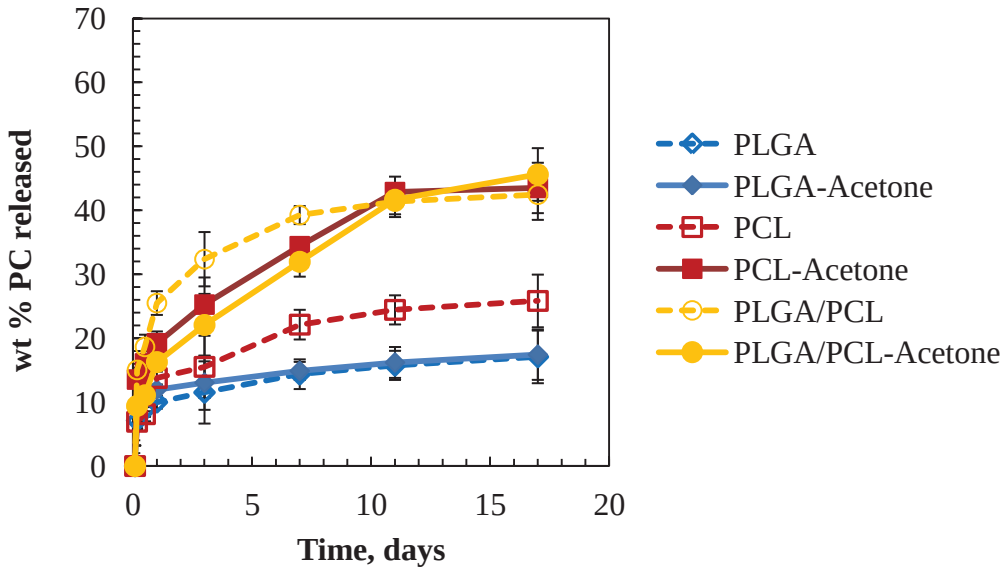

Figure 93. Effect of polymer material on drug release behavior from foams incorporated with 10 wt% IC and generated using CO_2 only (solid lines) and CO_2 + 0.2 wt% acetone (dashed lines) (n=3).

8.6 Conclusions

The effect of incorporating drug release components on the pore morphology of PLGA and PCL foams was investigated by SEM, and the presence of drug or PM within the polymers was found to lead to an increase in pore size. This was attributed to the depression of polymer foam T_m or T_g by incorporating the drug release components, which led to an increase in pore size, due to extended cell growth times before vitrification, and a corresponding decrease in pore density. Even though the presence of heterogeneous nucleation sites introduced a competing effect, which was expected to reduce pore size and increase pore density, the resulting pore structure was found to be dominated by the T_g and T_m depression of the polymer. An exception to this explanation was PLGA foams incorporated with inclusion compounds, which displayed smaller pore sizes and a higher pore density than foams incorporated with pure drug or drug:CD physical

mixtures, suggesting improved distribution of the ICs within the polymer matrix, where heterogeneous nucleation became the dominant factor in the resulting pore structure. Drug release profiles pointed to the complexities of these systems, although interesting trends were observed, including the similar drug release behavior of the PMs and ICs in many foams. This suggests that complex formation occurs in situ during the foaming process, providing a one-step pathway for generating polymer foams and promoting inclusion complex formation of physical mixtures. In comparing the drug release profiles from different polymers, improved drug dispersion between PCL and PLGA with acetone addition was observed. In addition, foaming of the polymers was found to result in a decrease in drug release rates with a more sustained release compared to un-foamed pellets containing the drug delivery component. By carefully choosing the foaming conditions and controlling the dispersion of the drug between PLGA and the amorphous domains of PCL, it may be possible to tailor drug release dynamics from these foams.

Chapter IX. Conclusions and Recommendations for Future Work

During this research activity, new methods for the preparation of porous biomedical scaffolds for applications in tissue engineering and drug delivery were investigated. Supercritical CO_2 and mixtures of carbon dioxide with a co-solvent like acetone, ethanol or ethyl acetate were considered as the main processing fluids. The first objective was to promote cyclodextrin-drug complex formation, such that the solubility of hydrophobic drug in aqueous media was improved via drug inclusion into the hydrophilic molecule, cyclodextrin. Non-steroidal anti-inflammatory drugs were considered, including ibuprofen, naproxen, piroxicam and ketoprofen. Among the cyclodextrins, α-, β-, γ- and 2-hydroxypropyl-β- cyclodextrins were considered. For the polymer matrix, two biodegradable polymers and a blend of the polymers were evaluated. These were the semi-crystalline polymer, poly(ε-caprolactone), and the amorphous copolymer, poly(lactide-*co*-glycolide), which are widely used and already have FDA approval.

9.1 The major accomplishments and findings towards the first objective of forming drug-CD inclusion complexes are as follows:

9.1.1 Differential scanning calorimetry was shown to be an effective tool for providing details of complex formation in all the systems explored. An in depth analysis of naproxen + β-cyclodextrin physical mixtures by differential scanning calorimetry was presented in Chapter IV and showed that inclusion complex formation occurred upon drug melting in the presence of cyclodextrin. This was an important observation which increased the

awareness of the difficulties in generating complex formation by drug melting if the drug was not stable at or near its melting temperature.

9.1.2 To take advantage of melt inclusion complex formation with thermally labile drugs which degrade at their melting temperature, such as piroxicam, a new method for melt processing in CO_2 + co-solvent mixtures was developed. This has been described in Chapter V. It has been shown that in the presence of supercritical CO_2, the melting temperature of piroxicam can be significantly depressed. Lowering of drug melting temperature provides a viable pathway to the promotion of inclusion complex formation with cyclodextrins while avoiding thermal degradation.

9.1.3 In situ drug-cyclodextrin complex formation was also found to occur in the polymer matrices containing their physical mixtures when exposed to carbon dioxide for foaming and porous scaffold generation. As discussed in Chapter VIII, occurrence of complex formation was indicated by the drug release behavior from the foams that were generated from systems that initially contained physical mixture versus inclusion complex. In situ inclusion complex formation was found to be further promoted in solvent mixtures containing acetone as a co-solvent, when added to the CO_2-based foaming process. These findings are important in suggesting that in creating polymer + inclusion complex system, one does not have to start with a pre-formed inclusion complex, and may potentially generate the polymer + inclusion complex system in one direct step starting with a physical mixture.

The second objective of this research was to produce porous polymeric matrices to serve as tissue engineering scaffolds and drug delivery system, using a CO_2-based foaming process. The addition of a small amount of co-solvent was investigated as a potential means of improving the foaming process. Poly(lactide-*co*-glycolide) and poly(ε-caprolactone) were investigated for foaming. The foams were evaluated in terms of their morphology by SEM and in terms of the dynamics of drug release from these matrices in phosphate buffered saline (PBS) media,

9.2 The major accomplishments toward this objective are as follows:

9.2.1 CO_2 foaming is a viable alternative pathway for producing polymeric foams to conventional solvent-intensive methods of generating porosity. The present observations of foaming with PCL and PLGA were consistent with the expectations based on literature with respect to the consequences of foaming temperature, pressure, and rate of depressurization as presented in Chapter VII. Exposure to CO_2 at higher pressures leads to smaller pores with higher cell density. Imposing faster depressurization rates leads to smaller pores. Foaming at higher temperatures lead to formation of larger pores.

9.2.2 Co-solvent addition to the CO_2 foaming process was investigated as an approach to minimize skin formation and improve pore interconnectivity that is often a limitation in foaming with CO_2 alone. As shown in Chapter VII, skin formation in the present system was not completely eliminated at the co-solvent addition levels employed. However, SEM images of polymer foams generated by CO_2 foaming with acetone addition indicated improved pore interconnectivity.

9.2.3 A special effort was made to develop further understanding of the polymer + CO_2 + acetone systems as the addition of small amount of acetone has favorable consequences. This part of the study was however focused on conditions where polymer completely dissolves in the fluid, in contrast to foaming conditions where the fluid dissolves in the polymer matrix. Regardless, the results provide valuable information on the interactions of the fluid components with the polymer as a function of temperature and pressure. The study involved full documentation of the density and related volumetric properties of these solutions. As described in Chapter VI, the observations point to complex dynamics of the competitive interaction of CO_2 with the carbonyl group in both the acetone and in the PLGA. The carbonyl group interactions were also later noted as possibly playing a role in polymer foaming in the presence of drug release compounds.

9.2.4 Incorporation of drug release compounds into polymers led to morphological changes in the resulting foams, as shown in Chapter VIII. Remarkably, the presence of the drug components in the mixture was found to cause a depression of the T_g of PLGA, which was expected and found to lead to the generation of larger pores arising from an extended duration of cell growth during depressurization before vitrification. Heterogeneous nucleation sites within the polymer due to the presence of immiscible drug release compounds provided a competing effect which was expected to decrease pore size. Generally, the effect of polymer T_g depression dominated the resulting pore structure, leading to the generation of larger pores in foams.

9.2.5 Foamed polymer blends of PCL/PLGA were found to display drug release behavior intermediate between that of PCL and that of PLGA when foamed with CO_2 + acetone. This observation suggests that acetone addition leads to a more even distribution of the drug release component between the two polymers. Since drug delivery from PLGA foams is much slower than drug release from PCL foams, foaming of PCL/PLGA blends of different blend compositions using CO_2 + acetone may provide a pathway for generating drug delivery systems with tunable drug release attributes.

9.3 The following are recommended future studies in this research area:

9.3.1 The concept of melting point depression in CO_2 to form drug –cyclodextrin inclusion complexes should be further explored. Other thermally labile drugs, such as carbamazepine which has a melting temperature of about 190 ^{o}C, should be investigated for possible melting point depression as an alternative pathway for melt processing of these compounds, including liquid state inclusion complex formation with cyclodextrins.

9.3.2 The depression of T_g or T_m in polymer foams incorporated with drug release components should be further investigated in terms of the effect of the incorporated compound, including its compatibility with the polymer, particle size and physical state (liquid/solid).

9.3.3 Polymer blends that incorporate a semi-crystalline and an amorphous polymer should be further explored with respect to the dynamics of foaming and the dynamics of drug

release from their foams. In this respect, blends of PCL/PLGA with other compositions are the logical systems to explore further.

9.3.4 Important information that is not easily generated experimentally is the direct assessment of the amount of CO_2 that dissolves in the polymer prior to depressurization at a given T / P and fluid composition conditions. Any future experimental system development that can provide reliable data on the dissolved CO_2 or CO_2 + co-solvent in the polymer matrix would help describe the resulting morphologies with greater clarity. This is an ongoing challenge in the literature.

Appendix A. Characterization of Drug-Cyclodextrin Inclusion Complexes

Drugs and CDs explored in this research, as well as their physical mixtures and inclusion complexes, were characterized by thermal and spectroscopic techniques including thermal gravimetric analysis, differential scanning calorimetry, Fourier transform infrared spectroscopy and powder x-ray diffraction. These characterization techniques were used to differentiate between pure compounds, drug:CD physical mixtures and drug:CD inclusion compounds, which was an important aspect of this research.

A.1 Materials and Methods

A.1.1 Materials

Ibuprofen (IB), Ketoprofen (KP), Naproxen (NA), Piroxicam (PC), α-cyclodextrin (α-CD), β-cyclodextrin (β-CD), γ-cyclodextrin (γ-CD) and 2-hydroxypropyl-β-cyclodextrin (HP-β-CD) were obtained as fine white powders from Sigma and used as received. 10 mg of 1:1 molar ratio physical mixtures of drug and CD were prepared by gentle mixing and grinding with a mortar and pestle. The mixtures were sampled for analysis by DSC and FTIR.

A.1.2 UV-Vis Spectroscopy

An Ocean Optics USB 4000 spectrometer equipped with a UV-VIS-NIR light source (DH-2000-BAL) was employed in the UV-Vis measurements. 450 μm XSR fiberoptic cables were used for the light source and detection. One cable was connected from the light source to the sample call, and the other cable was connected from the sample cell to the detector. Samples were placed

into quartz cuvettes with a 1 cm pathlength. Ocean Optics Spectra Suite software was used in data acquisition and analysis. The beam was attenuated using a pin-hole card between the sample and the detector. 200 scans were averaged with a boxcar width of 3.

A.1.3 Differential Scanning Calorimetry

Differential scanning calorimetry (DSC) was performed using a Pyris Diamond DSC. Samples were analyzed by heating and cooling at a rate of 20 ^{o}C/min with a nitrogen purge at 10 ml/min. Pyris software was use in the data analysis.

A.1.4 Thermogravimetric Analysis

TGA was used in the determination of thermal degradation onset temperature of each compound investigated. A DuPont Instruments 951 thermogravimetric analyzer was employed in the TGA measurements. The instrument was modified in house for data digitization and recording in real-time. Platinum pans were used to hold the samples. N_2 was used as a purge gas at 10 ml/min, and a temperature ramp of 10 ^{o}C/min was used. A Python 2.7 graphical user interface was used to monitor and record sample temperature and sample mass during the experiments.

A.1.5 Fourier Transform Infrared Spectroscopy

Fourier transform infrared (FTIR) spectroscopy was carried out on a Digilab Excaliber HE Series FTS 3100 spectrometer with a 4 cm^{-1} resolution and 32 scans in the wavenumber range of 4000 to 400 cm^{-1}. Samples were prepared into KBr pellets for analysis.

A.1.6 Powder X-ray Diffraction

Powder X-ray diffraction (XRD) was carried out on a PANalytical X-Pert PRO instrument.

A.1.7 Preparation of Freeze Dried Complexes

Stoichiometric quantities (1:1 mol:mol) of drug and CD were dissolved in water. A small amount of ammonium hydroxide solution was used to dissolve the drug completely, and the solution was stirred for 24 hours. The solution was frozen by submerging into liquid nitrogen followed by lyophilization for 72 hours. The recovered powder was gently ground using a mortar and pestle.

A.2 Results

A.2.1 UV-Vis Spectroscopy

Each drug displayed a unique, characteristic wavelength of maximum absorbance, which are summarized in Table 20. As an example of the UV-Vis spectra acquired in these measurements, Figure 94 shows the absorbance of each drug in ethanol.

Table 20. Characteristic wavelength of maximum absorbance.

Drug	λ_{max}, nm
IB	265
KP	276
NA	272
PC	334

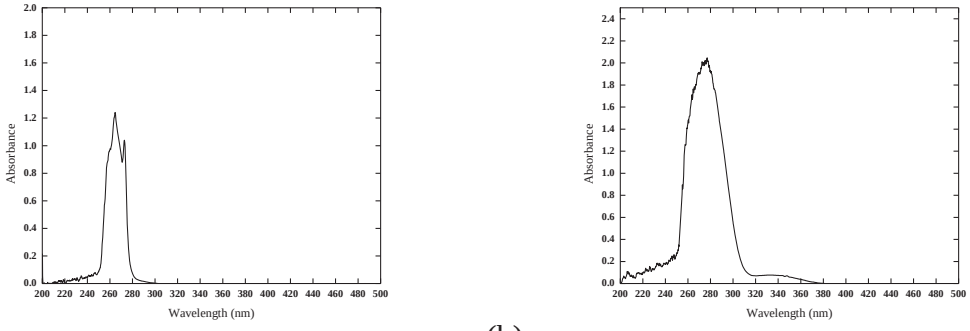

Figure 94. UV-Vis spectra for (a) IB, (b) KP, (c) NA and (d) PC in ethanol.

A.2.2 Differential Scanning Calorimetry

DSC experiments were performed for each pure drug by first heating to 250 ^{o}C to determine the melting temperature. Then DSC experiments were conducted for each drug by heating to slightly above the melting temperature, holding for 1 minute and then cooling to room temperature at 20 ^{o}C/min. The resulting phase change information is reported in Table 21. Each drug displayed a characteristic melting endotherm in the heating cycle, as shown in Figure 95 (left). In the cooling scan, only NA displayed a crystallization exotherm. However, after allowing the same samples to sit for 24 hours at room temperature and performing the same DSC experiment, a melting endotherm was observed only for IB and NA, as shown in Figure 95

(right). KP and PC seemed to remain amorphous for up to five months at room temperature after the initial DSC experiment. In the heating scan of PC, the slope of the heat flow curve changes significantly upon melting. This could be an indication of thermal degradation of the drug, which is further investigated by TGA.

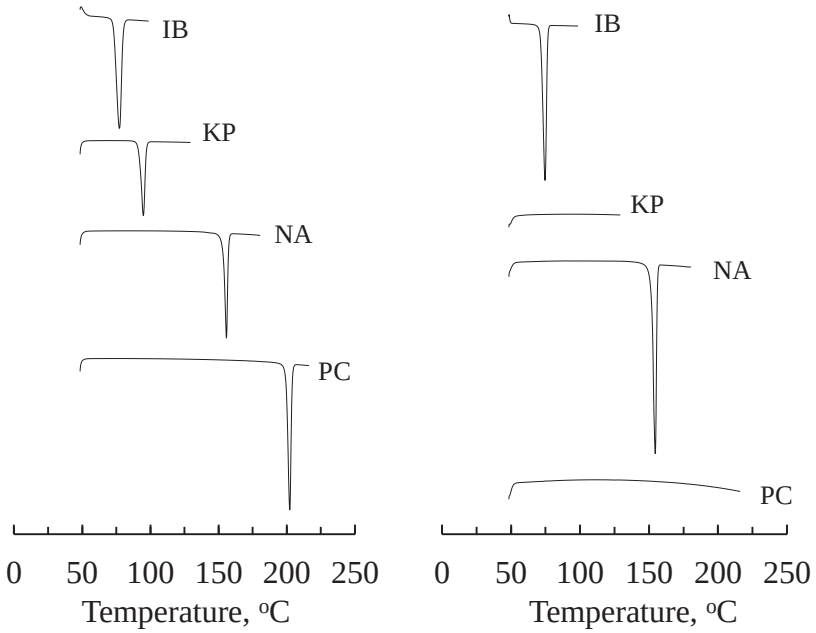

Figure 95. Heating scans of pure drugs; first heating scan (left) and reheating scan after 24 hours at room temperature (right).

The heating scans for each pure CD are shown in Figure 96. In each CD a broad endotherm is observed in the range of 75 - 150 ^{o}C and is representative of the dehydration of the CD cavity. At temperatures up to 250 ^{o}C, no melting is observed for any of the CDs.

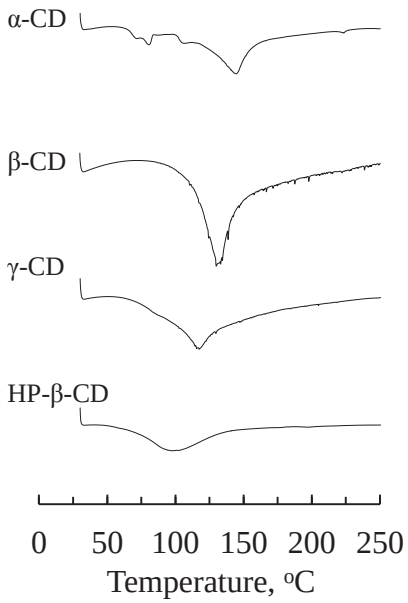

Figure 96. Heating scans of pure cyclodextrins.

Table 21. Melting information for pure drugs obtained from DSC heating curves.

Drug	T_m, °C	ΔH_m, J/g
Ibuprofen	77.12 ± 1.29	114.84 ± 5.29
Ketoprofen	96.03 ± 1.29	106.64 ± 1.81
Naproxen	157.95 ± 1.30	128.67 ± 2.45
Piroxicam	203.40 ± 0.94	105.03 ± 5.19

The same DSC programs were carried out with 1:1 (mol:mol) CD:drug physical mixtures with IB and NA. The first heating curves for the mixtures are shown in Figure 97. The IB melting endotherm is observed in each mixture. For NA:CD mixture, the NA melting peak is observed in mixtures only with the native CDs, α-, β- and γ-CD, but not with HP-β-CD. However, a shallow broadened peak is observed in the NA:HP-β-CD mixture, which likely indicates the NA melting transition. In the NA:β-CD physical mixture, the dehydration of the CD cavity is

observed followed by the NA melting peak and then a small exothermic peak at a temperature just higher than the NA melting peak. This peak was discussed in depth in Chapter IV and was found to be an indication of NA:β-CD inclusion complex formation occurring upon NA melting in the DSC.

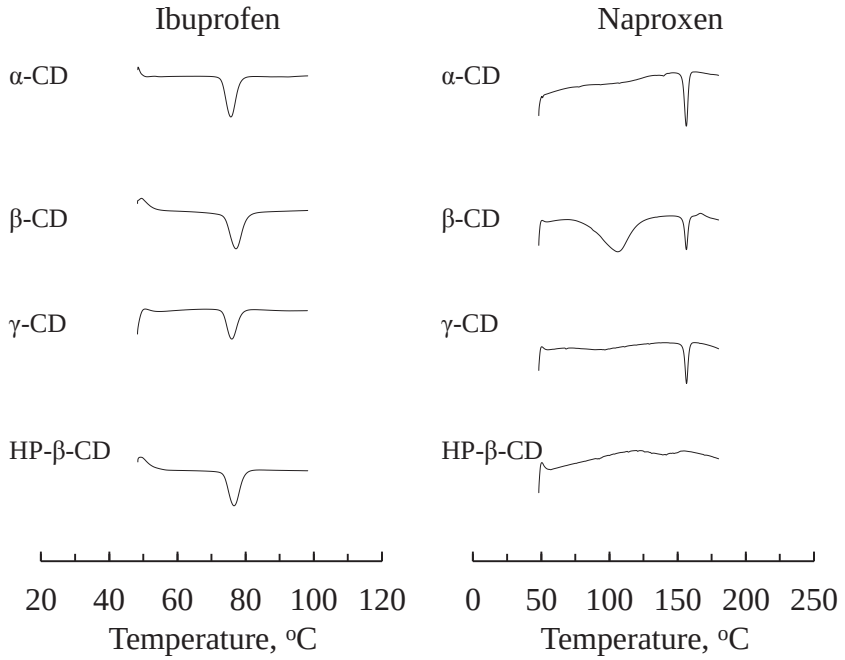

Figure 97. First heating scans of 1:1 molar ratio physical mixtures of IB:CD (left) and NA:CD (right)

The samples were left at room temperature for 24 hours before being reheated in the DSC. The reheating scans for IB:CD and NA:CD physical mixtures are shown in Figure 98. Since IB and NA recrystallize within 24 hours at room temperature, remelting of the drugs is expected in the reheating scan. The IB melting peak is only observed in the mixture with γ-CD, which could indicate that IB has fully complexed with α-, β- and HP-β-CD upon melting in the DSC. The

NA melting peak is reduced resulting in a lower ΔH_m, in physical mixtures with each CD, which could indicate partial complex formation of NA upon melting in the DSC.

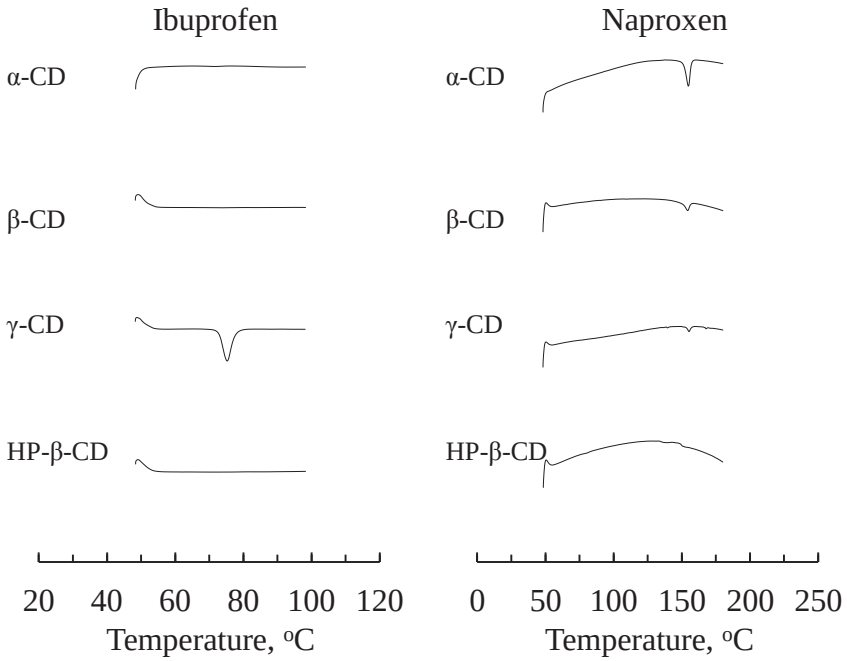

Figure 98. Reheating scans of 1:1 molar ratio physical mixtures of IB:CD (left) and NA:CD (right)

For comparison, the DSC heating scans of the freeze-dried complexes of IB:β-CD and NA:β-CD are shown in Figure 99. The drug melting endotherms are not observed in either of the freeze dried samples which supports the notion that disappearance of drug melting peaks may indicate drug:CD inclusion complex formation. However, further investigation is required to confirm the event of complex formation in these mixtures, as DSC alone is not conclusive. The absence of drug melting peak in the reheat scans indicates that the drug has become amorphous. Since the possibility of drug amorphization due to effects other than complex formation, further investigation is required.

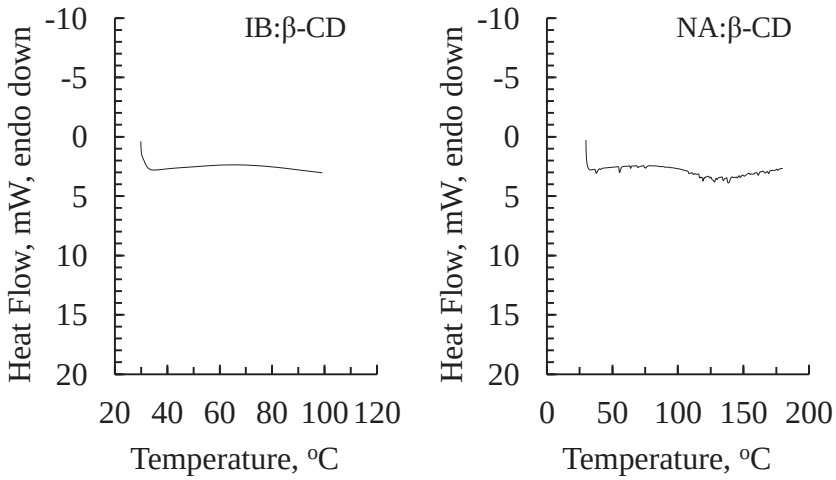

Figure 99. DSC heating scans of 1:1 molar ratio IB:β-CD and NA:β-CD inclusion complexes prepared by freeze drying.

A.2.3 TGA

Thermal stability of the drugs investigated in this research was explored using TGA. The weight loss curves are shown for each drug in Figure 100. The onset of thermal degradation is indicated with arrows for each compound, and was used as a measure of thermal stability. Thus, thermal stability was found to increase in going from IB to KP to NA to PC. An important outcome of this analysis is the fact that PC thermal degradation occurs at 200 ^{o}C, which is nearly the same as the 203.4 ^{o}C melting temperature determined by DSC. Therefore, the lack of recrystallization of PC after melting by DSC is likely due to the onset of thermal degradation, rather than to the amorphization of the intact drug. Since PC simultaneously melts and degrades, this drug is a poor candidate for inclusion complex formation via drug melting. This subject was thoroughly discussed and circumvented in research presented in our second publication in Chapter V.

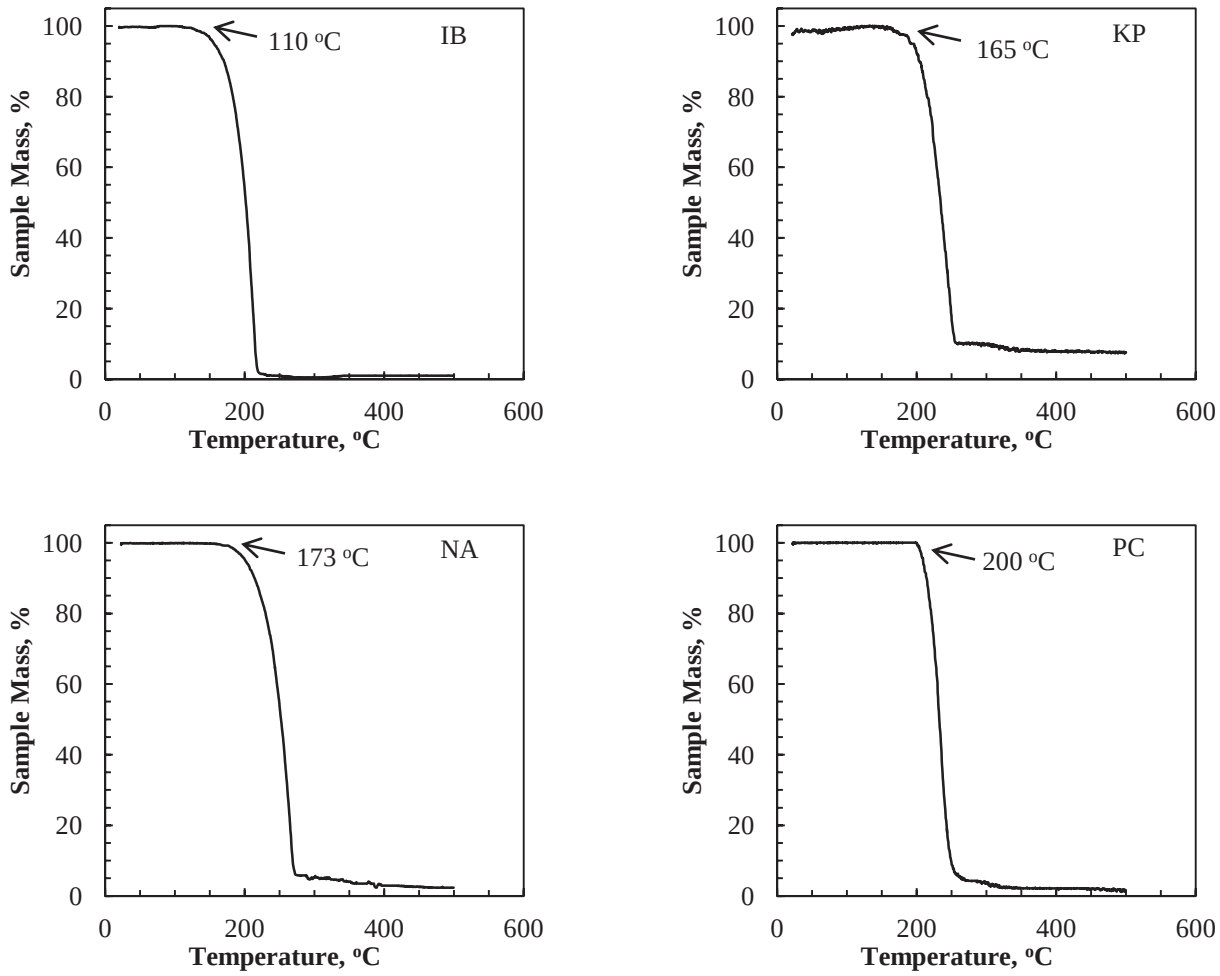

Figure 100. Thermogravimetric analysis of drugs investigated in this research.

The thermal behavior of CDs explored in this research was also investigated and the weight loss curves are shown in Figure 101. Each CD displayed some degree of water loss, which was important to know during the preparation of stoichiometric drug-CD physical mixtures. The water loss and onset of thermal degradation is show for each CD in Table 22.

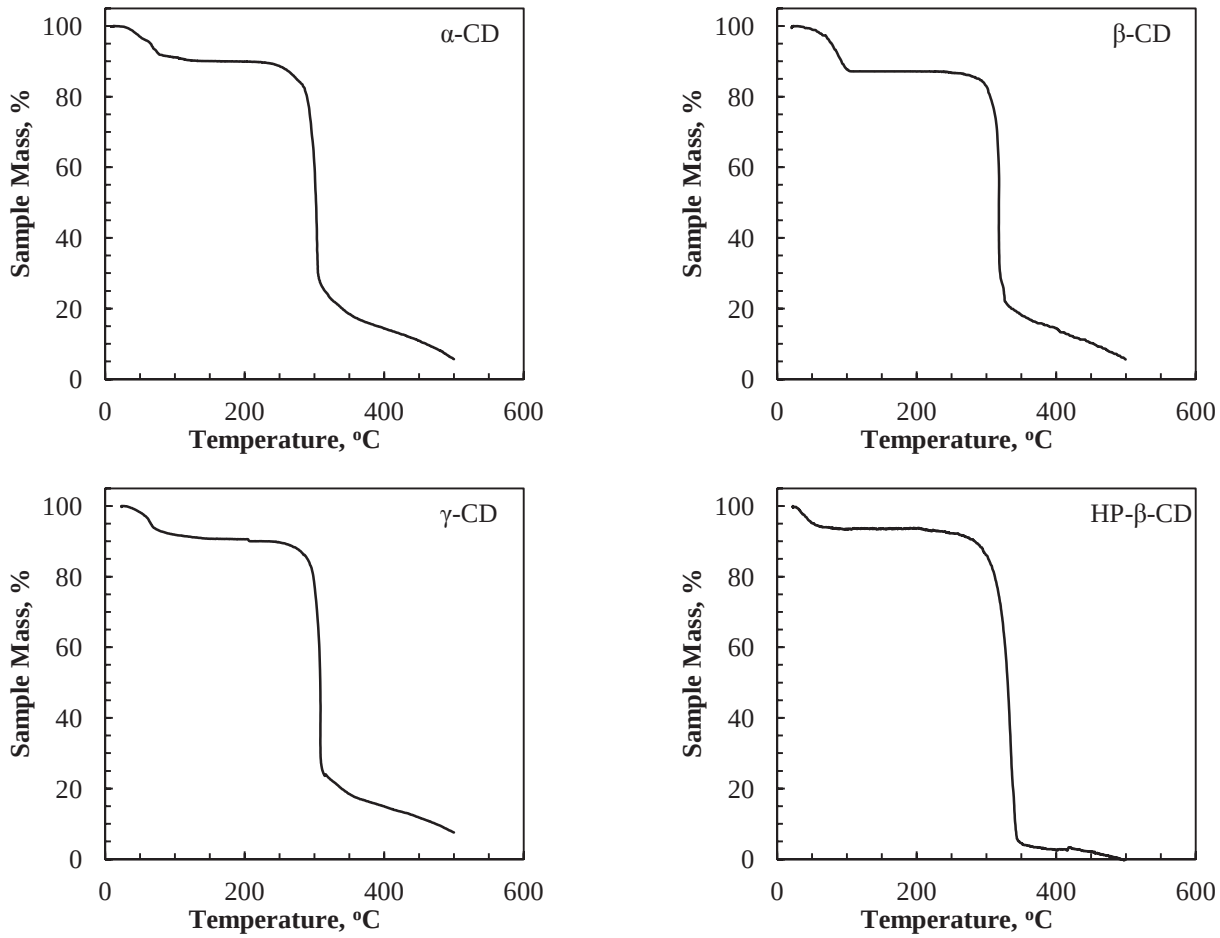

Figure 101. Thermogravimetric analysis of cyclodextrins investigated in this research.

Table 22. Thermal behavior of CDs

CD	% Water Loss	Onset of Thermal Degradation, °C
α-CD	9.9	222
β-CD	11.5	259
γ-CD	9.4	247
HP-β-CD	6.4	210

A.2.4 FTIR

Infrared spectroscopy was used to compare the pure compounds, drug:CD physical mixtures and drug:CD inclusion compounds generated by melting in the DSC, as well as those produced via freeze drying. The FTIR spectra of the pure drugs and CDs are presented in Figure 102 and Figure 103, respectively. For IB, the –OH stretch is observed between 3300-2500 cm^{-1}, and the carbonyl =O stretch is seen at 1721 cm^{-1}. The most distinctive band for IB is the peak at 1721 cm^{-1}. For KP, the ketone =O stretch is observed at 1229 cm^{-1}, the carbonyl =O stretch is observed at 1698 cm^{-1} and 1656 cm^{-1}, and the –OH stretch is observed from 3300-2500 cm^{-1}. The most distinctive bands for KP are the peaks at 1698 cm^{-1} and 1656 cm^{-1}. For NA, the asymmetric -O- stretch is observed at 1228 cm^{-1}, the carbonyl =O stretch is seen at 1729 and 1685 cm^{-1}, and the –OH stretch is observed in 3300-2500 cm^{-1}. The distinctive bands for NA are seen at 1729 and 1685 cm^{-1}. For PC, the O=S=O stretch is observed at 1330 cm^{-1}, the =O stretch is seen at 1531 cm^{-1}, 1577 cm^{-1}, and 1630 cm^{-1}, and the -NH- stretch is observed at 3339 cm^{-1}. The distinctive band for PC is the sharp peak at 3338 cm^{-1}. The key peaks for each drug used for comparison with their inclusion compounds with CDs are summarized in Table 23.

Table 23. Key peaks for each pure drug

Drug	Key Peaks, cm^{-1}	Related Bond
IB	1721	carbonyl stretch; C=O
KP	1698, 1656	carbonyl stretch; C=O
NA	3201	hydroxyl stretch; -OH
PC	3338	-NH- stretch

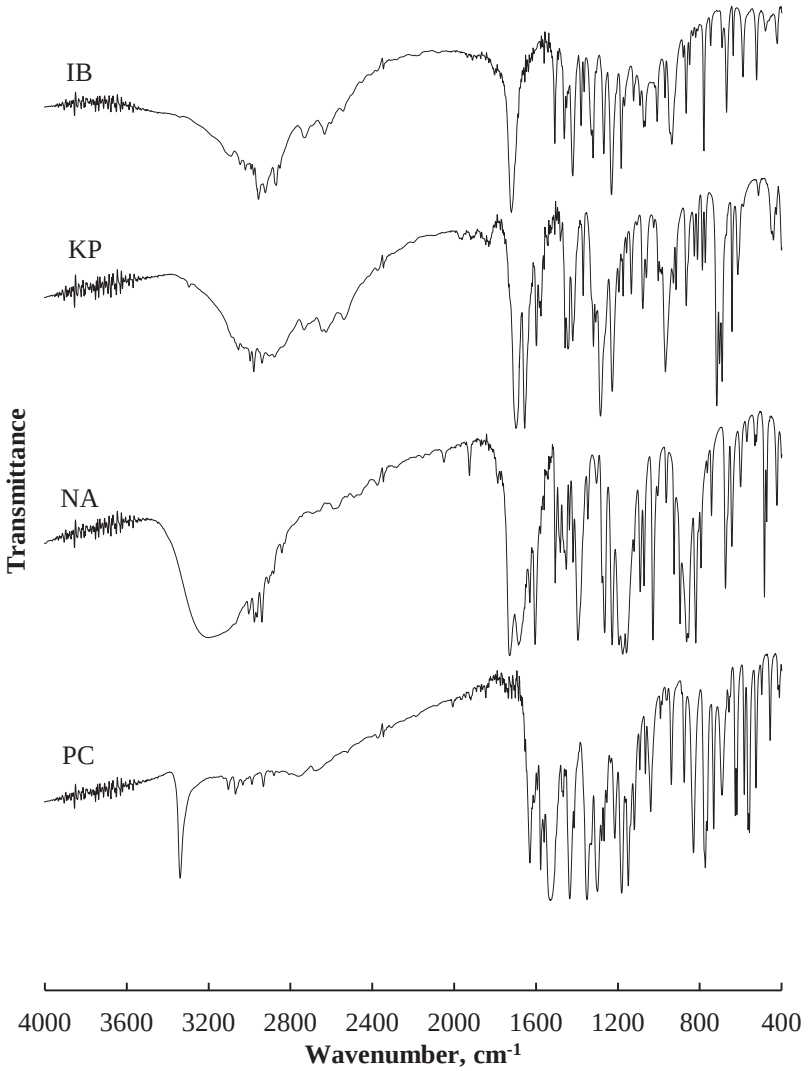

Figure 102. Infrared spectra of pure drugs

All of the cyclodextrins display the same key bands. The broad band at 3410-3300 cm^{-1} represents the –OH stretch. The peaks at 2930-2925 cm^{-1} and at 1157-1159 cm^{-1} are present in each spectrum. HP-β-CD is the only cyclodextrin investigated with a distinct peak seen at approximately 3000 cm^{-1} as a shoulder on the peak at 2930 cm^{-1}.

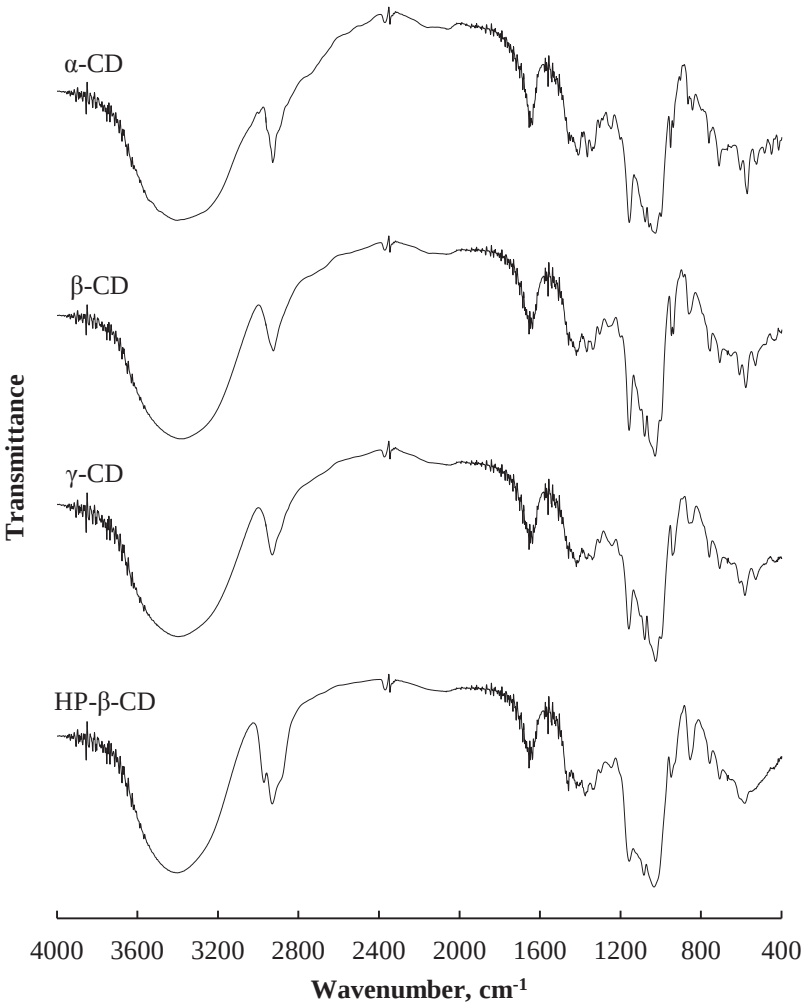

Figure 103. Infrared spectra of pure cyclodextrins

The FTIR spectra are shown for the physical mixtures of 1:1 mol drug:mol CD in Figure 104-Figure 107. The spectra of each drug:CD physical mixture is representative of an overlay of each pure component. For example, looking at the IB:α-CD physical mixture spectrum in Figure 10, it is seen that the distinctive carbonyl stretch is present at 1721 cm^{-1}, while the broad hydroxyl stretch from α-CD is also observed between 3410-3300 cm^{-1}. This is similar for the other drug:CD physical mixtures.

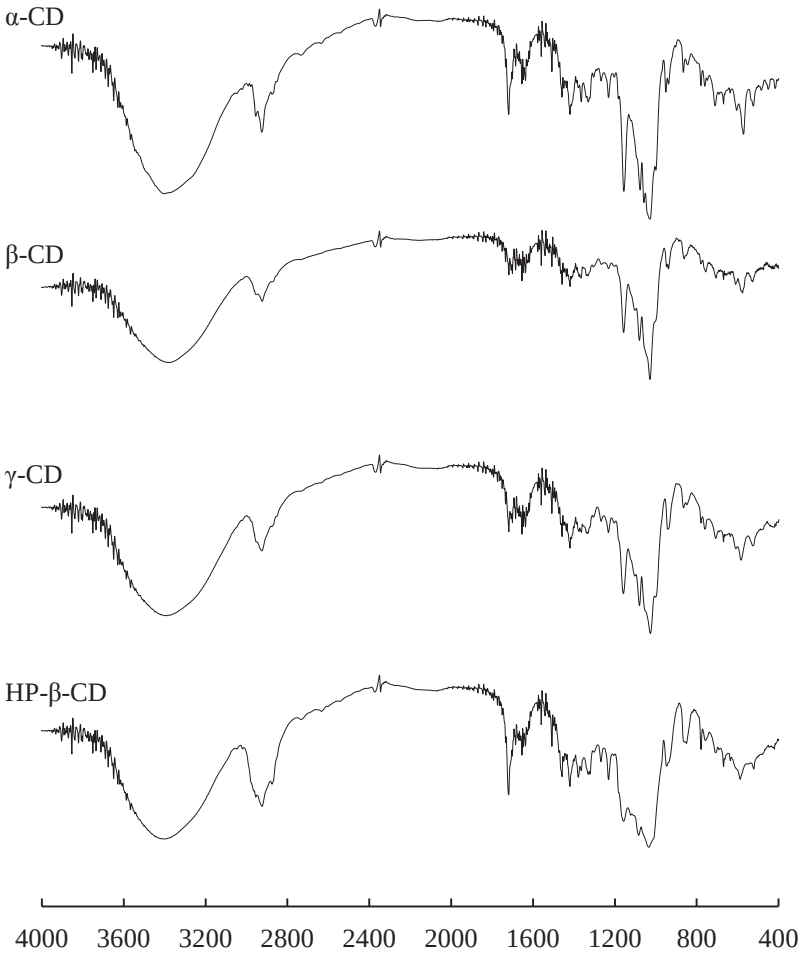

Figure 104. FTIR spectra of 1:1 molar ratio IB:CD physical mixtures.

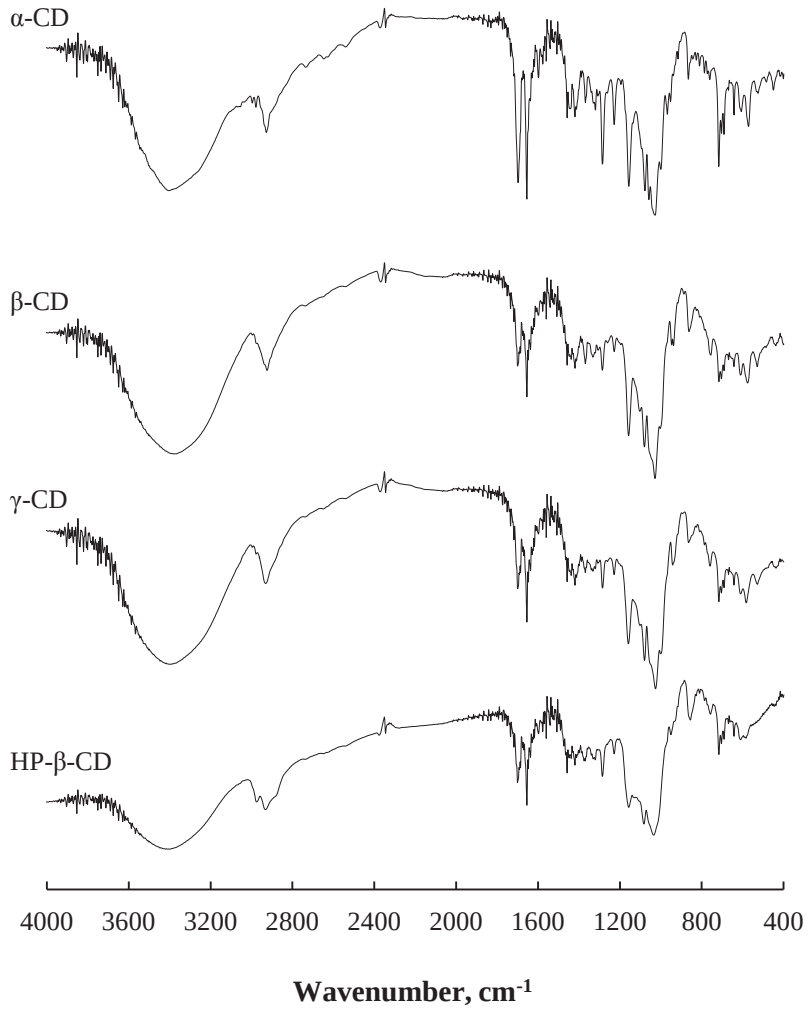

Figure 105. FTIR spectra of 1:1 molar ratio KP:CD physical mixtures.

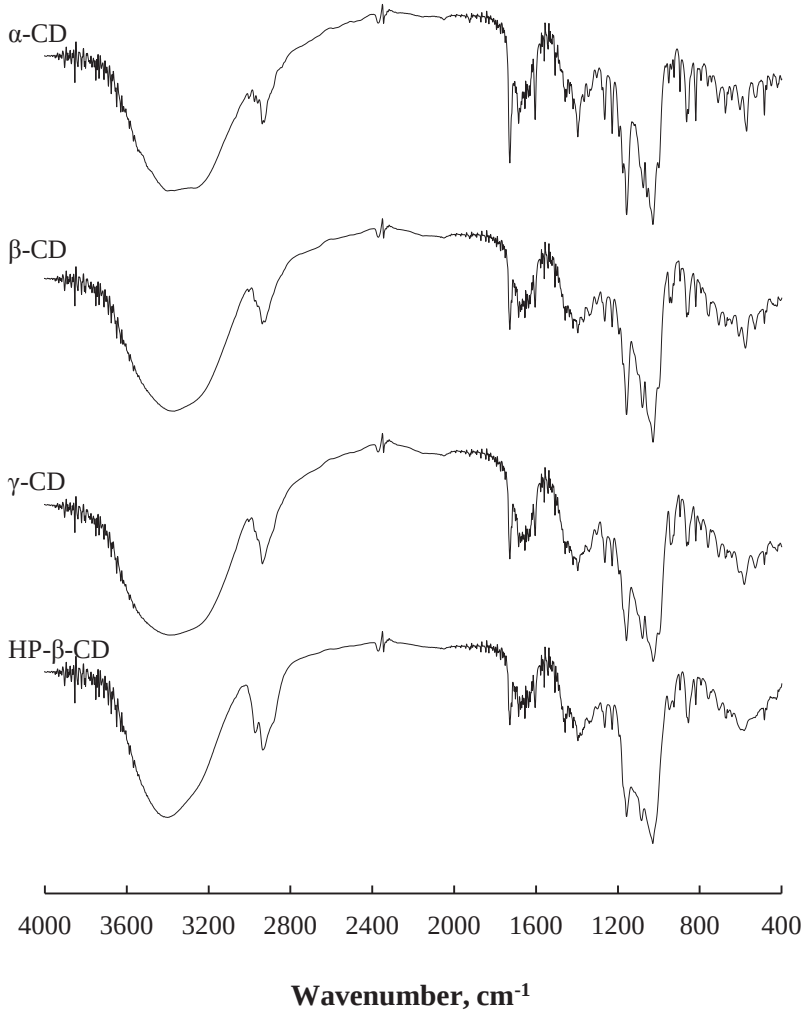

Figure 106. FTIR spectra of 1:1 molar ratio NA:CD physical mixtures.

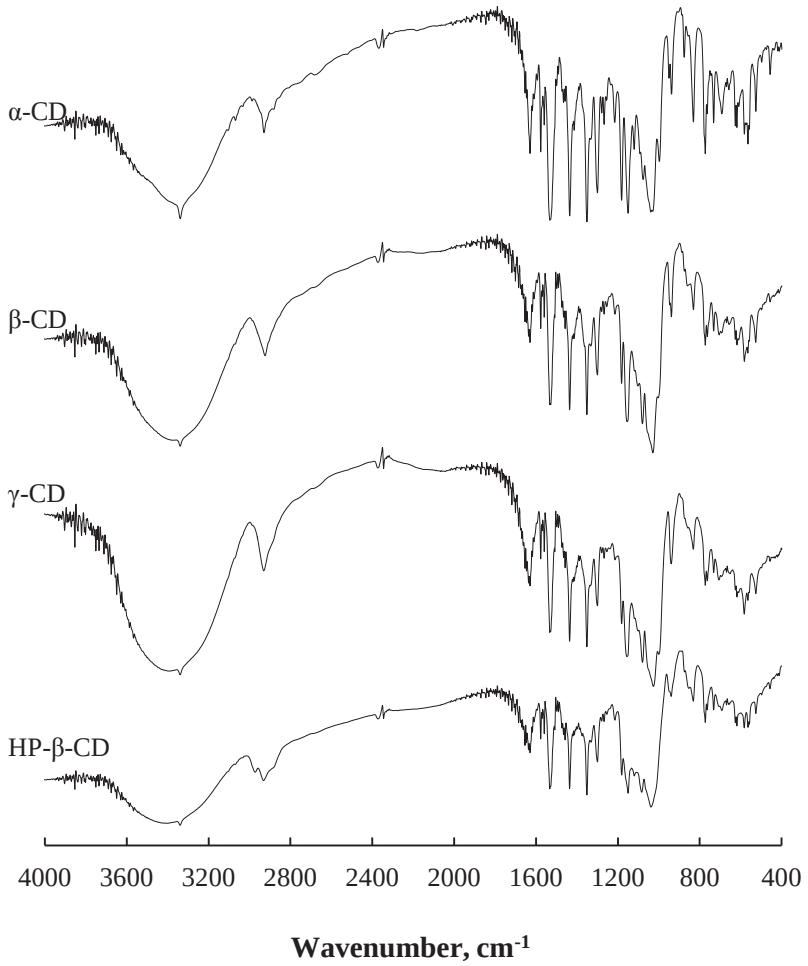

Figure 107. FTIR spectra of 1:1 molar ratio PC:CD physical mixtures.

Figure 108 and Figure 109 show the FTIR spectra of the IB:CD and NA:CD samples melted in DSC heating scans and cooled back to room temperature. The characteristic peaks of each drug are still visible in both samples, with the carbonyl stretch of IB visible at 1721 cm^{-1} and the carbonyl stretch of NA visible but shifted to about 1724 and 1638 cm^{-1}.

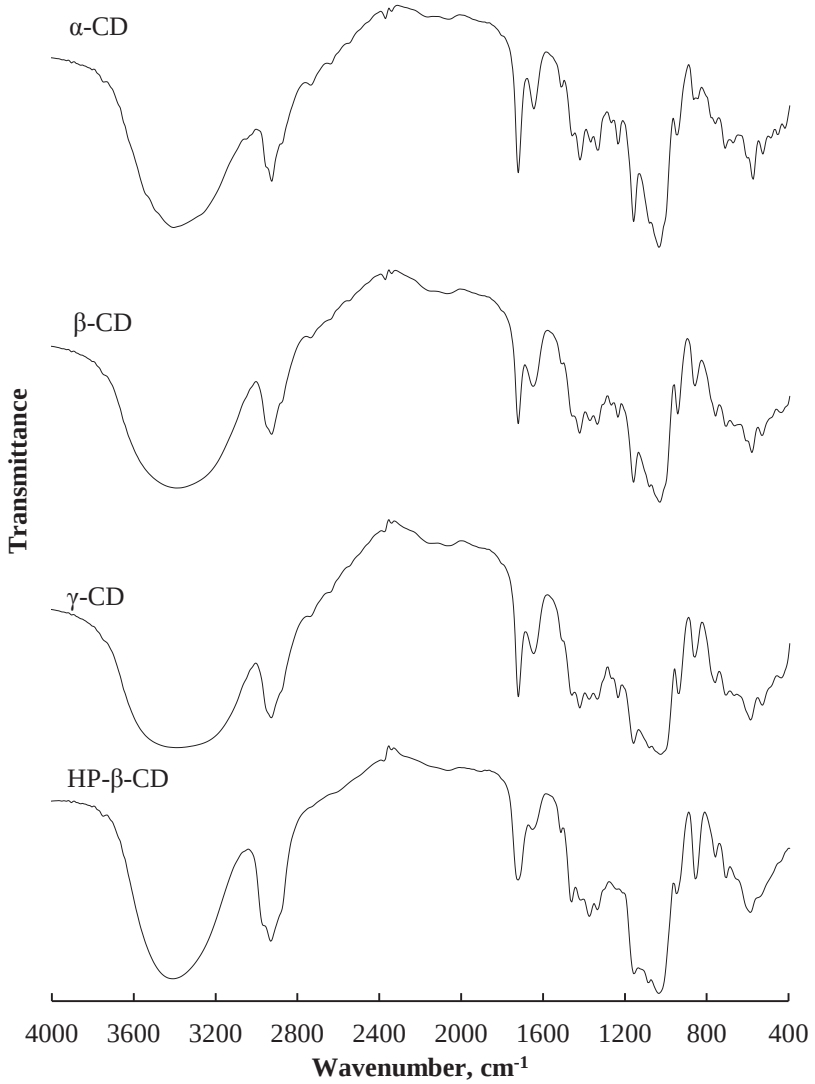

Figure 108. Infrared spectra of 1:1 molar ratio IB:CD samples after melting in DSC experiments.

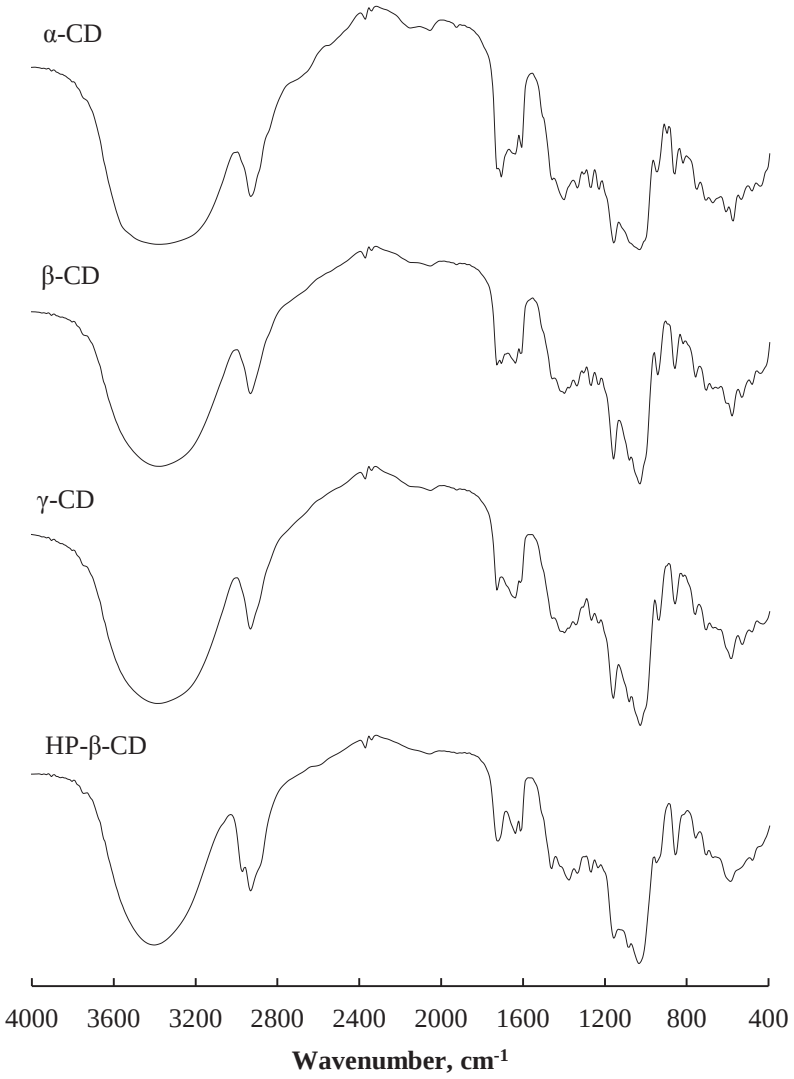

Figure 109. Infrared spectra of 1:1 molar ratio NA:CD samples after melting in DSC experiments.

The FTIR spectra of the freeze dried complexes of IB:β-CD and NA: β-CD are shown in Figure 110 and Figure 111, respectively. The spectrum of the IB:β-CD freeze dried sample appears to be consistent with the spectrum of β-CD alone with the exception of the appearance of new peaks at 1652 and 1567 cm^{-1}. These peaks may be associated with the carbonyl stretch in the IB

molecules, but may be shifted if IB is included in the β-CD cavity. Similarly, the spectrum of the NA:β-CD freeze dried mixture is mostly consistent with the β-CD spectrum alone except for the peaks at 1642 and 1547 cm^{-1}. These peaks could be associated with the carbonyl stretch in the NA molecule although shifted due to inclusion with β-CD. As discussed in Chapter II, any changes in the FTIR spectra may indicate potential inclusion complex formation between guest molecules as CDs, including disappearance, intensity reduction or shifting of key guest compound peaks.

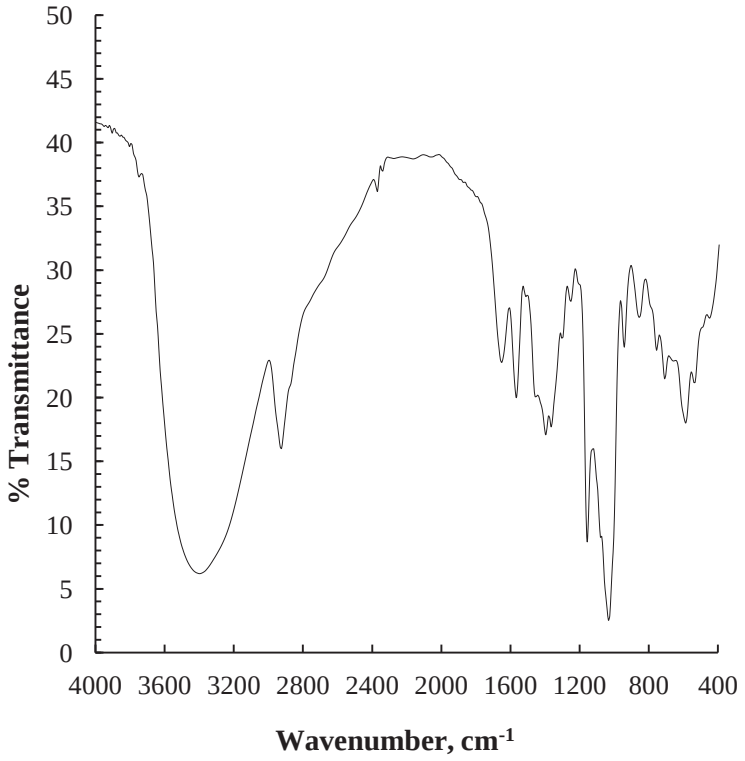

Figure 110. FTIR spectrum of IB:β-CD inclusion complex prepared by freeze drying.

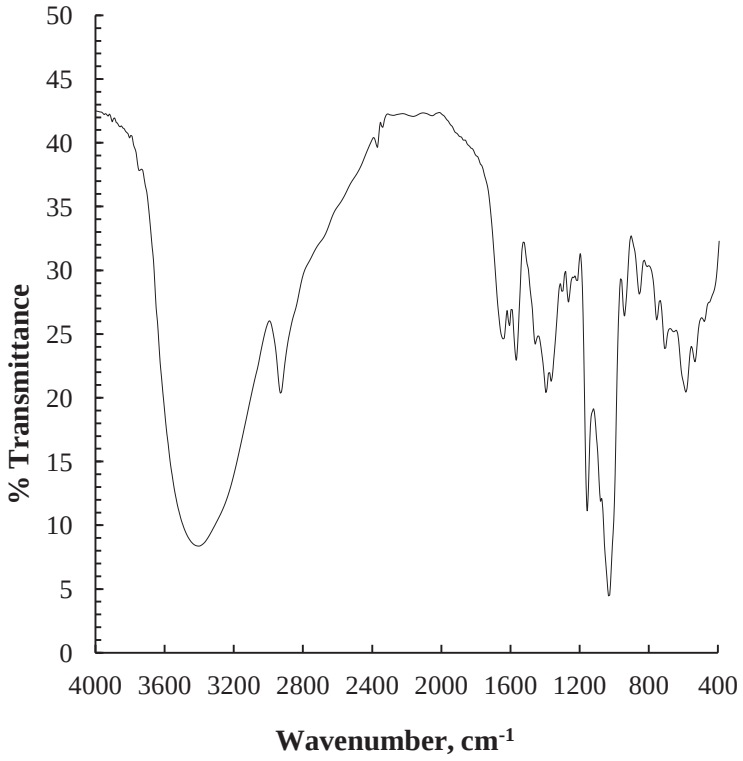

Figure 111. FTIR spectrum of NA:β-CD inclusion complex prepared by freeze drying.

A.2.5 Powder X-ray Diffraction

Powder XRD patterns are shown for the pure drugs, IB, NA and PC in Figure 112. KP was not analyzed by XRD, since it was a poor candidate for inclusion complex formation based on the DSC and FTIR results. Each drug displays a distinct diffraction pattern with sharp peaks indicative of crystalline compounds. IB key peaks are observed at 2θ values of 6.12, 12.24, 16.78, 18.77, 19.10, 20.16, 22.35 and 24.61^{o}, which match well with reference patterns provided in the PANalytical software. NA key peaks are observed at 2θ values of 6.74, 12.76, 13.46, 16.94, 18.14, 19.13, 20.46, 22.72, 23.87, 24.11, 27.43, 27.97 and 28.63^{o}, which also match well with the reference patterns found the XRD software. PC key peaks are observed at 2θ values of 8.75, 8.78, 11.78, 11.81, 12.61, 12.64, 14.63, 14.67, 15.98, 16.02, 16.80, 16.85, 17.82, 17.87, 18.96, 19.00, 21.86, 21.92, 22.55, 22.61, 25.96, 26.86, 26.93, 27.52, 27.59, 29.40, 31.40, 32.20, 34.44 and 43.62^{o}. These peaks match well with the reference patterns from the software as well.

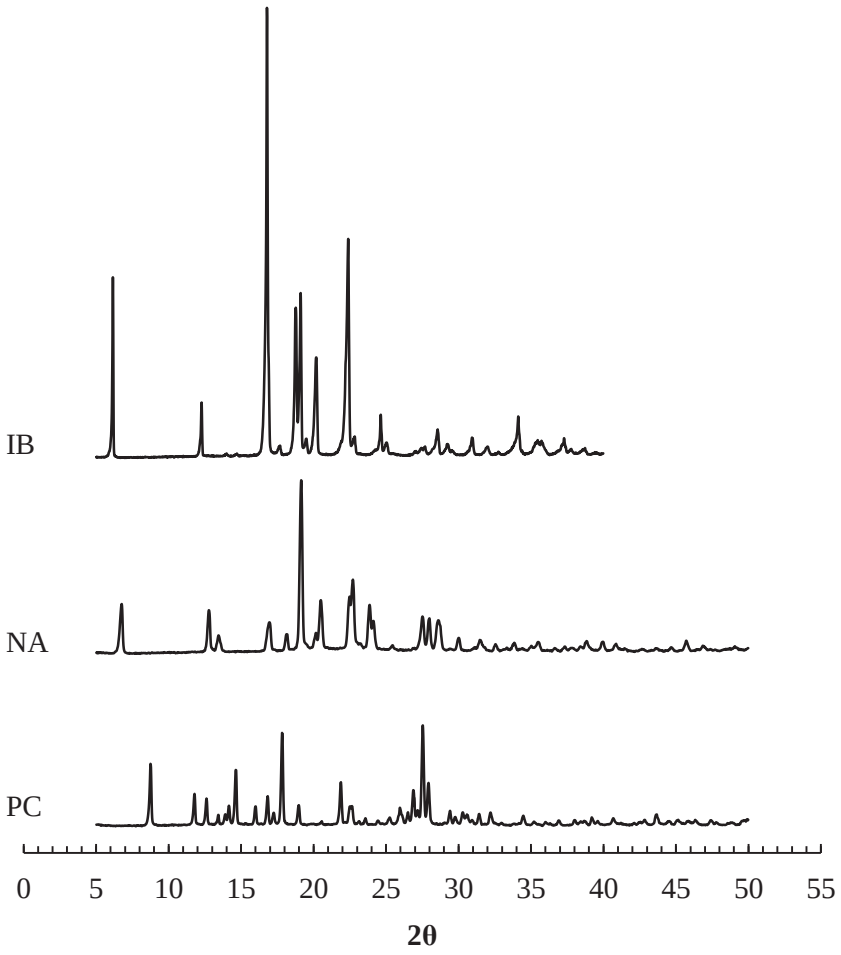

Figure 112. XRD patterns for pure drugs

The diffraction patterns for each CD are shown in Figure 113. Although these compounds are chemically similar, the different CDs clearly vary crystallographically. The native CDs all display crystallinity, while the HP-β-CD displays only an amorphous diffraction pattern indicated by the broad peak observed in the pattern of the substituted CD.

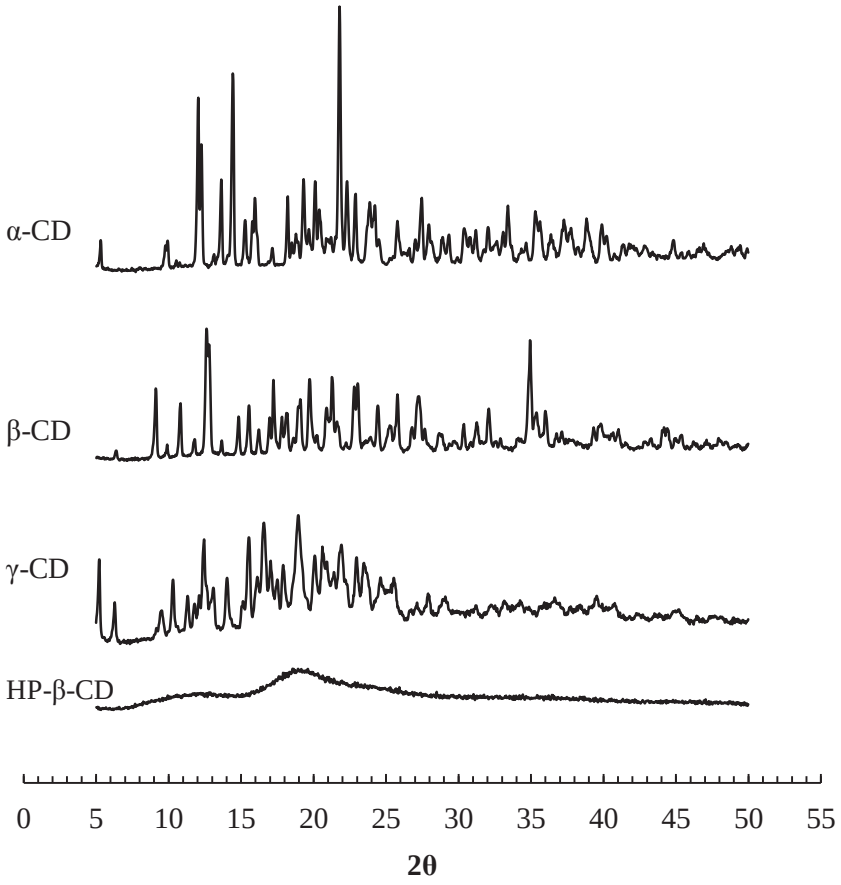

Figure 113. XRD patterns for pure CDs

The XRD patterns for IB:β-CD and NA:β-CD freeze dried samples are shown in Figure 114 and Figure 115, respectively. Both patterns are representative of an amorphous compound, which has been described in the literature as an indication of inclusion complex formation. The premise is that the inclusion of the drug molecule into the CD cavity prevents the crystalline CDs from crystallizing. However, what is not clear is whether the processing of the physical mixture has caused the amorphization of both compounds without leading to inclusion complex formation. This has been the topic of a publication in which the authors try to differentiate

between an amorphous PC:β-CD inclusion complex and an amorphous physical mixture of the two components [254].

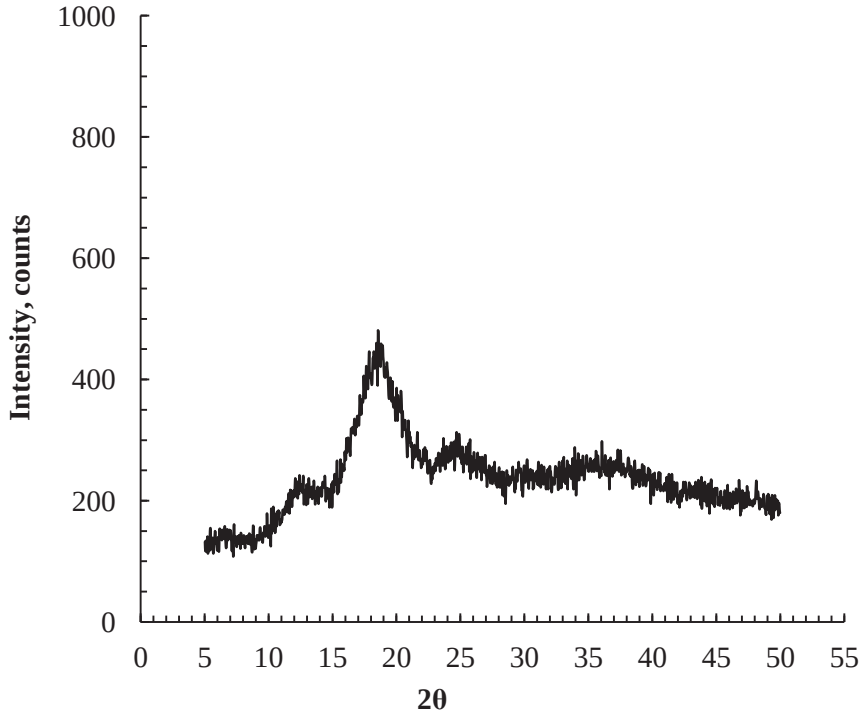

Figure 114. XRD pattern for 1:1 molar ratio IB:β-CD freeze dried complex.

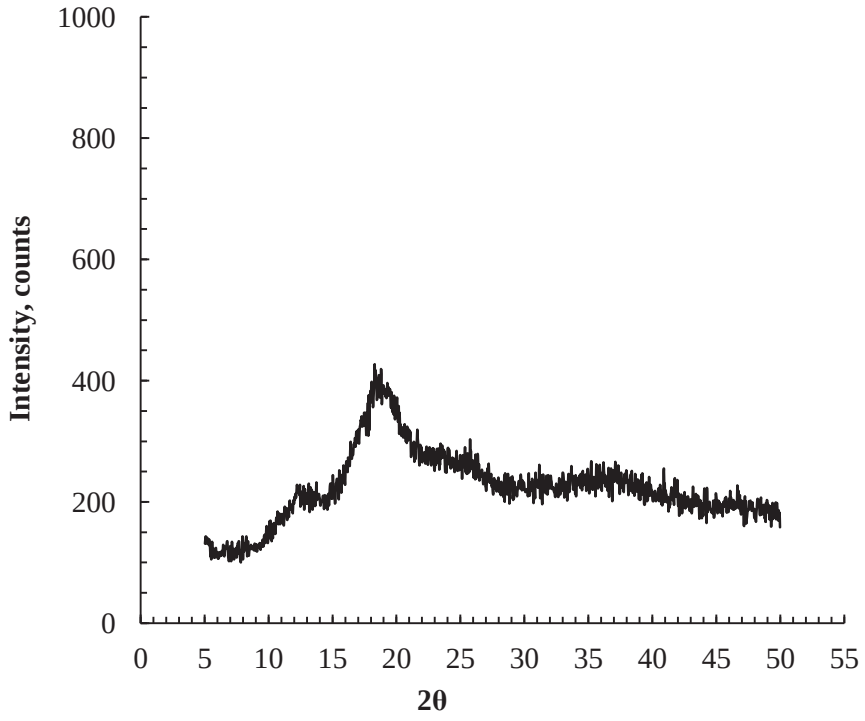

Figure 115. XRD pattern for 1:1 molar ratio NA:β-CD freeze dried complex.

A.3 Conclusions

Each of these analyses on their own do not seem to be conclusive in the determination of drug:CD inclusion complex formation. However, combined, these characterizations can provide strong evidence of the presence of inclusion compounds versus a partial complex.

Appendix B. High Pressure Complex Formation

Additional high pressure complex formation experiments were carried out with IB and β-CD, which were integral in the design of reported high pressure complex formation experiments but not reported elsewhere in this dissertation.

B.1 Materials

Ibuprofen, piroxicam, β-cyclodextrin and 2-hydroxypropyl-β-cyclodextrin were purchased from Sigma Aldrich and used as received.

B.2 Methods

B.2.1 High Pressure Complex Formation

A new high pressure view-cell, which is illustrated in Figure 116, was designed and built in order to perform complex formation experiments. Limitations of previous systems included complex interior geometries from which sample recovery was difficult, poor mixing capabilities and poor visualization capabilities (i.e. small windows). This simple system was designed to circumvent these limitations by incorporating larger windows, modification and implementation of a commercial magnetically driven high pressure mixer with greater torque than small magnetic stirbar mixers, and creating a inner geometry capable of containing a transparent glass vial for containing the samples for easier product recovery. This system is currently a constant volume system, with temperature control maintained by symmetrically positioned heater cartridges in the bottom and middle segments of the vessel and heating tape around the bottom of the mixer. A

Dynisco pressure transducer is used to monitor system pressure within +/- 10 psi. Pressure is altered by changing the loading to the system. Aside from its utilization in this research activity, this system holds high potential and flexibility for future additions, if needed, such as a variable-volume portion.

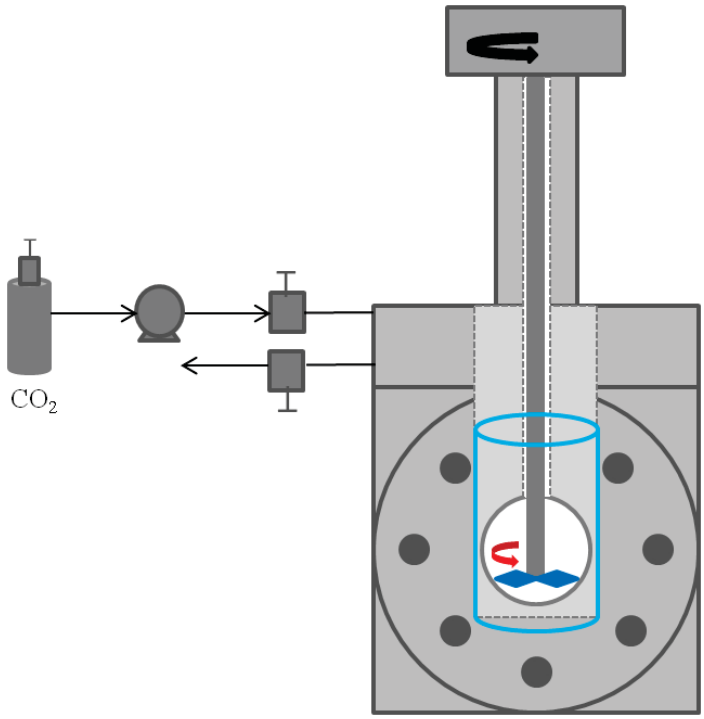

Figure 116. View-cell apparatus developed for and used in high pressure complex formation experiments.

In a typical high pressure inclusion complex formation experiment, 500 mg of a specified stoichiometric drug:CD mixture was added to the glass vial. The vial was place into the high pressure vessel and co-solvent, if used, was added. The vessel was sealed closed and CO_2 was charged to the system. The temperature was increased to the desired set point and the mixer was

turned on. After the desired exposure time had been reached, the heaters and mixer were turned off and the sample was recovered.

B.2.2 DSC

Differential scanning calorimetry (DSC) experiments were carried out on a Perkin Elmer Diamond DSC unit at a heating rate of 20 ^{o}C/ min with a 10 mL/min nitrogen purge.

B.2.3 TGA

Thermal gravimetric analysis (TGA) was carried out using a modified DuPont Instruments 951 TGA unit with a heating rate of 10 ^{o}C/min and a nitrogen purge of about 10 mL/min.

B.2.4 FTIR

Infrared spectroscopy was carried using a Digilab Excaliber HE Series FTS 3100 spectrometer. Samples were prepared into KBr pellets at 1 wt% concentrations for analysis.

B.2.5 Powder XRD

X-ray diffraction patterns were acquired on a PANalytical X-Pert PRO instrument.

B.3 Results

B.3.1 Ibuprofen and β-Cyclodextrin Mixtures

The melting temperature of IB has been shown to be depressed in the presence of CO_2 [255], as shown in Figure 117. In our DSC characterization, β-CD and IB form a complex upon IB melting which was visualized by the disappearance of the IB melting peak when reheated. Attempts to form a complex between β-CD and IB using $scCO_2$ have generally used the approach of dissolving IB in CO_2 and passing through a bed of β-CD [62]. This work attempts to melt the IB in the presence of CO_2 and β-CD to form the complex in a one-step batch process.

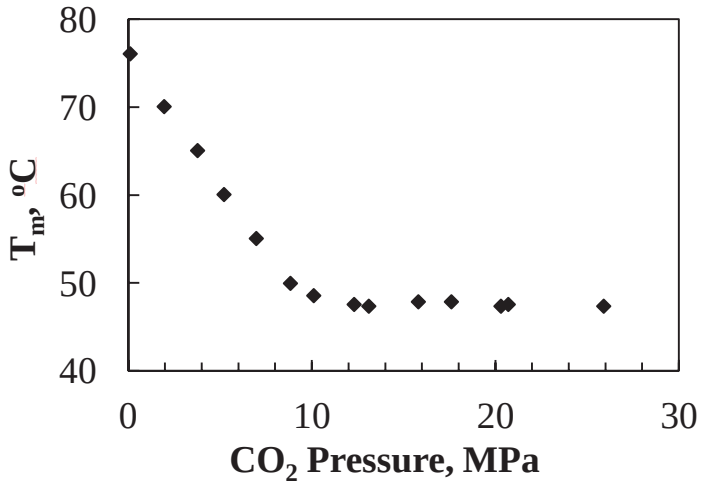

Figure 117. Pressure dependent melting point depression of IB in CO_2 [255].

For high pressure complex formation experiments to be successful, the thermal properties of the incorporated drug cannot be compromised. Therefore, preliminary work was done exposing IB alone to CO_2 at conditions reported to melt the drug (50 ^oC / 10 MPa) [62, 255]. During the high pressure experiments, melting of IB was visually confirmed since the drug would remain as an

immiscible liquid lay at the bottom of the vessel. The recovered product was analyzed by DSC and TGA, and the results are shown in Figure 118 and Figure 119, respectively.

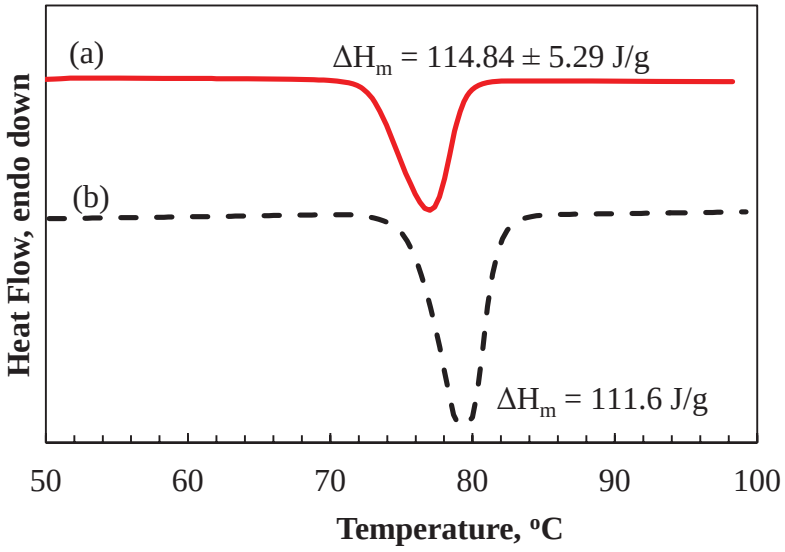

Figure 118. DSC heating scan of (a) unprocessed IB vs. (b) IB exposed to CO_2 for 2 hours at 50 ^{o}C / 10 MPa.

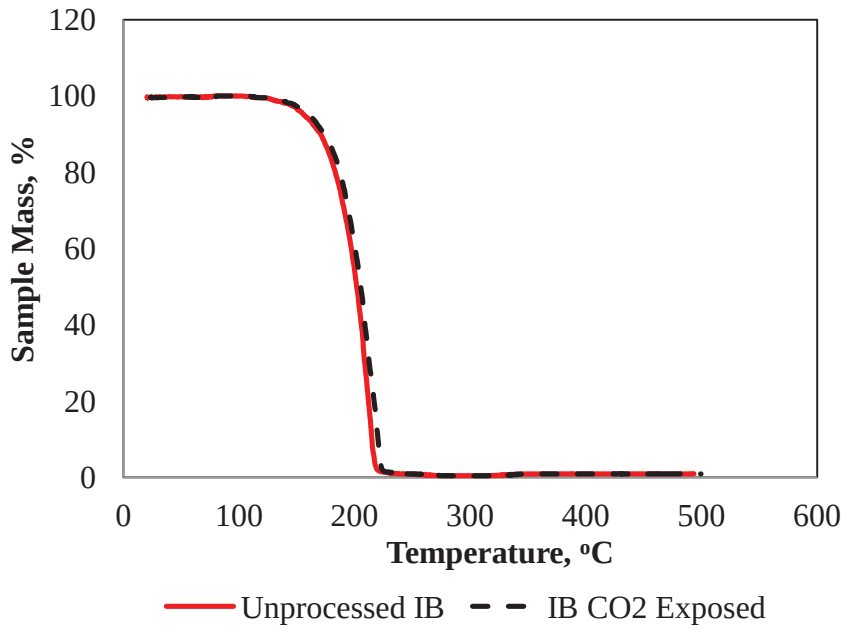

Figure 119. TGA thermogram of unprocessed IB vs. IB exposed to CO_2 for 2 hours at 50 ^{o}C / 10 MPa.

As indicated by the melting peak seen in the DSC heating scan in Figure 118, the IB which has been exposed to CO_2 exhibits a slightly higher melting temperature than the unprocessed IB while heat of melting is in the same range. Based on the TGA thermogram shown in Figure 119, the thermal stability of the CO_2 exposed IB seems to be nearly identical to that of the unprocessed IB. Thus, these conditions were deemed appropriate for high pressure complex formation experiments of IB:β-CD mixtures, since IB properties do not seem to be compromised by the $scCO_2$ processing. Table 24 provides the experimental conditions employed in four high pressure complex formation experiments with 1:1 molar ratio mixture of IB:β-CD. All experiments were conducted at constant temperature of 50 ^{o}C. At all experimental conditions employed in this work, IB is known to be in the liquid state, as indicated in the literature [62, 255] and confirmed in the view-cell in our lab.

Table 24. High pressure complex formation experiments carried out with IB:β-CD mixtures. Inclusion yields were calculated from integrating the melting peak of IB in DSC heating scans.

Trial	IB mass, g	β-CD mass, g	Molar Ratio, β-CD:IB	Pressure, MPa	Exposure time, hr	% Inclusion
1	0.15653	0.96095	1.09	10.34	2	10
2	0.15724	0.96222	1.09	15.17	2	66
3	0.15554	0.96288	1.10	24.83	2	79
4	0.15518	0.96173	1.10	34.48	2	82

The DSC results are shown comparatively in Figure 120. The melting peak of unprocessed IB is clearly seen in Figure 120a. β-CD does not display any thermal events over the temperature range investigated, since the sample was first dehydrated by heating to 100 ^{o}C then reheated for the displayed heating curve. As processing pressure increases, the intensity of the IB melting peak decreases indicating a lower amount of free (uncomplexed) IB in the sample. This was taken as a result of increased IB inclusion complex formation with β-CD at higher pressures. The equation below was used to calculate the percentage inclusion yield.

$$\%\ complexed = \left[1 - \frac{H_m^{product}}{H_m^{IB}}\right] \times 100$$

Table 25. Inclusion yield for IB:β-CD mixtures processed at 50 ^{o}C in CO_2.

Pressure, MPa	ΔH_m, J/g	% Complexed
10	106	7
15	41	64
25	24	79
35	21	82

As shown in Table 25, a significant increase in complex formation was seen when increasing the pressure was from 10 MPa to 15 MPa, and again from 15 to 25 MPa. However, the pressure increase from 25 to 35 MPa did not increase the inclusion yield significantly further.

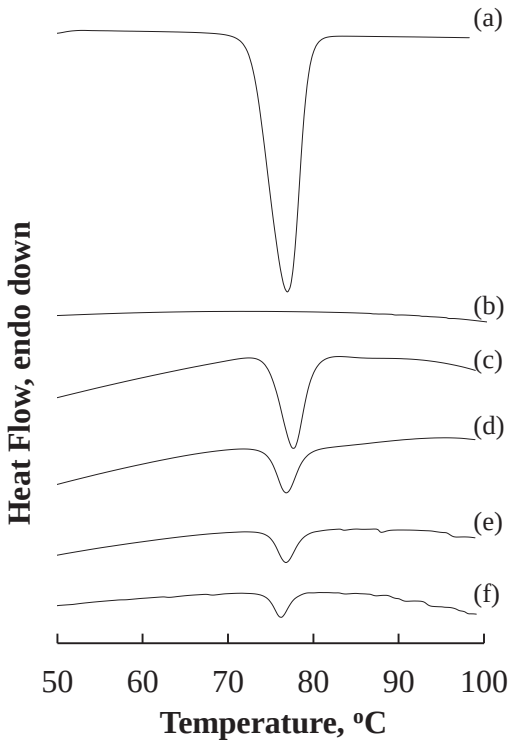

Figure 120. DSC heating scans of (a) unprocessed IB, (b) unprocessed β-CD and 1:1 molar ratio IB:β-CD exposed to CO_2 at 50 °C and (c) 10 MPa, (d) 15 MPa, (e) 25 MPa and (f) 35 MPa.

The FTIR analysis is shown in Figure 121. The key peak of interested in the FTIR spectra of IB is the carbonyl stretch at 1721 cm^{-1}. In pure IB (Figure 121a), the peak is very intense, while there is no peak observed at 1721 cm^{-1} for β-CD (Figure 121b). The spectrum of the IB:β-CD mixture processed at 10 MPa (Figure 121c) contains the same IB carbonyl stretch, although the peak is diminished compared with pure IB. The peak is hardly visible in the spectrum acquired for the mixture processed at 20 MPa, and with higher processing pressure, the peak is no longer

visible. This supports the DSC information that the amount of free, uncomplexed IB in the mixture is decreasing as processing pressure increases.

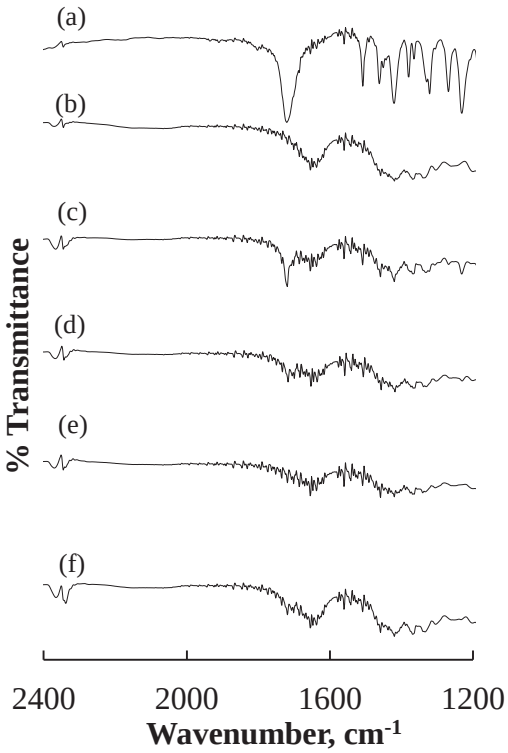

Figure 121. FTIR spectra of (a) unprocessed IB, (b) unprocessed β-CD and 1:1 molar ratio IB:β-CD exposed to CO_2 at 50 ^{o}C and (c) 10 MPa, (d) 15 MPa, (e) 25 MPa and (f) 35 MPa.

The XRD patterns for unprocessed components and CO_2 exposed IB:β-CD mixtures are shown in Figure 122. Both IB and β-CD have distinct diffraction patterns as shown in Figure 122a and b, respectively. In the mixtures, the diffraction pattern is nearly identical to that of β-CD and does not seem to vary based on the processing pressure. This indicates that IB is not present in the mixtures in the same crystalline form as the unprocessed IB, which could in turn be an indication of inclusion complex formation.

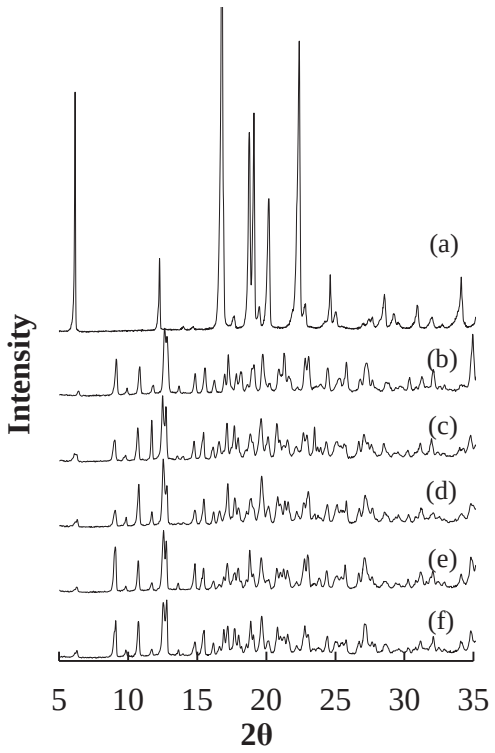

Figure 122. XRD patterns for (a) unprocessed IB, (b) unprocessed β-CD and 1:1 molar ratio IB:β-CD exposed to CO_2 at 50 ^{o}C and (c) 10 MPa, (d) 15 MPa, (e) 25 MPa and (f) 35 MPa.

B.3.2 Piroxicam and 2-Hydroxypropyl-β-Cyclodextrin Mixtures

The high pressure inclusion complex formation procedure described in Chapter V was employed to form a PC:HP-β-CD complex by PC melting point depression in a 90:10 wth% CO_2:ethanol mixture. The 1:1 molar ratio physical mixture of HP-β-CD:PC and desired amount of ethanol were added to a high pressure mixing vessel. The vessel was then charged with CO_2 for a total solvent composition of 90:10 wt% CO_2:ethanol. A processing temperature of 165 ^{o}C was achieved using four symmetrically positioned heater cartridges and stirred for 1.5 h. Pressure was allowed to increase with temperature to about 30 MPa. The heaters were turned off and the vessel was then allowed to gradually cool to room temperature while mixing the sample. The

sample was collected after depressurizing and was dried under vacuum at 80 ^{o}C to remove any remaining co-solvent. The product was characterized by DSC and FTIR, which are shown in Figure 123 and Figure 124, respectively. The DSC melting endotherm displayed a PC heat of melting of 15.8 J/g, compared to the unprocessed PC heat of melting of 105.0 J/g, indicating that an inclusion yield of 85% was achieved in this process.

The FTIR spectra show that the inclusion complex produced only displays the HP-β-CD key peaks, and the PC key peaks at 1330 cm^{-1} (O=S=O stretch), 1630 cm^{-1} (=O stretch) and 3339 cm^{-1} (-NH- stretch) are not visible. This is consistent with the evidence provided in Chapter V on the formation of an inclusion complex between HP-β-CD and PC.

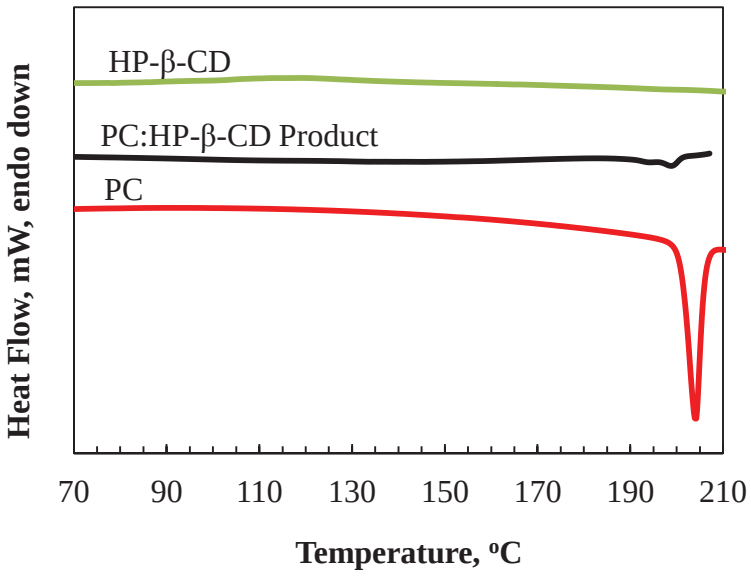

Figure 123. Comparison of DSC heating scans of HP-β-CD, PC and the PC:HP-β-CD complex formed by the high pressure melting point depression technique described in Chapter V.

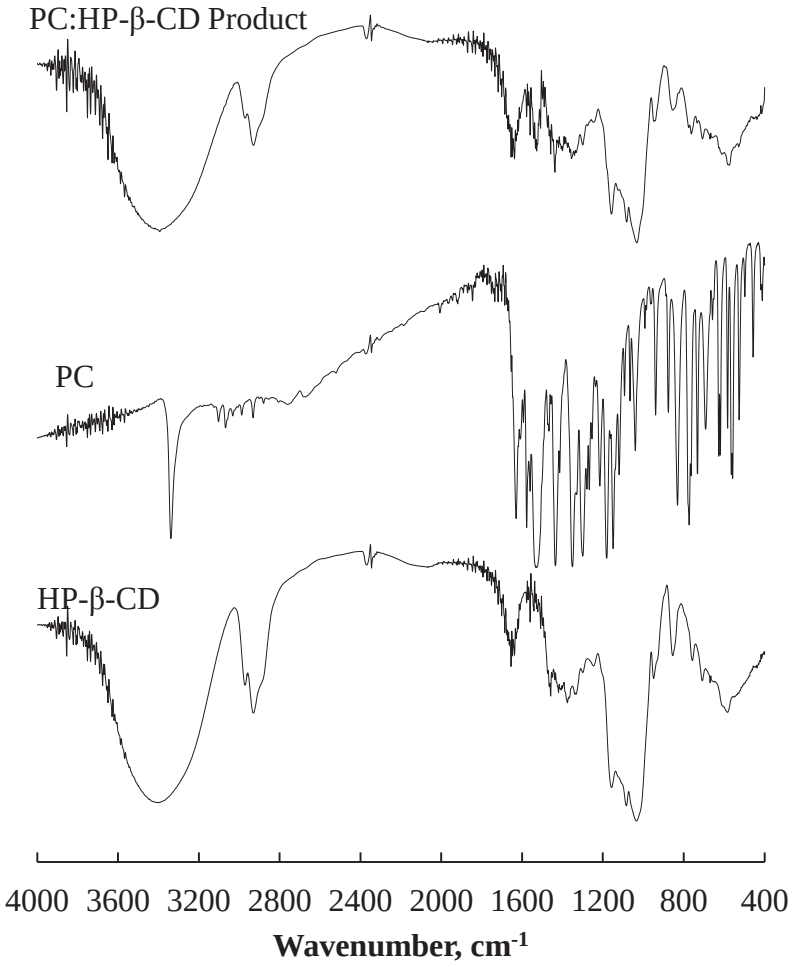

Figure 124. Comparison of the FTIR spectra of HP-β-CD, PC and the PC:HP-β-CD complex formed by the high pressure melting point depression technique described in Chapter V.

Appendix C. Synthesis of a β-cyclodextrin Containing Monomer

Synthesis of a mono-vinyl substituted β-CD was attempted in this research to be polymerized alone or co-polymerized with a biocompatible polymer for TE and drug delivery applications. This synthesis has been described in the literature [256-258].

C.1 Materials and Methods

C.1.1 Materials

All compounds used in the synthesis are shown in Table 26. All chemicals were obtained from Sigma and used as received with no further purification.

Table 26. Purity of chemicals used in monomer synthesis

Compound	Purity, %
β-cyclodextrin	≥ 97
Sodium Hydroxide	99.99
p-Toluenesulfonyl Chloride	≥ 99
Acetonitrile	99.8
Hydrogen Chloride	≥ 99.8
Ethylene Diamine	≥ 99
Acetone	≥ 99.5
Diethyl Ether	≥ 99
Methanol	≥ 99.8
Glycidyl Methacrylate	97
Dimethylformamide	≥ 99.8
Hydroquinone	≥ 99

C.1.2 Synthesis

Synthesis of a monovinyl – substituted β-cyclodextrin was attempted and can be broken into three steps:

(1) Synthesis of mono-6-OTs-β-cyclodextrin, where Ts represents *p*-toluenesulfonyl.

(2) Replace the OTs group with ethylenediamine (EDA).

(3) Attach glycidyl methacrylate (GMA) to the amine, generating the monomer, glycidyl methacrylate ethylenediamene (GMA-EDA) substituted β-cyclodextrin.

Synthesis of Mono-6-OTs-β-Cyclodextrin

The method described by Petter, et al. was employed in conjuction with the method described by Xie, et al. to produce mono-6-OTs-β-cyclodextrin (mono-6-OTs-β-CD). 30 g β-CD was added to 250 ml ACS reagent grade water at 24^{o}C with stirring. A supersaturated, opaque white solution was produced. 10 ml of 8.2M NaOH aqueous solution was added dropwise over 5 minutes while mixing. The solution became transparent and slightly yellow in color with the addition of NaOH. A solution of 5.04 g *p*-toluenesulfonyl chloride (*p*-TsCl) was added to 15 ml anhydrous acetonitrile (ACN) and mixed until the solution became homogeneous. The ACN/*p*-TsCl solution was added dropwise to the β-CD/NaOH/H_2O solution dropwise over 45 minutes. A white precipitate formed immediately. The slurry was stirred for 2 hours after the addition was complete at 24 ^{o}C. 1M HCl was added to neutralize the solution (pH = 7), which caused the precipitation of the reaction product and any unreacted β-CD. The solution was placed in the refrigerator overnight at about 9 ^{o}C. Vacuum filtration was used to collect the precipitate using a Millipore 0.22 um filter. The precipitate was washed with ethyl ether and hot water three times to remove unreacted *p*-TsCl and β-CD, respectively. The precipitate was collected by vacuum

filtration after each washing then dried under vacuum at 70 ^{o}C. The product was characterized by H-NMR, DSC and FTIR.

Synthesis of EDA-β-CD

The product recovered from the mono-6-OTs-β-CD synthesis was dissolved in 30 ml ethylenediamine. The solution was placed into a constant temperature water bath at 75 ^{o}C and left to react for 4 hours. After cooling to room temperature overnight, the reaction mixture was poured into 400 ml of acetone at 8 ^{o}C, instantly forming a white precipitate. The precipitate was collected by vacuum filtration using a Whatman 7.0 cm qualitative filter paper. Two distinct precipitates were observed: (1) a free flowing, particle-like precipitate which readily dissolved in 3:1 (v/v) water-methanol solution and (2) a sticky precipitate yellow in color, which dissolved in 3:1 (v/v) water-methanol solution with gentle heating of the solution. The precipitation and re-dissolving procedures were repeated once. The precipitate was placed under vacuum at 50 ^{o}C for 5 days.

Synthesis of GMA-EDA-β-CD

A 4:1 molar ratio of GMA to EDA-β-CD was dissolved in 30 ml dimethylformamide. A small amount of 1,4-dihydroxybenzene was added to the solution. The solution was stirred and heated to 60 ^{o}C. The reaction took place at 60 ^{o}C for 6 hours. The mixture was allowed to cool to room temperature over night.

C.1.3 Differential Scanning Calorimetry

Differential scanning calorimetry (DSC) was performed using a Pyris Diamond DSC. Samples were analyzed by heating and cooling at a rate of 20 ^{o}C/min with a nitrogen purge at 10 ml/min. Pyris software was use in the data analysis.

C.1.4 Fourier Transform Infrared Spectroscopy

Fourier transform infrared (FTIR) spectroscopy was carried out on a Digilab Excaliber HE Series FTS 3100 spectrometer with a 4 cm^{-1} resolution and 32 scans in the wavenumber range of 4000 to 400 cm^{-1}. Samples were prepared into KBr pellets for analysis.

C.1.5 Nuclear Magnetic Resonance Spectroscopy

Proton nuclear magnetic resonance (H-NMR) spectroscopy was carried out on a Varian Inova 400 MHz spectrometer. Mono-6-OTs-β-CD was dissolved in deuterated dimethylsulfoxide, and EDA-β-CD and GMA-EDA-β-CD were dissolved in deuterated water for H-NMR analysis. Expected chemical shifts are reported for the product of each step in Table 27.

Table 27. Reported chemical shifts of each product of the synthesis from a [256] and b [258].

mono-6-OTs-β-CD[a]		EDA-β-CD[b]		GMA-EDA-β-CD[b]	
δ	Protons	δ	Protons	δ	Protons
7.74	2 H	4.9	7 H, C(1)-*H*	6.02	1 H, C*H*H=
7.42	2 H	3.83-3.68	28 H, C(3)-*H*, C(6)-*H*, C(5)-*H*	5.64	1 H, CH*H*=
5.87-5.58	14 H	3.51-3.25	14 H, C(2)-*H*, C(4)-*H*	4.91	7 H, C(1)-*H*
4.82	4 H	2.89	2 H, -CH_2NH-β-CD	3.79-3.24	β-CD *H*
4.76	3 H			2.9	2 H, CH_2NH-β-CD
4.55-4.13	6 H			2.07	2 H, NHCH_2-CH_2NH-β-CD
3.74-3.43	28 H			1.83	3 H, -CH_3
3.42-3.18	overlaps HOD				
2.42	3 H				

C.2 Results

Batch 1

The first batch of mono-6-OTs-β-CD produced 0.3055 g of a white powder, using twice the batch described above, which is a very low yield. Petter's method, which was followed in this batch, does not describe a neutralization step at the end of the reaction, but Xie's method does. Without the neutralization step, the product is not precipitated out of the solution, resulting in a low yield.

Petter, et al. reported the melting point of the product to be 179 ^{o}C with a key FTIR peak at 1320 cm^{-1}. Using DSC to determine the melting temperature, the recovered product had a melting point of 204.74 ^{o}C, as shown in Figure 125, which is significantly higher than the reported value. In addition, the key peak was not observed in the FTIR spectrum displayed in Figure 126. The H-NMR spectrum is shown in Figure 127, and the peaks do not correspond exactly to those described by Petter, et al., as shown in Table 27. However, the H-NMR does show proton chemical shifts in the correct regions with δ 7.72, 7.45-7.41, 5.73-5.67, 4.81, 4.44, 3.60, 3.31 and 2.48-2.26. The product of this reaction was not used in any further synthesis, and another batch of mono-6-OTs-β-CD was attempted.

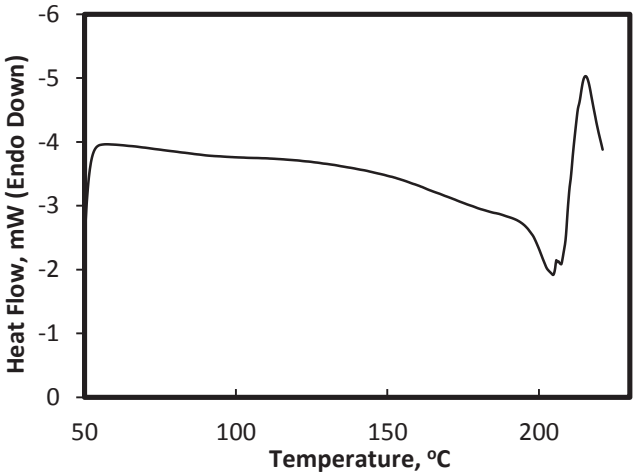

Figure 125. DSC of Batch 1 mono-6-OTs-β-CD reaction product

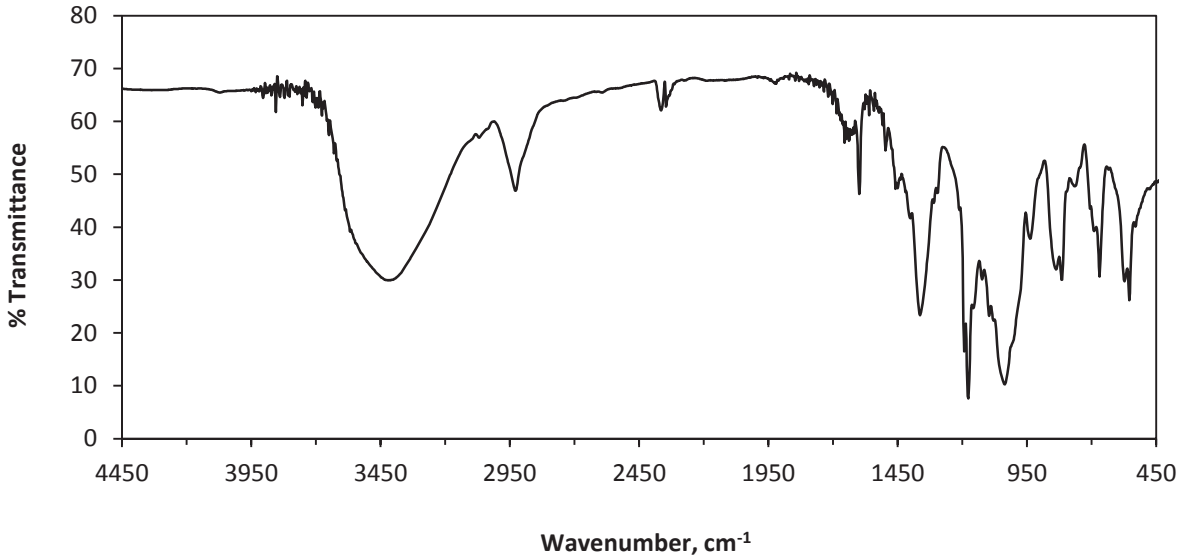

Figure 126. FTIR of Batch 1 mono-6-OTs-β-CD reaction product

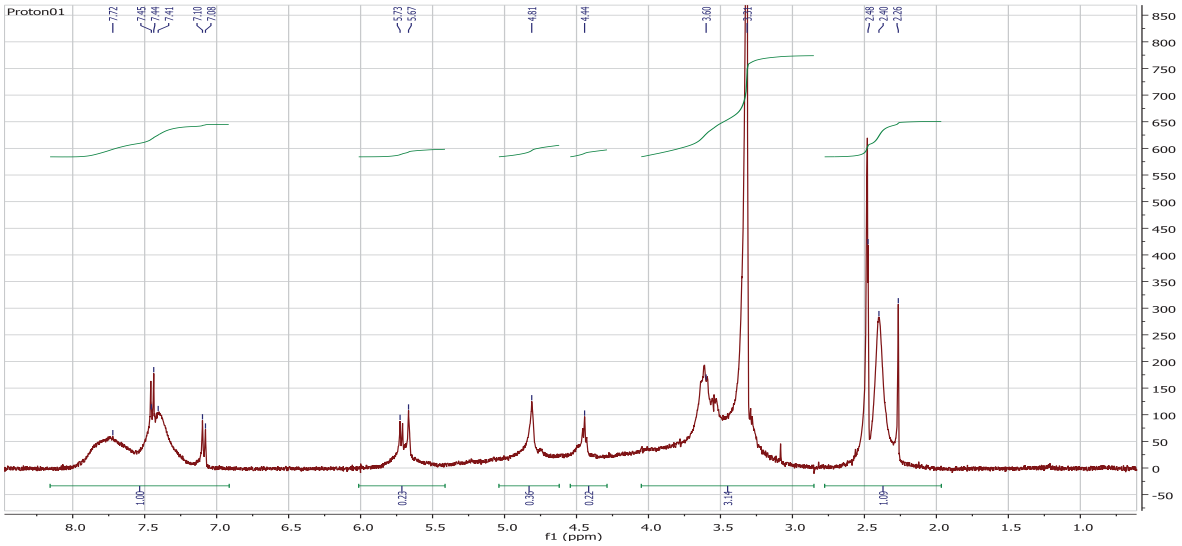

Figure 127. H-NMR of Batch 1 mono-6-OTs-β-CD reaction product.

Batch 2

In the second batch of mono-6-OTs-β-CD, the neutralization step was included as described in the procedure above, adapted from Xie's method. A precipitate forms during neutralization, which improved the product yield significantly. 5.9115 g of precipitate was obtained after filtering and drying. The DSC heating scan provided in Figure 128 showed two endothermic peaks at 186 ^{o}C and 192 ^{o}C. The FTIR analysis shown in Figure 129 displayed peaks at 1365 cm^{-1} and 1330 cm^{-1}. The H-NMR spectrum is shown in Figure 130. The values are not exactly the same as Petter, et al. reported; however, the synthesis was continued to produce EDA-β-CD.

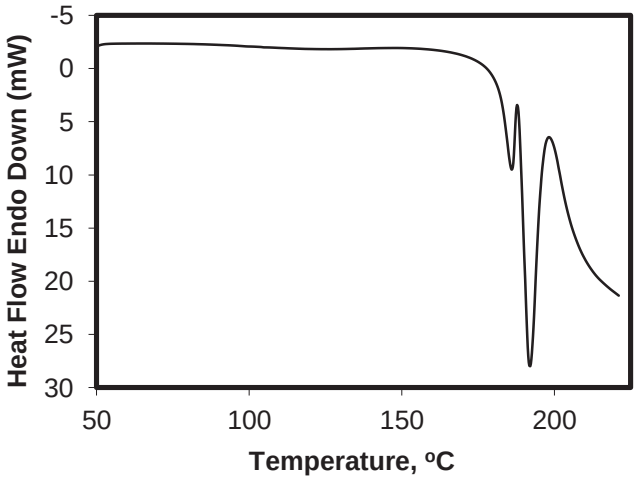

Figure 128. DSC of Batch 2 mono-6-OTs-β-CD reaction product.

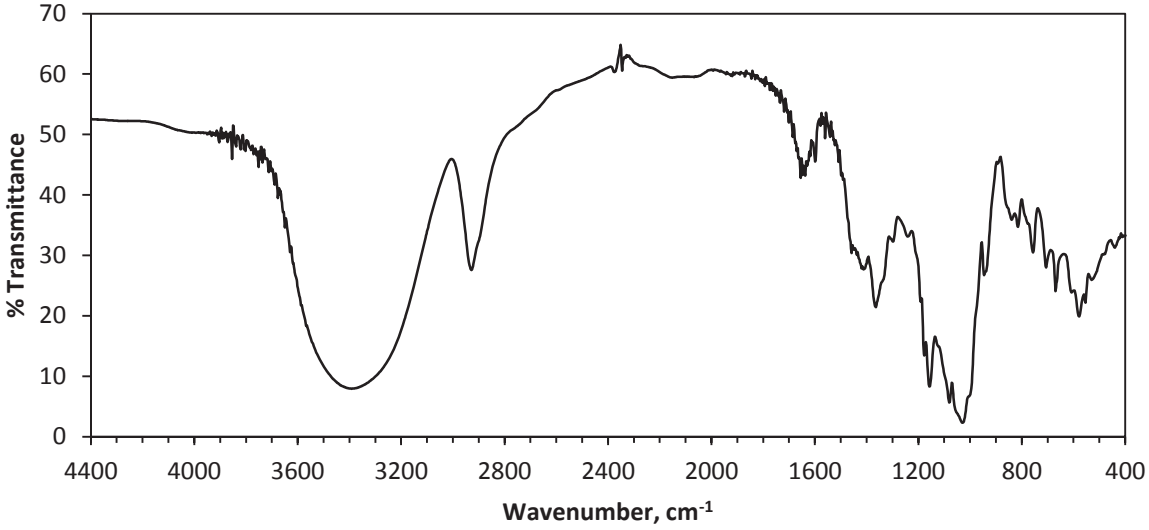

Figure 129. FTIR of Batch 2 mono-6-OTs-β-CD reaction product.

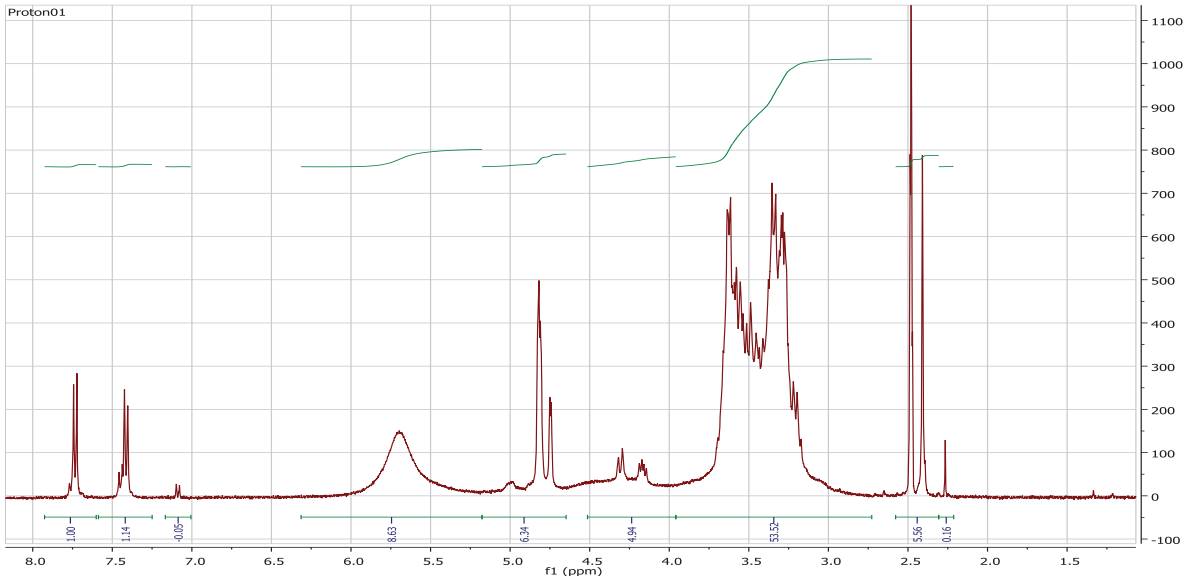

Figure 130. H-NMR of Batch 2 mono-6-OTs-β-CD reaction product.

The next step of the synthesis was carried out for Batch 2. 0.253 g of the EDA-β-CD product was recovered and spared for reaction with GMA. Only FTIR analysis was carried out for the EDA- β-CD product due to low sample yield, and the spectrum is shown in Figure 131. The reported key peaks for EDA-β-CD are 3382 cm^{-1} (-OH stretch), 2927 cm^{-1} (-CH_2) and 1029 cm^{-1} (C-OH) [258]. Related peaks are observed at 3369, 2928 and 1032 cm^{-1} in Figure 131. These peaks are close enough to the reported values to continue the synthesis with the GMA addition. For a 4:1 molar ratio of GMA:EDA-β-CD, all of the recovered EDA-β-CD was mixed with 0.122 g GMA.

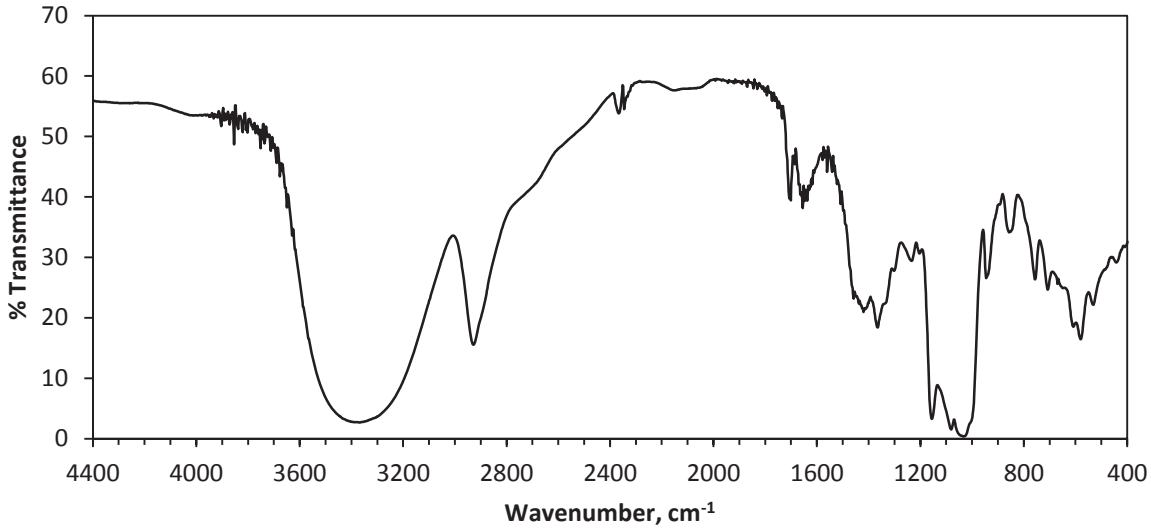

Figure 131. FTIR of EDA-β-CD product from Batch 2.

0.151 g of precipitate was collected from the GMA-EDA-β-CD reaction. The FTIR spectrum of the GMA-EDA-β-CD product is shown in Figure 132. Key bands described in the literature are 3385 cm^{-1} (-OH stretch), 2928 cm^{-1} ($-CH_2$), 1715 cm^{-1} (C=O) and 1031 cm^{-1} (C-O). The –OH stretch is observed in Figure 132 at 3368 cm^{-1}. The $-CH_2$ absorbance is observed at 2928 cm^{-1}. The carbonyl C=O stretch is clearly observed as a distinct peak at 1662 cm^{-1}. The -C-O stretch is observed at 1031 cm^{-1} in Figure 132. Figure 133 shows the H-NMR spectrum of the GMA-EDA-β-CD product, and it does not resemble the reported spectrum [258].

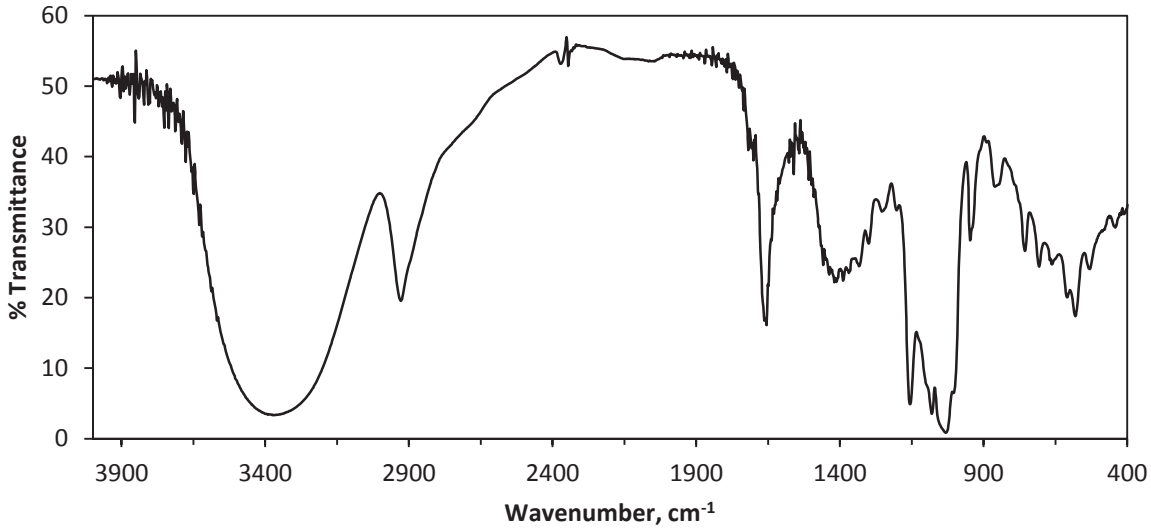

Figure 132. FTIR of Batch 2 GMA-EDA-β-CD reaction product.

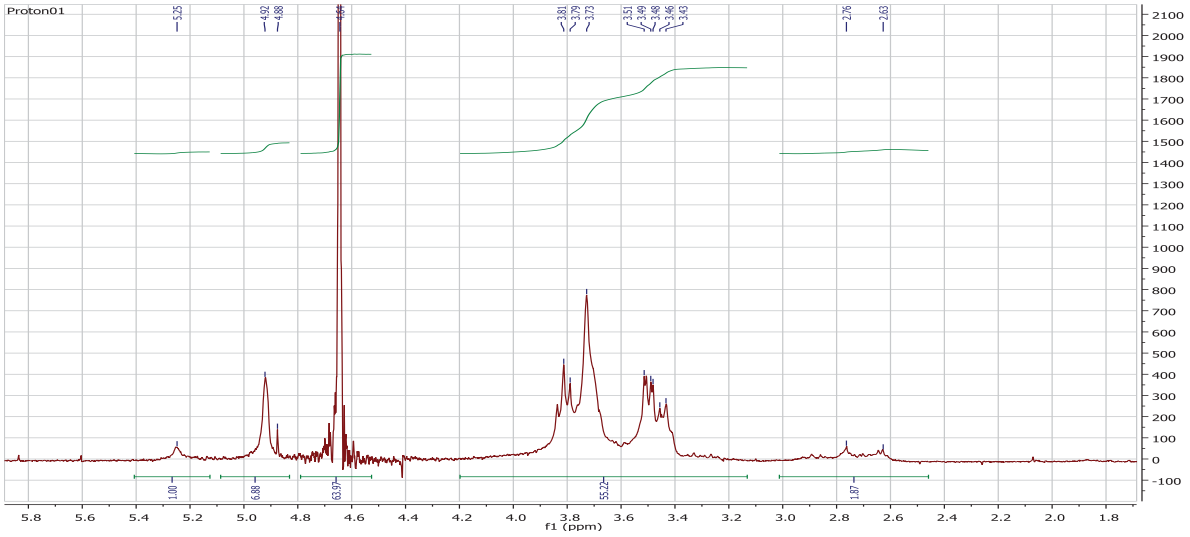

Figure 133. H-NMR of Batch 2 GMA-EDA-β-CD reaction product.

Batch 3

A third batch of mono-6-OTs-β-CD was synthesized, since the GMA-EDA-β-CD from Batch 2 did not appear to be successfully synthesized. 7.022 g of precipitated product was recovered. The DSC of the mono-6-OTs-β-CD product from Batch 3 is shown in Figure 134. The melting peak is observed at 189 ^{o}C, which is 10 ^{o}C higher than what Petter, et al. reported for this compound. The FTIR spectrum shown in Figure 135 does not display the reported key peak at 1320 cm^{-1}. However, the H-NMR spectrum shown in Figure 136 does correspond fairly closely with Petter's reports, and the next step of the synthesis was carried out.

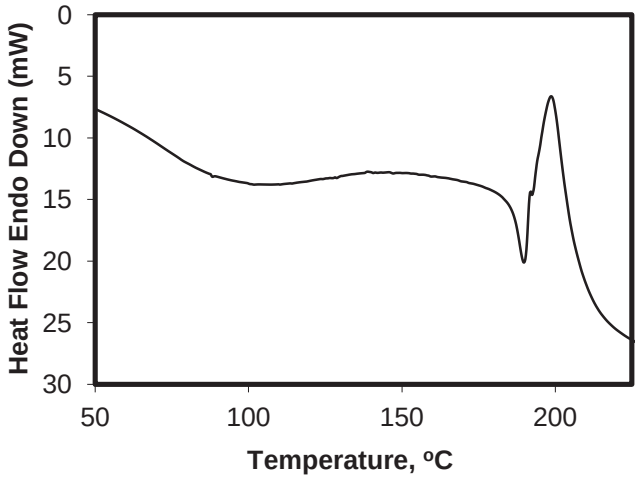

Figure 134. DSC of Batch 3 mono-6-OTs-β-CD reaction product.

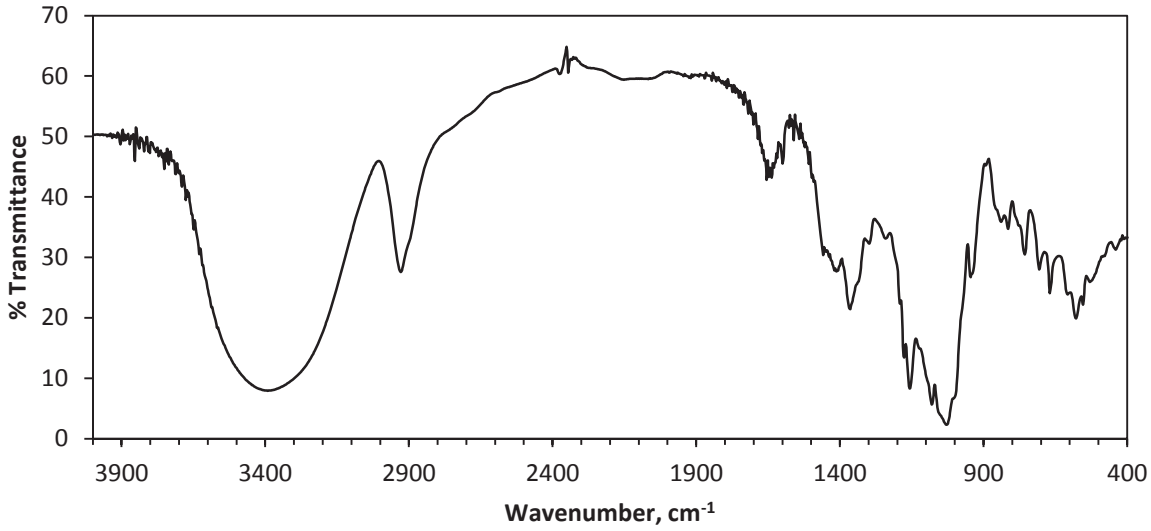

Figure 135. FTIR of Batch 3 mono-6-OTs-β-CD reaction product.

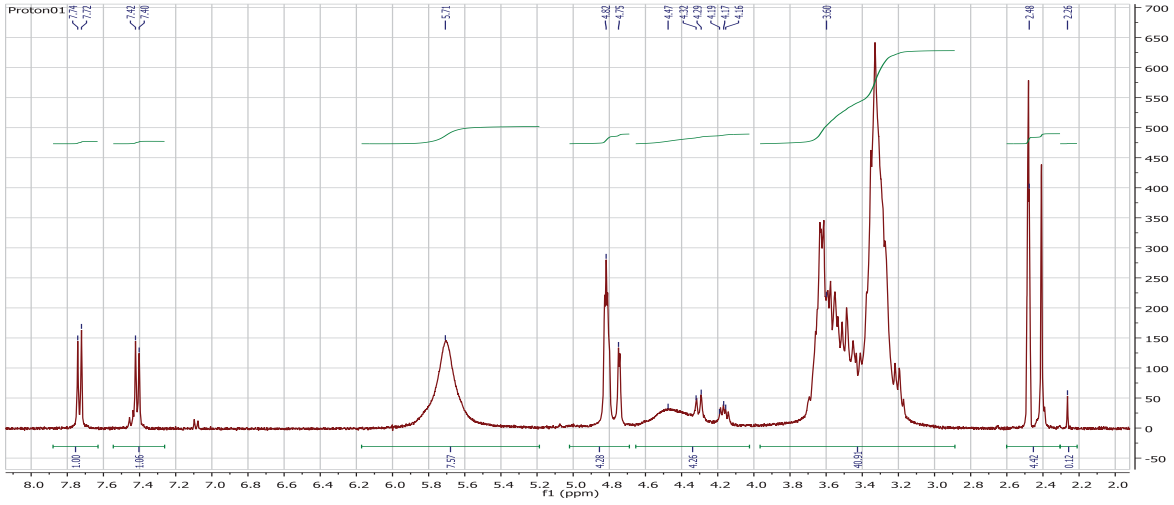

Figure 136. H-NMR of Batch 3 mono-6-OTs-β-CD reaction product.

1.7585 g of powder was recovered from the EDA-β-CD synthesis. The FTIR and H-NMR spectra for the Batch 3 EDA-β-CD reaction product are shown in Figure 137 and Figure 138, respectively. In the FTIR spectrum key peaks corresponding to those reported by Y.Y. Liu, et al. are found at 3385, 2928, 1018 cm^{-1}. The H-NMR spectrum corresponds almost exactly with the

spectrum reported by Y.Y. Liu, et al. with the exception of the peak at 2.89, for which integration does not relate to 2 protons, but only one in the –CH_2NH-β-CD. The next step of the synthesis was carried out, since the FTIR and the H-NMR data were very similar to those reported.

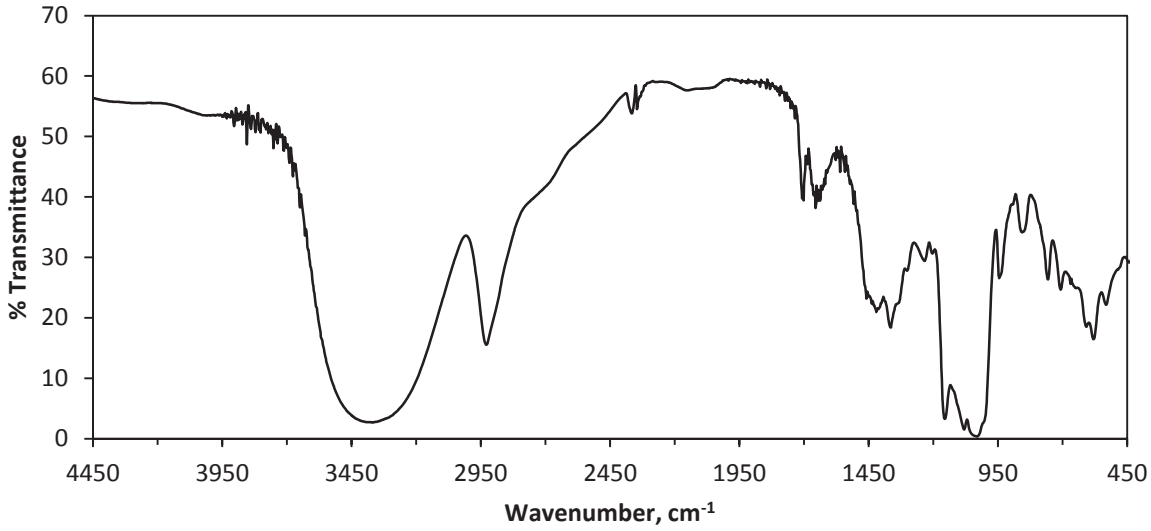

Figure 137. FTIR of Batch 3 EDA-β-CD reaction product.

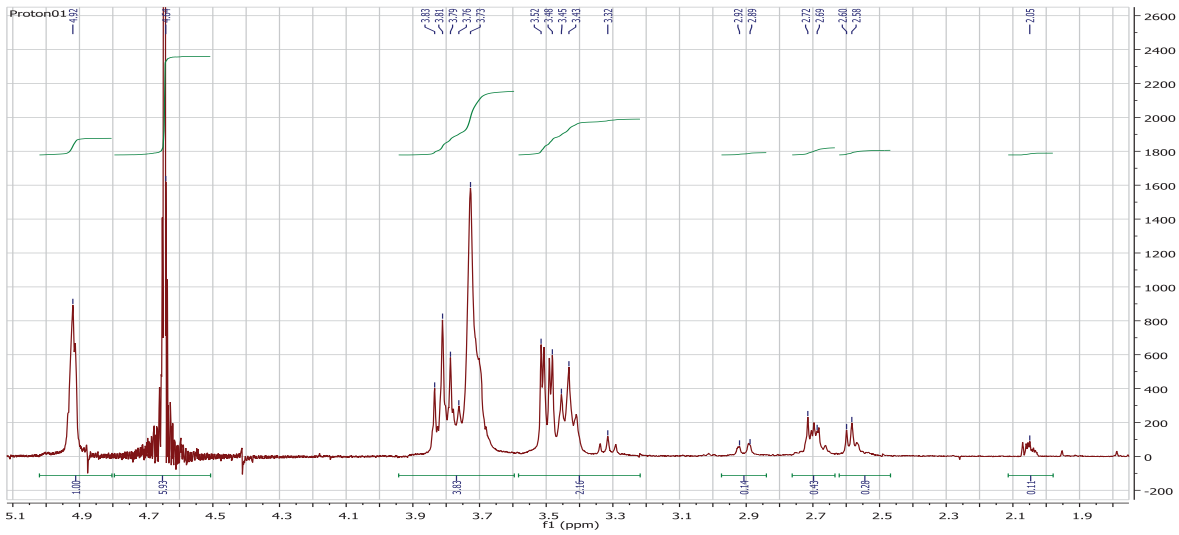

Figure 138. H-NMR of Batch 3 EDA-β-CD reaction product.

For a 4:1 molar ratio GMA:EDA-β-CD reaction mixture, 1.5 g EDA-β-CD product was mixed with 0.7245 g GMA. The FTIR and H-NMR spectra of the GMA-EDA-β-CD product are shown in Figure 139 and Figure 140, respectively. The FTIR spectrum corresponds with that reported by Y.Y. Liu, et al. with key peaks observed at 3369, 2929, 1655 and 1031 cm^{-1}, as expected. The H-NMR, however, does not correspond with the spectrum described in the literature, as the majority of the protons are not observed at the expected chemical shifts.

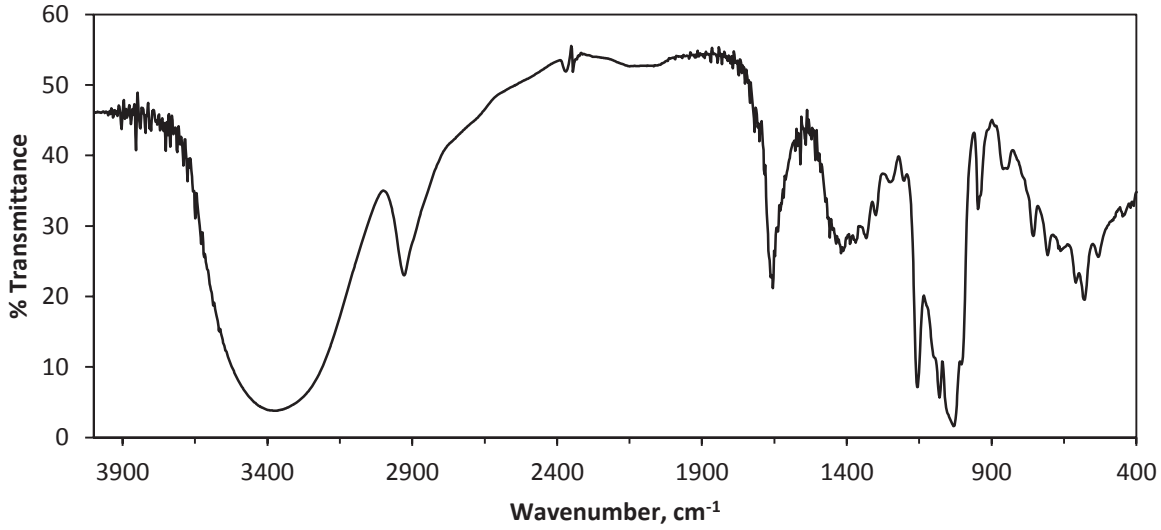

Figure 139. FTIR of Batch 3 GMA-EDA-β-CD reaction product.

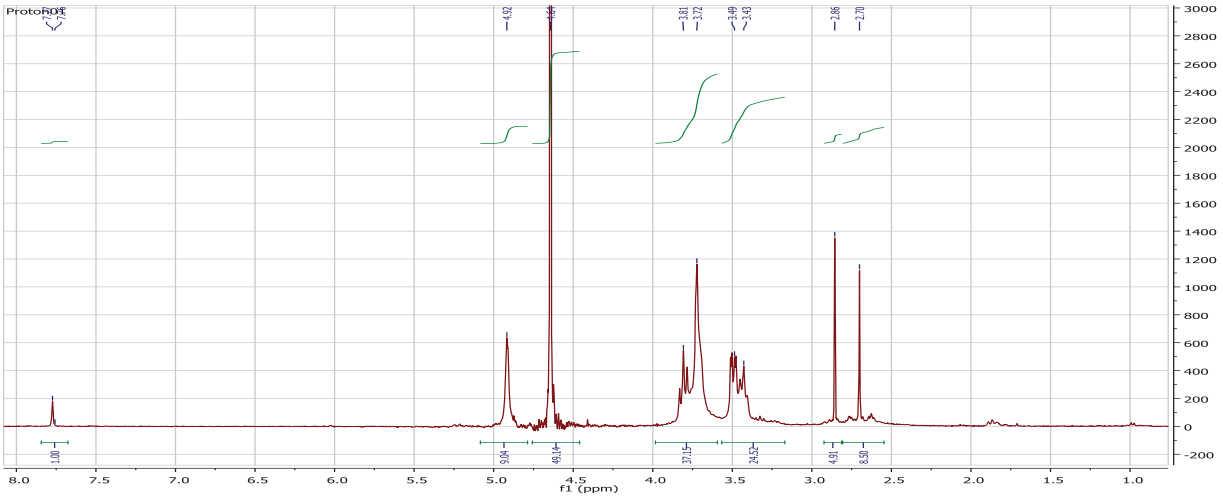

Figure 140. H-NMR of Batch 3 GMA-EDA-β-CD reaction product.

Batch 4

Since the GMA-EDA-β-CD monomer was not successfully synthesized in Batch 3, a fourth batch was attempted from the beginning. 4.14 g of mono-6-OTs-βCD product was recovered from the Batch 4 synthesis. The DSC heating scan shown in Figure 141 displayed a melting endotherm at 186 ^{o}C, which is higher than the 179 ^{o}C melting point described by Petter, et al. The FTIR spectrum shown in Figure 142 does not display the reported peak at 1320 cm^{-1}, but a peak is observed at 1364 cm^{-1}, which may represent the tosyl group. The H-NMR spectrum is shown in Figure 143 but does not closely correspond to the spectrum described by Petter, et al.

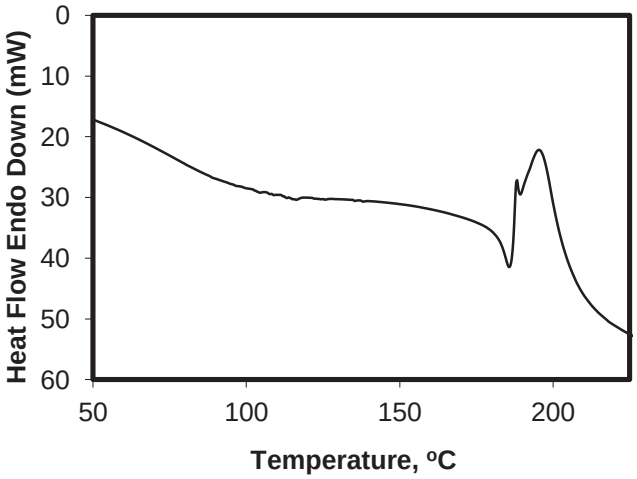

Figure 141. DSC of Batch 4 mono-6-OTs-β-CD reaction product.

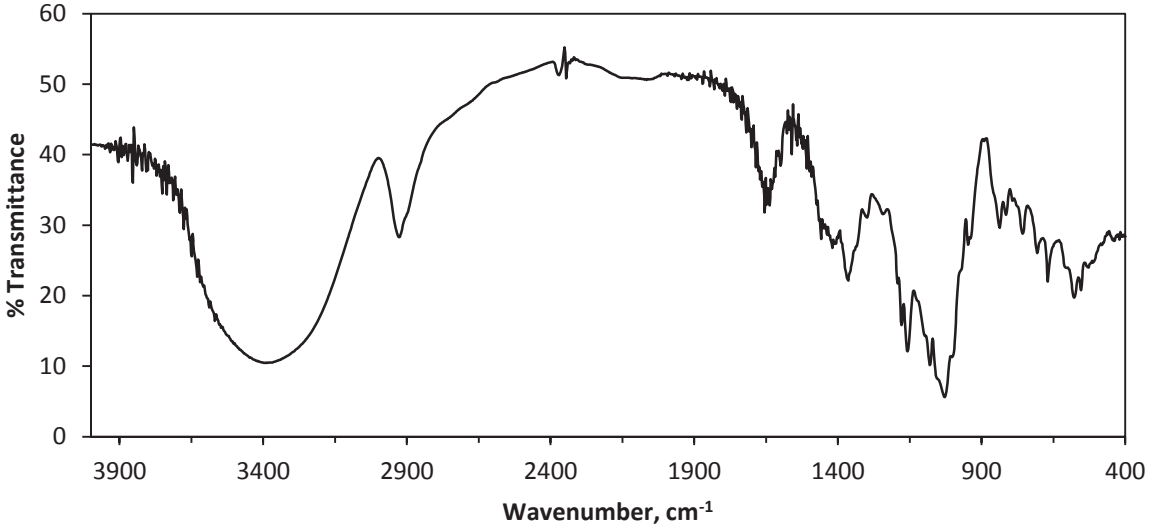

Figure 142. FTIR of Batch 4 mono-6-OTs-β-CD reaction product.

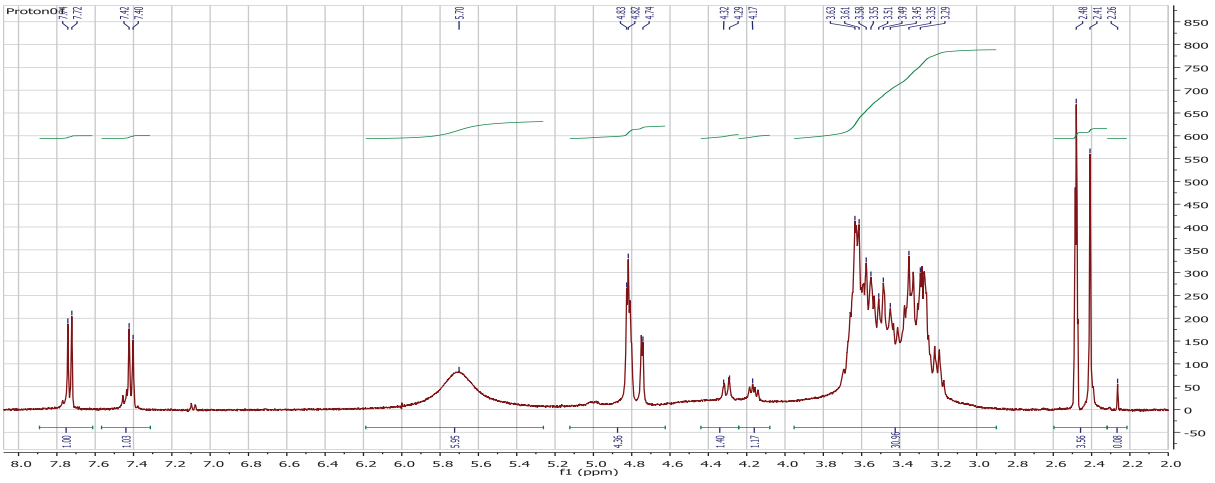

Figure 143. H-NMR of Batch 4 mono-6-OTs-β-CD reaction product.

The synthesis was continued, as this was the final effort to generate the monomer. Only 0.055 g EDA-β-CD product was recovered, thus, only FTIR characterization was carried out to spare some product for the GMA reaction. The FTIR spectrum is shown in Figure 144. Key peaks are observed at 3367, 2929 and 1031 cm^{-1}, as reported by Y.Y. Liu, et al.

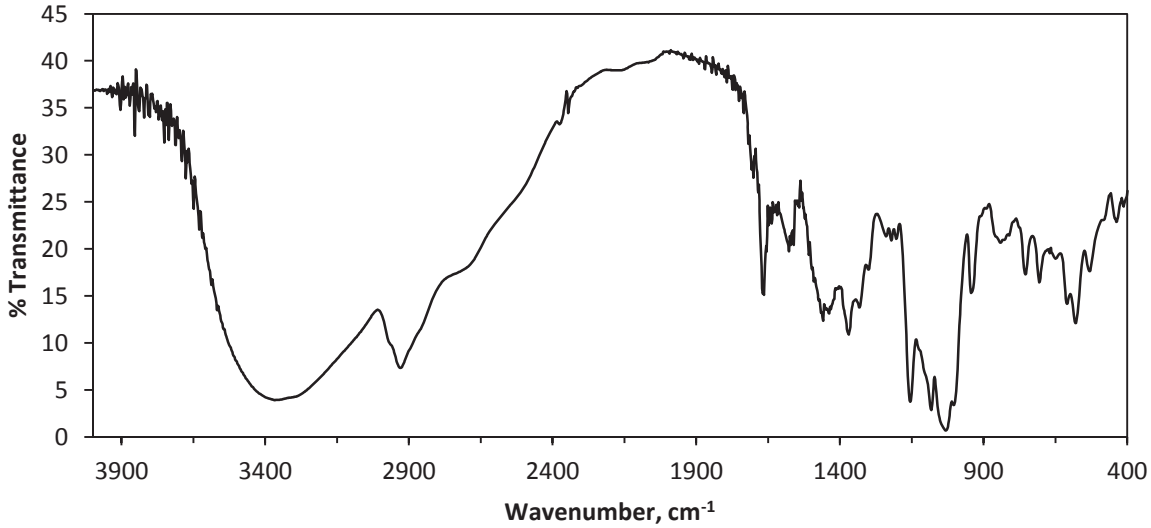

Figure 144. FTIR of Batch 4 EDA-β-CD reaction product.

The final step of the synthesis was carried out to add the GMA group to the substituted CD. A very low yield of the GMA-EDA-β-CD reaction product resulted, due to poor yield in the previous step of the synthesis. The H-NMR spectrum of the Batch 4 GMA-EDA-β-CD reaction product is shown in Figure 145. The spectrum does not fully represent the spectrum described in the literature for this product, and the synthesis was not attempted beyond this batch.

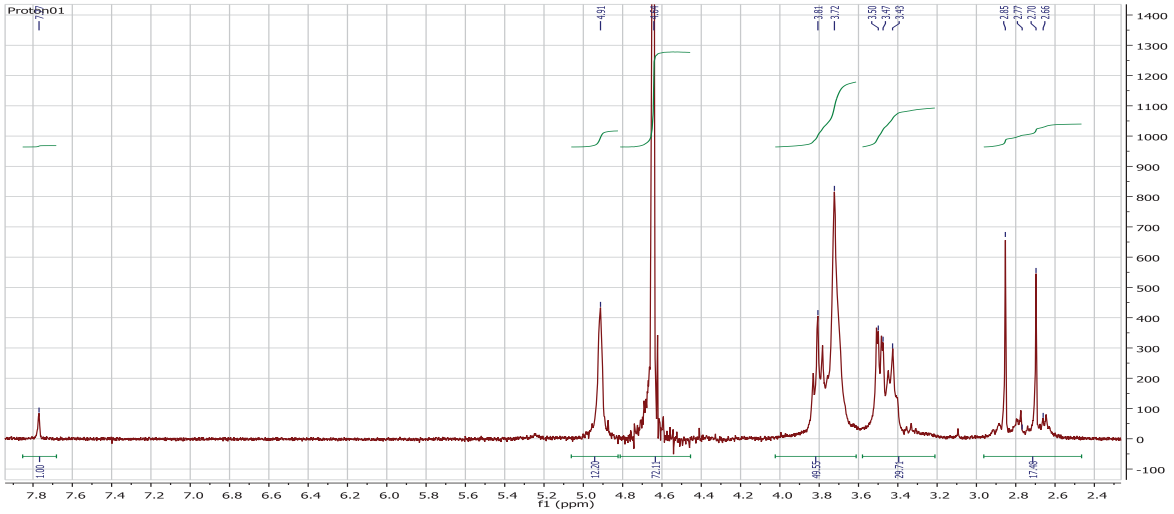

Figure 145. H-NMR of Batch 4 GMA-EDA-β-CD reaction product.

C.3 Conclusions

The attempted monomer synthesis was not conclusive and not continued throughout this research activity.

Appendix D. Annotated List of Figures

References

[1] E. Kiran, P.G. Debenedetti, C.J. Peters, Supercritical fluids : fundamentals and applications, Kluwer Academic Publishers, Dordrecht ; Boston, 2000.

[2] P. Munshi, S. Bhaduri, Supercritical CO(2): a twenty-first century solvent for the chemical industry, Current Science, 97 (2009) 63-72.

[3] M. Perrut, Supercritical fluids applications in the pharmaceutical industry, Stp Pharma Sciences, 13 (2003) 83-91.

[4] N. Foster, R. Mammucari, F. Dehghani, A. Barrett, K. Bezanehtak, E. Coen, G. Combes, L. Meure, A. Ng, H.L. Regtop, A. Tandya, Processing pharmaceutical compounds using dense gas technology, Industrial & Engineering Chemistry Research, 42 (2003) 6476-6493.

[5] S.D. Yeo, E. Kiran, Formation of polymer particles with supercritical fluids: A review, Journal of Supercritical Fluids, 34 (2005) 287-308.

[6] G. Bertoloni, A. Bertucco, M. Rassu, K. Vezzu, Medical device disinfection by dense carbon dioxide, Journal of Hospital Infection, 77 (2011) 42-46.

[7] C. Cinquemani, C. Boyle, E. Bach, E. Schollmeyer, Inactivation of microbes using compressed carbon dioxide - An environmentally sound disinfection process for medical fabrics, Journal of Supercritical Fluids, 42 (2007) 392-397.

[8] M. Zougagh, M. Valcarcel, A. Rios, Supercritical fluid extraction: a critical review of its analytical usefulness, Trac-Trends in Analytical Chemistry, 23 (2004) 399-405.

[9] S.G. Kazarian, Polymer Processing with Supercritical Fluids, Polymer Science, Series C, 42 (2000) 78-101.

[10] S.E. Conway, H.S. Byun, M.A. McHugh, J.D. Wang, F.S. Mandel, Poly(lactide-co-glycolide) solution behavior in supercritical CO2, CHF3, and CHClF2, Journal of Applied Polymer Science, 80 (2001) 1155-1161.

[11] H. Pöhler, E. Kiran, Volumetric Properties of Carbon Dioxide + Acetone at High Pressures, Journal of Chemical & Engineering Data, 42 (1997) 379-383.

[12] H. Pohler, E. Kiran, Volumetric properties of carbon dioxide plus ethanol at high pressures, Journal of Chemical and Engineering Data, 42 (1997) 384-388.

[13] D.R. Burgess, Thermochemical Data, in: P.J.L.a.W.G. Mallard (Ed.) NIST Chemistry WebBook, NIST Standard Reference Database Number 69, National Institute of Standards and Technology, Gaithersburg MD, 20899.

[14] T.L. Chester, B.S. Haynes, Estimation of pressure-temperature critical loci of CO2 binary mixtures with methyl-tert-butyl ether, ethyl acetate, methyl-ethyl ketone, dioxane and decane, Journal of Supercritical Fluids, 11 (1997) 15-20.

[15] H. Pohler, E. Kiran, Volumetric properties of carbon dioxide plus toluene at high pressures, Journal of Chemical and Engineering Data, 41 (1996) 482-486.

[16] R. Langer, Tissue engineering, Molecular Therapy, 1 (2000) 12-15.

[17] S. Levenberg, R. Langer, Advances in tissue engineering, Current Topics in Developmental Biology, Vol. 61, 61 (2004) 113-+.

[18] L.S. Nair, C.T. Laurencin, Biodegradable polymers as biomaterials, Progress in Polymer Science, 32 (2007) 762-798.

[19] B.D. Ulery, L.S. Nair, C.T. Laurencin, Biomedical Applications of Biodegradable Polymers, Journal of Polymer Science Part B-Polymer Physics, 49 (2011) 832-864.

[20] L.G. Griffith, Polymeric biomaterials, Acta Materialia, 48 (2000) 263-277.

[21] N.A. Peppas, R. Langer, New Challenges in Biomaterials, Science, 263 (1994) 1715-1720.

[22] D.S. Kohane, R. Langer, Polymeric biomaterials in tissue engineering, Pediatric Research, 63 (2008) 487-491.

[23] A.G. Mikos, G. Sarakinos, S.M. Leite, J.P. Vacanti, R. Langer, Laminated 3-Dimensional Biodegradable Foams for Use in Tissue Engineering, Biomaterials, 14 (1993) 323-330.

[24] S. Samavedi, C.O. Horton, S.A. Guelcher, A.S. Goldstein, A.R. Whittington, Fabrication of a model continuously graded co-electrospun mesh for regeneration of the ligament-bone interface, Acta Biomaterialia, 7 (2011) 4131-4138.

[25] Y.S. Nam, T.G. Park, Porous biodegradable polymer scaffolds for tissue engineering prepared by thermally-induced phase separation., Abstracts of Papers of the American Chemical Society, 216 (1998) U270-U270.

[26] A.R.C. Duarte, J.F. Mano, R.L. Reis, Supercritical fluids in biomedical and tissue engineering applications: a review, International Materials Reviews, 54 (2009) 214-222.

[27] E. Kiran, Polymer miscibility, phase separation, morphological modifications and polymorphic transformations in dense fluids, Journal of Supercritical Fluids, 47 (2009) 466-483.

[28] D.J. Mooney, D.F. Baldwin, N.P. Suh, L.P. Vacanti, R. Langer, Novel approach to fabricate porous sponges of poly(D,L-lactic-co-glycolic acid) without the use of organic solvents, Biomaterials, 17 (1996) 1417-1422.

[29] O.R. Davies, A.L. Lewis, M.J. Whitaker, H.Y. Tai, K.M. Shakesheff, S.M. Howdle, Applications of supercritical CO(2) in the fabrication of polymer systems for drug delivery and tissue engineering, Advanced Drug Delivery Reviews, 60 (2008) 373-387.

[30] E. Kiran, Modification of biomedical polymers in dense fluids. Miscibility and foaming of poly(p-dioxanone) in carbon dioxide plus acetone fluid mixtures, Journal of Supercritical Fluids, 66 (2012) 372-379.

[31] E. Kiran, Foaming strategies for bioabsorbable polymers in supercritical fluid mixtures. Part II. Foaming of poly(epsilon-caprolactone-co-lactide) in carbon dioxide and carbon dioxide plus acetone fluid mixtures and formation of tubular foams via solution extrusion, Journal of Supercritical Fluids, 54 (2010) 308-319.

[32] E. Kiran, Foaming strategies for bioabsorbable polymers in supercritical fluid mixtures. Part I. Miscibility and foaming of poly(L-lactic acid) in carbon dioxide plus acetone binary fluid mixtures, Journal of Supercritical Fluids, 54 (2010) 296-307.

[33] J.A. Hubbell, Synthetic biodegradable polymers for tissue engineering and drug delivery, Current Opinion in Solid State & Materials Science, 3 (1998) 246-251.

[34] R. Langer, Invited Review: Polymeric Delivery Systems for Controlled Drug Release, Chemical Engineering Communications, 3 (1980) 1-48.

[35] L.L. Lao, S.S. Venkatraman, N.A. Peppas, Modeling of drug release from biodegradable polymer blends, European Journal of Pharmaceutics and Biopharmaceutics, 70 (2008) 796-803.

[36] S.K.S. Anuj Kumar, Kumud Padhee, Prithi Pal Singh Kochar, Ajit Satapathy and Naveen Pathak, Review on Solubility Enhancement Techniques for Hydrophobic Drugs, Pharmacie Globale (IJCP), 2 (2011) 1-7.

[37] G.A. Green, Understanding NSAIDs: From Aspirin to COX-2, Sports Medicine, 3 50-59.

[38] J.G. Lombardino, Nonsteroidal antiinflammatory drugs, Wiley, New York, 1985.

[39] T. Spyriouni, X. Krokidis, I.G. Economou, Thermodynamics of pharmaceuticals: Prediction of solubility in pure and mixed solvents with PC-SAFT, Fluid Phase Equilibria, 302 (2011) 331-337.

[40] D.P. Pacheco, Y.J. Manrique, F. Martinez, Thermodynamic study of the solubility of ibuprofen and naproxen in some ethanol plus propylene glycol mixtures, Fluid Phase Equilibria, 262 (2007) 23-31.

[41] C.R. Daniels, A.K. Charlton, W.E. Acree, M.H. Abraham, Thermochemical behavior of dissolved carboxylic acid solutes: Part 2 - Mathematical correlation of ketoprofen solubilities with the Abraham general solvation model, Physics and Chemistry of Liquids, 42 (2004) 305-312.

[42] S. Gracin, A.C. Rasmuson, Solubility of phenylacetic acid, p-hydroxyphenylacetic acid, p-aminophenylacetic acid, p-hydroxybenzoic acid, and ibuprofen in pure solvents, Journal of Chemical and Engineering Data, 47 (2002) 1379-1383.

[43] S. Wang, Z.Q. Song, J.D. Wang, Y.L. Dong, M. Wu, Solubilities of Ibuprofen in Different Pure Solvents, Journal of Chemical and Engineering Data, 55 (2010) 5283-5285.

[44] M. Sorrenti, A. Negri, G.P. Bettinetti, DSC study of crystallinity changes of naproxen in ground mixtures with linear maltooligomers, Journal of Thermal Analysis and Calorimetry, 51 (1998) 993-1000.

[45] M.C.T. de Ilarduya, C. Martin, M.M. Goni, M.C. Martinez-Oharriz, Solubilization and interaction of sulindac with beta-cyclodextrin in the solid state and in aqueous solution, Drug Development and Industrial Pharmacy, 24 (1998) 301-306.

[46] M.L. Bender, M. Komiyama, Cyclodextrin chemistry, Springer-Verlag, Berlin ; New York, 1978.

[47] V.J. Stella, R.A. Rajewski, Cyclodextrins: Their future in drug formulation and delivery, Pharmaceutical Research, 14 (1997) 556-567.

[48] T. Loftsson, M.E. Brewster, Pharmaceutical applications of cyclodextrins .1. Drug solubilization and stabilization, Journal of Pharmaceutical Sciences, 85 (1996) 1017-1025.

[49] V.J. Stella, V.M. Rao, E.A. Zannou, V. Zia, Mechanisms of drug release from cyclodextrin complexes, Advanced Drug Delivery Reviews, 36 (1999) 3-16.

[50] S.O. Fakayode, M. Lowry, K.A. Fletcher, X.D. Huang, A.M. Powe, I.M. Warner, Cyclodextrins host-guest chemistry in analytical and environmental chemistry, Current Analytical Chemistry, 3 (2007) 171-181.

[51] J. Szejtli, Introduction and general overview of cyclodextrin chemistry, Chemical Reviews, 98 (1998) 1743-1753.

[52] M. Abdel-Tawab, H. Zettl, M. Schubert-Zsilavecz, Nonsteroidal Anti-Inflammatory Drugs: A Critical Review on Current Concepts Applied to Reduce Gastrointestinal Toxicity, Current Medicinal Chemistry, 16 (2009) 2042-2063.

[53] K. Moribe, Y. Tozuka, K. Yamamoto, Supercritical carbon dioxide processing of active pharmaceutical ingredients for polymorphic control and for complex formation, Advanced Drug Delivery Reviews, 60 (2008) 328-338.

[54] T. Loftsson, M.E. Brewster, Pharmaceutical applications of cyclodextrins: basic science and product development, Journal of Pharmacy and Pharmacology, 62 (2010) 1607-1621.

[55] E.M. Martin Del Valle, Cyclodextrins and their uses: a review, Process Biochemistry, 39 (2004) 1033-1046.

[56] T. Loftsson, D. Duchene, Cyclodextrins and their pharmaceutical applications, International Journal of Pharmaceutics, 329 (2007) 1-11.

[57] H. Dodziuk, Cyclodextrins and their complexes : chemistry, analytical methods, applications, Wiley-VCH, Weinheim, 2006.

[58] J. Szejtli, Past, present, and future of cyclodextrin research, Pure and Applied Chemistry, 76 (2004) 1825-1845.

[59] K.L. Larsen, Large cyclodextrins, Journal of Inclusion Phenomena and Macrocyclic Chemistry, 43 (2002) 1-13.

[60] L. Szente, J. Szejtli, Highly soluble cyclodextrin derivatives: chemistry, properties, and trends in development, Advanced Drug Delivery Reviews, 36 (1999) 17-28.

[61] M.E. Brewster, R. Vandecruys, J. Peeters, P. Neeskens, G. Verreck, T. Loftsson, Comparative interaction of 2-hydroxypropyl-β-cyclodextrin and sulfobutylether-β-cyclodextrin with itraconazole: Phase-solubility behavior and stabilization of supersaturated drug solutions, European Journal of Pharmaceutical Sciences, 34 (2008) 94-103.

[62] M. Charoenchaitrakool, F. Dehghani, N.R. Foster, Utilization of supercritical carbon dioxide for complex formation of ibuprofen and methyl-beta-cyclodextrin, International Journal of Pharmaceutics, 239 (2002) 103-112.

[63] Cyclodextrins in Pharmaceutics, Cosmetics, and Biomedicine: Current and Future Industrial Applications, John Wiley & Sons, Inc., Hoboken, 2011.

[64] A.R. Hedges, Industrial Applications of Cyclodextrins, Chemical Reviews, 98 (1998) 2035-2044.

[65] H. Cabral-Marques, R. Almeida, Optimisation of spray-drying process variables for dry powder inhalation (DPI) formulations of corticosteroid/cyclodextrin inclusion complexes, European Journal of Pharmaceutics and Biopharmaceutics, 73 (2009) 121-129.

[66] J.F. Pinto, P.J. Salustio, H.M. Cabral-Marques, P.C. Costa, Comparison of ibuprofen release from minitablets and capsules containing ibuprofen: beta-Cyclodextrin complex, European Journal of Pharmaceutics and Biopharmaceutics, 78 (2011) 58-66.

[67] C. Mekjaruskul, Y.T. Yang, M.G.D. Leed, M.P. Sadgrove, M. Jay, B. Sripanidkulchai, Novel formulation strategies for enhancing oral delivery of methoxyflavones in Kaempferia parviflora by SMEDDS or complexation with 2-hydroxypropyl-beta-cyclodextrin, International Journal of Pharmaceutics, 445 (2013) 1-11.

[68] C. Rogel, N. Mendoza, J. Troncoso, J. Gonzalez, C. Von Plessing, Formulation and Characterization of Inclusion Complexes Using Hydroxypropyl-Beta-Cyclodextrin and Florfenicol with Chitosan Microparticles, Journal of the Chilean Chemical Society, 56 (2011) 574-579.

[69] A.K. Mahapatra, P.N. Murthy, S. Biswal, A.P.K. Mahapatra, S.P. Pradhan, Dissolution Enhancement and Physicochemical Characterization of Valsartan in Solid Dispersions with beta-CD, HP beta-CD, and PVP K-30, Dissolution Technologies, 18 (2011) 39-45.

[70] C. Arama, C. Nicolescu, A. Nedelcu, C.M. Monciu, Synthesis and characterization of the inclusion complex between repaglinide and sulfobutylether-beta-cyclodextrin (Captisol (R)), Journal of Inclusion Phenomena and Macrocyclic Chemistry, 70 (2011) 421-428.

[71] Y.J. Su, S.Q. Rao, Y.J. Cai, Y.J. Yang, Preparation and characterization of the inclusion complex of hypocrellin A with hydroxypropyl-beta-cyclodextrin, European Food Research and Technology, 231 (2010) 781-788.

[72] CAVAMAX Cyclodextrins Forming and Analyzing Drug Inclusion Complexes, in: I.S. Products (Ed.) ISP Group, 2006.

[73] V. Nekkanti, T. Muniyappan, P. Karatgi, M.S. Hari, S. Marella, R. Pillai, Spray-drying process optimization for manufacture of drug-cyclodextrin complex powder using design of experiments, Drug Development and Industrial Pharmacy, 35 (2009) 1219-1229.

[74] Y. Zheng, A.H.L. Chow, Production and characterization of a spray-dried hydroxypropyl-beta-cyclodextrin/quercetin complex, Drug Development and Industrial Pharmacy, 35 (2009) 727-734.

[75] T. Mihajlovic, K. Kachrimanis, A. Graovac, Z. Djuric, S. Ibric, Improvement of Aripiprazole Solubility by Complexation with (2-Hydroxy)propyl-beta-cyclodextrin Using Spray Drying Technique, Aaps Pharmscitech, 13 (2012) 623-631.

[76] K. Kawakami, A. Fujita, T. Mikami, H. Yoshii, V. Paramita, T.L. Neoh, T. Furuta, Formation of rice flavor powder with alpha-cyclodextrin by spray drying, European Food Research and Technology, 229 (2009) 239-245.

[77] G.S. Borghetti, I.S. Lula, R.D. Sinisterra, V.L. Bassani, Quercetin/beta-Cyclodextrin Solid Complexes Prepared in Aqueous Solution Followed by Spray-drying or by Physical Mixture, Aaps Pharmscitech, 10 (2009) 235-242.

[78] Z.S. Wang, Y.J. Deng, S.Y. Sun, X.P. Zhang, Preparation of hydrophobic drugs cyclodextrin complex by lyophilization monophase solution, Drug Development and Industrial Pharmacy, 32 (2006) 73-83.

[79] Z.X. Wang, Y.J. Deng, X.P. Zhang, The novel application of tertiary butyl alcohol in the preparation of hydrophobic drug-HP beta CD complex, Journal of Pharmacy and Pharmacology, 58 (2006) 409-414.

[80] S. Junco, T. Casimiro, N. Ribeiro, M.N. Da Ponte, H.C. Marques, A comparative study of naproxen - Beta cyclodextrin complexes prepared by conventional methods and using

Supercritical carbon dioxide, Journal of Inclusion Phenomena and Macrocyclic Chemistry, 44 (2002) 117-121.

[81] T. Van Hees, V. Barillaro, G. Piel, P. Bertholet, S.H. De Hassonville, B. Evrard, L. Delattre, Application of Supercritical carbon dioxide for the preparation of drug-cyclodextrin inclusion compounds, Journal of Inclusion Phenomena and Macrocyclic Chemistry, 44 (2002) 271-274.

[82] T. Van Hees, G. Piel, B. Evrard, X. Otte, L. Thunus, L. Delattre, Application of supercritical carbon dioxide for the preparation of a piroxicam-beta-cyclodextrin inclusion compound, Pharmaceutical Research, 16 (1999) 1864-1870.

[83] Y. Tozuka, T. Fujito, K. Moribe, K. Yamamoto, Ibuprofen-cyclodextrin inclusion complex formation using supercritical carbon dioxide, Journal of Inclusion Phenomena and Macrocyclic Chemistry, 56 (2006) 33-37.

[84] M. Turk, G. Upper, M. Steurenthaler, K. Hussein, M.A. Wahl, Complex formation of ibuprofen and beta-cyclodextrin by controlled particle deposition (CPD) using SC-CO(2), Journal of Supercritical Fluids, 39 (2007) 435-443.

[85] K. Hussein, M. Turk, M.A. Wahl, Drug loading into beta-cyclodextrin granules using a supercritical fluid process for improved drug dissolution, European Journal of Pharmaceutical Sciences, 33 (2008) 306-312.

[86] M. Charoenchaitrakool, F. Dehghani, N.R. Foster, H.K. Chan, Micronization by rapid expansion of supercritical solutions to enhance the dissolution rates of poorly water-soluble pharmaceuticals, Industrial & Engineering Chemistry Research, 39 (2000) 4794-4802.

[87] M.A. Sabegh, H. Rajaei, F. Esmaeilzadeh, M. Lashkarbolooki, Solubility of ketoprofen in supercritical carbon dioxide, Journal of Supercritical Fluids, 72 (2012) 191-197.

[88] A. Garmroodi, J. Hassan, Y. Yamini, Solubilities of the drugs benzocaine, metronidazole benzoate, and naproxen in supercritical carbon dioxide, Journal of Chemical and Engineering Data, 49 (2004) 709-712.

[89] M. Sauceau, J. Fages, J.J. Letourneau, D. Richon, A novel apparatus for accurate measurements of solid solubilities in supercritical phases, Industrial & Engineering Chemistry Research, 39 (2000) 4609-4614.

[90] M. Munto, N. Ventosa, S. Sala, J. Veciana, Solubility behaviors of ibuprofen and naproxen drugs in liquid "CO2-organic solvent" mixtures, Journal of Supercritical Fluids, 47 (2008) 147-153.

[91] S.S.T. Ting, S.J. Macnaughton, D.L. Tomasko, N.R. Foster, Solubility of Naproxen in Supercritical Carbon-Dioxide with and without Cosolvents, Industrial & Engineering Chemistry Research, 32 (1993) 1471-1481.

[92] T. Van Hees, G. Piel, S.H. de Hassonville, B. Evrard, L. Delattre, Determination of the free/included piroxicam ratio in cyclodextrin complexes: comparison between UV spectrophotometry and differential scanning calorimetry, European Journal of Pharmaceutical Sciences, 15 (2002) 347-353.

[93] M. Sauceau, E. Rodier, J. Fages, Preparation of inclusion complex of piroxicam with cyclodextrin by using supercritical carbon dioxide, Journal of Supercritical Fluids, 47 (2008) 326-332.

[94] M. Banchero, L. Manna, Investigation of the piroxicam/hydroxypropyl-beta-cyclodextrin inclusion complexation by means of a supercritical solvent in the presence of auxiliary agents, Journal of Supercritical Fluids, 57 (2011) 259-266.

[95] M. Banchero, L. Manna, The use of lysine to enhance the supercritical complexation of ketoprofen and cyclodextrins, The Journal of Supercritical Fluids, 67 (2012) 76-83.
[96] A. Galia, E.C. Navarre, G. Filardo, O. Scialdone, E. Monflier, Inclusion complexes of triphenylphosphine derivatives and peracetylated-beta-cyclodextrin in supercritical carbon dioxide, Joint 21st Airapt and 45th Ehprg International Conference on High Pressure Science and Technology, 121 (2008).
[97] S.W. Jun, M.S. Kim, J.S. Kim, H.J. Park, S. Lee, J.S. Woo, S.J. Hwang, Preparation and characterization of simvastatin/hydroxypropyl-beta-cyclodextrin inclusion complex using supercritical antisolvent (SAS) process, European Journal of Pharmaceutics and Biopharmaceutics, 66 (2007) 413-421.
[98] K. Moribe, T. Fujito, Y. Tozuka, K. Yamamoto, Solubility-dependent complexation of active pharmaceutical ingredients with trimethyl-beta-cyclodextrin under supercritical fluid condition, Journal of Inclusion Phenomena and Macrocyclic Chemistry, 57 (2007) 289-295.
[99] B. Wang, J. He, D.H. Sun, R. Zhang, B.X. Han, Utilization of supercritical carbon dioxide for the preparation of 3-hydroxyflavone and beta-cyclodextrin complex, Journal of Inclusion Phenomena and Macrocyclic Chemistry, 55 (2006) 37-40.
[100] A.H. Al-Marzouqi, I. Shehatta, B. Jobe, A. Dowaidar, Phase solubility and inclusion complex of itraconazole with beta-cyclodextrin using supercritical carbon dioxide, Journal of Pharmaceutical Sciences, 95 (2006) 292-304.
[101] A. Al-Marzouqi, B. Jobe, G. Corti, M. Cirri, P. Mura, Physicochemical characterization of drug-cyclodextrin complexes prepared by supercritical carbon dioxide and by conventional techniques, Journal of Inclusion Phenomena and Macrocyclic Chemistry, 57 (2007) 223-231.

[102] M. Banchero, S. Ronchetti, L. Manna, Characterization of Ketoprofen/Methyl-beta-Cyclodextrin Complexes Prepared Using Supercritical Carbon Dioxide, Journal of Chemistry, (2013).

[103] M. Banchero, L. Manna, Investigation of the piroxicam/hydroxypropyl-β-cyclodextrin inclusion complexation by means of a supercritical solvent in the presence of auxiliary agents, The Journal of Supercritical Fluids, 57 (2011) 259-266.

[104] R. Singh, N. Bharti, J. Madan, S. Hiremath, Characterization of Cyclodextrin Inclusion Complexes - A Review, Journal of Pharmaceutical Science and Technology, 2 (2010) 171-183.

[105] F.B.T. Pessine, A. Calderini, Synthesis and characterization of inclusion complex of the vasodilator drug minoxidil with beta-cyclodextrin, Journal of Inclusion Phenomena and Macrocyclic Chemistry, 60 (2008) 369-377.

[106] R. Hirlekar, V. Kadam, Preparation and characterization of inclusion complexes of carvedilol with methyl-beta-cyclodextrin, Journal of Inclusion Phenomena and Macrocyclic Chemistry, 63 (2009) 219-224.

[107] O. Exner, Calculating equilibrium constants from spectral data: reliability of the Benesi-Hildebrand method and its modifications, Chemometrics and Intelligent Laboratory Systems, 39 (1997) 85-93.

[108] Y.X. Bai, J.P. Wang, M. Bashari, X.T. Hu, T. Feng, X.M. Xu, Z.Y. Jin, Y.Q. Tian, A thermogravimetric analysis (TGA) method developed for estimating the stoichiometric ratio of solid-state alpha-cyclodextrin-based inclusion complexes, Thermochimica Acta, 541 (2012) 62-69.

[109] J.R. Cruz, B.A. Becker, K.F. Morris, C.K. Larive, NMR characterization of the host-guest inclusion complex between beta-cyclodextrin and doxepin, Magnetic Resonance in Chemistry, 46 (2008) 838-845.

[110] J.S. Li, H.N. Xiao, J.H. Li, Y.P. Zhong, Drug carrier systems based on water-soluble cationic beta-cyclodextrin polymers, International Journal of Pharmaceutics, 278 (2004) 329-342.

[111] M.J. Arias, J.R. Moyano, J.M. Gines, Investigation of the triamterene-beta-cyclodextrin system prepared by co-grinding, International Journal of Pharmaceutics, 153 (1997) 181-189.

[112] R. Singh, H.H. Tonnesen, S.B. Vogensen, T. Loftsson, M. Masson, Studies of curcumin and curcuminoids. XXXVI. The stoichiometry and complexation constants of cyclodextrin complexes as determined by the phase-solubility method and UV-Vis titration, Journal of Inclusion Phenomena and Macrocyclic Chemistry, 66 (2010) 335-348.

[113] A.J. Chen, M. Liu, L.N. Dong, D.Z. Sun, Study on the effect of solvent on the inclusion interaction of hydroxypropyl-beta-cyclodextrin with three kinds of coumarins by phase solubility method, Fluid Phase Equilibria, 341 (2013) 42-47.

[114] K.A. Al-Sou'od, Investigation of the hydrocortisone-beta-cyclodextrin complex by phase solubility method: Some theoretical and practical considerations, Journal of Solution Chemistry, 37 (2008) 119-133.

[115] I.V. Terekhova, M.N. Tikhova, T.V. Volkova, R.S. Kumeev, G.L. Perlovich, Inclusion complex formation of alpha- and beta-cyclodextrins with riboflavin and alloxazine in aqueous solution: thermodynamic study, Journal of Inclusion Phenomena and Macrocyclic Chemistry, 69 (2011) 167-172.

[116] I.V. Terekhova, R.S. Kumeev, G.A. Alper, A.V. Agafonov, Thermodynamic characteristics of the formation of alpha- and beta-cyclodextrin complexes with lumichrome, lumazine, and uracil in aqueous solution, Russian Journal of Physical Chemistry A, 85 (2011) 1844-1849.

[117] W. Zielenkiewicz, I.V. Terekhova, M. Wszelaka-Rylik, R.S. Kumeev, Thermodynamics of inclusion complex formation of hydroxypropylated alpha- and beta-cyclodextrins with aminobenzoic acids in water, Journal of Thermal Analysis and Calorimetry, 101 (2010) 15-23.

[118] W. Zielenkiewicz, I.V. Terekhova, M. Kozbial, R.S. Kumeev, Thermodynamic study on inclusion complex formation of riboflavin with hydroxypropyl-beta-cyclodextrin in water, Journal of Thermal Analysis and Calorimetry, 101 (2010) 595-600.

[119] M.M. Al Omari, M.I. El-Barghouthi, M.B. Zughul, J.E.D. Davies, A.A. Badwan, The role of drug hydrophobicity in beta-cyclodextrin complexes, Journal of Molecular Liquids, 155 (2010) 103-108.

[120] A. Ghuzlaan, M.M. Al Omari, K.A. Al-Sou'od, Prednisone/Cyclodextrin Inclusion Complexation: Phase Solubility, Thermodynamic, Physicochemical and Computational Analysis, Journal of Solution Chemistry, 38 (2009) 83-94.

[121] Y.I. Mikhail V. Rekharsky, Complexation Thermodynamics of Cyclodextrins, Chemical Reviews, 98 (1998) 1875-1917.

[122] T. Loftsson, A. Magnusdottir, M. Masson, J.F. Sigurjonsdottir, Self-association and cyclodextrin solubilization of drugs, Journal of Pharmaceutical Sciences, 91 (2002) 2307-2316.

[123] H. Beiginejad, A. Bagheri, L.S. Yekta, Z.B. Nojini, Thermodynamic studies of inclusion complex formation between alkylpyridinium chlorides and beta-cyclodextrin using

conductometric method, Journal of Inclusion Phenomena and Macrocyclic Chemistry, 67 (2010) 247-252.

[124] L.J. Waters, S. Bedford, G.M.B. Parkes, J.C. Mitchell, Influence of lipophilicity on drug-cyclodextrin interactions: A calorimetric study, Thermochimica Acta, 511 (2010) 102-106.

[125] P. Lo Meo, F. D'Anna, S. Riela, M. Gruttadauria, R. Noto, Binding equilibria between beta-cyclodextrin and p-nitro-aniline derivatives: the first systematic study in mixed water-methanol solvent systems, Tetrahedron, 65 (2009) 2037-2042.

[126] M.M. Al Omari, M.I. El-Barghouthi, M.B. Zughul, J.E.D. Davies, A.A. Badwan, Dipyridamole/beta-cyclodextrin complexation: effect of buffer species, thermodynamics, and guest-host interactions probed by (1)H-NMR and molecular modeling studies, Journal of Inclusion Phenomena and Macrocyclic Chemistry, 64 (2009) 305-315.

[127] M. Jug, M. Becirevic-Lacan, S. Bengez, Novel cyclodextrin-based film formulation intended for buccal delivery of atenolol, Drug Development and Industrial Pharmacy, 35 (2009) 796-807.

[128] M. Jug, M. Becirevic-Lacan, Development of a cyclodextrin-based nasal delivery system for lorazepam, Drug Development and Industrial Pharmacy, 34 (2008) 817-826.

[129] F.J.O. Espinar, S.A. Igea, J.B. Mendez, J.L.V. Jato, Reduction in the Ulcerogenicity of Naproxen by Complexation with Beta-Cyclodextrin, International Journal of Pharmaceutics, 70 (1991) 35-41.

[130] G. Wenz, Cyclodextrin Polyrotaxanes Assembled from a Molecular Construction Kit in Aqueous Solution, Journal of Polymer Science Part a-Polymer Chemistry, 47 (2009) 6333-6341.

[131] P. Lo Nostro, J.R. Lopes, C. Cardelli, Formation of cyclodextrin-based polypseudorotaxanes: Solvent effect and kinetic study, Langmuir, 17 (2001) 4610-4615.

[132] F. van de Manakker, T. Vermonden, C.F. van Nostrum, W.E. Hennink, Cyclodextrin-Based Polymeric Materials: Synthesis, Properties, and Pharmaceutical/Biomedical Applications, Biomacromolecules, 10 (2009) 3157-3175.

[133] K. Kato, H. Komatsu, K. Ito, A Versatile Synthesis of Diverse Polyrotaxanes with a Dual Role of Cyclodextrin as both the Cyclic and Capping Components, Macromolecules, 43 (2010) 8799-8804.

[134] F. Yhaya, A.M. Gregory, M.H. Stenzel, Polymers with Sugar Buckets - The Attachment of Cyclodextrins onto Polymer Chains, Australian Journal of Chemistry, 63 (2010) 195-210.

[135] S.E. Wolf, L.S. Edelman, N. Kemalyan, L. Donison, J. Cross, M. Underwood, R.J. Spence, D. Noppenberger, T.L. Palmieri, D.G. Greenhalgh, M. Lawless, D. Voigt, P. Edwards, P. Warner, R. Kagan, S. Hatfield, J. Jeng, D. Crean, J. Hunt, G. Purdue, A. Burris, B. Cairns, M. Kessler, R.L. Klein, R. Baker, C. Yowler, W. Tutulo, K. Foster, D. Caruso, B. Hildebrand, W. Benjamin, C. Villarreal, A.P. Sanford, J. Saffle, Effects of oxandrolone on outcome measures in the severely burned: A multicenter prospective randomized double-blind trial, Journal of Burn Care & Research, 27 (2006) 131-139.

[136] V. Wintgens, C. Amiel, Water-soluble gamma-cyclodextrin polymers with high molecular weight and their complex forming properties, European Polymer Journal, 46 (2010) 1915-1922.

[137] C. Manuelli, G. Galli, P. Biondi, P. Perri, P. Melani, R. Zonefrati, A. Casini, G. Vannelli, L. Gloria, C. Surrenti, D. Shuppan, A. Conti, M.L. Brandi, C.M. Rotella, Characterization and Cloning of Bovine Retinal Endothelial-Cells (Brec) in Long-Term Culture, Diabetes Nutrition & Metabolism, 8 (1995) 281-291.

[138] A. Martinotti, A. Stoppacciaro, M. Vagliani, C. Melani, F. Spreafico, M. Wysocka, G. Parmiani, G. Trinchieri, M.P. Colombo, Cd4 T-Cells Inhibit in-Vivo the Cd8-Mediated Immune-

Response against Murine Colon-Carcinoma Cells Transduced with Interleukin-12 Genes, European Journal of Immunology, 25 (1995) 137-146.

[139] S. Daoud-Mahammed, J.L. Grossiord, T. Bergua, C. Amiel, P. Couvreur, R. Gref, Self-assembling cyclodextrin based hydrogels for the sustained delivery of hydrophobic drugs, Journal of Biomedical Materials Research Part A, 86A (2008) 736-748.

[140] K.Y. Lee, Design parameters of polymers for tissue engineering applications, Macromolecular Research, 13 (2005) 277-284.

[141] M. Sokolsky-Papkov, K. Agashi, A. Olaye, K. Shakesheff, A.J. Domb, Polymer carriers for drug delivery in tissue engineering, Advanced Drug Delivery Reviews, 59 (2007) 187-206.

[142] D.F. Williams, On the mechanisms of biocompatibility, Biomaterials, 29 (2008) 2941-2953.

[143] J. Jagur-Grodzinski, Polymers for tissue engineering, medical devices, and regenerative medicine. Concise general review of recent studies, Polymers for Advanced Technologies, 17 (2006) 395-418.

[144] J.P. Santerre, K. Woodhouse, G. Laroche, R.S. Labow, Understanding the biodegradation of polyurethanes: From classical implants to tissue engineering materials, Biomaterials, 26 (2005) 7457-7470.

[145] K. Hemmrich, J. Salber, M. Meersch, U. Wiesemann, T. Gries, N. Pallua, D. Klee, Three-dimensional nonwoven scaffolds from a novel biodegradable poly(ester amide) for tissue engineering applications, Journal of Materials Science: Materials in Medicine, 19 (2008) 257-267.

[146] C.M. Agrawal, R.B. Ray, Biodegradable polymeric scaffolds for musculoskeletal tissue engineering, Journal of Biomedical Materials Research, 55 (2001) 141-150.

[147] N.Y.C. Yu, A. Schindeler, D.G. Little, A.J. Ruys, Biodegradable Poly(alpha-hydroxy acid) Polymer Scaffolds for Bone Tissue Engineering, Journal of Biomedical Materials Research Part B-Applied Biomaterials, 93B (2010) 285-295.

[148] L. Lu, S.J. Peter, M.D. Lyman, H.L. Lai, S.M. Leite, J.A. Tamada, S. Uyama, J.P. Vacanti, R. Langer, A.G. Mikos, In vitro and in vivo degradation of porous poly(DL-lactic-co-glycolic acid) foams, Biomaterials, 21 (2000) 1837-1845.

[149] K.M. Nampoothiri, N.R. Nair, R.P. John, An overview of the recent developments in polylactide (PLA) research, Bioresource Technology, 101 (2010) 8493-8501.

[150] W. Wei, X.D. Yu, H.X. Ju, Simultaneous determination of several antalgic drugs based on their interactions with beta-cyclodextrin by capillary zone electrophoresis, Journal of Chromatographic Science, 42 (2004) 155-160.

[151] L.S.S. Ribeiro, D.C. Ferreira, F.J.B. Veiga, Physicochemical investigation of the effects of water-soluble polymers on vinpocetine complexation with beta-cyclodextrin and its sulfobutyl ether derivative in solution and solid state, European Journal of Pharmaceutical Sciences, 20 (2003) 253-266.

[152] R.A. Quirk, R.M. France, K.M. Shakesheff, S.M. Howdle, Supercritical fluid technologies and tissue engineering scaffolds, Current Opinion in Solid State & Materials Science, 8 (2004) 313-321.

[153] Y.S. Nam, T.G. Park, Porous biodegradable polymeric scaffolds prepared by thermally induced phase separation, Journal of Biomedical Materials Research, 47 (1999) 8-17.

[154] K. Iwasaki, H. Uchida, Y. Dobashi, T. Nishita, Fast Particle-based Visual Simulation of Ice Melting, Computer Graphics Forum, 29 (2010) 2215-2223.

[155] L.J.M. Jacobs, M.F. Kemmere, J.T.F. Keurentjes, Sustainable polymer foaming using high pressure carbon dioxide: a review on fundamentals, processes and applications, Green Chemistry, 10 (2008) 731-738.

[156] W.S. Koegler, C. Patrick, M.J. Cima, L.G. Griffith, Carbon dioxide extraction of residual chloroform from biodegradable polymers, Journal of Biomedical Materials Research, 63 (2002) 567-576.

[157] S. Takahashi, J.C. Hassler, E. Kiran, Melting behavior of biodegradable polyesters in carbon dioxide at high pressures, The Journal of Supercritical Fluids, 72 (2012) 278-287.

[158] B. Krause, R. Mettinkhof, N.F.A. van der Vegt, M. Wessling, Microcellular foaming of amorphous high-T-g polymers using carbon dioxide, Macromolecules, 34 (2001) 874-884.

[159] Z.M. Xu, X.L. Jiang, T. Liu, G.H. Hu, L. Zhao, Z.N. Zhu, W.K. Yuan, Foaming of polypropylene with supercritical carbon dioxide, Journal of Supercritical Fluids, 41 (2007) 299-310.

[160] B. Krause, N.F.A. van der Vegt, M. Wessling, New way to produce porous polymeric membranes by carbon dioxide foaming., Abstracts of Papers of the American Chemical Society, 222 (2001) U326-U326.

[161] E. Kiran, K. Liu, K. Ramsdell, Morphological changes in poly(ε-caprolactone) in dense carbon dioxide, Polymer, 49 (2008) 1853-1859.

[162] S. Siripurapu, J.A. Coughlan, R.J. Spontak, S.A. Khan, Surface-constrained foaming of polymer thin films with supercritical carbon dioxide, Macromolecules, 37 (2004) 9872-9879.

[163] L.J.M. Jacobs, K.C.H. Danen, M.F. Kemmere, J.T.F. Keurentjes, A parametric study into the morphology of polystyrene-co-methyl methacrylate foams using supercritical carbon dioxide as a blowing agent, Polymer, 48 (2007) 3771-3780.

[164] Z. Knez, E. Markocic, Z. Novak, M.K. Hrncic, Processing Polymeric Biomaterials using Supercritical CO(2), Chemie Ingenieur Technik, 83 (2011) 1371-1380.

[165] I. Tsivintzelis, A.G. Angelopoulou, C. Panayiotou, Foaming of polymers with supercritical CO2: An experimental and theoretical study, Polymer, 48 (2007) 5928-5939.

[166] E. Reverchon, S. Cardea, Production of controlled polymeric foams by supercritical CO2, Journal of Supercritical Fluids, 40 (2007) 144-152.

[167] H.Y. Tai, M.L. Mather, D. Howard, W.X. Wang, L.J. White, J.A. Crowe, S.P. Morgan, A. Chandra, D.J. Williams, S.M. Howdle, K.M. Shakesheff, Control of pore size and structure of tissue engineering scaffolds produced by supercritical fluid processing, European Cells & Materials, 14 (2007) 64-76.

[168] A. Salerno, S. Zeppetelli, E. Di Maio, S. Iannace, P.A. Netti, Architecture and properties of bi-modal porous scaffolds for bone regeneration prepared via supercritical CO2 foaming and porogen leaching combined process, Journal of Supercritical Fluids, 67 (2012) 114-122.

[169] I. Tsivintzelis, E. Pavlidou, C. Panayiotou, Biodegradable polymer foams prepared with supercritical CO2-ethanol mixtures as blowing agents, Journal of Supercritical Fluids, 42 (2007) 265-272.

[170] M. Sauceau, C. Nikitine, E. Rodier, J. Fages, Effect of supercritical carbon dioxide on polystyrene extrusion, Journal of Supercritical Fluids, 43 (2007) 367-373.

[171] M. Sauceau, J. Fages, A. Common, C. Nikitine, E. Rodier, New challenges in polymer foaming: A review of extrusion processes assisted by supercritical carbon dioxide, Progress in Polymer Science, 36 (2011) 749-766.

[172] C. Nikitine, E. Rodier, M. Sauceau, J.J. Letourneau, J. Fages, Controlling the Structure of a Porous Polymer by Coupling Supercritical CO(2) and Single Screw Extrusion Process, Journal of Applied Polymer Science, 115 (2010) 981-990.

[173] F. Wolff, H. Munstedt, Continuous direct melt foaming of a preceramic polymer using carbon dioxide: extrusion device and first results, Journal of Materials Science, 46 (2011) 6162-6167.

[174] X.M. Han, C.C. Zeng, L.J. Lee, K.W. Koelling, D.L. Tomasko, Extrusion of polystyrene nanocomposite foams with supercritical CO2, Polymer Engineering and Science, 43 (2003) 1261-1275.

[175] P.C. Lee, J. Wang, C.B. Park, Extruded open-cell foams using two semicrystalline polymers with different crystallization temperatures, Industrial & Engineering Chemistry Research, 45 (2006) 175-181.

[176] G. Della Porta, N. Falco, E. Reverchon, NSAID drugs release from injectable microspheres produced by supercritical fluid emulsion extraction, Journal of Pharmaceutical Sciences, 99 (2010) 1484-1499.

[177] G. Della Porta, E. Reverchon, Nanostructured microspheres produced by supercritical fluid extraction of emulsions, Biotechnology and Bioengineering, 100 (2008) 1020-1033.

[178] A.M. Lopez-Periago, A. Vega, P. Subra, A. Argemi, J. Saurina, C.A. Garcia-Gonzalez, C. Domingo, Supercritical CO(2) processing of polymers for the production of materials with applications in tissue engineering and drug delivery, Journal of Materials Science, 43 (2008) 1939-1947.

[179] D. Velasco, L. Benito, M. Fernandez-Gutierrez, J.S. Roman, C. Elvira, Preparation in supercritical CO(2) of porous poly(methyl methacrylate)-poly(L-lactic acid) (PMMA-PLA) scaffolds incorporating ibuprofen, Journal of Supercritical Fluids, 54 (2010) 335-341.

[180] D.D. Hile, M.L. Amirpour, A. Akgerman, M.V. Pishko, Active growth factor delivery from poly(D,L-lactide-co-glycolide) foams prepared in supercritical CO2, Journal of Controlled Release, 66 (2000) 177-185.

[181] E. Junquera, E. Aicart, A fluorimetric, potentiometric and conductimetric study of the aqueous solutions of naproxen and its association with hydroxypropyl-beta-cyclodextrin, International Journal of Pharmaceutics, 176 (1999) 169-178.

[182] A. Kawabata, Prostaglandin E(2) and Pain-An Update, Biological & Pharmaceutical Bulletin, 34 (2011) 1170-1173.

[183] R.L. Carrier, L.A. Miller, I. Ahmed, The utility of cyclodextrins for enhancing oral bioavailability, Journal of Controlled Release, 123 (2007) 78-99.

[184] R. Challa, A. Ahuja, J. Ali, R.K. Khar, Cyclodextrins in drug delivery: An updated review, Aaps Pharmscitech, 6 (2005) E329-357.

[185] H. Dodziuk, Rigidity versus flexibility. A review of experimental and theoretical studies pertaining to the cyclodextrin nonrigidity, Journal of Molecular Structure, 614 (2002) 33-45.

[186] N. Sadlej-Sosnowska, L. Kozerski, E. Bednarek, J. Sitkowski, Fluorometric and NMR studies of the naproxen-cyclodextrin inclusion complexes in aqueous solutions, Journal of Inclusion Phenomena and Macrocyclic Chemistry, 37 (2000) 383-394.

[187] G. Bettinetti, M. Sorrenti, A. Negri, M. Setti, P. Mura, F. Melani, Interaction of naproxen with alpha-cyclodextrin and its noncyclic analog maltohexaose, Pharmaceutical Research, 16 (1999) 689-694.

[188] J. Wang, I.M. Warner, Studies of the Naproxen-Beta-Cyclodextrin Inclusion Complex, Microchemical Journal, 48 (1993) 229-239.

[189] G. Bettinetti, P. Mura, M.T. Faucci, M. Sorrenti, M. Setti, Interaction of naproxen with noncrystalline acetyl beta- and acetyl gamma-cyclodextrins in the solid and liquid state, European Journal of Pharmaceutical Sciences, 15 (2002) 21-29.

[190] G.P. Bettinetti, M. Sorrenti, S. Rossi, F. Ferrari, P. Mura, M.T. Faucci, Assessment of solid-state interactions of naproxen with amorphous cyclodextrin derivatives by DSC, Journal of Pharmaceutical and Biomedical Analysis, 30 (2002) 1173-1179.

[191] S. Junco, T. Casimiro, N. Ribeiro, M.N. Da Ponte, H.M.C. Marques, Optimisation of supercritical carbon dioxide systems for complexation of naproxen: Beta-cyclodextrin, Journal of Inclusion Phenomena and Macrocyclic Chemistry, 44 (2002) 69-73.

[192] P. Mura, G.P. Bettinetti, M. Cirri, F. Maestrelli, M. Sorrenti, L. Catenacci, Solid-state characterization and dissolution properties of naproxen-arginine-hydroxypropyl-beta-cyclodextrin ternary system, European Journal of Pharmaceutics and Biopharmaceutics, 59 (2005) 99-106.

[193] R. Machin, J.R. Isasi, I. Velaz, beta-Cyclodextrin hydrogels as potential drug delivery systems, Carbohydrate Polymers, 87 (2012) 2024-2030.

[194] A. Banik, P. Gogoi, M.D. Saikia, Interaction of naproxen with beta-cyclodextrin and its derivatives/polymer: experimental and molecular modeling studies, Journal of Inclusion Phenomena and Macrocyclic Chemistry, 72 (2012) 449-458.

[195] P. Mura, F. Maestrelli, M. Cirri, Ternary systems of naproxen with hydroxypropyl-beta-cyclodextrin and aminoacids, International Journal of Pharmaceutics, 260 (2003) 293-302.

[196] A. Ganzagonzalez, J.L. Vilajato, S. Anguianoigea, F.J. Oteroespinar, J. Blancomendez, A Proton Nuclear-Magnetic-Resonance Study of the Inclusion Complex of Naproxen with Beta-Cyclodextrin, International Journal of Pharmaceutics, 106 (1994) 179-185.

[197] J.A. Arancibia, G.M. Escandar, Determination of naproxen in pharmaceutical preparations by room-temperature phosphorescence. A comparative study of several organized media, Analyst, 126 (2001) 917-922.

[198] S.V. Kurkov, E.V. Ukhatskaya, T. Loftsson, Drug/cyclodextrin: beyond inclusion complexation, Journal of Inclusion Phenomena and Macrocyclic Chemistry, 69 (2011) 297-301.

[199] J.M. Gines, M.J. Arias, J.I. Perez-Martinez, J.R. Moyano, E. Morillo, P.J. Sanchez-Soto, Determination of the stoichiometry of 2,3-dichlorophenoxyacetic acid beta-cyclodextrin complexes in solution and in solid state, Thermochimica Acta, 321 (1998) 53-58.

[200] P. Mura, F. Maestrelli, M. Cirri, S. Furlanetto, S. Pinzauti, Differential scanning calorimetry as an analytical tool in the study of drug-cyclodextrin interactions, Journal of Thermal Analysis and Calorimetry, 73 (2003) 635-646.

[201] A.H. Al-Marzouqi, H.M. Elwy, I. Shehadi, A. Adem, Physicochemical properties of antifungal drug-cyclodextrin complexes prepared by supercritical carbon dioxide and by conventional techniques, Journal of Pharmaceutical and Biomedical Analysis, 49 (2009) 227-233.

[202] L.S. Koester, C.R. Xavier, P. Mayorga, V.L. Bassani, Influence of beta-cyclodextrin complexation on carbamazepine release from hydroxypropyl methylcellulose matrix tablets, European Journal of Pharmaceutics and Biopharmaceutics, 55 (2003) 85-91.

[203] H.A. Hassan, A.H. Al-Marzouqi, B. Jobe, A.A. Hamza, G.A. Ramadan, Enhancement of dissolution amount and in vivo bioavailability of itraconazole by complexation with beta-

cyclodextrin using supercritical carbon dioxide, Journal of Pharmaceutical and Biomedical Analysis, 45 (2007) 243-250.

[204] I. Shehatta, A. Al-Marzouqi, B. Jobe, A. Dowaidar, Enhancement of aqueous solubility of itraconazole by complexation with cyclodextrins using supercritical carbon dioxide, Canadian Journal of Chemistry-Revue Canadienne De Chimie, 83 (2005) 1833-1838.

[205] Z.Y. Lian, S.A. Epstein, C.W. Blenk, A.D. Shine, Carbon dioxide-induced melting point depression of biodegradable semicrystalline polymers, Journal of Supercritical Fluids, 39 (2006) 107-117.

[206] X. Liao, G. Li, X.H. Sun, J.S. He, Effect of supercritical CO2 and cosolvent on the crystallization and melting behavior of bisphenol-A polycarbonate, Acta Chimica Sinica, 61 (2003) 1697-1699.

[207] B. Li, X.Y. Zhu, G.H. Hu, T. Liu, G.P. Cao, L. Zhao, W.K. Yuan, Supercritical carbon dioxide-induced melting temperature depression and crystallization of syndiotactic polypropylene, Polymer Engineering and Science, 48 (2008) 1608-1614.

[208] H. Uchida, M. Yoshida, Y. Kojima, Y. Yamazoe, M. Matsuoka, Measurement and correlation of the solid-liquid-gas equilibria for the carbon dioxide plus S-(+)-ibuprofen and carbon dioxide plus RS-(+/-)-ibuprofen systems, Journal of Chemical and Engineering Data, 50 (2005) 11-15.

[209] M. Turk, G. Upper, P. Hils, Formation of composite drug-polymer particles by co-precipitation during the rapid expansion of supercritical fluids, Journal of Supercritical Fluids, 39 (2006) 253-263.

[210] M. Turk, T. Kraska, Experimental and Theoretical Investigation of the Phase Behavior of Naproxen in Supercritical CO(2), Journal of Chemical and Engineering Data, 54 (2009) 1592-1597.

[211] F. Vrecer, M. Vrbinc, A. Meden, Characterization of piroxicam crystal modifications, International Journal of Pharmaceutics, 256 (2003) 3-15.

[212] M. Janik, Z. Malarski, J. Mrozinski, J. Wajcht, Z. Zborucki, Influence of Solvent Effect on Polymorphism of 4-Hydroxy-2-Methyl-N-2-Pyridyl-2h-1,2-Benzothiazine-3-Carboxamide-1, 1-Dioxide (Piroxicam), Journal of Crystallographic and Spectroscopic Research, 21 (1991) 519-522.

[213] F. Vrecer, S. Srcic, J. Smidkorbar, Investigation of Piroxicam Polymorphism, International Journal of Pharmaceutics, 68 (1991) 35-41.

[214] F. Kozjek, L. Golic, P. Zupet, E. Palka, P. Vodopivec, M. Japelj, Physicochemical Properties and Biovailability of 2 Crystal Forms of Piroxicam, Acta Pharmaceutica Jugoslavica, 35 (1985) 275-281.

[215] N. De Zordi, I. Kikic, M. Moneghini, D. Solinas, Piroxicam solid state studies after processing with SAS technique, Journal of Supercritical Fluids, 55 (2010) 340-347.

[216] J. Fang, E. Kiran, Crystallization and gelation of isotactic poly(4-methyl-1-pentene) in n-pentane and in n-pentane plus Co-2 at high pressures, Journal of Supercritical Fluids, 38 (2006) 132-145.

[217] J. Fang, E. Kiran, Thermoreversible Gelation and Polymorphic Transformations of Syndiotactic Polystyrene in Toluene and Toluene plus Carbon Dioxide Fluid Mixtures at High Pressures, Macromolecules, 41 (2008) 7525-7535.

[218] O. Guney, A. Akgerman, Synthesis of controlled-release products in supercritical medium, Aiche Journal, 48 (2002) 856-866.

[219] T.K. Kim, J.J. Yoon, D.S. Lee, T.G. Park, Gas foamed open porous biodegradable polymeric microspheres, Biomaterials, 27 (2006) 152-159.

[220] E. Kiran, K. Liu, K. Ramsdell, Morphological changes in poly(epsilon-caprolactone) in dense carbon dioxide, Polymer, 49 (2008) 1853-1859.

[221] X.H. Zhu, L.Y. Lee, J.S.H. Jackson, Y.W. Tong, C.-H. Wang, Characterization of porous poly(D,L-lactic-co-glycolic acid) sponges fabricated by supercritical CO2 gas-foaming method as a scaffold for three-dimensional growth of Hep3B cells, Biotechnology and Bioengineering, 100 (2008) 998-1009.

[222] G. Lemon, Y. Reinwald, L.J. White, S.M. Howdle, K.M. Shakesheff, J.R. King, Interconnectivity analysis of supercritical CO2-foamed scaffolds, Computer Methods and Programs in Biomedicine, 106 (2012) 139-149.

[223] A. Kasturirangan, A.S. Teja, Phase behavior of CO2 + biopolymer and CO2 + fluoropolymer systems, Fluid Phase Equilibria, 261 (2007) 64-68.

[224] H.-S. Byun, H.-Y. Lee, Cloud-point measurement of the biodegradable poly(d,l-lactide-co-glycolide) solution in supercritical fluid solvents, Korean Journal of Chemical Engineering, 23 (2006) 1003-1008.

[225] P. Arce, M. Aznar, Modeling the thermodynamic behavior of poly (lactide-co-glycolide) plus supercritical fluid mixtures with equations of state, Fluid Phase Equilibria, 244 (2006) 16-25.

[226] A. Kasturirangan, C. Grant, A.S. Teja, Compressible lattice model for phase equilibria in CO2+polymer systems, Industrial & Engineering Chemistry Research, 47 (2008) 645-649.

[227] Y.M. Kuk, B.C. Lee, Y.W. Lee, J.S. Lim, Phase behavior of biodegradable polymers in dimethyl ether and dimethyl ether plus carbon dioxide, Journal of Chemical and Engineering Data, 46 (2001) 1344-1348.

[228] J.M. Lee, B.C. Lee, S.H. Lee, Cloud points of biodegradable polymers in compressed liquid and supercritical chlorodifluoromethane, Journal of Chemical and Engineering Data, 45 (2000) 851-856.

[229] S.G. Kazarian, M.F. Vincent, F.V. Bright, C.L. Liotta, C.A. Eckert, Specific Intermolecular Interaction of Carbon Dioxide with Polymers, Journal of the American Chemical Society, 118 (1996) 1729-1736.

[230] S.P. Nalawade, F. Picchioni, L.P.B.M. Janssen, D.W. Grijpma, J. Feijen, Investigation of the interaction of CO2 with poly (L-lactide), poly(DL-lactide) and poly(epsilon-caprolactone) using FTIR spectroscopy, Journal of Applied Polymer Science, 109 (2008) 3376-3381.

[231] Y.H. Yuan, A.S. Teja, Quantification of specific interactions between CO2 and the carbonyl group in polymers via ATR-FTIR measurements, Journal of Supercritical Fluids, 56 (2011) 208-212.

[232] Z. Shen, M.A. McHugh, J. Xu, J. Belardi, S. Kilic, A. Mesiano, S. Bane, C. Karnikas, E. Beckman, R. Enick, CO2-solubility of oligomers and polymers that contain the carbonyl group, Polymer, 44 (2003) 1491-1498.

[233] S.P. Nalawade, F. Picchioni, J.H. Marsman, L.P.B.M. Janssen, The FT-IR studies of the interactions of CO2 and polymers having different chain groups, Journal of Supercritical Fluids, 36 (2006) 236-244.

[234] M. Altarsha, F. Ingrosso, M.F. Ruiz-Lopez, A New Glimpse into the CO2-Philicity of Carbonyl Compounds, Chemphyschem, 13 (2012) 3397-3403.

[235] J.Y. Wang, M.Y. Wang, J.M. Hao, S. Fujita, M. Arai, Z.J. Wu, F.Y. Zhao, Theoretical study on interaction between CO2 and carbonyl compounds: Influence of CO2 on infrared spectroscopy and activity of C = O, Journal of Supercritical Fluids, 54 (2010) 9-15.

[236] M. Besnard, M.I. Cabaco, S. Longelin, T. Tassaing, Y. Danten, Raman investigation of the CO2 complex formation in CO2-acetone mixtures, Journal of Physical Chemistry A, 111 (2007) 13371-13379.

[237] Y. Danten, T. Tassaing, M. Besnard, Vibrational spectra of CO2-electron donor - Acceptor complexes from ab initio, Journal of Physical Chemistry A, 106 (2002) 11831-11840.

[238] K. Liu, E. Kiran, Viscosity, density and excess volume of acetone plus carbon dioxide mixtures at high pressures, Industrial & Engineering Chemistry Research, 46 (2007) 5453-5462.

[239] W.H. Zhuang, E. Kiran, An automated high pressure PVT apparatus for continuous recording of density and isothermal compressibility of fluids, Review of Scientific Instruments, 67 (1996) 244-250.

[240] N. Falco, E. Kiran, Volumetric properties of ethyl acetate plus carbon dioxide binary fluid mixtures at high pressures, Journal of Supercritical Fluids, 61 (2012) 9-24.

[241] K. Liu, E. Kiran, Miscibility, viscosity and density of poly(epsilon-caprolactone) in acetone plus CO(2) binary fluid mixtures, Journal of Supercritical Fluids, 39 (2006) 192-200.

[242] K. Liu, E. Kiran, A tunable mixture solvent for poly (epsilon-caprolactone): Acetone+CO2, Polymer, 48 (2007) 5612-5625.

[243] K. Liu, E. Kiran, High-pressure solution blending of poly(epsilon-caprolactone) with poly(methyl methacrylate) in acetone plus carbon dioxide, Polymer, 49 (2008) 1555-1561.

[244] L. Singh, V. Kumar, B.D. Ratner, Generation of porous microcellular 85/15 poly ((DL)-lactide-co-glycolide) foams for biomedical applications, Biomaterials, 25 (2004) 2611-2617.

[245] L.Y. Lee, S.H. Ranganath, Y.L. Fu, J.L. Zheng, H.S. Lee, C.H. Wang, K.A. Smith, Paclitaxel release from micro-porous PLGA disks, Chemical Engineering Science, 64 (2009) 4341-4349.

[246] R. Pini, G. Storti, M. Mazzotti, H.Y. Tai, K.M. Shakesheff, S.M. Howdle, Sorption and swelling of poly(DL-lactic acid) and poly(lactic-co-glycolic acid) in supercritical CO2: An experimental and modeling study, Journal of Polymer Science Part B-Polymer Physics, 46 (2008) 483-496.

[247] C. Hansen, The Universality of the Solubility Parameter, I & EC Produce Research and Development, 8 (1969) 2-11.

[248] C. Panayiotou, Solubility parameter revisited: an equatio-of-state approach for its estimation, Fluid Phase Equilibria, 131 (1997) 21-35.

[249] Polycaprolactone, in, Sigma-Aldrich, Saint Louis, MO.

[250] PLGA (Poly Lactic co-Glycolic Acid) Uniform Dry Microspheres, in, Polysciences, Inc., Warrington, PA.

[251] J. Tatibouet, R. Gendron, Heterogeneous nucleation in foams as assessed by in-line ultrasonic measurements, Journal of Cellular Plastics, 41 (2005) 57-72.

[252] S.J. Macnaughton, I. Kikic, N.R. Foster, P. Alessi, A. Cortesi, I. Colombo, Solubility of Anti-Inflammatory Drugs in Supercritical Carbon Dioxide, Journal of Chemical & Engineering Data, 41 (1996) 1083-1086.

[253] D.C. Bibby, N.M. Davies, I.G. Tucker, Mechanisms by which cyclodextrins modify drug release from polymeric drug delivery systems, International Journal of Pharmaceutics, 197 (2000) 1-11.

[254] E. Redenti, T. Peveri, M. Zanol, P. Ventura, G. Gnappi, A. Montenero, A study on the differentiation between amorphous piroxicam:beta-cyclodextrin complex and a mixture of the two amorphous components, International Journal of Pharmaceutics, 129 (1996) 289-294.

[255] H. Uchida, A. Yoshida, H. Kojima, Y. Yamazoe, M. Matsuoka, Measurement and correlation of the solid-liquid-gas equilibria for the carbon dioxide plus S-(+)-ibuprofen and carbon dioxide plus RS-(+/-)-ibuprofen systems, Journal of Chemical and Engineering Data, 50 (2005) 11-15.

[256] J.S. R. Petter, D. Sikorski, G. Kumaravel, F. Lin, Cooperative binding by aggregated mono-6-(alkylamino)-beta-cyclodextrins, Journal of the American Chemical Society, 112 (1990) 3860-3868.

[257] S.B.Z. R. Xie, H.D. Wang, Temperature-dependent molecular-recognizable membranes based on poly(N-isopropylacrylamide) and β-cyclodextrin, Journal of Membrane Science, 326 (2009) 618-626.

[258] X.D.F. Y.Y. Liu, L. Gao, Synthesis and Characterization of β-Cyclodextrin Based Functional Monomers and its Copolymers with N-isopropylacrylamide, Macromolecular Bioscience, 3 (2003) 715-719.